NATURAL CONVECTION IN TWO-DIMENSIONAL IRREGULAR CAVITIES

by

MARTIN FOURNIER

A THESIS SUBMITTED IN PARTIAL FULFILMENT OF

THE REQUIREMENTS FOR THE DEGREE OF

MASTER OF APPLIED SCIENCE

in

THE FACULTY OF GRADUATE STUDIES

Department of Chemical Engineering

We accept this thesis as conforming

to the required standard

THE UNIVERSITY OF BRITISH COLUMBIA

September 1986

In presenting this thesis in partial fulfilment of the requirements for an advanced degree at the The University of British Columbia, I agree that the Library shall make it freely available for reference and study. I further agree that permission for extensive copying of this thesis for scholarly purposes may be granted by the Head of my Department or by his or her representatives. It is understood that copying or publication of this thesis for financial gain shall not be allowed without my written permission.

Department of Chemical Engineering

The University of British Columbia
2075 Wesbrook Place
Vancouver, Canada
V6T 1W5

Date: September 1986

ABSTRACT

Natural convection in two-dimensional irregular cavities was simulated by numerically solving the steady-state conservation equations written in terms of stream function, vorticity and temperature dependent variables and for a general orthogonal coordinate system. It was assumed that the Boussinesq approximations were valid, that the fluid was Newtonian and that the properties other than density were constant. The use of orthogonal coordinates and the above set of dependent variables was found to have several advantages over the use of Cartesian or non-orthogonal systems and the set of primitive dependent variables (velocities, pressure and temperature). The body-fitted orthogonal coordinate system was numerically generated by means of the weak constraint method of Ryskin and Leal [26]. Special forms of the Wood and second-order vorticity boundary conditions were derived for a general two-dimensional body-fitted orthogonal coordinate system. Finite difference techniques were used to solve the resulting set of differential equations.

The effects of the mapping characteristics, the vorticity boundary conditions and the finite difference grid size on the accuracy of the natural convection solution were investigated first. For the cavity geometries studied, it was observed that, except for grid boundary conditions which led to undesirable grids, most combinations of grid and vorticity boundary conditions gave results of acceptable

accuracy (relative error less than one percent) as long as a sufficiently fine grid size (28x28 or finer) was employed.

The effects of the cavity geometry and the Rayleigh number on natural convection were investigated in Part II. It was found that increasing the Rayleigh number always acted to enhance both the natural convection circulation and the heat transfer rate, a result which was easily explained by examining the source term of the momentum equation. The effect of the cavity geometry was more complex but these results could also be interpreted by examining the influence of the cavity shape in impeding or enhancing fluid circulation and the opposing effects of the distance between isothermal walls on conductive and convective heat transfer.

The possibility of using a similar numerical procedure to simulate a melting or a freezing process was investigated in Part III. Numerical predictions of the circulating flow in the liquid phase of an ice forming process were obtained by digitizing the photographic image of a real ice interface and using the true non-linear relationship between density and temperature for water at low temperature. The numerical results were in reasonable agreement with the flow visualization experiments carried out by Eckert [42].

Table of Contents

LIST OF TABLES

LIST OF FIGURES

ACKNOWLEDGEMENTS

I would like to express my thanks to the people who have contributed to this work: my wife and family, who have stimulated me throughout the course of this work; Dr. Bruce Bowen, my supervisor, who has guided me, provided me knowledge and assisted me in the writing of this thesis; and Frank Laytner, a friend, who helped me in the writing of an intermediate report presented to my committee.

The financial assistance provided by the Natural Sciences and Engineering Research Council of Canada in the form of a Graduate Scholarship is gratefully acknowledged.

I. INTRODUCTION

Natural convection is a topic which has received growing attention in the last few decades. It is a subject of interest for both engineers and physicists. Natural convection takes place in many geophysical phenomena and has numerous engineering applications. Recently, the most important engineering applications of natural convection have been related either to the design of solar collectors for passive heating or to the storage of solar energy by phase change materials.

Natural convection is promoted by the presence of a density gradient in a body force field. The density gradient is usually due to a temperature difference, and the body force is often gravity.

Natural convection can be investigated theoretically by solving simultaneously the mass, momentum and energy conservation equations. Because these equations are strongly coupled and are nonlinear, their solution generally requires the application of numerical methods. In only a few very simple cases, the numerical approach can be replaced by an analytical approach.

Experimental and numerical studies of natural convection have been carried out for many geometries, but it is the one-dimensional isothermal flat plate and the two-dimensional rectangular cavity which have received the most attention. The rectangular cavity consists of two opposing isothermal walls at different temperatures and two

adiabatic walls which complete the enclosure (Fig. 1). Each rectangular cavity problem is specified by four independent variables: the Rayleigh and Prandtl numbers (calculated with respect to a characteristic length, usually taken to be the length of the adiabatic wall; the characteristic temperature difference, $T_h - T_c$; and the properties evaluated at a fluid reference temperature, usually the average temperature of the cavity), the cavity aspect ratio (length of the isothermal wall divided by the length of the adiabatic wall) and the angle of tilt.

Natural convection in two-dimensional nonrectangular cavities (other than axisymmetric cylindrical cavities) has hardly been investigated. The natural convection in the liquid phase of a melting or freezing process taking place in a vertical rectangular cavity creates a nonrectangular enclosure of particular interest. Most of the numerical studies of natural convection in nonrectangular enclosures have used either the finite element method or the finite difference method in combination with a nonorthogonal transformation to solve the conservation equations.

Recently, Ryskin and Leal [26] have developed a new method for numerically generating body-fitted orthogonal coordinates which are better suited to the finite difference method. As well as producing orthogonal grids, the method allows very flexible control over the spacing of grid lines as well as nodal correspondence at boundaries between contiguous solution domains. Its ability to map irregular

Figure 1. Two-dimensional rectangular cavity.

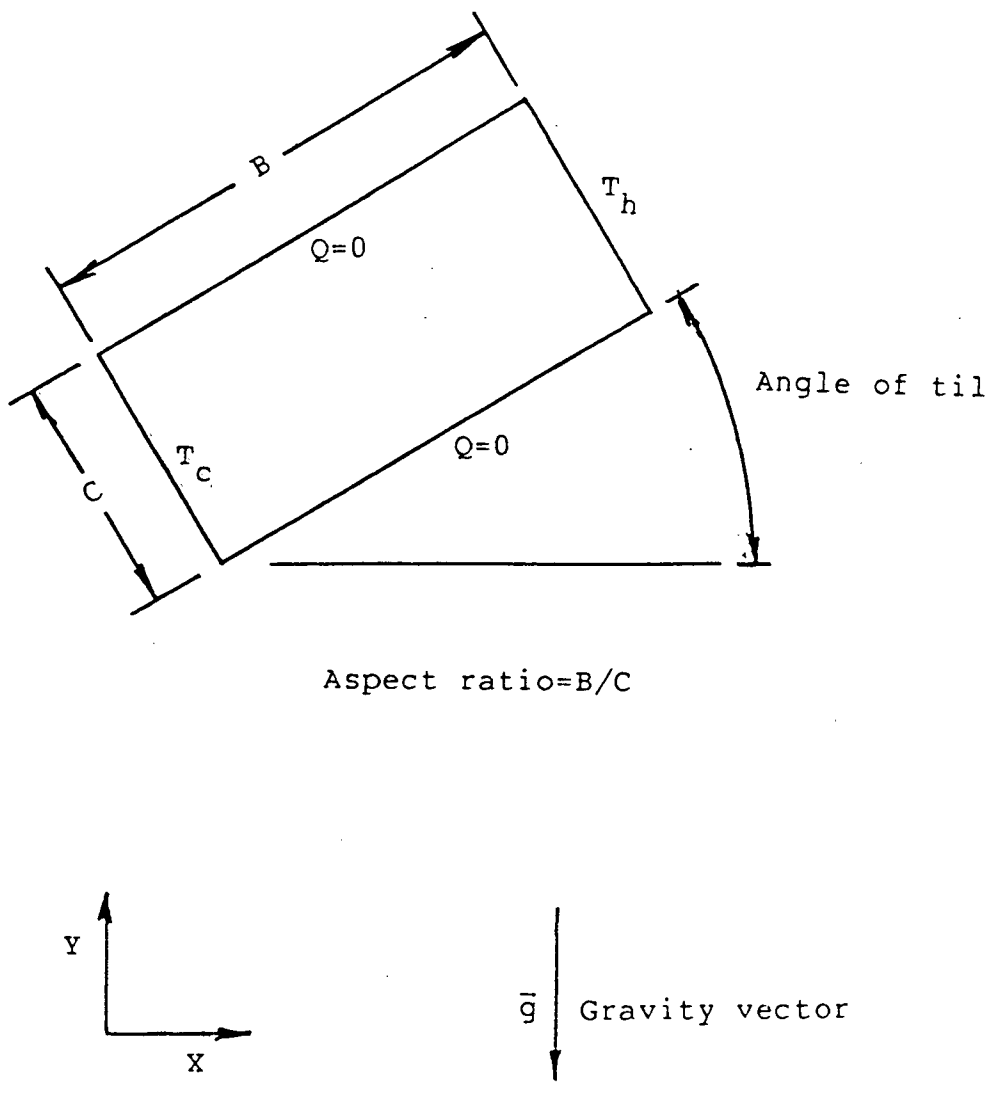

cavities is shown in Fig. 2. Some of the different characteristics which can be imposed on the mapping are shown in Fig. 3. This new mapping procedure has never been used before to study natural convection in nonrectangular enclosures.

The primary objective of the present thesis is to develop a general procedure for using numerically generated body-fitted orthogonal coordinate transformations to solve problems of natural convection in nonrectangular cavities. The cavities considered here are those that are likely to arise in phase change situations and can be seen as extensions of the vertical square enclosure problem. In the main part of the work, two general cavity shapes are investigated. Both enclosures have nonflat right walls which are analytically defined by the cosine functions: one cavity employs a half cycle, i.e.

$$X=1+A-(A\ \cos(\pi Y)) \qquad 0<=Y<=1 \qquad (1)$$

while the other uses a full cycle, i.e.

$$X=1+A-(A\ \cos(2\pi Y)) \qquad 0<=Y<=1 \qquad (2)$$

For convenience, these two types of cavities are referred to as C1 and C2, respectively, and are shown in Fig. 4.

Natural convection in such deformed cavities is affected by five independent variables; the Rayleigh and

Figure 2. Body-fitted orthogonal grids generated by the weak constraint method of Ryskin and Leal [26] for several different irregular cavities.

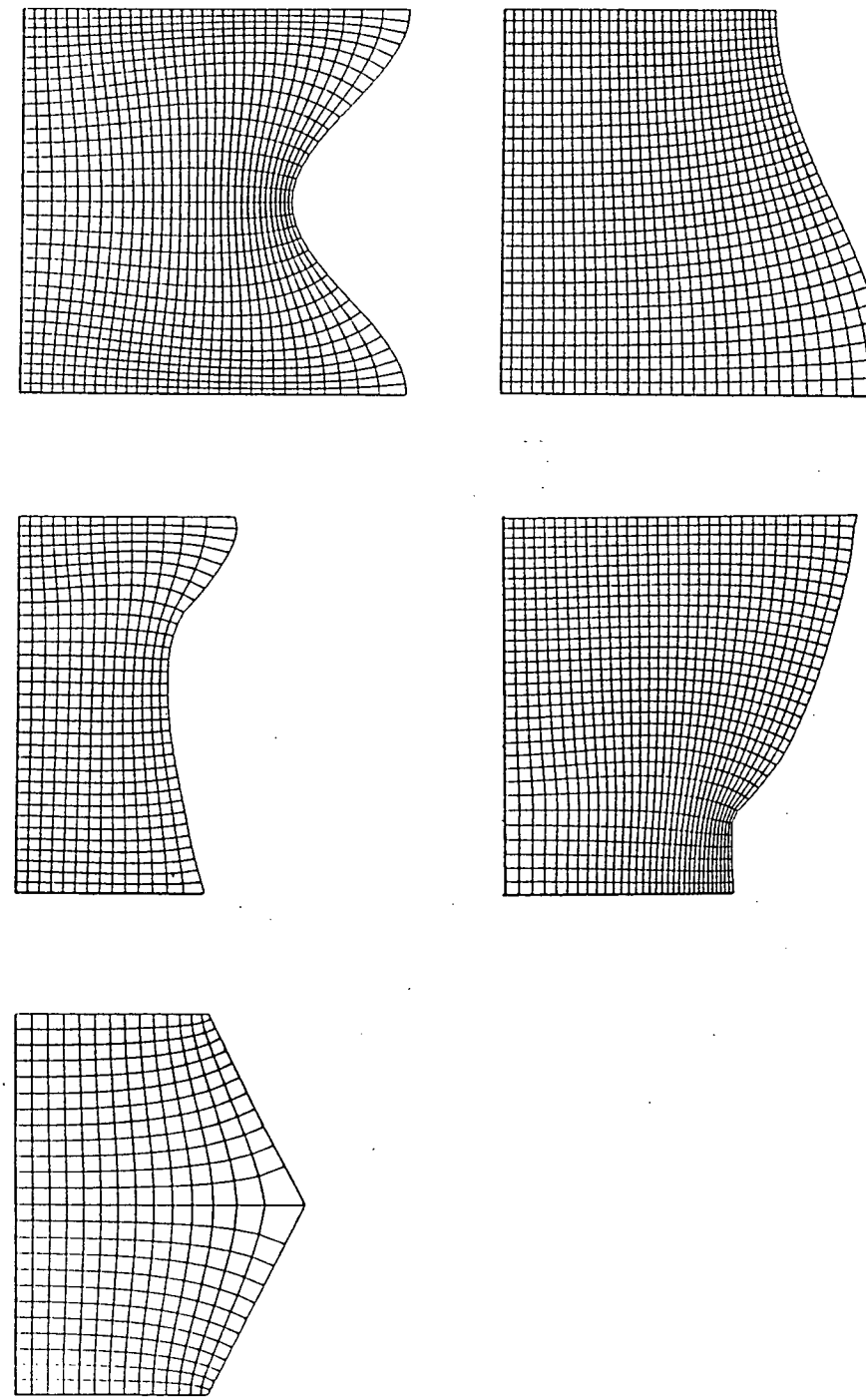

Figure 3. Three different body-fitted orthogonal grids generated by the weak constraint method of Ryskin and Leal [26] for a single irregular cavity.

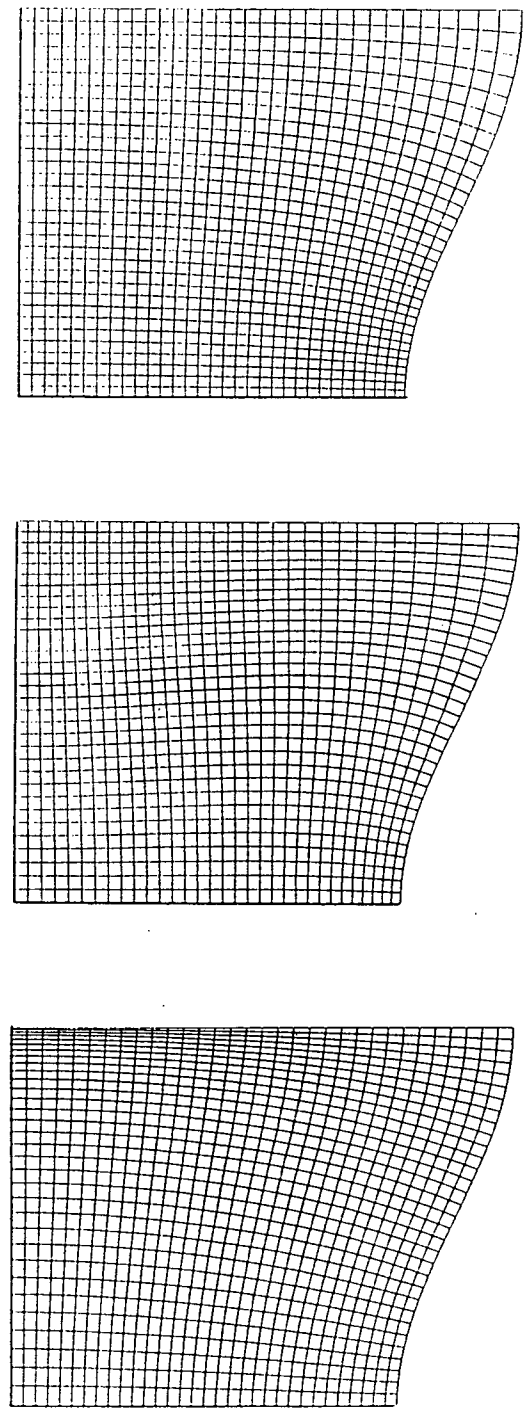

Figure 4. General shape of cavity types C1 (a) and C2 (b).

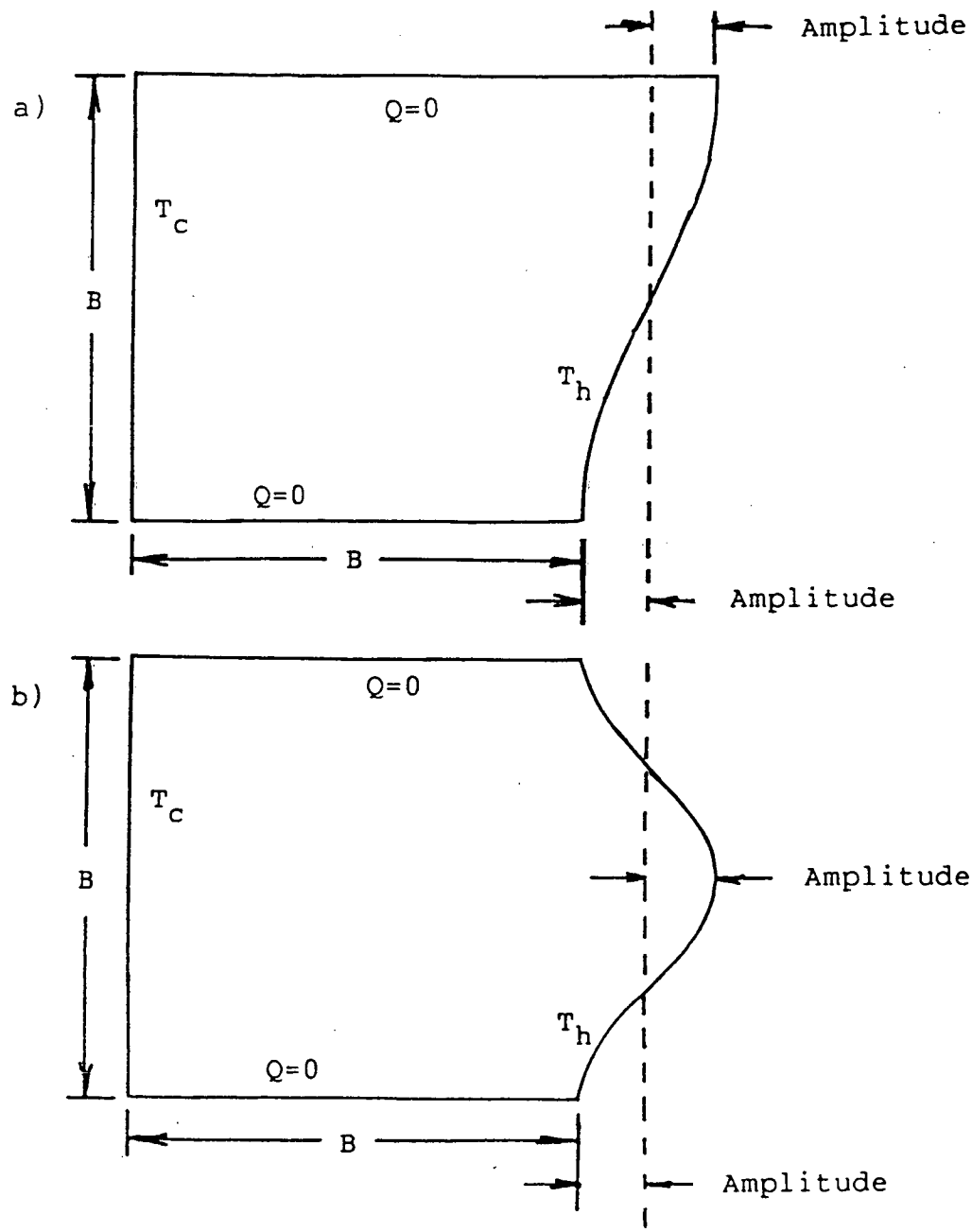

Prandtl numbers (calculated with respect to the length of the cavity bottom wall; the characteristic temperature difference, T_h-T_c; and the properties evaluated at the fluid reference temperature, $(T_h-T_c)/2$), the dimensionless amplitude (amplitude divided by length of the bottom wall), the aspect ratio (length of the left wall divided by the length of the bottom wall) and the angle of tilt. The independent variable values which are investigated are presented in Table 1. Only two parameters are varied in the present study: the Rayleigh number and the dimensionless amplitude. The Prandtl number, the cavity aspect ratio and the angle of tilt remain constant.

The method of Ryskin and Leal [26] is used to generate a two-dimensional body-fitted orthogonal coordinate system. The steady-state mass, momentum and energy conservation equations, written in terms of the stream function, vorticity and temperature dependent variables, are then solved in transformed coordinates using a finite difference method. The analysis assumes that the Boussinesq approximations are valid, that the fluid properties other than density are constant, and that the fluid is Newtonian.

The study is subdivided into three parts. The objective of the first part is to determine the effects of the mapping characteristics (which are described in a later chapter), the vorticity boundary conditions (either Wood or second order) and the finite difference grid size on the accuracy of the numerical results. For this purpose, only the most

Table 1. Independent variables considered for the cavity types C1 and C2.

Rayleigh Number	Prandtl Number	Dimensionless Amplitude	Cavity Aspect Ratio	Cavity Angle of Tilt (Degree)
0 1000 3000 10000 30000 100000	1	-0.150 -0.075 0.000 0.075 0.150	1	0

extreme cases are considered. Thus, only the most distorted cavities of types C1 and C2 are used. A moderate Rayleigh number of 10000 is employed because it ensures that both the conductive and convective heat transfer modes are involved. From the results of these simulations, the best set of mapping characteristics and vorticity boundary conditions is determined for each extreme case. Also, an optimum finite difference grid size is selected which yields reasonable numerical error with minimal computational cost.

In the second part, the optimal conditions selected in the first section are used to thoroughly investigate the effects of dimensionless amplitude and Rayleigh number on the heat transfer by natural convection in cavity types C1 and C2. As well as generating flow maps and temperature distributions for each case, local and average Nusselt numbers are also calculated and compared with standard correlations for rectangular cavities.

The objective of the third part is to demonstrate the applicability of the numerical procedure to real phase change problems. Several different quasi-steady flow patterns which occur during ice formation are simulated and compared to available experimental stream-line photographs taken by Eckert [42].

II. LITERATURE REVIEW

A. NATURAL CONVECTION NEAR A VERTICAL ISOTHERMAL FLAT PLATE

For this simple case, an analytical solution of the conservation equations is made possible by assuming that the fluid is Newtonian, that a laminar boundary-layer exists, that the Boussinesq approximations are valid and that the fluid properties other than density are constant. Under these conditions a similarity transformation can be applied which reduces the set of partial differential equations to a pair of ordinary differential equations [30,32,33]. Also, similarity profiles can be used in conjunction with the integral method to approximately solve the conservation equations [30,31]. The temperature and velocity results from the analytic theory are found to be in good agreement with experimental measurements [30]. However, the experimental average Nusselt numbers are slightly higher than those predicted analytically. The differences in the average Nusselt numbers are larger for both small and large Rayleigh numbers. At low Rayleigh numbers, the discrepancies between predicted and experimental average Nusselt numbers are likely due to the increasing inaccuracy of the boundary-layer assumptions. At high Rayleigh numbers, the differences are attributed to the development of turbulence. The analytical average Nusselt number is correlated to the Rayleigh number by an equation of the form

$$Nu_{x,ave}=a(Ra_x)^b \tag{3}$$

where

$$Nu_{x,ave}=\frac{h_{ave}x}{k_\infty} \tag{4}$$

$$Ra_x=g\beta_\infty\rho_\infty^2\, x^3(T_w-T_\infty)C_{p\infty}/\mu_\infty k_\infty \tag{5}$$

and x is the distance along the plate in the flow direction. The value of the coefficient a in Eq. 3 is weakly dependent on the Prandtl number, and the value of the coefficient b is equal to 0.25 for the laminar boundary-layer regime. For Prandtl number approaching 0 and Prandtl numbers larger than 100, Eq. 3 becomes, respectively,

$$Nu_{x,ave}=0.8(PrRa_x)^{0.25} \tag{6}$$

and

$$Nu_{x,ave}=0.67(Ra_x)^{0.25} \tag{7}$$

where Pr is the Prandtl number.

B. NATURAL CONVECTION IN RECTANGULAR ENCLOSURES

The two-dimensional rectangular cavity is called a vertical rectangular cavity if the isothermal walls are vertical, and a horizontal rectangular cavity if the

isothermal walls are horizontal. This classification arises from the differences in the convection patterns observed for the two cases [1,2]. In the vertical rectangular cavity, the flow starts immediately because the density gradient is perpendicular to the gravity vector. On the other hand, for the horizontal rectangular cavity, two cases are possible:

1. if the density gradient is parallel and opposed to the gravity vector, the flow starts only if the gradient is sufficiently large, and
2. if the density gradient is parallel to and in the same direction as the gravity vector, no flow takes place in the cavity.

The independent variables associated with the rectangular cavity are the Rayleigh number, the Prandtl number, the cavity aspect ratio and the angle of tilt. Extensive experimental and numerical investigations have been carried out on the rectangular cavity to establish flow regimes and to determine average Nusselt numbers. The results of these investigations are thoroughly discussed in two excellent review articles [1,2]. The different flow regimes and dominant heat transfer mechanisms observed as a function of Rayleigh number are shown in Table 2 for the case of the vertical square cavity filled with air [1,3]. Two example flow patterns are illustrated in Fig. 5. For the vertical square enclosure, the following identification scheme for the various heat transfer regimes was proposed [14]:

Table 2. Flow and heat transfer observations for the vertical square cavity filled with air.

Rayleigh Number Range	Observations
0 to 1000	- Weak unicellular flow pattern - Conduction heat transfer regime
1000 to 10000	- Unicellular boundary-layer like flow pattern - Transition heat transfer regime
10000 to 100000	- Unicellular boundary-layer like flow pattern - Boundary-layer heat transfer regime
100000 to 1000000	- Onset of a secondary flow cat's-eye pattern - Boundary-layer heat transfer regime

Figure 5. Typical flow patterns observed in a vertical square cavity. (a) Ra=10000, unicellular flow, (b) Ra=100000, "cat's-eye" pattern.

a)

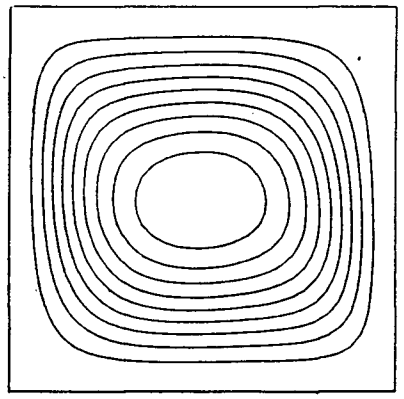

b)

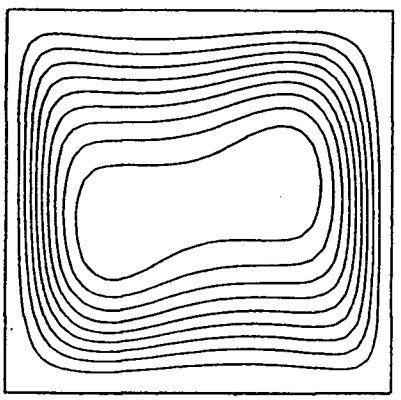

1. the end of the conduction regime is attained when the horizontal temperature derivative at the center of the cavity differs by 10 percent from the value for pure conduction, and
2. the beginning of the boundary-layer regime is reached when the horizontal temperature derivative at the center of the cavity is equal to zero.

The average Nusselt number is found to be significantly affected by the Rayleigh number [3-8,11,13], low Prandtl number [3,7,8], the cavity aspect ratio [6,7,13] and the angle of tilt [4-6]. The effect of large Prandtl number on the average Nusselt number is negligible [3,7,8]. The general relationship used to correlate the Nusselt number with the Rayleigh number (other independent variables being constant) is similar to that employed for the isothermal flat plate (Eq. 3):

$$Nu_{ave}=a(Ra)^{b} \tag{8}$$

where

$$Nu_{ave}=\frac{h_{ave}L_c}{k_o} \tag{9}$$

and

$$Ra=g\beta_o\rho_o^2L_c^3(T_h-T_c)C_{p_o}/\mu_o k_o \qquad (10)$$

The characteristic length, L_c, is the length of the adiabatic wall and the fluid reference temperature is the average temperature through the cavity. For the laminar boundary-layer regime, the value of the exponent b is somewhat greater for the vertical rectangular cavity than for the vertical isothermal flat plate. For the enclosure, b ranges from 0.25 to 0.35 [3,7,9,10]. This fact demonstrates the importance of the core of the cavity and the significant interaction it has with the boundary-layer at the wall [1,2,4].

Natural convection in a vertical square cavity has become a benchmark problem for numerical studies, primarily because this is the simplest case for which all terms of the Navier-Stokes equations must be included and where the energy and motion equations are coupled. In 1982, under the auspices of De Vahl Davis and Jones [15], a comparison exercise was carried out to test the ability of a large number of different numerical techniques to successfully solve this problem. Of the 36 contributions, 21 used finite difference methods while 10 others used finite element methods. Also, among all contributions, 11 considered the primitive variable form (two velocities, pressure and temperature) of the governing equations while 9 others used the stream function, vorticity and temperature form. A large variety of finite difference discretization methods were

used. Of the various finite difference solutions submitted, one of the most successful was that of Wong and Raithby [12], who employed the exponential differencing scheme and a second order accurate vorticity boundary condition.

Investigations have also been carried out on the validity of the commonly used assumptions in numerical natural convection studies. The validity of the Boussinesq approximations and constant fluid properties (with the exception of the density) assumption was studied by examining the effects of variable properties on laminar natural convection in a vertical square enclosure [10]. In this study, the unsteady-state conservation equations written in terms of primitive variables were solved using finite difference methods. To determine the validity limits of the Boussinesq approximations (constant properties evaluated at the cavity cold wall temperature), a compressible Newtonian fluid (air) whose density follows the perfect gas law and whose other fluid properties are constant was considered. It was found that the Boussinesq approximations were valid if the overall temperature difference satisfied the following criterion:

$$\frac{T_h - T_c}{T_c} < 0.1 \qquad (11)$$

where the temperatures are expressed in Kelvins. Considering a compressible Newtonian fluid (air) whose density is still

given by the perfect gas law but whose properties are temperature dependent, it was found that

1. the average Nusselt number was unaffected by the assumptions made about the fluid properties over a range of $(T_h-T_c)/T_c$ from 0.2 to 2.0 as long as an appropriate reference temperature, i.e.

$$T_0=T_c+0.25(T_h-T_c) \qquad (12)$$

was chosen, and

2. the velocity and temperature profiles were influenced to a greater or lesser degree by the choices made concerning the property assumptions.

The Newtonian fluid and constant property assumptions were also investigated by studying the natural convection in a rectangular enclosure of a fluid whose viscosity was temperature dependent or whose behaviour was non-Newtonian [9]. In this study, the steady-state conservation equations written in terms of stream function, vorticity and temperature were solved using finite difference methods. It was assumed that the Boussinesq approximations were valid and that the fluid properties other than density, viscosity and elasticity were constant. It was found that, while the velocity distribution is affected significantly, the overall rate of heat transfer through the enclosure is negligibly influenced by assuming

Newtonian behaviour.

Natural convection has been studied in modified rectangular cavities [16,17]. Chang and al. [17] numerically investigated the effects of internal baffles located opposite one another on the top and bottom walls of a vertical cavity. The unsteady-state conservation equations written in terms of primitive variables were solved using a finite difference method. It was assumed that the fluid was Newtonian and obeyed the perfect gas law and that its properties other than density were constant. The numerical results are discussed but are not compared with experimental measurements. Kim and Viskanta [16] studied the effect of wall heat conduction on natural convection heat transfer in a square enclosure. The unsteady-state conservation equations written in terms of stream function, vorticity and temperature were solved with finite difference methods. It was assumed that the Boussinesq approximations were valid, that the fluid was Newtonian, its properties other than density were constant and that the wall properties were isotropic and temperature-independent. Their numerical results were compared with measurements carried out by the same authors [16]. Very good agreement was found between the numerical and experimental results for the temperature distribution in the solid while a reasonable agreement was obtained for the temperature distribution in the liquid.

C. PHASE CHANGE PROBLEMS

The problem of melting or solidification in an enclosure has not been extensively investigated either numerically or experimentally. The lack of theoretical information about this case can be attributed to the difficulty of solving the equations of motion and energy in an irregular-shaped cavity with a moving boundary [19]. It has been amply demonstrated that natural convection plays a significant role in such phase change problems [18,19,20]. Numerical results are available for melting or solidification in a vertical rectangular cavity [18,19] and in an annular cavity [20]. In these studies, a non-orthogonal coordinate system and a quasi-steady approach were used to solve either the steady-state [19] or unsteady-state [18,20] conservation equations. In all cases, it was assumed that the fluid phase properties other than density were constant, that the fluid was Newtonian and that the Boussinesq assumptions were valid while all properties of the solid were assumed to be constant. Both primitive variables and stream function, vorticity and temperature variables were used in these numerical investigations. Only the numerical results of Ho and Viskanta [18] were extensively compared with measurements obtain by the same authors [18]. The liquid volume fraction, the local and average Nusselt numbers along the vertical hot wall, and the shape of the solid-liquid interface were compared at different times during the transient melting process. At

early times, good quantitative agreement was found between the numerical and experimental results, but with increasing time, the numerical results were found to display only similar qualitative trends in time and space with the measured results. Natural convection phase change problems also occur during casting processes. For instance, Kroeger and Ostrach [21] have carried out a theoretical study of the continuous casting of a slab. A numerically generated conformal orthogonal coordinate system was used along with finite difference methods to solve the steady-state conservation equations, written in terms of stream function, vorticity and temperature dependent variables. It was assumed that the fluid phase properties other that density were constant, that the fluid was Newtonian and that the Boussinesq approximations were valid. Unfortunately, the numerical results were not compared with measured data.

D. NATURAL CONVECTION IN NONRECTANGULAR ENCLOSURES

Natural convection in two-dimensional nonrectangular enclosures (other than cylindrical) has also been little investigated. Some experimental work on natural convection in parallelogrammic enclosures has been carried out [23]. A major study which involved numerical analyses as well as some experimental measurements investigated natural convection in two-dimensional vee-corrugated channels (bottom left image of Fig. 2) [22,24,34-37]. In the numerical investigation [22,24], a Schwartz-Christoffel

transformation was used to analytically determine a conformal boundary-fitted orthogonal coordinate system. The usual assumptions (constant fluid properties other than density, Boussinesq, Newtonian fluid) were made in order to solve the unsteady-state conservation equations, written in terms of stream function, vorticity and temperature, using finite difference methods. Average Nusselt numbers along the flat surface were compared with measurements [34-37] for different channel aspect ratios, angles of tilt and Rayleigh numbers. Similar trends were noticed although quantitative discrepancies (up to 20 percent) were found.

E. BODY-FITTED ORTHOGONAL TRANSFORMATIONS

Body-fitted orthogonal transformations for mapping nonrectangular domains into rectangular domains can be obtained using either an analytical or a numerical approach. The analytical approach involves tedious mathematical manipulations and is restricted to the mapping of very simple nonrectangular domains. However, the numerical approach can be used to map nearly any irregular domain and allows for far more flexible mapping characteristics.

Numerical coordinate generation is a relatively new area of numerical analysis and its progression has been reviewed in several recent articles [25,26]. Of the numerical mapping procedures available for enclosures with specified boundaries, the so-called weak constraint method of Ryskin and Leal [26] appears to be most powerful. It not

only generates orthogonal grids which have distinct advantages over non-orthogonal coordinate systems, but it also allows for the convenient matching of boundary conditions at the interface of neighbouring regions, an important consideration in phase change problems. Despite its many advantageous features, the weak constraint method appears to have had limited use in solving fluid flow problems. The only reference to the procedure that has appeared in the literature so far is a paper by Chikhliwala and Yortsos [27] who used it to map the irregular domains likely to arise during immiscible fluid-fluid displacement in porous media. However, the paper was concerned only with the mapping process; there were no accompagning solutions to the fluid flow problem. Several earlier studies have solved the Navier-Stokes equations using less elaborate numerical procedures than the weak constraint method. For example, Pope [29] used a numerically generated orthogonal grid (constant shape factor) to investigate turbulent forced convection flows in an irregular channel while Kroeger and Ostrach [21] used a numerically generated orthogonal grid to study the continuous casting process of a slab in which natural convection was taken into account.

III. COORDINATE SYSTEM

In mapping a nonrectangular two-dimensional domain, many coordinate systems could be considered. For example, either a Cartesian, a body-fitted nonorthogonal or a body-fitted orthogonal coordinate system could be used (Fig. 6). Whichever coordinate system is adopted, the mass, momentum and energy conservation principles required to solve the natural convection problem are still applicable; however, the mathematical formulation of these conservation principles in a particular coordinate system is complicated to a greater or lesser extent depending on which coordinate system is chosen.

The steady-state natural convection problem which is described by a set of elliptic partial differential equations is subject to a corresponding set of boundary conditions. These boundary conditions are either of the Dirichlet, Neumann or mixed (Robin) type. A Dirichlet boundary condition specifies the value of a dependent variable at the domain boundary. A Neumann boundary condition specifies the values of the derivative of a dependent variable in the direction normal to the boundary. The mixed boundary condition as, its name implies, relates the normal derivative of a dependent variable with its value at the boundary. Thus, the way the coordinate system matches the cavity boundary is an important factor to consider. The easier and the more accurately the boundary conditions can be prescribed, the better will be the numerical

Figure 6. Different coordinate systems which can be used to map an irregular cavity. (a) Cartesian, (b) body-fitted nonorthogonal, (c) body-fitted orthogonal.

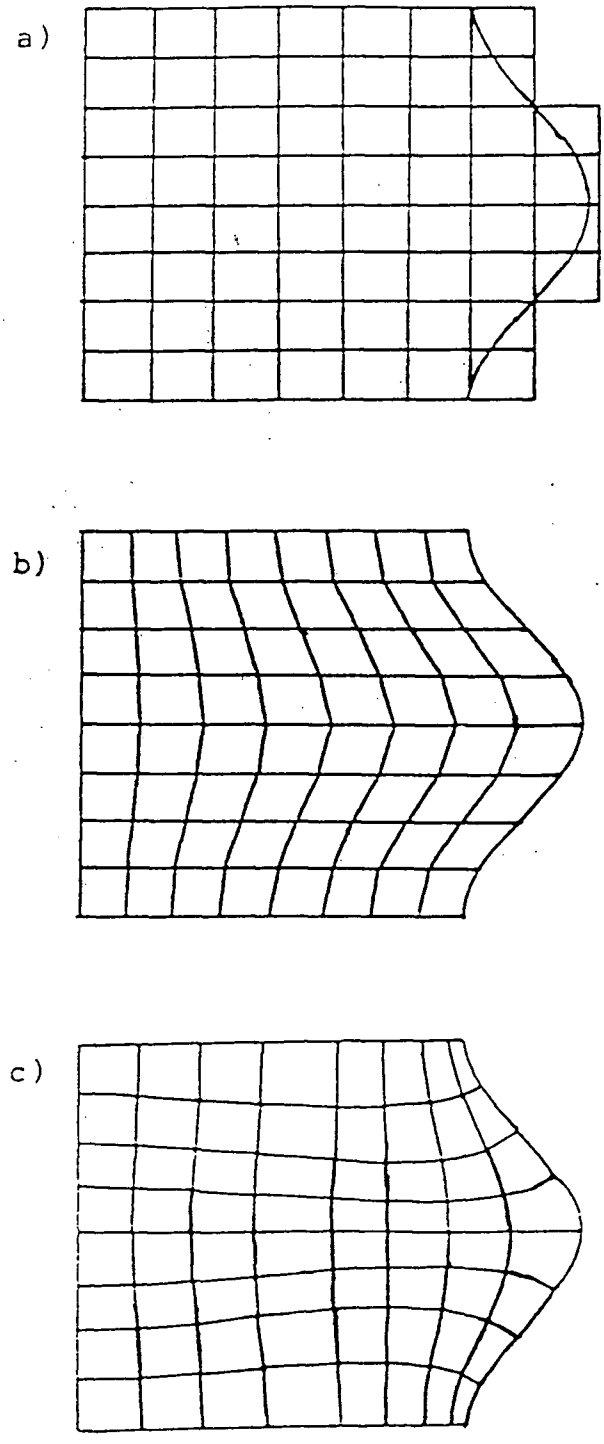

solution [24].

The body-fitted orthogonal coordinate system is the only one which matches the domain boundary, allows easy specification of Dirichlet, Neumann and mixed conditions at the boundary and reduces the conservation equations to a relatively compact form. The choice of the Cartesian coordinate system was eliminated because not all of the finite difference nodes lie on the boundary, nor do the grid lines intercept it at right angles. As a consequence, it becomes very difficult to accurately specify any type of boundary condition. The body-fitted non-orthogonal coordinate system makes the setting of Dirichlet conditions a simple matter, but it is also a poor choice because the Neumann and mixed conditions cannot be accurately specified and furthermore, the governing equations, due to the fact that cross-derivative terms must be retained, become very cumbersome.

A. BODY-FITTED ORTHOGONAL MAPPING USING THE WEAK CONSTRAINT METHOD

In the following discussion, two domains are considered (Fig. 7) which are referred to as the physical and the transformed domains, respectively. The coordinate system of the physical domain is Cartesian, and it has an irregular shape whose boundaries can be expressed in terms of analytic formulae. Regardless of its shape, the boundary of the physical domain can be divided into four sections. The

Figure 7. Physical domain (a) and transformed domain (b).

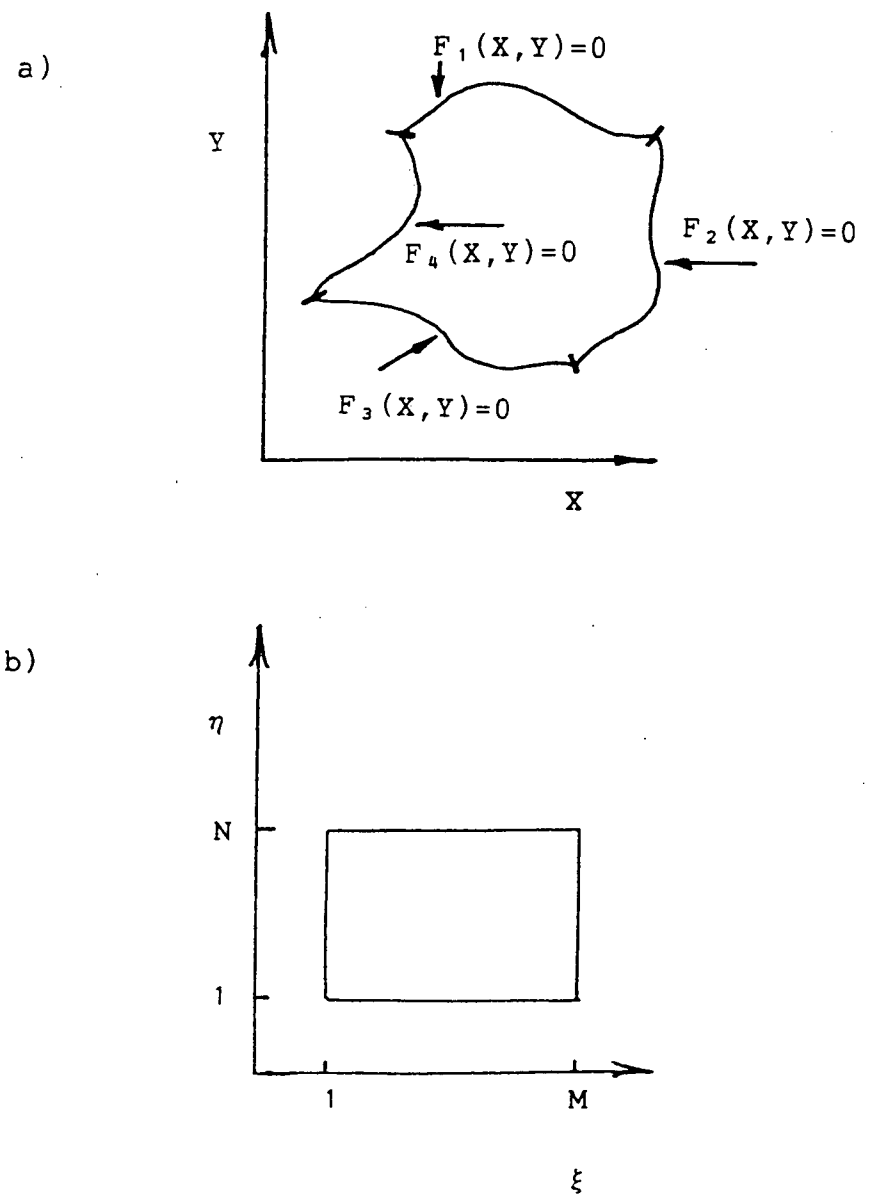

sections are numbered from 1 to 4 following the boundary in its clockwise direction. The coordinate system of the transformed domain is orthogonal. The transformed domain always has a rectangular shape which is the image, in the orthogonal coordinate system, of the physical domain. The four boundaries of the transformed domain are referred to as the top, right, bottom and left walls and are expressed in analytical form by the following relationships:

left wall, $\xi=1$;

right wall, $\xi=M$;

bottom wall, $\eta=1$;

and

top wall, $\eta=N$;

where M and N are the number of rows or columns of nodal points in the ξ and η directions, respectively.

If it is arbitrarily considered that the images of the top wall and the top right corner of the transformed domain correspond to section 1 and the junction of sections 1 and 2 of the physical domain, respectively, then the following statements can be made about the transformation:

1. the images of the top, right, bottom and left walls of the transformed domain must correspond to sections 1 to 4 of the physical domain boundary, respectively, and
2. the image of the top left, bottom left, bottom

right and top right corner points of the transformed domain boundary must correspond to the junctions of the physical domain boundary sections 1 and 2, 2 and 3, 3 and 4, and 4 and 1, respectively.

The point-by-point coordinate mapping of the transformed domain into the physical domain is obtained numerically by solving an appropriate set of differential equations. In the weak constraint method of Ryskin and Leal [26], the orthogonal mapping is defined by the folowing pair of elliptic partial differential equations:

$$\frac{1}{H_\xi H_\eta}\left[\frac{\partial}{\partial \xi}\left[f\frac{\partial X}{\partial \xi}\right]+\frac{\partial}{\partial \eta}\left[\frac{1}{f}\frac{\partial X}{\partial \eta}\right]\right]=0 \tag{13}$$

and

$$\frac{1}{H_\xi H_\eta}\left[\frac{\partial}{\partial \xi}\left[f\frac{\partial Y}{\partial \xi}\right]+\frac{\partial}{\partial \eta}\left[\frac{1}{f}\frac{\partial Y}{\partial \eta}\right]\right]=0 \tag{14}$$

where

$$f=\frac{H_\eta}{H_\xi} \tag{15}$$

$$H_\xi^2=\left[\frac{\partial X}{\partial \xi}\right]^2+\left[\frac{\partial Y}{\partial \xi}\right]^2 \tag{16}$$

and

$$H_{\eta}^{2}=\left[\frac{\partial X}{\partial \eta}\right]^{2}+\left[\frac{\partial Y}{\partial \eta}\right]^{2} \qquad (17)$$

Equations 13 and 14 are Laplace's equations in general orthogonal coordinates, and they arise from consideration of the fact that all coordinate lines in both the physical and transformed domains must meet at right angles. The two equations must be solved simultaneously over the whole of the transformed domain subject to an appropriate set of boundary conditions.

The quantities, H_{ξ} and H_{η}, are called scale factors. They relate the length of infinitesimal displacements in both domains. The shape factor, f, specifies the aspect ratio of an infinitesimal rectangular element in the physical domain which is the image of an infinitesimal square element in the transformed domain. The shape factor is prescribed over the interior of the transformed domain by a function which is called the distortion function. The distortion function can be any positive scalar function including, in its simplest form, a constant. If the shape factor is everywhere equal to unity, then the mapping which results is called conformal. The mapping of an irregular shape using a constant distortion function is said to be "stiff" because such a condition is a major and unnecessary restriction [26]. A distortion function which varies with ξ and η is much more desirable because it gives the user more control over the mapping process. Ryskin and Leal [26] recommend the following algebraic interpolation formula

which considers the shape factors along the transformed domain boundary in order to determine the shape factors in the interior of the transformed domain:

$$f(\xi,\eta)=(1-\xi)f(1,\eta)+\xi f(M,\eta)+(1-\eta)f(\xi,1)+\eta f(\xi,N)$$
$$-(1-\xi)(1-\eta)f(1,1)-(1-\xi)\eta f(1,N)$$
$$-\xi(1-\eta)f(M,1)-\xi\eta f(M,N) \qquad (18)$$

It has been demonstrated that Eq. 18 can be used with great success to map a variety of different irregular-shaped domains with body-fitted orthogonal coordinates [26,27].

B. BOUNDARY CONDITIONS OF THE BODY-FITTED ORTHOGONAL MAPPING

The imposition of the boundary conditions in body-fitted orthogonal mapping is of primary importance. Two boundary conditions, one for each Cartesian coordinate, are required along each section of the transformed domain boundary. The possible boundary conditions, which must be either of the Dirichlet or Neumann type, are reported below.

Dirichlet boundary conditions:

$$X=F(Y) \qquad (19)$$

and

$$Y=F(X) \tag{20}$$

Neumann boundary conditions:

$$f\frac{\partial X}{\partial \xi}=\frac{\partial Y}{\partial \eta} \tag{21}$$

and

$$\frac{\partial X}{\partial \eta}=-f\frac{\partial Y}{\partial \xi} \tag{22}$$

In the weak constraint method, two different choices of boundary conditions for each boundary section are possible. In one case, the correspondence between Cartesian and orthogonal coordinates is completely specified along the transformed domain boundary section while the shape factors along the same boundary section required for Eq. 18 are obtained numerically from Eqs. 15 to 17. This case requires the specification of two Dirichlet conditions. This method of prescribing boundary conditions allows complete control of the spacing between ξ or η coordinate lines at a boundary section of the physical domain and also for complete matching of ξ or η coordinates lines at the interface of adjoining physical domains. The other possible choice is to specify the shape factors along the transformed domain boundary section (usually by linearly interpolating the pre-assigned values at the two corner points) and allow the mapping to determine the correspondence between Cartesian

and orthogonal coordinates. Therefore, in this case, it is the mapping which determines where the ξ and η coordinate lines intersect on the physical domain boundary for the section considered. This second choice requires the specification of one Dirichlet and one Neumann condition at the boundary. The Neumann condition (Eqs. 21 or 22) simply indicates that the coordinate line of ξ or η must be orthogonal to the physical domain boundary. In practice, the best mapping results are usually obtained by requiring boundary correspondence only at one or at most three boundary sections [27]. Attempting to impose the correspondence between Cartesian and orthogonal coordinates on all four boundary sections may lead to a mapping in which the orthogonality condition is not necessarily respected. Such mappings would be ill-suited for numerical solutions.

IV. CONSERVATION EQUATIONS

The natural convection problem is described by the mass, momentum and energy conservation equations. These equations can be written in terms of different sets of dependent variables. One common choice is to use the velocity components, the temperature and the pressure as the dependent variables. This set is known as the set of primitive variables. An alternative set of dependent variables consists of the stream function, vorticity and temperature. An advantage of the second set over the first set, at least in two-dimensional natural convection problems, is that the four conservation equations associated with the primitive variables are reduced to three. This advantage is offset to some extent by the fact that the vorticity boundary conditions are difficult to specify and the pressure distribution, which is very important in forced convection, is not obtained explicitly. However, the latter information is not usually of direct interest in natural convection situations.

The simplicity of the conservation equations written in general two-dimensional orthogonal coordinates also has to be taken into account in the choice of dependent variables. Because the stream function and the vorticity are scalar quantities in two dimensions whereas velocity is always a vector, the conservation equations in general coordinates have less complex formulations when the stream function, vorticity and temperature variables are used.

For the above reasons, the stream function, vorticity and temperature were adopted as dependent variables in the present study.

A. ASSUMPTIONS

The assumptions used in the analysis of laminar natural convection occuring in an enclosure are stated below:

1. Problem is independent of time.
2. Problem is two-dimensional.
3. Fluid is Newtonian.
4. Fourier's law is valid.
5. Boussinesq approximations are valid:
   a. the density variations are considered only insofar as they contribute to buoyancy, but are otherwise neglected, and
   b. the density difference which causes the buoyancy is approximated as a pure temperature effect.
6. Fluid properties other than density are constant.
7. The body force is due only to the gravity.
8. Viscous dissipation is negligible.
9. Compressible work is negligible.
10. Energy is not generated.

B. CONSERVATION EQUATIONS IN CARTESIAN SYSTEM

To obtain the correct formulation of the relevant conservation equations of the natural convection problem in a general orthogonal system, the equations are first derived for the Cartesian system in the present section and then modified for the general system in the section which follows.

Using the assumptions stated in Section A, the relevant mass, momentum and energy conservation equations become, respectively,

$$\frac{\partial}{\partial x}(v_x)+\frac{\partial}{\partial y}(v_y)=0 \tag{23}$$

$$\rho_o\left[v_x\frac{\partial}{\partial x}(v_x)+v_y\frac{\partial}{\partial y}(v_x)\right]=-\frac{\partial}{\partial x}(p_{dyn})+\mu_o\left[\frac{\partial^2}{\partial x^2}(v_x)+\frac{\partial^2}{\partial y^2}(v_x)\right] \tag{24}$$

$$\rho_o\left[v_x\frac{\partial}{\partial x}(v_y)+v_y\frac{\partial}{\partial y}(v_y)\right]=-\frac{\partial}{\partial y}(p_{dyn})+\mu_o\left[\frac{\partial^2}{\partial x^2}(v_y)+\frac{\partial^2}{\partial y^2}(v_y)\right]+g\beta_o\rho_o(T-T_o) \tag{25}$$

$$\rho_o C_{p_o}\left[v_x\frac{\partial T}{\partial x}+v_y\frac{\partial T}{\partial y}\right]=k_o\left[\frac{\partial^2 T}{\partial x^2}+\frac{\partial^2 T}{\partial y^2}\right] \tag{26}$$

where the gravity vector direction is opposed to the Y axis, as shown in Figs. 1 and 4. The natural convection driving mechanism, which is represented by the last term on the right hand side of Eq. 25, results from the interaction of

the hydrostatic pressure gradient and the body force term [30-33]. Thus, the pressure in Eqs. 24 and 25 is the dynamic pressure (local pressure minus the hydrostatic pressure).

Dimensionless variables and characteristic groups are introduced to reduce the number of parameters that need to be specified in the numerical experiments. Let

$$\theta=\frac{T-T_c}{T_h-T_c} \tag{27}$$

$$X=\frac{x}{L_c} \tag{28}$$

$$Y=\frac{y}{L_c} \tag{29}$$

$$V_x=\rho_o C_{po} L_c v_x/k_o \tag{30}$$

$$V_y=\rho_o C_{po} L_c v_y/k_o \tag{31}$$

$$P_{dyn}=p_{dyn}\rho_o C_{po}^2 L_c^2/k_o^2 \tag{32}$$

$$Ra=g\beta_o\rho_o^2 L_c^3(T_h-T_c)C_{po}/\mu_o k_o \tag{33}$$

and

$$Pr=\mu_o C_{po}/k_o \tag{34}$$

where Ra represents the Rayleigh number, Pr represents the

Prandtl number and L_c, the characteristic length, is equal to the length of the cavity bottom wall. Using these dimensionless variables and groups, the mass, momentum and energy equations are transformed to

$$\frac{\partial}{\partial X}(V_x)+\frac{\partial}{\partial Y}(V_y)=0 \tag{35}$$

$$V_x\frac{\partial}{\partial X}(V_x)+V_y\frac{\partial}{\partial Y}(V_x)=-\frac{\partial}{\partial X}(P_{dyn})+Pr\left[\frac{\partial^2}{\partial X^2}(V_x)+\frac{\partial^2}{\partial Y^2}(V_x)\right] \tag{36}$$

$$V_x\frac{\partial}{\partial X}(V_y)+V_y\frac{\partial}{\partial Y}(V_y)=-\frac{\partial}{\partial Y}(P_{dyn})+Pr\left[\frac{\partial^2}{\partial X^2}(V_y)+\frac{\partial^2}{\partial Y^2}(V_y)\right]$$

$$+RaPr(\theta-\theta_o) \tag{37}$$

and

$$V_x\frac{\partial\theta}{\partial X}+V_y\frac{\partial\theta}{\partial Y}=\frac{\partial^2\theta}{\partial X^2}+\frac{\partial^2\theta}{\partial Y^2} \tag{38}$$

At this point, let us introduce the stream function and vorticity variables. The stream function is defined in such a way as to satisfy the mass conservation equation. Thus, the stream function definition is

$$V_x=\frac{\partial\psi}{\partial Y} \tag{39}$$

and

$$V_y = -\frac{\partial \psi}{\partial X} \tag{40}$$

The vorticity represents the amount of anticlockwise rotation that the fluid possesses. It is obtained mathematically as the curl of the velocity vector, i.e.

$$\bar{\Omega} = \left[\frac{\partial}{\partial X}(V_y) - \frac{\partial}{\partial Y}(V_x)\right]\bar{e}_z \tag{41}$$

The vorticity is a vector by definition. However, because the vector orientation in a two-dimensional Cartesian situation is everywhere the same (perpendicular to the two-dimensional Cartesian plane), the vorticity can be considered as a scalar variable. Thus, we can write that

$$\Omega = \frac{\partial}{\partial X}(V_y) - \frac{\partial}{\partial Y}(V_x) \tag{42}$$

When the stream function definition (Eqs. 39 and 40) is introduced into the above equation, the final vorticity definition becomes

$$\Omega = -\left[\frac{\partial^2 \psi}{\partial X^2} + \frac{\partial^2 \psi}{\partial Y^2}\right] \tag{43}$$

The two momentum equations can be linked together to cancel the pressure terms by subtracting the X momentum equation differentiated with respect to Y from the Y momentum equation differentiated with respect to X. Using the vorticity definition (Eq. 42), the momentum equations

then reduce to

$$\frac{\partial}{\partial X}(V_x \Omega)+\frac{\partial}{\partial Y}(V_y \Omega)=Pr\left[\frac{\partial^2 \Omega}{\partial X^2}+\frac{\partial^2 \Omega}{\partial Y^2}\right]+RaPr\frac{\partial \theta}{\partial X} \qquad (44)$$

The velocity components that appear in Eq. 44 (and also in the temperature Eq. 38) can be rewritten in term of stream function but are retained because their presence simplifies the discretization process (see Chapter V). The set of semitransformed equations (Eqs. 43, 44 and 38) are called the stream function, vorticity and temperature equations, respectively.

C. CONSERVATION EQUATIONS IN A GENERAL ORTHOGONAL SYSTEM

The conservation equations written for a Cartesian system cannot be directly applied to a general two-dimensional orthogonal system because the domain is locally stretched or shrunk. This fact must be taken into account when deriving alternate forms of the conservation equations for general orthogonal coordinates.

To derive these alternate forms, the following two steps were used:

1. the Cartesian conservation equations were first rewritten in forms which are independent of the coordinate system chosen by using the Cartesian gradient, divergence, curl and Laplacian operators, and then
2. the same vector operators defined for a general

orthogonal system were simply substituted into the coordinate-free conservation equations.

The definitions of the gradient, divergence, curl and Laplacian operators in a general orthogonal system can be found in many standard textbooks [41,45-47] and, in order, are

$$\nabla\phi=\frac{1}{H_{z1}}\frac{\partial\phi}{\partial Z1}\bar{e}_{z1}+\frac{1}{H_{z2}}\frac{\partial\phi}{\partial Z2}\bar{e}_{z2} \tag{45}$$

$$\nabla\cdot\bar{a}=\frac{1}{H_{z1}H_{z2}}\left[\frac{\partial}{\partial Z1}(H_{z2}a_{z1})+\frac{\partial}{\partial Z2}(H_{z1}a_{z2})\right] \tag{46}$$

$$\nabla\times\bar{a}=\frac{1}{H_{z1}H_{z2}}\left[\frac{\partial}{\partial Z1}(H_{z2}a_{z2})-\frac{\partial}{\partial Z2}(H_{z1}a_{z1})\right]\bar{e}_{z3} \tag{47}$$

and

$$\nabla^2\phi=\frac{1}{H_{z1}H_{z2}}\left[\frac{\partial}{\partial Z1}\left[\frac{H_{z2}}{H_{z1}}\frac{\partial\phi}{\partial Z1}\right]+\frac{\partial}{\partial Z2}\left[\frac{H_{z1}}{H_{z2}}\frac{\partial\phi}{\partial Z2}\right]\right] \tag{48}$$

The operator definitions for a Cartesian system can be obtained from the above equations by substituting unity scale factors.

Let us first rewrite the mass conservation equation in a general orthogonal system in order to derive the appropriate definition of the stream function. Using the Cartesian and orthogonal operator definitions, the mass conservation Eq. 35 can be rewritten in the general orthogonal system as

$$\frac{1}{H_\xi H_\eta}\left[\frac{\partial}{\partial \xi}(H_\eta V_\xi)+\frac{\partial}{\partial \eta}(H_\xi V_\eta)\right]=0 \qquad (49)$$

By definition, the stream function must satisfy the mass conservation equation. Therefore, in the general orthogonal system, the stream function is defined by

$$H_\eta V_\xi=\frac{\partial \psi}{\partial \eta} \qquad (50)$$

and

$$H_\xi V_\eta=-\frac{\partial \psi}{\partial \xi} \qquad (51)$$

The vorticity, which is defined as the curl of the velocity vector, becomes in the general orthogonal system

$$\vec{\Omega}=\frac{1}{H_\xi H_\eta}\left[\frac{\partial}{\partial \xi}(H_\eta V_\eta)-\frac{\partial}{\partial \eta}(H_\xi V_\xi)\right]\vec{e}_z \qquad (52)$$

Because the coordinate system is two-dimensional, the vorticity can once again be considered as a scalar variable for reasons similar to those discussed for the Cartesian system. Therefore, Eq. 52 can be written as

$$\Omega=\frac{1}{H_\xi H_\eta}\left[\frac{\partial}{\partial \xi}(H_\eta V_\eta)-\frac{\partial}{\partial \eta}(H_\xi V_\xi)\right] \qquad (53)$$

When the stream function definition for an orthogonal system is introduced into the above equation, the vorticity

definition becomes

$$\Omega=-\frac{1}{H_\xi H_\eta}\left[\frac{\partial}{\partial\xi}\left[\frac{H_\eta\partial\psi}{H_\xi\partial\xi}\right]+\left[\frac{\partial}{\partial\eta}\left[\frac{H_\xi\partial\psi}{H_\eta\partial\eta}\right]\right]\right] \tag{54}$$

This equation is the stream function equation in general orthogonal coordinates.

To derive the appropriate form of the vorticity equation (Eq. 44) in the general orthogonal system, the Cartesian and general orthogonal operator definitions are required along with the relation

$$\frac{\partial\phi}{\partial X}=\frac{1}{H_{z1}H_{z2}}\left[\frac{\partial Y}{\partial Z2}\frac{\partial\phi}{\partial Z1}-\frac{\partial Y}{\partial Z1}\frac{\partial\phi}{\partial Z2}\right] \tag{55}$$

which can be found in the literature [43]. In Eq. 55, X is a Cartesian coordinate and Z1 and Z2 are general orthogonal coordinates. After some manipulation, the vorticity equation in general orthogonal coordinates is found to be

$$\frac{1}{H_\xi H_\eta}\left[\frac{\partial}{\partial\xi}(H_\eta V_\xi\Omega)+\frac{\partial}{\partial\eta}(H_\xi V_\eta\Omega)\right]=\frac{Pr}{H_\xi H_\eta}\left[\frac{\partial}{\partial\xi}\left[\frac{H_\eta\partial\Omega}{H_\xi\partial\xi}\right]+\frac{\partial}{\partial\eta}\left[\frac{H_\xi\partial\Omega}{H_\eta\partial\eta}\right]\right]+\frac{RaPr}{H_\xi H_\eta}\left[\frac{\partial Y\partial\theta}{\partial\eta\partial\xi}-\frac{\partial Y\partial\theta}{\partial\xi\partial\eta}\right] \tag{56}$$

Similarly, the temperature equation (Eq. 38), whose transformation also requires the use of the Cartesian and general orthogonal operators, becomes

$$\frac{1}{H_\xi H_\eta}\left[\frac{\partial}{\partial \xi}(H_\eta V_\xi \theta)+\frac{\partial}{\partial \eta}(H_\xi V_\eta \theta)\right]=\frac{1}{H_\xi H_\eta}\left[\frac{\partial}{\partial \xi}\left[\frac{H_\eta \partial \theta}{H_\xi \partial \xi}\right]+\frac{\partial}{\partial \eta}\left[\frac{H_\xi \partial \theta}{H_\eta \partial \eta}\right]\right] \tag{57}$$

The velocity components V_ξ and V_η can be rewritten in terms of the stream function but are allowed to remain in Eqs. 56 and 57 to simplify the discretization procedure described in Chapter V.

In summary, the mass, momentum and energy conservation equations for a two-dimensional orthogonal system are given by Eqs. 54, 56 and 57, respectively.

D. BOUNDARY CONDITIONS OF THE CONSERVATION EQUATIONS

The four types of boundary conditions needed to complete the specification of the natural convection problem are:

1. the four walls of the cavity are impermeable (i.e. the normal component of the fluid velocity at the wall is zero),
2. the top and bottom walls of the cavity are adiabatic,
3. the left and right walls of the cavity are isothermal, and
4. the no-slip condition applies at all four bounding surfaces (i.e. the tangential component of fluid velocity is zero).

It is now necessary to translate the above boundary conditions, which are given in terms of primitive variables, to their equivalent forms written for stream function, vorticity and temperature variables.

The first boundary condition is satisfied by specifying a constant stream function value along the domain boundary. By convention, this value is arbitrarily assigned as zero. Thus, the first boundary condition is given by

$$\psi_{db}=0 \tag{58}$$

The second boundary condition specifies a null heat flux throught the top and bottom walls. This can be written as

$$\left.\frac{\partial\theta}{\partial\eta}\right|_{\eta=1}=0 \tag{59}$$

and

$$\left.\frac{\partial\theta}{\partial\eta}\right|_{\eta=N}=0 \tag{60}$$

where η=1 and η=N correspond to the bottom and top walls, respectively.

The isothermal wall boundary conditions are given by assigning the dimensionless temperature at the wall to

$$\theta\Big|_{\xi=1} = 0 \tag{61}$$

and

$$\theta\Big|_{\xi=M} = 1 \tag{62}$$

where $\xi=1$ and $\xi=M$ correspond to the left and right walls, respectively.

The no-slip boundary condition is satisfied by specifying a zero stream function derivative in the direction normal to each wall. Because the first three boundary conditions have already been used to specify the stream function and temperature variations along the domain boundary, the fourth condition is used to derive the vorticity boundary condition. Many different representations of the vorticity boundary condition which satisfy the no-slip criterion can be found in the literature [12,38,40,43,44]. Each is derived somewhat differently and each describes the no-slip condition with differing degrees of accuracy. The Wood and the second order vorticity boundary conditions are considered in this work because they are expected to be the most accurate [12]. Derivations of these two forms of the vorticity boundary condition can be found for the two-dimensional Cartesian system [12,38,40,43,44] and the general two-dimensional conformal orthogonal system [24]. However, these vorticity boundary conditions have never been derived for the case of

the general two-dimensional non-conformal orthogonal system used in the present study. Such a derivation is presented in the chapter on discretization which follows.

V. FINITE DIFFERENCE DISCRETIZATION

Sets of simultaneous partial differential equations along with their attendant boundary conditions are very difficult to solve analytically even under the simplest of circumstances. Because of the non-linearity of the vorticity and temperature equations and because of the strong linkage between all three conservation equations, an analytical solution to the present set is not possible. Thus it becomes necessary to resort to approximate numerical techniques. The most common numerical methods used for solving sets of elliptic partial differential equations are finite difference, finite element and collocation methods.

In the finite difference method chosen for the present study, the idea of obtaining a continuous solution over the whole of the physical domain is abandoned for one of determining approximate values of the dependent variables at discrete positions within and on the boundaries of the domain. These discrete positions are not randomly scattered, but are specified by, in the present case, an orthogonal grid which covers the domain in a fairly homogeneous fashion. At each grid point or node, the differential equation is substituted by a corresponding algebraic equation obtained by somewhat compromisingly replacing the exact differentials by finite difference analogues. This procedure leads to a set of simultaneous algebraic equations in which each nodal value is linked to those of its neighbouring nodes. The set is then solved using standard

sparse matrix techniques.

The finite difference form of any partial differential equation can be derived using either Taylor series expansions or the control volume approach [39]. In the latter discretization technique, the partial differential equation is integrated over the finite control volume which surrounds each nodal point. The control volume approach has several distinct advantages over the Taylor series method:

1. it is easy to understand and lends itself to direct physical interpretation,
2. it ensures that the conservation of each dependent variable is maintained over every control volume and hence globally over the whole domain, and
3. it allows the use of far more realistic dependent variable profiles between nodal points.

In the present work, the control volume approach is used to discretize all of the partial differential equations. However, on a few occasions, Taylor series expansions are used to approximate first order derivatives in some boundary conditions. Equations 63 to 65 list three first order derivative approximations of second order accuracy obtained using series expansions. They are referred to as the forward, central and backward finite difference approximations, respectively, and are written as

$$\left.\frac{d\phi}{dZ1}\right|_{Z1=Z1_o} \simeq \left[-3\phi\Big|_{Z1=Z1_o} + 4\phi\Big|_{Z1=Z1_o+\Delta Z1} - \phi\Big|_{Z1=Z1_o+2\Delta Z1}\right]/(2\Delta Z1) \quad (63)$$

$$\left.\frac{d\phi}{dZ1}\right|_{Z1=Z1_o+\Delta Z1} \simeq \left[\phi\Big|_{Z1=Z1_o+2\Delta Z1} - \phi\Big|_{Z1=Z1_o}\right]/(2\Delta Z1) \quad (64)$$

and

$$\left.\frac{d\phi}{dZ1}\right|_{Z1=Z1_o+2\Delta Z1} \simeq \left[3\phi\Big|_{Z1=Z1_o+2\Delta Z1} - 4\phi\Big|_{Z1=Z1_o+\Delta Z1} + \phi\Big|_{Z1=Z1_o}\right]/(2\Delta Z1) \quad (65)$$

A. DISCRETIZATION OF THE GRID GENERATION EQUATIONS

The mapping equations (Eqs. 13 and 14) must be transformed into a set of algebraic equations in order to generate the body-fitted orthogonal grid. A grid which is uniform in the two general orthogonal coordinate directions (i.e. $\Delta\xi=\Delta\eta=1$) is used in to specify the positions of the discrete values in the transformed domain. The grid is represented in Fig. 8 by the solid lines; the dashed lines delimit the control volumes associated with each discrete value. The discrete values in this case are the Cartesian coordinates from which the scale factors, the shape factors and various first order derivatives of Cartesian coordinates with respect to the orthogonal coordinates can be derived.

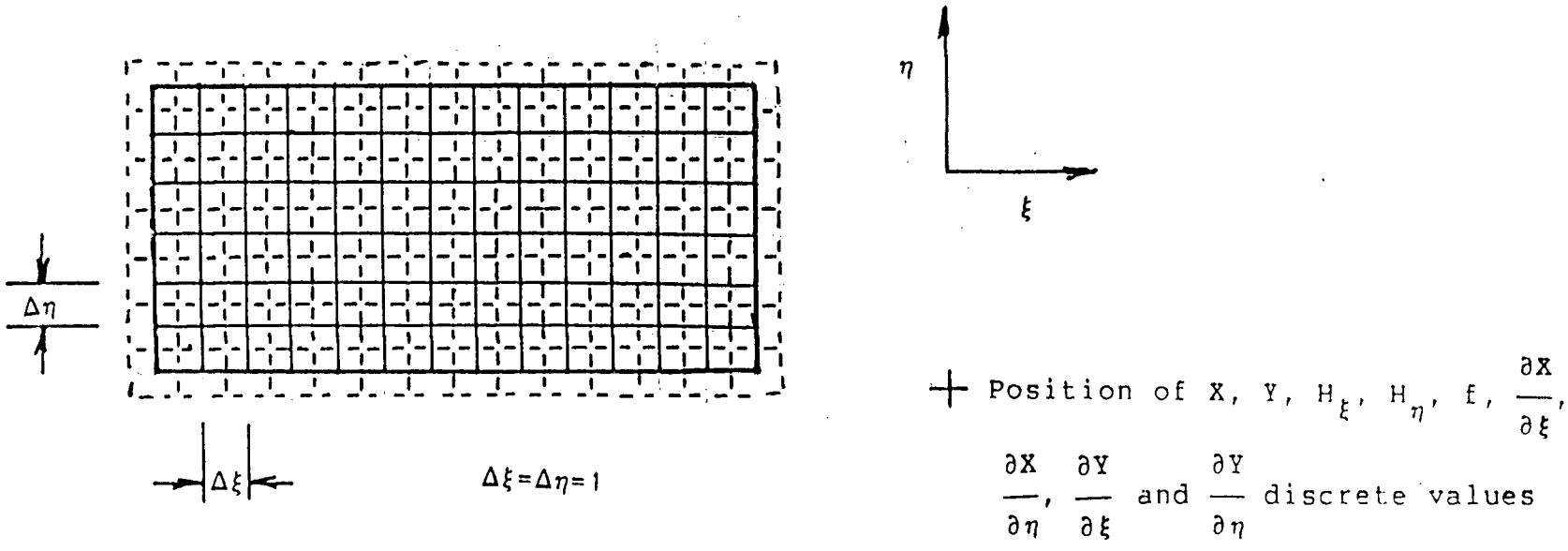

Figure 8. Uniform grid in the transformed domain used to discretize the differential equations of governing the body-fitted orthogonal coordinate transformation.

The algebraic form of the body-fitted orthogonal mapping equation involving X is obtained by integrating Eq. 13 over a general control volume (Fig. 9). Thus, after integrating, Eq. 13 becomes

$$\int_{\xi_o}^{\xi_o+\Delta\xi}\int_{\eta_o}^{\eta_o+\Delta\eta}\frac{1}{H_\xi H_\eta}\left[\left[\frac{\partial}{\partial\xi}\left[f\frac{\partial X}{\partial\xi}\right]+\frac{\partial}{\partial\eta}\left[\frac{1}{f}\frac{\partial X}{\partial\eta}\right]\right]\right]H_\xi H_\eta d\xi d\eta=0 \qquad (66)$$

The product of scale factors appears in Eq. 66 because the Jacobian must be accounted for when integrating in general orthogonal coordinates. Equation 66 can be partially integrated to give

$$\int_{\eta_o}^{\eta_o+\Delta\eta}\left[f\frac{\partial X}{\partial\xi}\bigg|_{\xi_o+\Delta\xi}-f\frac{\partial X}{\partial\xi}\bigg|_{\xi_o}\right]d\eta + \int_{\xi_o}^{\xi_o+\Delta\xi}\left[\frac{1}{f}\frac{\partial X}{\partial\eta}\bigg|_{\eta_o+\Delta\eta}-\frac{1}{f}\frac{\partial X}{\partial\eta}\bigg|_{\eta_o}\right]d\xi=0 \qquad (67)$$

At this stage, assumptions are required in order to continue. Let us assume that the normal derivative and the shape factor at a control volume face are constant over the entire face and are evaluated by assuming a linear profile between the pair of nodal points involved [39]. Using these assumptions, it can be easily shown that the above equation reduces to the following algebraic equation

$$aX=a_{i+1}X_{i+1}+a_{i-1}X_{i-1}+a_{j+1}X_{j+1}+a_{j-1}X_{j-1} \qquad (68)$$

where

Figure 9. General control volume for the Cartesian coordinate discrete values.

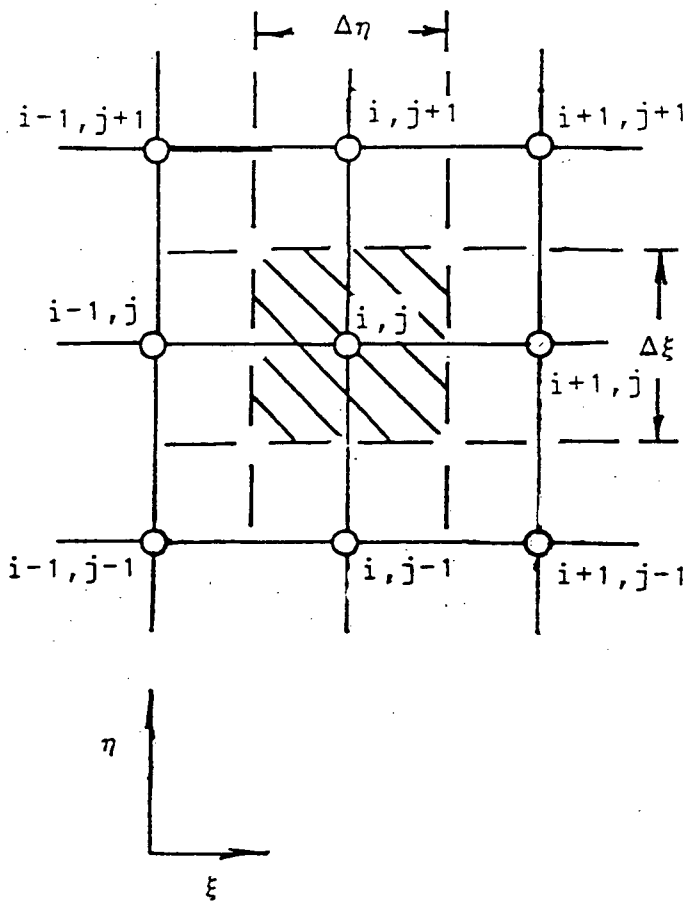

○ Position of X, Y, H_ξ, H_η, f, $\frac{\partial X}{\partial \xi}$, $\frac{\partial X}{\partial \eta}$, $\frac{\partial Y}{\partial \xi}$ and $\frac{\partial Y}{\partial \eta}$ discrete values

$$a=a_{i+1}+a_{i-1}+a_{j+1}+a_{j-1} \tag{69}$$

$$a_{i+1}=(f+f_{i+1})/2 \tag{70}$$

$$a_{i-1}=(f+f_{i-1})/2 \tag{71}$$

$$a_{j+1}=2/(f+f_{j+1}) \tag{72}$$

and

$$a_{j-1}=2/(f+f_{j-1}) \tag{73}$$

In the above equations, the missing indices are understood to be i and j. This nomenclature is used throughout the rest of this work.

Because the mapping equation for Y (Eq. 14) is similar to the one for X and because both X and Y share the same control volume, the derivation of the algebraic analogue of the mapping equation for Y can be deduced from Eq. 68. Thus, the algebraic equation which defines the body-fitted orthogonal mapping for Y is given by

$$aY=a_{i+1}Y_{i+1}+a_{i-1}Y_{i-1}+a_{j+1}Y_{j+1}+a_{j-1}Y_{j-1} \tag{74}$$

where the coefficients are again given by Eqs. 69 to 73.

Equations 68 and 74 define a set of algebraic equations for X and Y which apply at all of the interior nodes of the

transformed domain. Once this set of equations along with the discretized forms of the boundary conditions have been solved, the scale factors are obtained by using second order accurate forward, backward or central differences to represent the first derivatives of the Cartesian coordinates with respect to the orthogonal coordinates which appear in Eqs. 16 and 17.

B. DISCRETIZATION OF THE GRID BOUNDARY CONDITIONS

The application of the Dirichlet boundary conditions of the grid generating equations is straight-forward; the boundary nodes are simply assigned to the appropriate value of X or Y. Two modified Neumann boundary conditions (Eqs. 75 and 76) have been found to give better results than the two original Neumann boundary conditions (Eqs. 21 and 22). These new conditions are derived from the old ones and are given by

$$\frac{\partial X}{\partial \eta} = -\frac{\partial Y \partial Y}{\partial X \partial \eta} \tag{75}$$

and

$$\frac{\partial Y}{\partial \xi} = \frac{\partial X \partial X}{\partial Y \partial \xi} \tag{76}$$

These modified Neumann boundary conditions yield improved numerical accuracy because they require the finite difference approximation of only two quantities: the X and Y

derivatives with respect to either ξ or η. The derivative of X with respect to Y or the derivative of Y with respect to X can be determined exactly from the analytical functions which define the physical domain boundary. However, the original Neumann boundary conditions involve the approximate evaluation of three quantities: the X and Y derivatives with respect to either ξ or η and the shape factor (see Eqs. 15, 16 and 17). The algebraic form of the modified Neumann conditions are obtained by using finite difference approximations of second order.

C. DISCRETIZATION OF THE NATURAL CONVECTION EQUATIONS

In order to solve the natural convection problem, the stream function, the vorticity and the temperature equations also have to be discretized. The scale factors, shape factors and various Cartesian coordinate derivatives required in these equations must be available from the numerical solution of the mapping equations. A staggered grid is used to specify the positions of the discrete values as shown in Fig. 10. The intersections of the dashed line grid determine the positions of the vorticity and temperature nodes; the solid line grid delimits the vorticity and temperature control volumes. The fictitious discrete temperature and vorticity nodes outside the transformed domain are used to specify the boundary conditions. The intersections of the solid grid correspond to the stream function nodes and indicate the positions

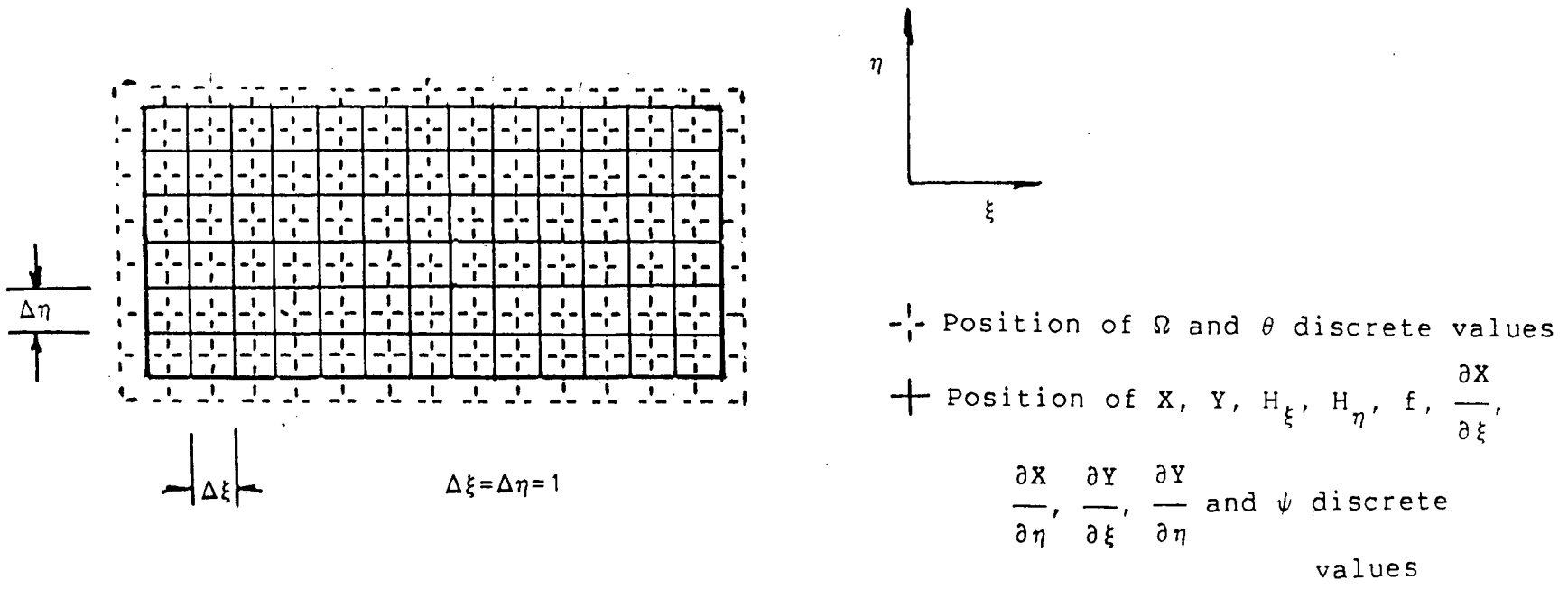

Figure 10. Staggered grid system used to discretize the natural convection conservation equations.

where the scale factors, shape factors and Cartesian coordinate derivatives are known from the converged numerical solution of the mapping equations. The stream function control volumes are delimited by the dashed grid. Both the solid and dashed grids are uniformly spaced in the two transformed coordinate directions (i.e. $\Delta\xi=\Delta\eta=1$). Of course, there is no loss of generality by using a uniform grid in the transformed coordinate system; the non-uniformities in the physical domain are accounted for in the transformation. Several advantages of staggered grids of the type shown in Fig. 10 over standard grids in which all three dependent variables are located at the same nodal positions have been claimed [12,39]. These advantages include:

1. the fluid flow across any vorticity or temperature control volume face is given exactly by the difference in discrete stream function values at the corresponding corners,
2. the use of fictitious vorticity and temperature nodes outside the solution domain allows more accurate specification of derivative boundary conditions (all vorticity and half of the temperature boundary conditions involve normal derivatives; the stream function is constant at the boundaries) and
3. there are no half or quarter control volumes for vorticity or temperature at the boundaries,

across which both energy and momentum may be transferred.

1. STREAM FUNCTION EQUATION

The algebraic form of the stream function equation (Eq. 54) can be deduced from the discretized version of the mapping equation for X because they both share the same control volume (Fig. 11) and have similar differential equations. In fact, the stream function differential equation has one additional term, the vorticity, which acts as a source term. If it is assumed that the vorticity and the scale factors are constant over a stream function control volume, this source term can be approximated by

$$b=\int_{\xi_o}^{\xi_o+\Delta\xi}\int_{\eta_o}^{\eta_o+\Delta\eta}(H_\xi H_\eta)\Omega d\xi d\eta$$

$$=H_\xi H_\eta(\Omega+\Omega_{i+1}+\Omega_{j+1}+\Omega_{i+1,j+1})/4 \qquad (77)$$

Thus, the discretized stream function equation can be written as

$$a\psi=a_{i+1}\psi_{i+1}+a_{i-1}\psi_{i-1}+a_{j+1}\psi_{j+1}+a_{j-1}\psi_{j-1}+b \qquad (78)$$

where the coefficients are once again given by Eqs. 69 to 73 and the coefficient b is defined by Eq. 77.

Figure 11. General control volume for discrete stream function values.

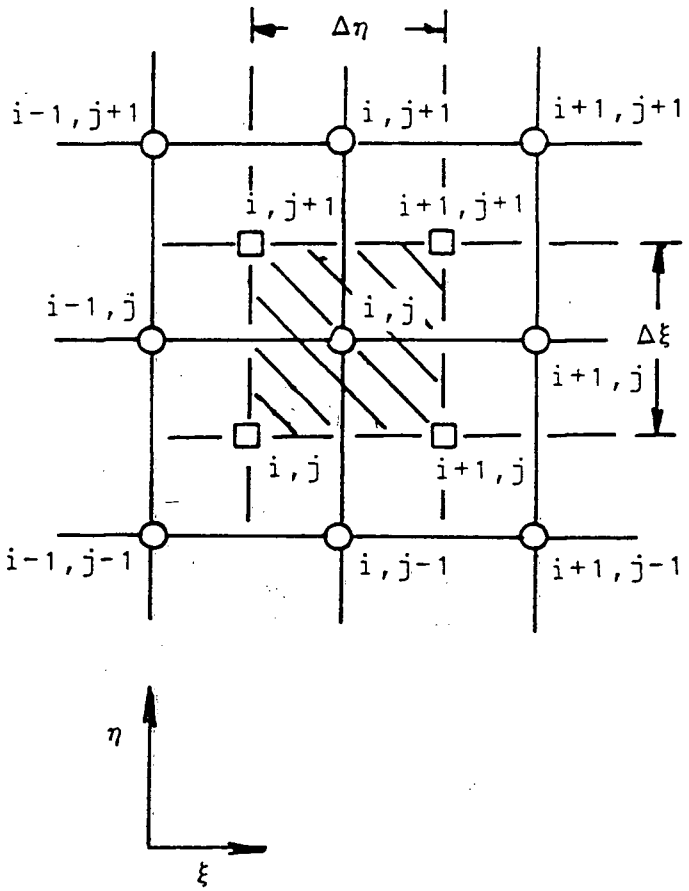

○ Position of X, Y, H_ξ, H_η, f, $\frac{\partial X}{\partial \xi}$, $\frac{\partial X}{\partial \eta}$, $\frac{\partial Y}{\partial \xi}$, $\frac{\partial Y}{\partial \eta}$ and ψ discrete values

□ Position of Ω and θ discrete values

2. VORTICITY EQUATION

First, the vorticity equation (Eq. 56) is integrated over the general vorticity control volume shown in Fig. 12 to obtain

$$\int_{\xi_o}^{\xi_o+\Delta\xi}\int_{\eta_o}^{\eta_o+\Delta\eta}\left[\frac{1}{H_\xi H_\eta}\left[\frac{\partial}{\partial\xi}(H_\eta V_\xi \Omega)+\frac{\partial}{\partial\eta}(H_\xi V_\eta \Omega)\right]\right.$$
$$-\frac{Pr}{H_\xi H_\eta}\left[\frac{\partial}{\partial\xi}\left[\frac{H_\eta}{H_\xi}\frac{\partial\Omega}{\partial\xi}\right]+\frac{\partial}{\partial\eta}\left[\frac{H_\xi}{H_\eta}\frac{\partial\Omega}{\partial\eta}\right]\right]$$
$$\left.-\frac{RaPr}{H_\xi H_\eta}\left[\frac{\partial Y}{\partial\eta}\frac{\partial\theta}{\partial\xi}-\frac{\partial Y}{\partial\xi}\frac{\partial\theta}{\partial\eta}\right]\right]H_\xi H_\eta\, d\xi\, d\eta=0 \qquad (79)$$

After a partial analytical integration, the above equation becomes

$$\int_{\eta_o}^{\eta_o+\Delta\eta}\left[\left[(H_\eta V_\xi\Omega)-Pr\frac{H_\eta}{H_\xi}\frac{\partial\Omega}{\partial\xi}\right]\Bigg|_{\xi_o+\Delta\xi}-\left[(H_\eta V_\xi\Omega)-Pr\frac{H_\eta}{H_\xi}\frac{\partial\Omega}{\partial\xi}\right]\Bigg|_{\xi_o}\right]d\eta$$
$$+\int_{\xi_o}^{\xi_o+\Delta\xi}\left[\left[(H_\xi V_\eta\Omega)-Pr\frac{H_\xi}{H_\eta}\frac{\partial\Omega}{\partial\eta}\right]\Bigg|_{\eta_o+\Delta\eta}-\left[(H_\xi V_\eta\Omega)-Pr\frac{H_\xi}{H_\eta}\frac{\partial\Omega}{\partial\eta}\right]\Bigg|_{\eta_o}\right]d\xi$$

$$-\int_{\xi_o}^{\xi_o+\Delta\xi}\int_{\eta_o}^{\eta_o+\Delta\eta}RaPr\left[\frac{\partial Y}{\partial\eta}\frac{\partial\theta}{\partial\xi}-\frac{\partial Y}{\partial\xi}\frac{\partial\theta}{\partial\eta}\right]d\xi\, d\eta=0 \qquad (80)$$

At this point, assumptions are required in order to continue. Thus, the vorticity and its normal derivative at a control volume face are assumed to be constant over the entire surface. It is not recommended that a linear profile of the vorticity between its discrete nodal values be used because it leads to a differencing scheme which is only

Figure 12. General control volume for either vorticity or temperature discrete values.

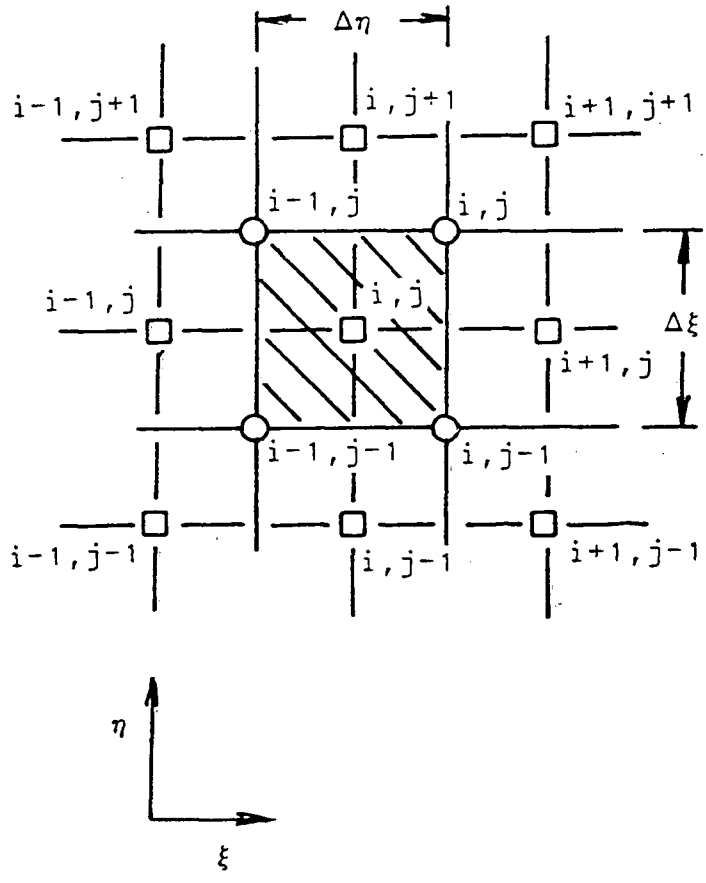

□ Position of Ω and θ discrete values

○ Position of X, Y, H_ξ, H_η, f, $\frac{\partial X}{\partial \xi}$, $\frac{\partial X}{\partial \eta}$, $\frac{\partial Y}{\partial \xi}$, $\frac{\partial Y}{\partial \eta}$ and ψ discrete values

conditionally stable [38-40]. Thus, to determine the values of the vorticity and its derivative at a control volume face, an exponential scheme [39] is employed. The exponential scheme uses as a profile between two neighbouring nodal points the analytical solution of a one-dimensional pure convection-diffusion problem. This problem can be written in a general form as

$$\frac{1}{H_{z1}H_{z2}}\frac{\partial}{\partial Z1}(H_{z2}V_{z1}\phi)=\frac{\Gamma}{H_{z1}H_{z2}}\frac{\partial}{\partial Z1}\left[\frac{H_{z2}\partial\phi}{H_{z1}\partial Z1}\right] \tag{81}$$

subject to

$$\phi\Big|_{Z1=0}=\phi_1 \tag{82}$$

$$\phi\Big|_{Z1=L}=\phi_2 \tag{83}$$

where ϕ is a general dependent variable and Γ is a general diffusion coefficient. If the distance between the discrete values, L, is small, then H_{z1}, H_{z2} and V_{z1} can be taken outside the differentials and assigned values of $H_{z1,ave}$, $H_{z2,ave}$ and $V_{z1,ave}$, respectively. Thus, the above equation is reduced to

$$H_{z2,ave}V_{z1,ave}\frac{\partial\phi}{\partial Z1}=\Gamma\frac{H_{z2,ave}}{H_{z1,ave}}\frac{\partial^2\phi}{\partial Z1^2} \tag{84}$$

or

$$a\frac{\partial \phi}{\partial Z1}=b\frac{\partial^2 \phi}{\partial Z1^2} \tag{85}$$

where

$$a=H_{z2,ave}V_{z1,ave} \tag{86}$$

and

$$b=\Gamma\frac{H_{z2,ave}}{H_{z1,ave}} \tag{87}$$

The profile of the general dependent variable, ϕ, in the interval between Z1=0 and Z1=L is obtained by solving the above differential equation with its boundary conditions (Eqs. 82 and 83). This profile is found to be

$$\phi=(\phi_2-\phi_1)\frac{\exp(PeZ1/L)-1}{\exp(Pe)-1}+\phi_1 \tag{88}$$

where

$$Pe=\frac{aL}{b} \tag{89}$$

is the local Peclet number which represents the ratio of the relative strengths of convection and diffusion in the direction Z1.

Using Eq. 88 together with Eq. 89, both the vorticity and its derivative can now be evaluated at each control volume face over which they are assumed to be constant.

Also, the scale factors are assumed to be constant between the discrete nodal values of Ω and over their common control volume face. The scale factors are evaluated by assuming a linear profile between their nodal values. Finally, the vorticity source term (the last term on the right hand side of Eq. 80) is assumed to be constant throughout the vorticity control volume and the values of the derivative of Y with respect to η and the derivative of X with respect to ξ are evaluated as a mathematical average. Using the above assumptions, it can be shown that the discretized form of Eq. 80 becomes

$$a\Omega = a_{i+1}\Omega_{i+1} + a_{i-1}\Omega_{i-1} + a_{j+1}\Omega_{j+1} + a_{j-1}\Omega_{j-1} + b \tag{90}$$

where

$$a = a_{i+1} + a_{i-1} + a_{j+1} + a_{j-1} \tag{91}$$

$$a_{i+1} = \frac{(\psi - \psi_{j-1})}{\exp(Pe_e) - 1} \tag{92}$$

$$a_{i-1} = \frac{(\psi_{i-1} - \psi_{i-1,j-1})\exp(Pe_w)}{\exp(Pe_w) - 1} \tag{93}$$

$$a_{j+1} = \frac{(\psi_{i-1} - \psi)}{\exp(Pe_n) - 1} \tag{94}$$

$$a_{j-1} = \frac{(\psi_{i-1,j-1} - \psi_{j-1})\exp(Pe_s)}{\exp(Pe_s) - 1} \tag{95}$$

$$Pe_e=\frac{\psi-\psi_{j-1}}{\Gamma}\left[\frac{H_\xi}{H_\eta}\right] \tag{96}$$

$$Pe_w=\frac{\psi_{i-1}-\psi_{i-1,j-1}}{\Gamma}\left[\frac{H_\xi}{H_\eta}\right] \tag{97}$$

$$Pe_n=\frac{\psi_{i-1}-\psi}{\Gamma}\left[\frac{H_\eta}{H_\xi}\right] \tag{98}$$

$$Pe_s=\frac{\psi_{i-1,j-1}-\psi_{j-1}}{\Gamma}\left[\frac{H_\eta}{H_\xi}\right] \tag{99}$$

$$b=RaPr\left[b_1\frac{\partial\theta}{\partial\xi}-b_2\frac{\partial\theta}{\partial\eta}\right] \tag{100}$$

$$b_1=\left[\left.\frac{\partial Y}{\partial\eta}+\frac{\partial Y}{\partial\eta}\right|_{\xi=i-1}+\left.\frac{\partial Y}{\partial\eta}\right|_{\eta=j-1}+\left.\frac{\partial Y}{\partial\eta}\right|_{\xi=i-1,\eta=j-1}\right]/4 \tag{101}$$

and

$$b_2=\left[\left.\frac{\partial Y}{\partial\xi}+\frac{\partial Y}{\partial\xi}\right|_{\xi=i-1}+\left.\frac{\partial Y}{\partial\xi}\right|_{\eta=j-1}+\left.\frac{\partial Y}{\partial\xi}\right|_{\xi=i-1,\eta=j-1}\right]/4 \tag{102}$$

where $\Gamma=Pr$. A central finite difference representation of second order is used to approximate the temperature derivatives which are present in Eq. 100.

The advantages of the exponential differencing scheme are that it more realistically accounts for the competing roles played by convection and diffusion in determining dependent variable profiles between nodes and that it has been shown to be unconditionally stable. Furthermore, as should be expected, the exponential formula reduces to a central difference equation when Pe approach zero (i.e. diffusion dominates convection) and an upwind or downwind

difference equation when Pe has either a large positive or large negative value (i.e. convection dominates diffusion).

3. TEMPERATURE EQUATION

Because the temperature equation (Eq. 57) has the same form as the vorticity equation (recognizable convection and diffusion terms, but no source terms in this case) and because they share the same control volume, the discretized form of the temperature equation can be deduced from the algebraic vorticity equation. Thus, the finite difference version of the temperature equation is given by

$$a\theta = a_{i+1}\theta_{i+1} + a_{i-1}\theta_{i-1} + a_{j+1}\theta_{j+1} + a_{j-1}\theta_{j-1} \qquad (103)$$

where the coefficient definitions are given by Eqs. 91 to 97 and $\Gamma = 1$.

D. DISCRETIZATION OF THE NATURAL CONVECTION BOUNDARY CONDITIONS

The Dirichlet conditions for the stream function (Eq. 54) are specified simply by assigning the value of zero to the boundary stream function nodes. The algebraic forms of the temperature boundary conditions, Eqs. 59 to 62 are obtained by using second-order accurate Taylor series approximations for the former two and mathematical averages for the latter two.

For the vorticity boundary conditions, two separate representations, called the Wood and second order equations, will be tested. However since the form of these equations appropriate to general orthogonal coordinates does not presently exist, this extension must first be carried out. The position and notation for the vorticity, stream function and scale factor values involved in these derivations are shown in Fig. 13. All of the variables and their differentials are evaluated at the wall unless otherwise specified.

The no-slip boundary condition and the impermeable wall condition imply, respectively, that

$$\frac{\partial \psi}{\partial Zn}=0 \tag{104}$$

$$\psi=\frac{\partial \psi}{\partial Zt}=\frac{\partial^2 \psi}{\partial Zt^2}=\frac{\partial^3 \psi}{\partial Zt^3}=\ldots=0 \tag{105}$$

where Zn and Zt refer to the normal and tangential general orthogonal coordinates, respectively. Thus, in the vicinity of the wall, the stream function equation (Eq. 54) is reduced to

$$\frac{H_{zt}}{H_{zn}}\frac{\partial^2 \psi}{\partial Zn^2}+(H_{zn}H_{zt}\Omega)=0 \tag{106}$$

Because a Neumann vorticity boundary condition was found to give more accurate results than a Dirichlet vorticity boundary condition [12], let us differentiate the above

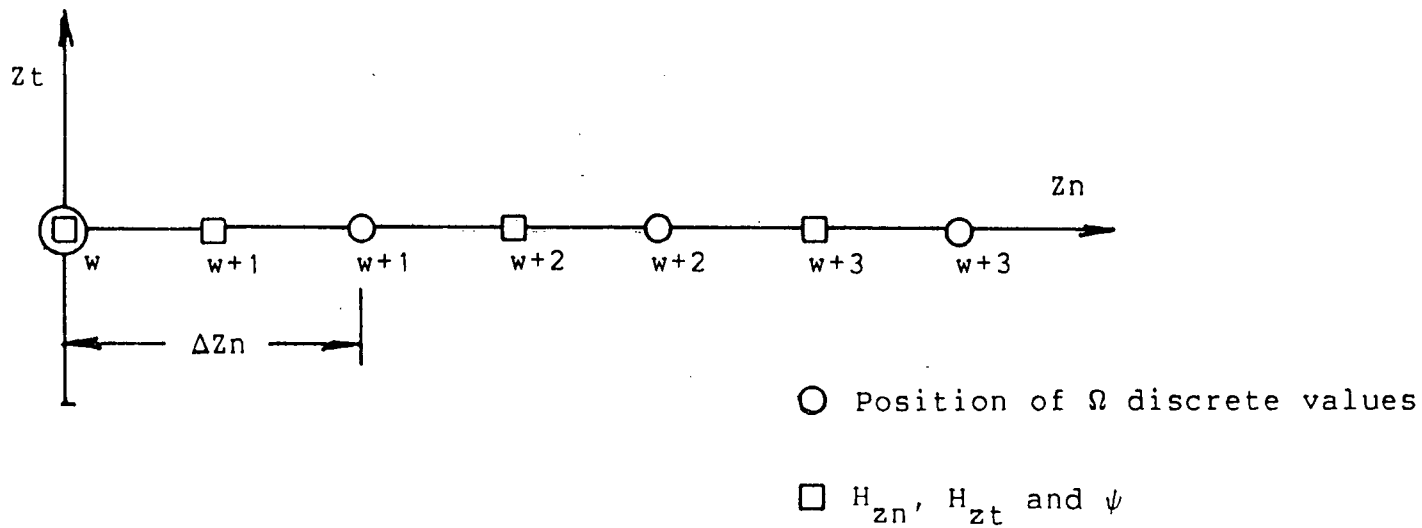

Figure 13. Staggered grid used to derive the different expressions for the vorticity boundary condition.

equation with respect to the coordinate normal to the wall to obtain

$$2\frac{\partial}{\partial Zn}\left[\frac{H_{zt}}{H_{zn}}\right]\frac{\partial^2\psi}{\partial Zn^2}+\frac{H_{zt}}{H_{zn}}\frac{\partial^3\psi}{\partial Zn^3}+\frac{\partial}{\partial Zn}(H_{zn}H_{zt})\Omega$$

$$+(H_{zn}H_{zt})\frac{\partial\Omega}{\partial Zn}=0 \qquad (107)$$

To derive the Wood and second order vorticity boundary conditions from Eq. 107, the following Taylor series expansions are required:

$$\psi_{w+1}=\psi+\frac{\partial\psi}{\partial Zn}\Delta Zn+\frac{1\partial^2\psi}{2\partial Zn^2}\Delta Zn^2+\frac{1\partial^3\psi}{6\partial Zn^3}\Delta Zn^3$$

$$+\frac{1\ \partial^4\psi}{24\partial Zn^4}\Delta Zn^4+O(\Delta Zn^5) \qquad (108)$$

$$\psi_{w+2}=\psi+2\frac{\partial\psi}{\partial Zn}\Delta Zn+2\frac{\partial^2\psi}{\partial Zn^2}\Delta Zn^2+\frac{4\partial^3\psi}{3\partial Zn^3}\Delta Zn^3$$

$$+\frac{2\partial^4\psi}{3\partial Zn^4}\Delta Zn^4+O(\Delta Zn^5) \qquad (109)$$

$$\Omega_{w+1}=\Omega+\frac{1\partial\Omega}{2\partial Zn}\Delta Zn+\frac{1\partial^2\Omega}{8\partial Zn^2}\Delta Zn^2+O(\Delta Zn^3) \qquad (110)$$

and

$$\Omega_{w+2}=\Omega+\frac{3\partial\Omega}{2\partial Zn}\Delta Zn+\frac{9\partial^2\Omega}{8\partial Zn^2}\Delta Zn^2+O(\Delta Zn^3) \qquad (111)$$

The Wood vorticity boundary condition is obtained by using one stream function Taylor series expansion (Eq. 108),

one vorticity Taylor series expansion (Eq. 110), the no-slip boundary condition (Eq. 104) and Eqs. 106 and 107. The no-slip boundary condition and Eqs. 106 and 107 are first substituted into the stream function Taylor series expansion, Eq. 108, truncated after the first four terms on the right hand side. The vorticity expansion, Eq. 110, truncated after the first two terms on the right hand side, is substituted into this modified stream function expansion. The final result of these manipulations is the expression for the Wood vorticity boundary condition for a general two-dimensional orthogonal coordinate system given below:

$$a_1 \frac{\partial \Omega}{\partial Zn} = a_2 \Omega_{w+1} + \psi - \psi_{w+1} \tag{112}$$

where

$$a_1 = -\frac{H_{zn}^2}{12} \Delta Zn^3 - \frac{H_{zn}}{12 H_{zt}} \frac{\partial}{\partial Zn} (H_{zn} H_{zt}) \Delta Zn^4 + \frac{H_{zn}^3}{6 H_{zt}} \frac{\partial}{\partial Zn} \left[\frac{H_{zt}}{H_{zn}} \right] \Delta Zn^4 \tag{113}$$

and

$$a_2 = -\frac{H_{zn}^2}{2} \Delta Zn^2 - \frac{H_{zn}}{6 H_{zt}} \frac{\partial}{\partial Zn} (H_{zn} H_{zt}) \Delta Zn^3 + \frac{H_{zn}^3}{3 H_{zt}} \frac{\partial}{\partial Zn} \left[\frac{H_{zt}}{H_{zn}} \right] \Delta Zn^3 \tag{114}$$

The discretized form of the Wood boundary condition is

easily generated from Eq. 112 by using a central difference to approximate the first derivative term. The stream function and scale factors needed in Eqs. 112 to 114 are obtained by linearly interpolating their nodal values.

The second order vorticity boundary condition uses both stream function Taylor series expansions (Eqs. 108 and 109), both vorticity Taylor series expansions (Eqs. 110 and 111), the no-slip boundary condition (Eq. 104) and Eqs. 106 and 107. Equations 108 and 109 are first linked together to eliminate the fourth order term from the resulting stream function series expansion. The no-slip boundary condition and Eqs. 106 and 107 are then substituted in this new stream function expansion. Equations 110 and 111 are also linked together to eliminate the second order term from the vorticity series expansions. Finally, the vorticity expansion is introduced into the last stream function expansion to obtain an expression for the second order vorticity boundary condition in a general two-dimensional orthogonal coordinate system. This expression is found to be

$$a_1\frac{\partial\Omega}{\partial Zn}=a_2\Omega_{w+1}+a_3\Omega_{w+2}+15\psi-16\psi_{w+1}+\psi_{w+2} \qquad (115)$$

where

$$a_1=-\frac{11H_{zn}^2}{12}\Delta Zn^3-\frac{H_{zn}}{2H_{zt}}\frac{\partial}{\partial Zn}(H_{zn}H_{zt})\Delta Zn^4$$
$$+\frac{H_{zn}^3}{H_{zt}}\frac{\partial}{\partial Zn}\left[\frac{H_{zt}}{H_{zn}}\right]\Delta Zn^4 \qquad (116)$$

$$a_2=-\frac{27H_{zn}^2}{4}\Delta Zn^2-\frac{3H_{zn}}{2H_{zt}}\frac{\partial}{\partial Zn}(H_{zn}H_{zt})\Delta Zn^3$$
$$+\frac{3H_{zn}^3}{H_{zt}}\frac{\partial}{\partial Zn}\left[\frac{H_{zt}}{H_{zn}}\right]\Delta Zn^3 \qquad (117)$$

and

$$a_3=\frac{3H_{zn}^2}{4}\Delta Zn^2+\frac{H_{zn}}{6H_{zt}}\frac{\partial}{\partial Zn}(H_{zn}H_{zt})\Delta Zn^3$$
$$-\frac{H_{zn}^3}{3H_{zt}}\frac{\partial}{\partial Zn}\left[\frac{H_{zt}}{H_{zn}}\right]\Delta Zn^3 \qquad (118)$$

As in the case of the discretized Wood boundary condition, the algebraic form of the second order boundary condition is obtained by using a second order accurate finite difference to represent the derivative, $\partial\Omega/\partial Zn$, and linearly interpolating the discrete stream function and scale factors to determine their mid-point values.

If scale factors of unity are introduced into Eqs. 112 and 115 above, the Wood and second order vorticity boundary conditions for a Cartesian system are recovered.

VI. COMPUTER PROGRAM

The computer program including the initialisation procedures, the techniques for solving the algebraic finite difference equations, the accuracy criteria and the performance indicators employed, and the methods for calculating local and average Nusselt numbers is described in this section and listed in Appendix A.

The computational procedure consists of two major parts: the generation of the body-fitted orthogonal grid and the solution of the corresponding natural convection problem. The general steps of the program are listed in Table 3. As can be seen from the Table, the procedure consists of 13 steps; the grid generation involves steps 3 to 6 while the natural convection calculation is carried out in steps 10 to 12.

In the program, the top, right, bottom and left walls of the transformed domain correspond to the top, right, bottom and left walls of the physical domain, respectively. The analytic functions (as well as the derivatives needed for the modified Neumann boundary conditions) which define the boundaries of the physical domain, i.e. Y=F(X) or X=F(Y), are introduced into the program through a function subroutine. The grid boundary conditions, two Dirichlet or one Dirichlet and one Neumann, are specified in a consistent manner at all grid points along each wall of the transformed domain. In the program, the desired grid boundary conditions at each wall of the transformed domain are specified by

Table 3. Program algorithm.

1) Set up the analytical functions and their derivatives for each physical domain boundary. Provide the program with the grid boundary condition flag values, the shape factors at the transformed domain corners, the vorticity boundary condition flag value, the grid size, the accuracy criteria, the allowed maximum number of iterations and the relaxation factors.

2) Initialize X, Y, θ, ψ and Ω at their appropriate boundary and internal grid points.

3) Update X and Y values using Eqs. 68 and 74 (where the coefficient definitions in both equations are given by Eqs. 69 to 73) and the appropriate boundary conditions (among Eqs. 19, 20, 75 or 76). One iteration consists of a complete sweep of rows followed by a complete sweep of colums using the line-by-line procedure. A line of X is followed immediately by the same line of Y to ensure the solution is as simultaneous as possible.

4) Update the shape factors using Eqs. 15 to 17 on walls (including the corner values) where two Dirichlet conditions are imposed. On walls where one Dirichlet and one Neumann condition are specified, the shape factors are evaluated by linearly interpolating the corner values. The shape factors inside the transformed domain are calculated by means of Eq. 18.

5) If the maximum absolute difference of X or Y is larger than 2, stop the execution. Otherwise, go to the next step.

6) If the convergence criteria are satisfied or if the maximum number of iterations for the grid generation part is exceeded, go on to the next step. Otherwise, return to step 3.

7) Calculate $\frac{\partial X}{\partial \xi}$, $\frac{\partial X}{\partial \eta}$, $\frac{\partial Y}{\partial \xi}$ and $\frac{\partial Y}{\partial \eta}$ at all grid points in the transformed domain.

8) Calculate the grid performance indicators using Eqs. 119 to 121.

9) Calculate the scale factors and the shape factors at all grid positions in the transformed domain using Eqs. 15 to 17.

10) Update the ψ, Ω and θ discrete values using Eqs. 78 (where the coefficient definitions are given by Eqs. 69 to 73 and 77), 90 (where the coefficient definitions are given by Eqs. 91 to 102) and 103 (where the coefficient definitions are given by Eqs. 90 to 99). The boundary conditions of these dependent variables are specified by Eqs. 58; either 112 (where the coefficients are given by Eqs. 113 and 114) 115 (where the coefficient are given by Eqs. 116 to 118); and 59 to 62. Again one iteration requires a complete sweep of rows and then columns. Since the grid is staggered, the temperature and the vorticity for any given line is updated before moving on to the adjacent line of stream function values.

11) If the maximum vorticity value is larger than 10^{10}, stop the execution. Otherwise, go to the next step.

12) If the convergence criterion is satisfied for all θ, ψ and Ω values, or if the maximum number of iterations for the natural convection part is exceeded, go to the next step. Otherwise, return to step 10.

13) Find the absolute maximum stream function value and calculate the local and average Nusselt numbers along the left and right walls of the enclosure using the Eqs. 124 and 125.

assigning a value of 0 or 1 to a flag variable. On walls where two Dirichlet boundary conditions are used, the initial values of the Cartesian coordinates at each nodal point remain unchanged during the computation. On walls where one Dirichlet and one Neumann boundary conditions are employed, the shape factors are obtained by linearly interpolating the corner values (other shape factor profiles could have been used). The shape factors at the corners of the transformed domain are assigned specific values at the beginning of the program. This corner shape factor value remains constant if one Dirichlet and one Neumann condition are specified on both walls which meet at that corner; otherwise, the corner value must be recalculated numerically using Eq. 15 with second order finite differences to represent the derivatives in Eqs. 16 and 17. Thus, it is through the choice of the grid boundary conditions, the initialisation of the Cartesian coordinates and the initialisation of the shape factors at the corner points that the grid characteristics are specified. The initial correspondence between Cartesian and orthogonal coordinates at each boundary node of the transformed domain is given in Table 4 for a MxN grid. Note that when two Dirichlet conditions are specified for any wall, Table 4 assumes that the nodes are to be uniformly spaced in the direction of the dependent Cartesian coordinate of the analytic function (other types of boundary point correspondence could have been prescribed).

Table 4. Initial correspondence between Cartesian and body-fitted orthogonal coordinates at the domain boundaries.

Wall	Physical Domain		New Domain
	Cavity C1	Cavity C2	
Top	$\left[\left[\frac{(i-1)(1+2A)}{M-1}\right], 1\right]$	$\left[\left[\frac{i-1}{M-1}\right], 1\right]$	(i,N)
Right	$\left[F1(Y), \left[\frac{j-1}{N-1}\right]\right]$	$\left[F2(Y), \left[\frac{j-1}{N-1}\right]\right]$	(M,j)
Bottom	$\left[\left[\frac{i-1}{M-1}\right], 0\right]$	$\left[\left[\frac{i-1}{M-1}\right], 0\right]$	(i,1)
Left	$\left[0, \left[\frac{j-1}{N-1}\right]\right]$	$\left[0, \left[\frac{j-1}{N-1}\right]\right]$	(1,j)

Because an iterative method will be used to solve the finite difference representation of the grid generation and natural convection equations, it becomes necessary to specify initial values for all dependent variables (X, Y, θ, ψ, and Ω) at the beginning of the program. The initial values of the Cartesian coordinates, X and Y, at all interior nodes of the transformed grid are assigned by linearly interpolating the boundary values. Initial temperature values are normally obtained by a linear interpolation between the isothermal walls of the enclosures. Since the stream function and vorticity values are difficult to specify beforehand and, in fact, can be either positive or negative, their initial values were normally assigned to zero. Provision is also made to use a converged solution of a similar problem (eg. at a slightly different Rayleigh number) to obtain starting θ, ψ and Ω values for a new problem. Of course, the initial values have no effect on the final converged solution other than to modify the number of iterations required to reach the final answer.

During each step of the iterative process, the Cartesian coordinates (during grid generation) and the temperature, the stream function and the vorticity (during the natural convection caculations) are updated using a line-by-line solution procedure along with successive relaxation. In the line-by-line method, the linear algebraic equations for a complete line of new dependent variable

values are written in implicit form. This procedure leads to a tridiagonal matrix which can then be solved using the very efficient Thomas algorithm [38-40]. The line-by-line implicit method has much better convergence properties than explicit methods like the Gauss-Seidel technique because information from the boundaries is transported in a single step throughout the domain. To ensure the rapid diffusion of all boundary information, the line-by-line method proceeds by rows in one sweep through the grid and then by columns in the next. Convergence can be further accelerated by applying successive relaxation to each set of solution values. Over-relaxation is used for the two Cartesian coordinates, the temperature and the stream function. It was found that under-relaxation was necessary in order to ensure the convergence of the vorticity.

Many criteria can be used to specify a desired level of convergence for a numerical solution. These criteria can be based on either absolute or relative errors. In this work, the absolute error of a dependent variable is defined as the maximum absolute difference between the discrete values obtained in the latest iteration and those obtained in the previous one. The relative error is then given by the ratio of the absolute error and the largest absolute value of that dependent variable in the latest iteration. The numerical procedure for generating the body-fitted orthogonal grid is stopped only when both Cartesian coordinates satisfy an absolute error criteria. The numerical procedure used to

solve the natural convection problem is considered to be converged when the temperature, stream function and vorticity discrete values meet a prescribed relative error criterion.

In most of the numerical experiments, both the absolute and relative errors were required to be less than 0.00001. The maximum absolute difference of X and Y at the end of each grid generation iteration and the maximum absolute vorticity value at the end of each natural convection iteration were used to detect a divergent solution. If the maximum difference of X or Y were larger than 2 or the maximum absolute vorticity value was greater than 10^{10}, the solution was assumed to be divergent and the procedure was stopped. Also, upper limits on the number of iterations for the grid generation and the natural convection calculation parts prevented the consumption of excessive CPU time.

Once each pair of grid generation and natural convection problems had successfully converged, the discrete results were used to calculate the following information:

1. the length of the curved right wall,
2. the average and maximum deviations of the numerically generated grid from orthogonality,
3. the maximum stream function value, and
4. the local and average Nusselt numbers of both the left and right isothermal walls.

The length of the right wall, which is the only curved boundary of both the C1 and C2 cavities, is calculated by

means of the integral

$$L_{rw}=\int_1^N H_\eta \Big|_{\xi=M} d\eta \qquad (119)$$

The integration in Eq. 119 is approximated numerically by using the trapezoid rule. The length of the right wall is used as an indicator of the performance of the numerical grid generation routine. The length, in general, is a function of the grid size. As the number of grid points increases, the calculated length converges asymptotically to the exact value which can be determined by an analytical integration of the boundary equation.

The deviation of the numerically generated grid from orthogonality is another indicator of the performance of the program. The deviation from orthogonality is also a function of the grid size. It should approach zero as the number of grid points increases. At each nodal point, the angle, Θ, at which the grid lines intersect can be determined from

$$COS(\Theta)=\frac{\frac{\partial X}{\partial \xi}\frac{\partial X}{\partial \eta}+\frac{\partial Y}{\partial \xi}\frac{\partial Y}{\partial \eta}}{\left[\left[\frac{\partial X}{\partial \xi}\right]^2+\left[\frac{\partial Y}{\partial \xi}\right]^2\right]^{0.5}\left[\left[\frac{\partial X}{\partial \eta}\right]^2+\left[\frac{\partial Y}{\partial \eta}\right]^2\right]^{0.5}} \qquad (120)$$

To evaluate Θ, the various derivatives appearing in Eq. 120 were approximated by second order accurate forward, backward and central finite differences. Finally, the deviation from orthogonality, Dev, was calculated as

$$Dev=|90°-\Theta| \tag{121}$$

The maximum stream function was taken to be the maximum absolute value of all of the discrete stream function values on the grid. The maximum stream function value is an important quantity because it is a measure of the total circulatory flow in the enclosure. If the sign associated with the maximum value is positive, the flow is anti-clockwise; otherwise, the flow is clockwise.

Probably the most important derived quantity in any convective heat transfer situation is the heat transfer coefficient at the fluid-solid interface. This quantity is essential in the design of any unit operation in which convection heat transfer occurs. The local heat flux at a solid-fluid interface is given in general orthogonal coordinates by

$$q_{zn}=-\frac{k_o \ \partial T}{H_{zn}L_c \partial Zn} \tag{122}$$

For design purposes, the local heat flux at the wall can also be written as the product of the characteristic temperature difference of the system and a coefficient called the convection heat transfer coefficient, i.e.

$$q_{zn}=h(T_h-T_c) \tag{123}$$

The dimensionless convection heat transfer coefficient,

called the Nusselt number, can now be derived by combining Eqs. 122 and 123 to obtain

$$Nu=\frac{hL_c}{k_o}=-\frac{1}{H_{zn}}\frac{\partial\theta}{\partial Zn} \qquad (124)$$

The local Nusselt number is calculated numerically from the above equation by using a second order accurate central difference to approximate the temperature derivative and by linearly interpolating the discrete scale factor values. The average Nusselt number along a wall is then given by

$$Nu_{ave}=\frac{\int_{wall} NuH_{zt}\,dZt}{\int_{wall} H_{zt}\,dZt} \qquad (125)$$

The average Nusselt number is calculated from Eq. 125 using the trapezoid rule integration technique.

VII. TEST PROBLEMS

Using results available from the literature, two different types of test problems were considered in order to ensure that the simulation program was running properly. The first problem was designed to test the program's ability to succesfully generate body-fitted orthogonal grids. The second test case examined the program's ability to solve a standard natural convection problem.

A. FIRST TEST

Chikhliwala and Yortsos [27] extensively investigated the ability of the weak constraint method to generate body-fitted orthogonal grids in two-dimensional domains which they suggest are encountered during immiscible fluid displacement in porous media. The general shape of the domain is identical to the cavity C1 with the only difference being that the bottom wall length is not B but 0.75B (see Fig. 4). Therefore, the function representing the right wall is

$$X=0.75+A\ \cos(\pi Y) \qquad (126)$$

where the amplitude, A, was allowed to vary from 0.0 (rectangular cavity) to 0.25. Two of the three different sets of boundary conditions considered by Chikhliwala and Yortsos are also investigated in this work. In case 1, the correspondence between Cartesian and general orthogonal

coordinates is prescribed at the right wall while the shape factors of the top left and bottom left corners are assigned to unity (i.e. the shape factors along the left wall are all unity, those along the right wall are calculated using Eqs. 15 to 17 and those along the top and bottom walls are linearly interpolated from their respective corners values). In case 2, boundary correspondence between the Cartesian and general orthogonal coordinates is prescribed at the the left, right and bottom walls (the shape factors are calculated for the left, right and bottom walls using Eqs. 15 to 17 and are determined for the top wall by linear interpolating its corner values). As a standard example, the authors chose a grid having 18 rows and 18 columns. Unfortunately, they give only very cursory information about their discretization methods.

These two cases were entered into the present program. An 18x18 grid was employed and the amplitude was allowed to range from 0.05 to 0.25 for both cases. The maximum deviations from orthogonality computed for the internal (non-boundary) grid points are compared to the results of reference [27] in Tables 5 (case 1) and 6 (case 2). It is of interest to note that the grids generated by the present program are more orthogonal than those obtained by Chikhliwala and Yortsos. The improved results obtained by the present program are probably attributable to the use of second order accurate finite difference approximations throughout, more stringent convergence criteria and the

Table 5. Comparison of the maximum deviations (in degrees) obtained in the present work and by Chikhliwala and Yortsos [27] - case 1.

Amplitude	Present Work	Reference [27]
0.05	0.106	0.300
0.10	0.221	1.000
0.15	0.352	2.000
0.20	0.809	3.600
0.25	1.510	5.700

Table 6. Comparison of the maximum deviations (in degrees) obtained in the present work and by Chikhliwala and Yortsos [27] - case 2.

Amplitude	Present Work	Reference [27]
0.05	0.251	1.300
0.10	0.743	2.400
0.15	1.780	3.700
0.20	3.310	5.000
0.25	6.050	6.500

modified Neumann boundary conditions (Eqs. 75 and 76). Tables 5 and 6 also reveal that the more the boundary nodes are constrained, i.e. the larger the number of bounding surfaces where complete boundary correspondence is required, the less orthogonal is the generated grid. In fact, Chikhliwala and Yortsos found that, in some cases, when the boundary nodes were initially prescribed over the entire perimeter of the domain, it was either impossible to obtain a converged set of interior grid points or the orthogonality condition was not satisfied. Apparently, the physical grid can be overconstrained at the boundaries to the point where a realistic solution is no longer achievable. However, this failure to obtain complete boundary correspondence should not be considered as a fatal deficiency of the weak constraint method. In most cases, including those considered in the present thesis, it is only essential to have boundary correspondence at one surface where two contiguous regions join (see Chapter X). The concentration of grid points can be varied by adjusting the scale factor values at the corners formed by the other three sides.

B. SECOND TEST

The natural convection portion of the program was tested by considering the case of a square cavity with vertical isothermal walls. As was mentioned earlier, this problem has been extensively investigated in the literature to the point where it is now considered to be a standard

problem for comparing different numerical heat transfer methods. De Vahl Davis and Jones [15] have summarized the results of a comparison exercise for the square cavity problem which included the solutions of 36 international contributors. As well, De Vahl Davis and Jones gave a benchmark solution which they consider to have a relative accuracy of better than 1 percent.

Using the present program, numerical simulations were carried out for the cases of Rayleigh number equal to 1000, 10000 and 100000. For each case, the Prandtl number was set equal to 0.71 (air) and a uniform Cartesian grid consisting of 42 rows and 42 columns was used. Contour plots of the stream function and temperature distributions as well as the local Nusselt number variations along the isothermal walls are shown on Figs. 14 to 16 for the three Rayleigh numbers studied. The maximum stream function value and the average cavity Nusselt number for each case are compared to the benchmark values of De Vahl Davis and Jones in Tables 7 and 8.

An examination of Tables 7 and 8 demonstrate that the results of the present program are in excellent agreement with the best solutions given by De Vahl Davis and Jones. The largest discrepancy was 0.72 percent and was associated with the maximum stream function at Ra=100000. The differences observed in Tables 7 and 8 are small compared to the total range of deviations listed in reference [15]. Thus, it can be concluded that, at least for a vertical

Figure 14. Selected natural convection results for a vertical square cavity with Ra=1000 and Pr=0.71. (a) Stream function contour plot, (b) Temperature contour plot (isotherms range from 0 to 1 in increments of 0.1), (c) Left wall Nusselt number distribution, (d) Right wall Nusselt number distribution.

AVERAGE NUSSELT NUMBER (RIGHT WALL)= 0.1117338E+01
AVERAGE NUSSELT NUMBER (LEFT WALL)= 0.1117107E+01

STREAM FUNCTION CONTOUR VALUES.
MIN= 0.0
MAX= 0.1172789E+01

CONTOUR #	1	0.1172788E+00
CONTOUR #	2	0.2345577E+00
CONTOUR #	3	0.3518366E+00
CONTOUR #	4	0.4691154E+00
CONTOUR #	5	0.5863943E+00
CONTOUR #	6	0.7036731E+00
CONTOUR #	7	0.8209520E+00
CONTOUR #	8	0.9382309E+00
CONTOUR #	9	0.1055510E+01

a)

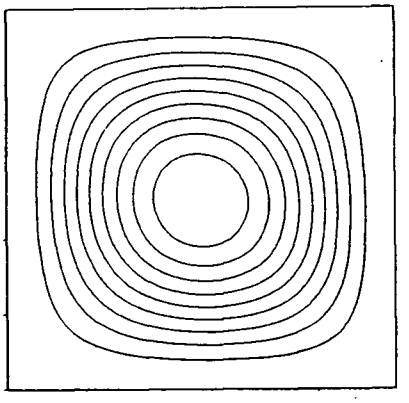

b)

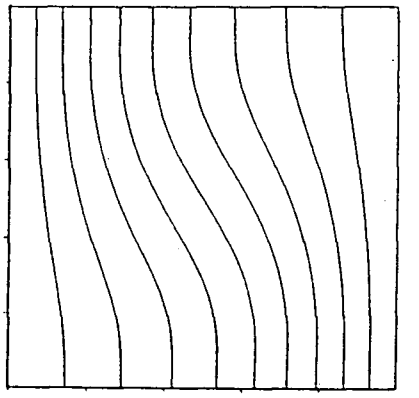

c)

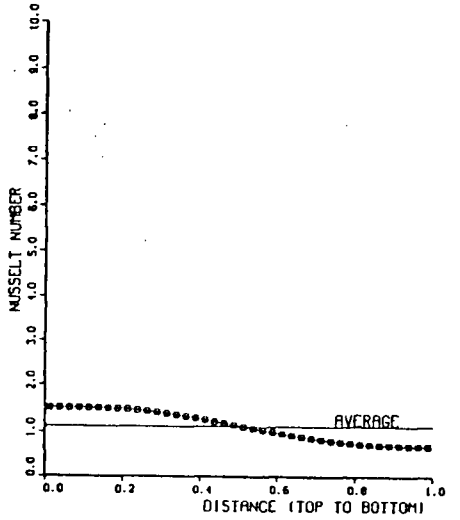

d)

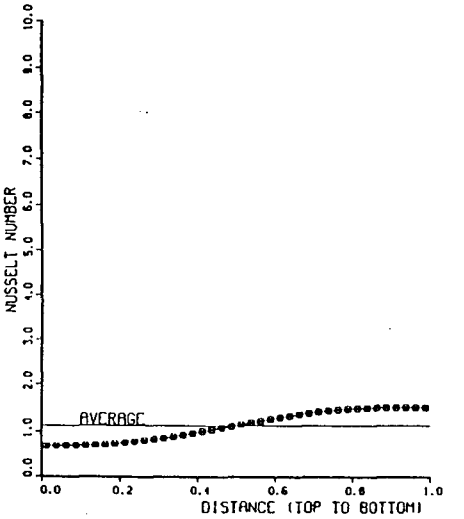

Figure 15. Selected natural convection results for a vertical square cavity with Ra=10000 and Pr=0.71. (a) Stream function contour plot, (b) Temperature contour plot (isotherms range from 0 to 1 in increments of 0.1), (c) Left wall Nusselt number distribution, (d) Right wall Nusselt number distribution.

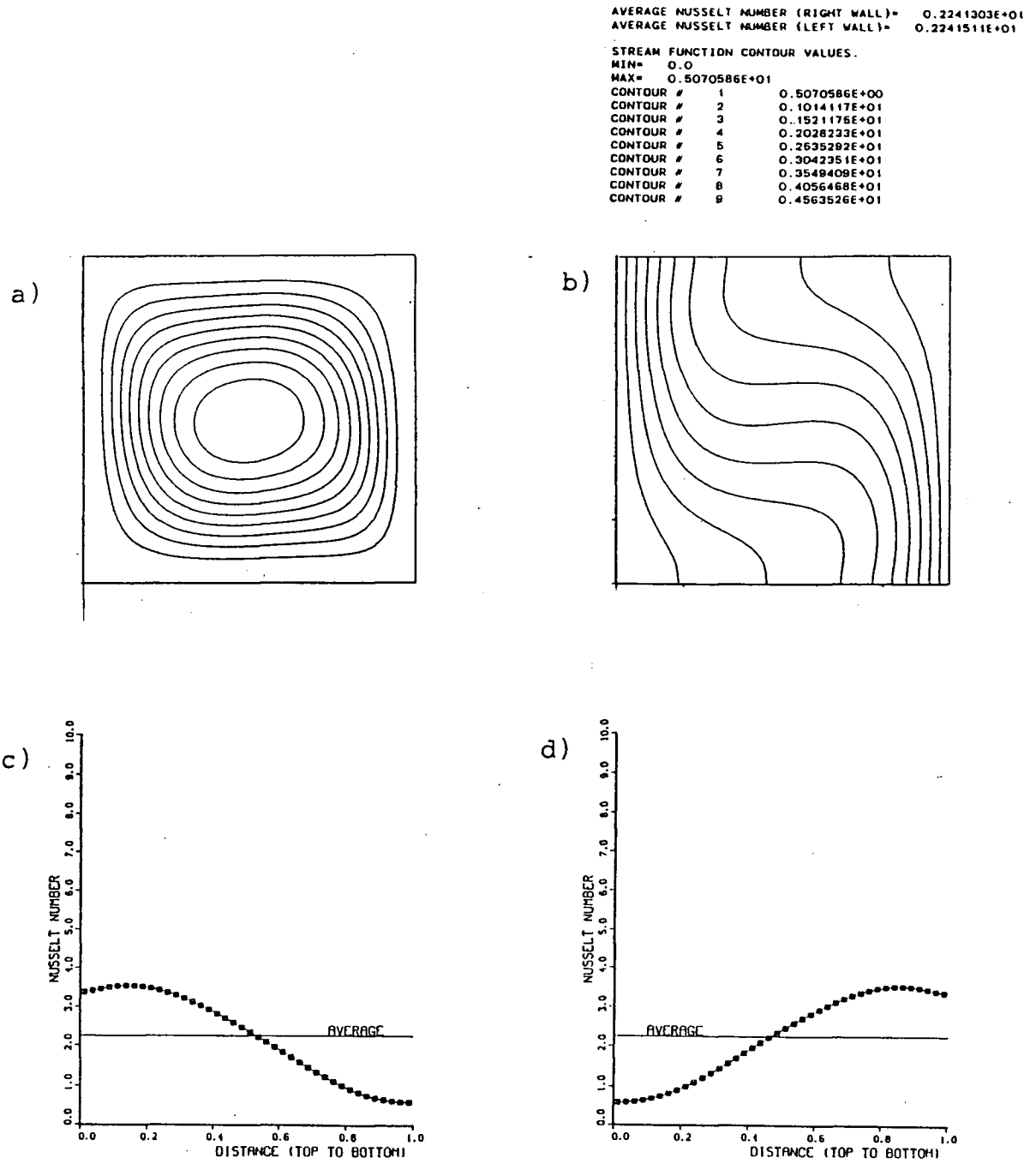

Figure 16. Selected natural convection results for a vertical square cavity with Ra=100000 and Pr=0.71. (a) Stream function contour plot, (b) Temperature contour plot (isotherms range from 0 to 1 in increments of 0.1), (c) Left wall Nusselt number distribution, (d) Right wall Nusselt number distribution.

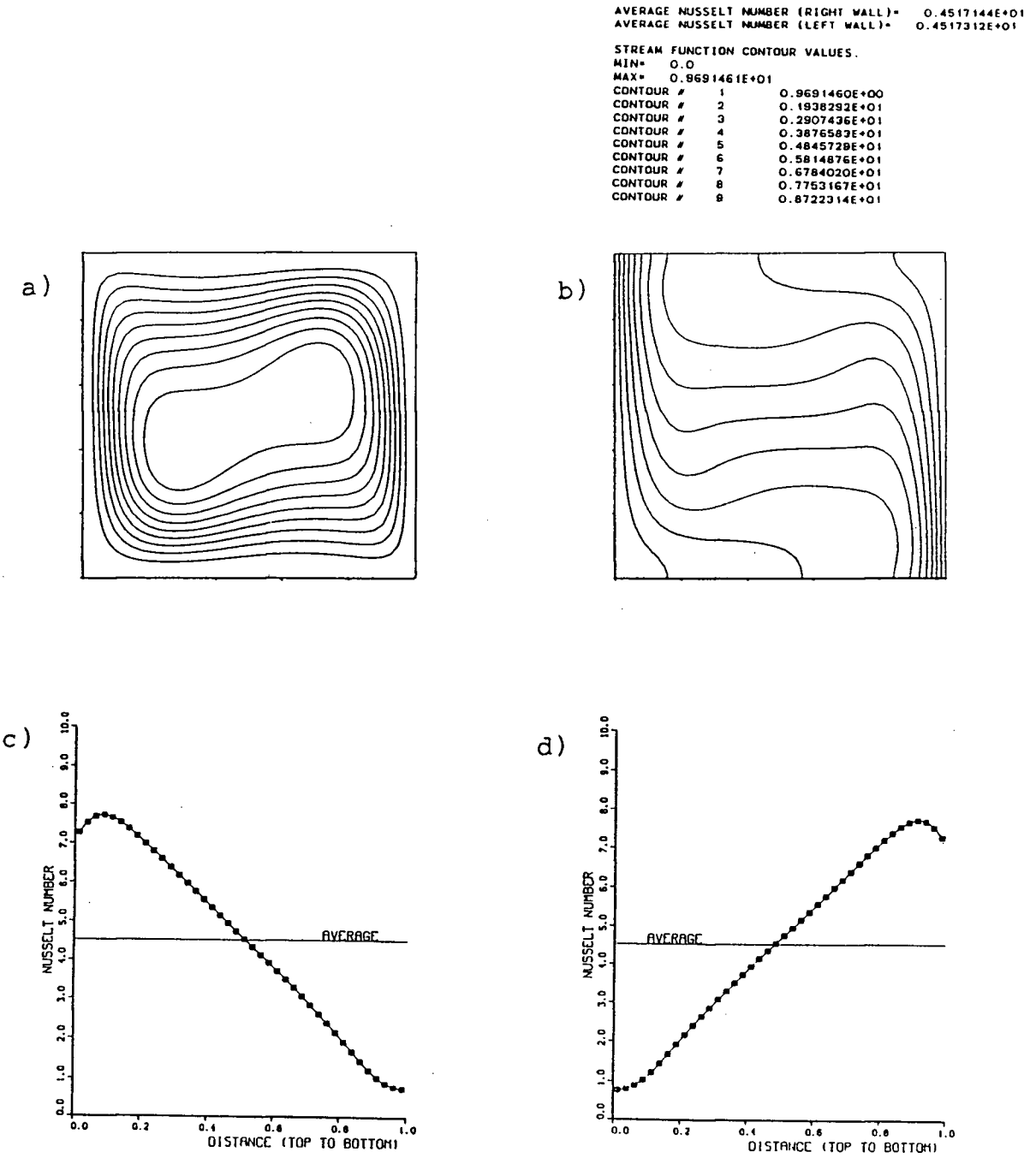

Table 7. Comparison of the maximum stream functions obtained in the present work with the benchmark results of De Vahl Davis and Jones [15].

Rayleigh Number	Present Work	Reference [15]
1000	1.172	1.174
10000	5.070	5.079
100000	9.691	9.622

Table 8. Comparison of the average Nusselt numbers obtained in the present work with the benchmark results of De Vahl Davis and Jones [15].

Rayleigh Number	Present Work	Reference [15]
1000	1.117	1.118
10000	2.241	2.238
100000	4.517	4.505

square cavity, the present program better than successfully solves simultaneous mass, momentum and energy balances.

The stream function and temperature contour plots shown in Figs. 14 to 16 illustrate the regimes typical of natural convection heat transfer in enclosures. For low Rayleigh numbers like 1000, the buoyancy-driven flow is very weak and hence the contribution of convection to the overall heat transfer is not very significant. This fact is clearly revealed in the temperature plot where the isotherms deviate only slightly from verticality; the state that would exist if convection were absent. In the latter case, the enclosure problem reduces to one of uni-directional conduction for which case it is possible to prove that the Nusselt number should be exactly unity. Thus, at Ra=1000, the calculated Nusselt number indicates that natural convection only increases the overall heat transfer rate by about 12 percent.

As the Rayleigh number is increased (for a given fluid, this can be achieved by increasing the characteristic temperature difference or the characteristic length of the cavity), the flow becomes stronger and convection makes a more important contribution to the overall transfer of heat. At a Rayleigh number of 100000, convection completely dominates conduction as a heat transfer mechanism and the flow is sufficiently strong that it begins to take on some of the attributes of a boundary layer. This is particularly noticeable in the temperature plot where the gradients are

very steep in the vicinity of the isothermal walls and essentially zero at the centre of the enclosure. For this case, it can be observed that secondary flows begin to develop in the core resulting in the formation of the characteristic "cat's eye" pattern.

VIII. PART I

A. NUMERICAL EXPERIMENTS

The natural convection problem treated here is totally defined by the specification of five independent parameters: the Rayleigh number, the Prandtl number, the dimensionless amplitude (referred to as the amplitude from this point onwards), the cavity aspect ratio and the cavity angle of tilt. The independent variable values investigated are presented in Table 1. For each cavity type (C1 or C2), the permutation of these independent variable values defines 30 different natural convection problems. Each natural convection problem is solved numerically by satisfying the difference forms of the body-fitted orthogonal mapping, stream function, vorticity and temperature equations along with their various boundary conditions. Six different sets of boundary conditions are considered in this work and these are presented in Tables 9 and 10. Also, 7 grid sizes are examined and are listed in Table 11. The permutation of the boundary conditions and grid sizes defines an additional 42 ways that each natural convection problem could be solved.

The primary objective of Part I is to determine the effect of the grid size and the set of boundary conditions used on the accuracy of the numerical solutions. Although each natural convection problem represents a particular case, 60x42 numerical simulations were not attempted in order to fulfil this first objective; rather only those

Table 9. Different grid, stream function, vorticity and temperature boundary conditions investigated in Part I.

Grid	Stream Function	Temperature	Vorticity
Case A Case B Case C	Eq. 58	Eqs. 59 to 62	Wood: Eqs. 112 to 114 Second Order: Eqs. 115 to 118

Table 10. Grid boundary conditions investigated in Part I; D=Dirichlet, N=Neumann.

Case	Top Wall		Right Wall		Bottom Wall		Left Wall	
	X	Y	X	Y	X	Y	X	Y
A	N	D	D	N	N	D	D	N
B	N	D	D	D	N	D	D	N
C	D	D	D	D	D	D	D	N

Grid Size	
M	N
7	7
9	9
13	13
17	17
25	25
33	33
49	49

Table 11. Grid sizes investigated in Part I.

cases expected to yield the greatest numerical difficulty were investigated in detail. Thus, five natural convection problems were selected for this purpose and are presented in Table 12. These five cases use only the most distorted cavities. A Rayleigh number of 10000 was chosen in four of the cases partly because the heat transfer at this condition exhibits both conduction and convection modes, and also because the computational cost of tackling a larger Rayleigh number was prohibitive. However, one case of Ra=100000 was included because it provides a more rigorous test of the accuracy of the numerical solution procedure. To minimize CPU time, the initial solution values for stream function, vorticity and temperature for each finer grid were obtained by linearly interpolating the converged answer for the previous coarser grid. In each case, once convergence had been attained, plots were made of the generated grids, the stream function, vorticity and temperature distributions as well as the local Nusselt number distributions on the left and right walls. Also, the length of the right wall, the maximum deviation of the grid from orthogonality, the maximum stream function and the average Nusselt numbers of the left and right walls were recorded in order to assess the accuracy of the solutions. Finally, a heat balance at the domain boundary was performed for each numerical experiment. Because the top and bottom walls are adiabatic, all of the heat energy which enters the cavity from the hot right wall must be removed from the cavity at the cold left

Table 12. Dimensionless amplitudes and Rayleigh numbers investigated in Part I.

Case	Cavity	Dimensionless Amplitude	Rayleigh Number
1	C1	-0.15	10000
2	C1	0.15	10000
3	C2	-0.15	10000
4	C2	0.15	10000
5	C1	-0.15	100000

wall if steady-state conditions are to prevail. This condition can be written dimensionally as

$$Q_{lw}=Q_{rw} \tag{127}$$

The above equation can be rewritten in terms of the average heat transfer coefficients of each wall, i.e.

$$h_{ave,lw}L_c L_{lw}(T_h-T_c)=h_{ave,rw}L_c L_{rw}(T_h-T_c) \tag{128}$$

assuming the cavity has a depth of unity. If Eq. 128 is divided through by k_o, it reduces to

$$Nu_{ave,lw}L_{lw}=Nu_{ave,rw}L_{rw} \tag{129}$$

where in the present investigation, L_{lw} is unity. Thus, as an additional measure of solution accuracy, the ratio of the difference between the left and right hand sides of Eq. 129 to their mean value was calculated.

B. RESULTS

There is not sufficient space or need to show all of Part I results. Some representative examples for a 33x33 grid are given in Figs. 17 to 21 for cases 1 to 5, respectively. Each figure includes three numerically generated grids corresponding to the three sets of boundary conditions (i.e. no boundary correspondence, boundary

Figure 17. Selected results obtained for case 1 of Table 12. (a), (b) and (c) 33x33 grids obtained with boundary conditions A, B and C, respectively, (d) Stream function contours, (e) Temperature contours, (f) and (g) Right and left wall Nusselt number distributions, respectively.

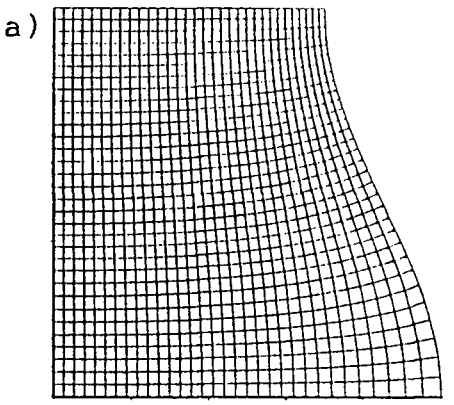

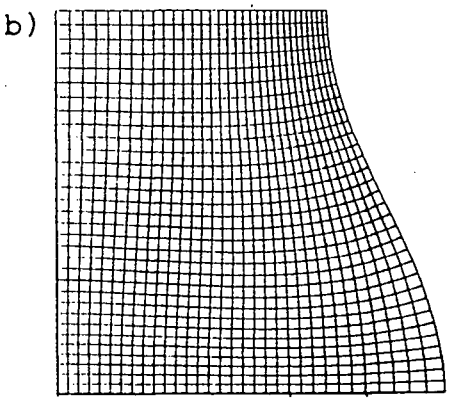

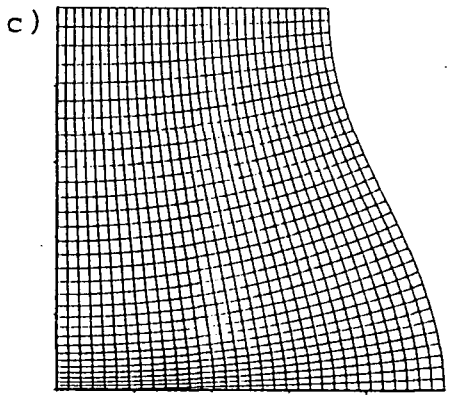

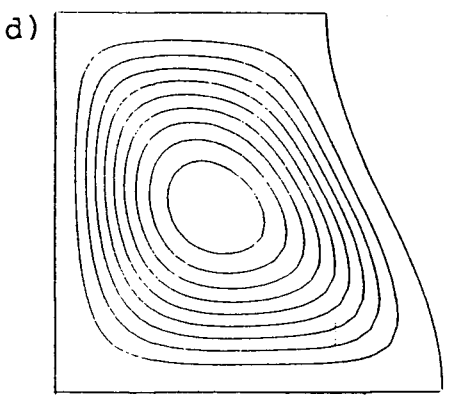

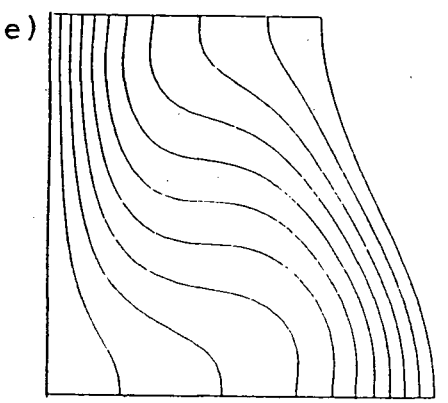

f)

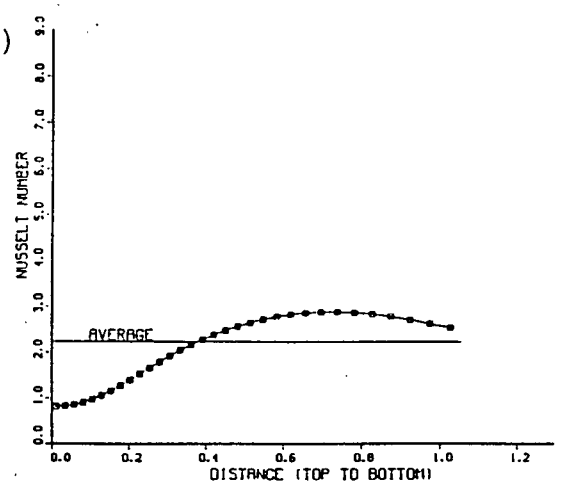
NUSSELT NUMBER
AVERAGE
DISTANCE (TOP TO BOTTOM)

g)

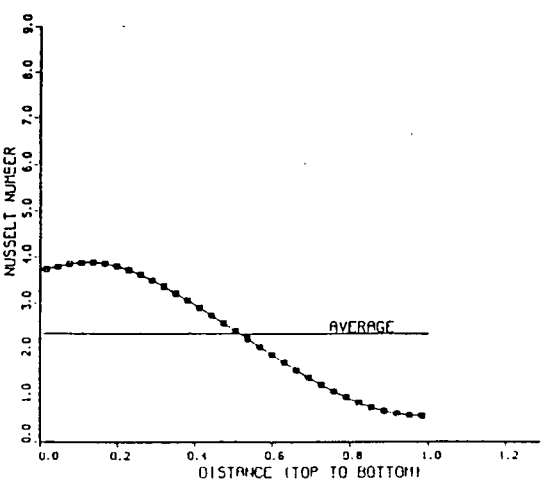
NUSSELT NUMBER
AVERAGE
DISTANCE (TOP TO BOTTOM)

Figure 18. Selected results obtained for case 2 of Table 12. (a), (b) and (c) 33x33 grids obtained with boundary conditions A, B and C, respectively, (d) Stream function contours, (e) Temperature contours, (f) and (g) Right and left wall Nusselt number distributions, respectively.

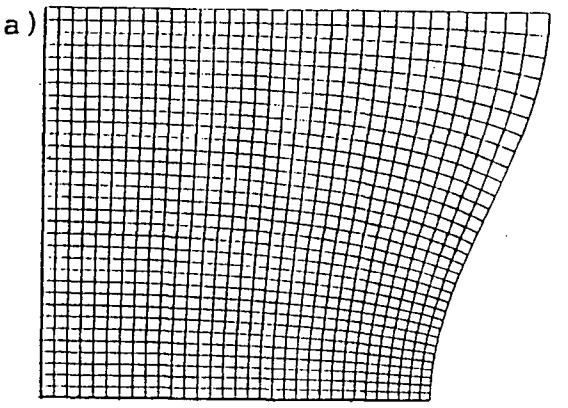

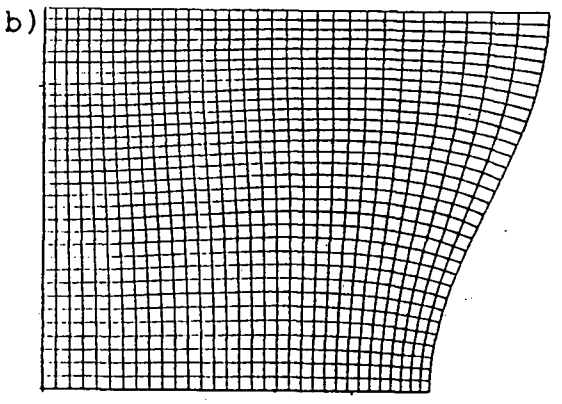

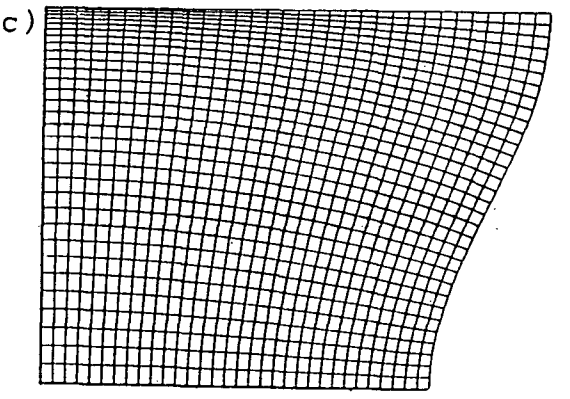

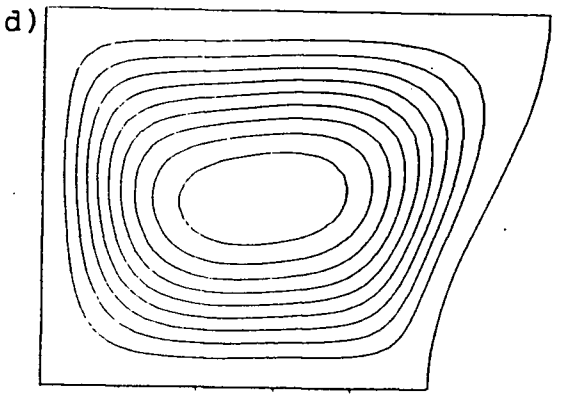

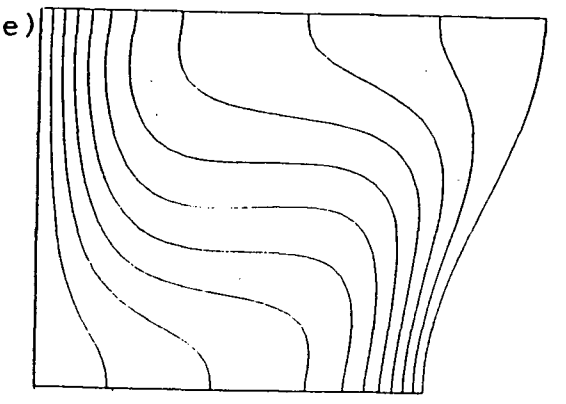

f)

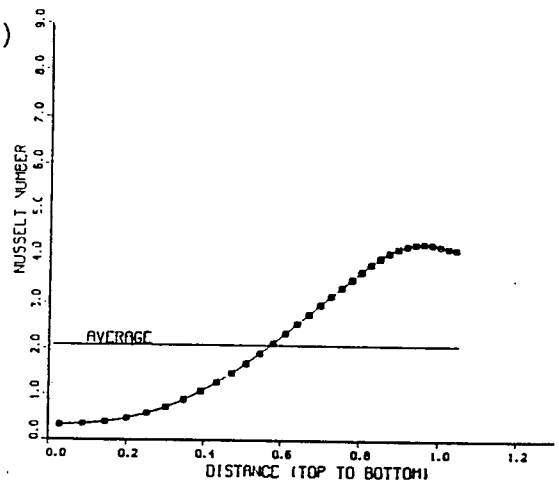
NUSSELT NUMBER
AVERAGE
DISTANCE (TOP TO BOTTOM)

g)

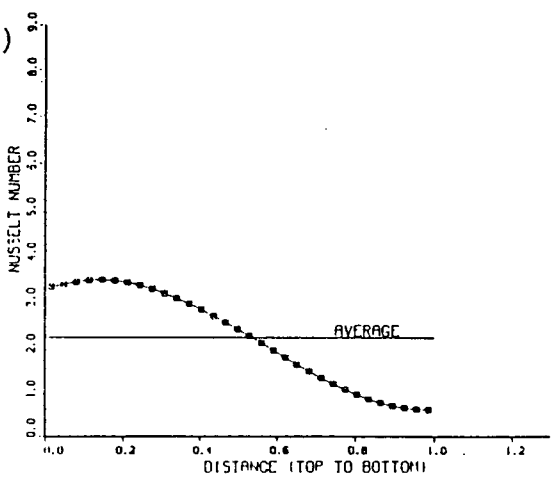
NUSSELT NUMBER
AVERAGE
DISTANCE (TOP TO BOTTOM)

Figure 19. Selected results obtained for case 3 of Table 12. (a) and (b) 33x33 grids obtained with boundary conditions A and B, respectively (grid boundary conditions C did not yield a converged result), (d) Stream function contours, (e) Temperature contours, (f) and (g) Right and left wall Nusselt number distributions, respectively.

a)

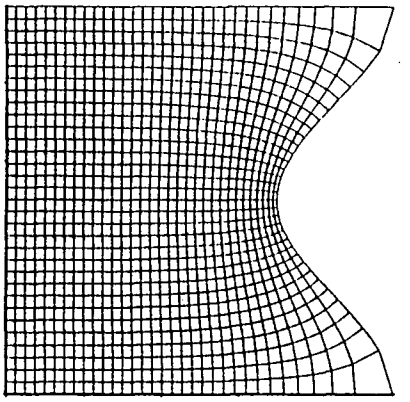

b)

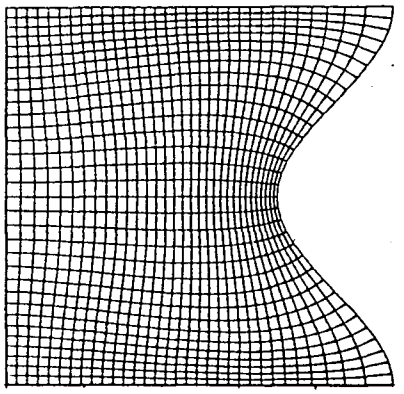

d)

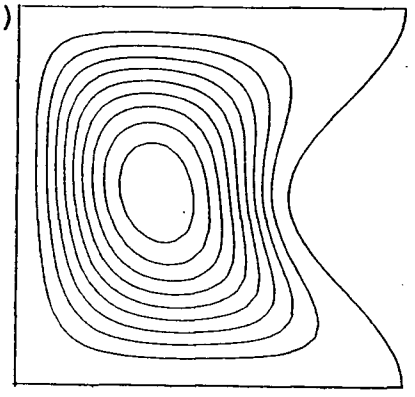

e)

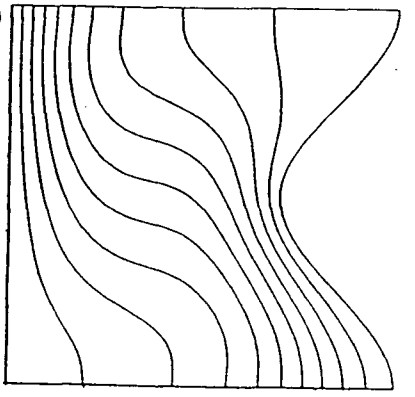

f)

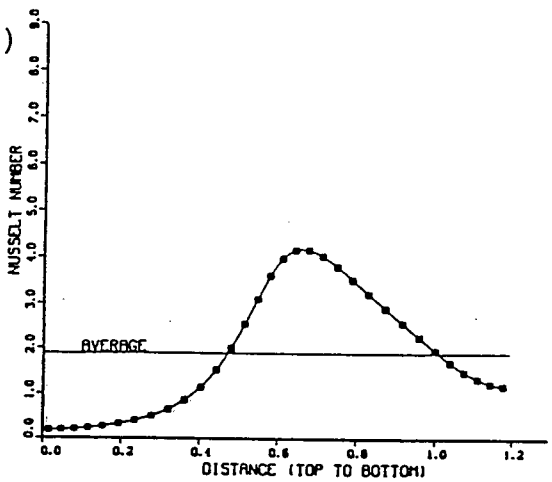
NUSSELT NUMBER
AVERAGE
DISTANCE (TOP TO BOTTOM)

g)

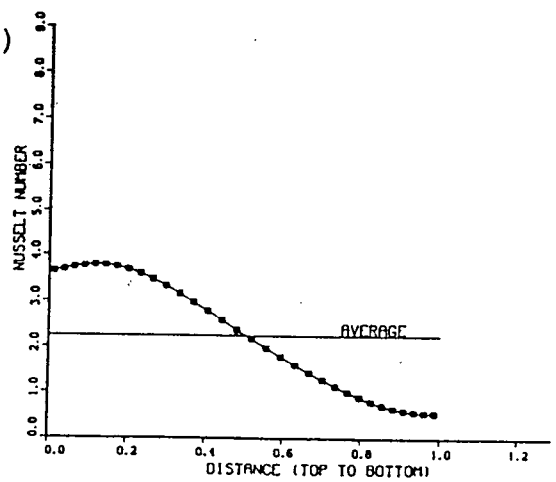
NUSSELT NUMBER
AVERAGE
DISTANCE (TOP TO BOTTOM)

Figure 20. Selected results obtained for case 4 of Table 12. (a), (b) and (c) 33x33 grids obtained with boundary conditions A, B and C, respectively, (d) Stream function contours, (e) Temperature contours, (f) and (g) Right and left wall Nusselt number distributions, respectively.

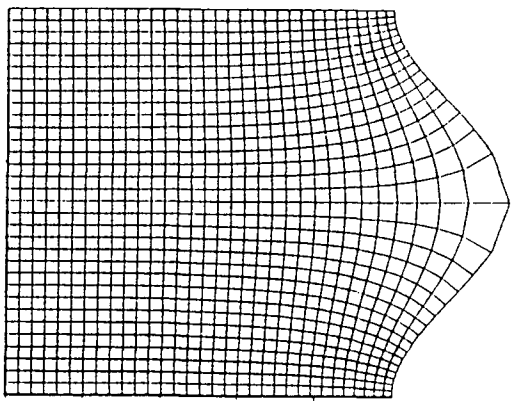

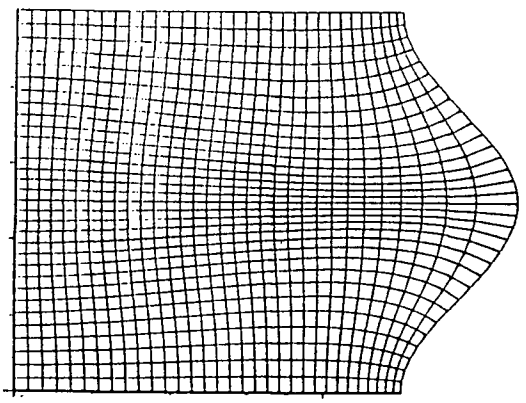

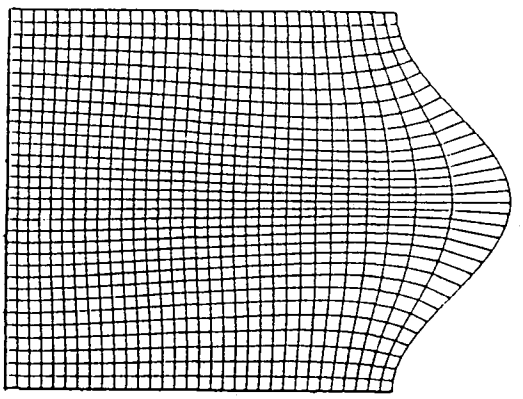

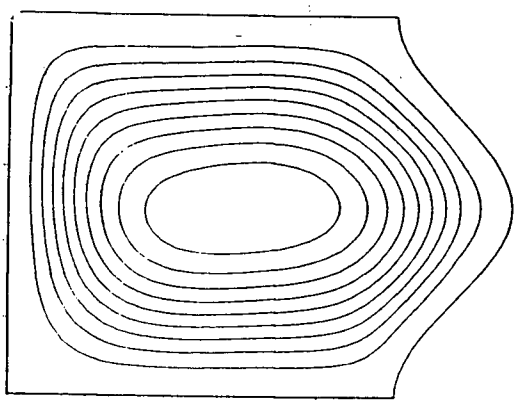

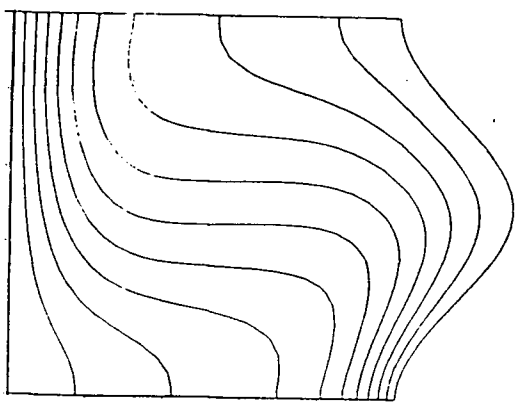

f)

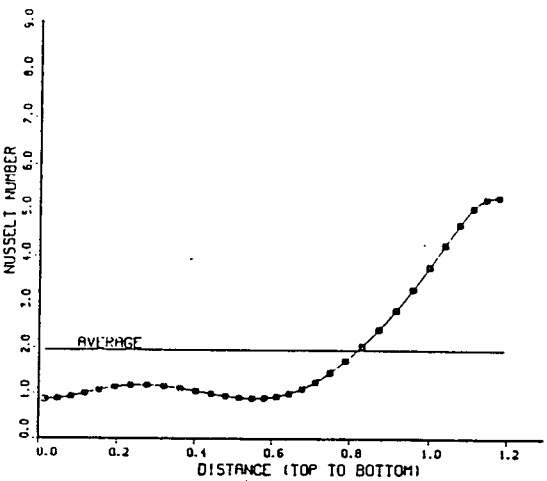
NUSSELT NUMBER
AVERAGE
DISTANCE (TOP TO BOTTOM)

g)

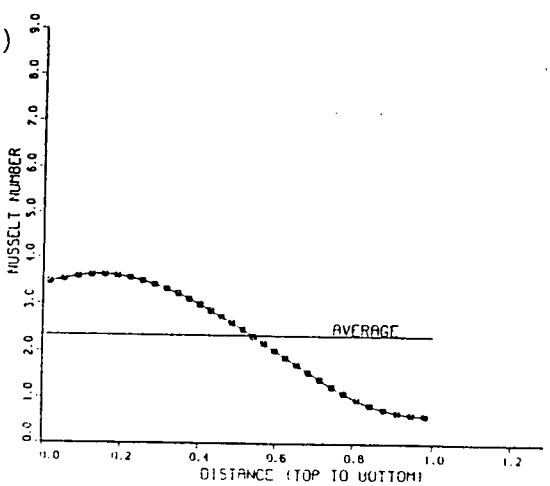
NUSSELT NUMBER
AVERAGE
DISTANCE (TOP TO BOTTOM)

Figure 21. Selected results obtained for case 5 of Table 12. (a), (b) and (c) 33x33 grids obtained with boundary conditions A, B and C, respectively, (d) Stream function contours, (e) Temperature contours, (f) and (g) Right and left wall Nusselt number distributions, respectively.

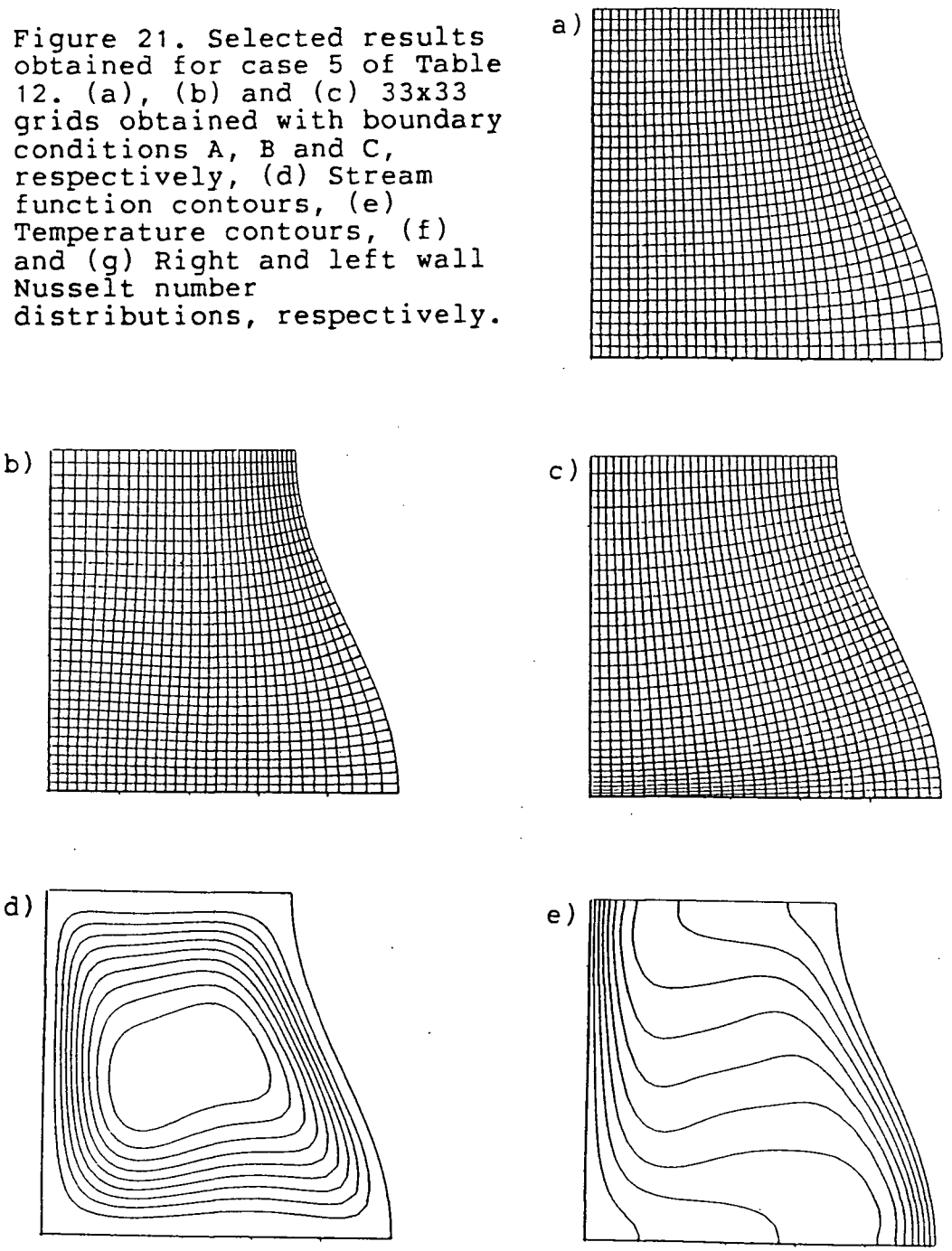

f)

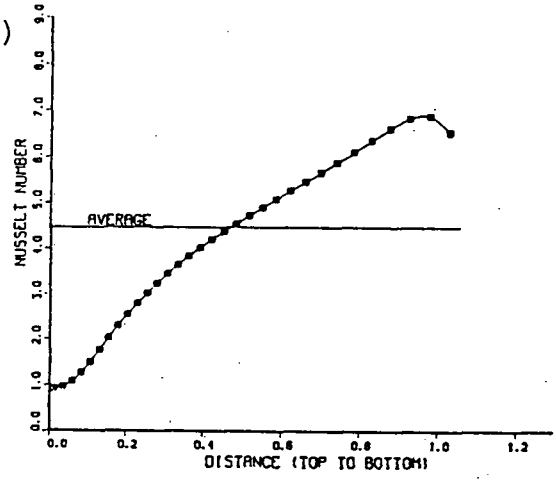
NUSSELT NUMBER
AVERAGE
DISTANCE (TOP TO BOTTOM)

g)

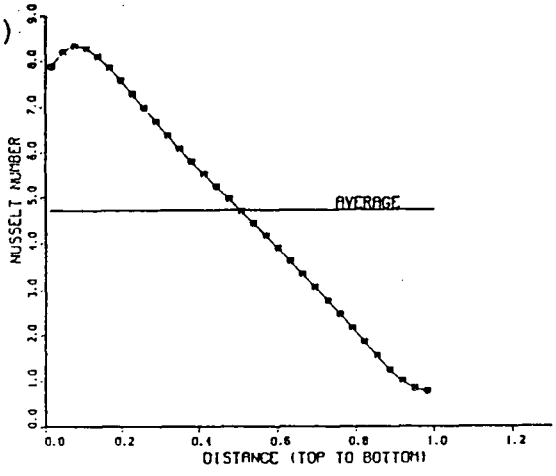
NUSSELT NUMBER
AVERAGE
DISTANCE (TOP TO BOTTOM)

correspondence on right wall and boundary correspondence on top, right and bottom walls) listed in Table 10. Also shown for purposes of discussion are contour plots of stream function and temperature as well as the local Nusselt number distributions along the two isothermal walls of the cavity. Note that these countour plots were generated using the results obtained with the finest grid (49x49) and were found to be unaffected by the set of grid and vorticity boundary conditions used.

The length of the right wall, the maximum deviation from orthogonality, the maximum stream function and the average Nusselt numbers used to monitor the accuracy of the solution are given in Figs. 22 to 26 for cases 1 to 5, respectively. These parameters are plotted as a function of the number of grid points (Table 11) and the type of boundary conditions used (Tables 9 and 10). As can be seen from Figs. 22 to 26, all of these monitored parameters eventually converge to asymptotic values as the number of grid points is increased. Considering these asymptotic values, relative errors associated with the length of the right wall, the maximum stream function and the average Nusselt numbers were calculated for the coarser grids. For example, the estimated relative errors obtained for a 33x33 grid are tabulated in Table 13 for the five extreme cases of interest. Also, the maximum deviation from orthogonality and the ratio of the difference between heat transfer rates through each isothermal wall and their mean values are

Figure 22. Plots of the monitored variables as a function of the number of discrete points for case 1.

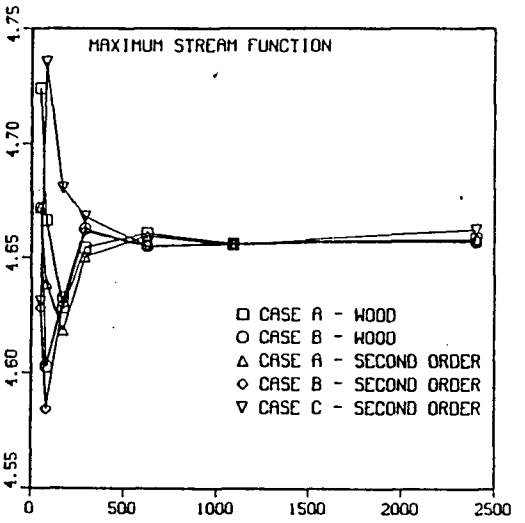

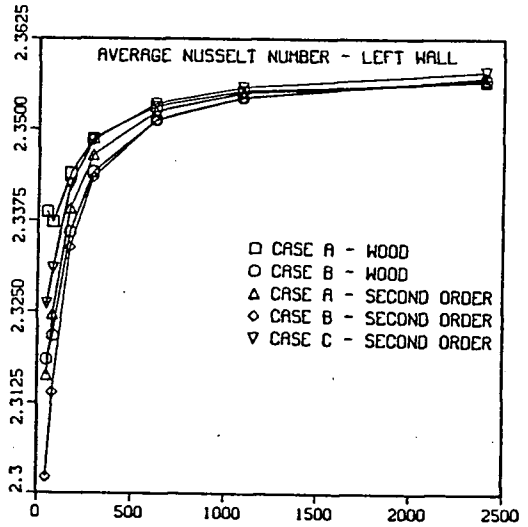

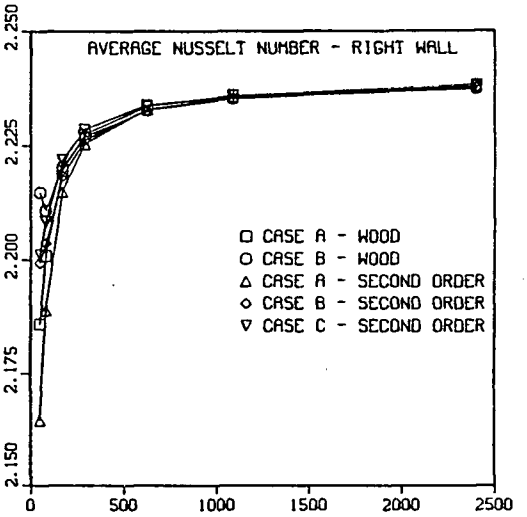

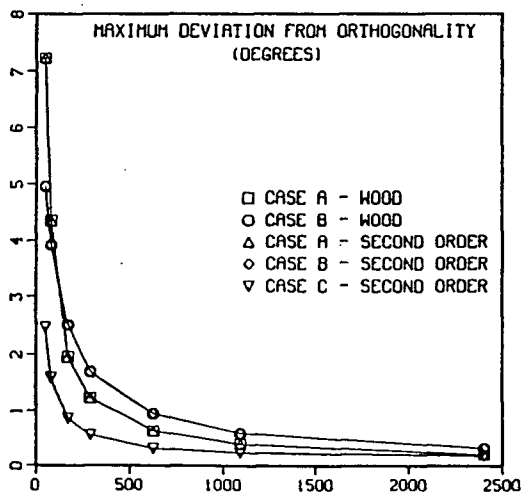

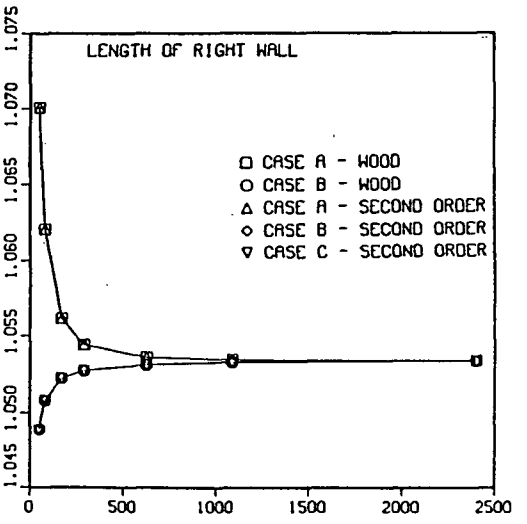

Figure 23. Plots of the monitored variables as a function of the number of discrete points for case 2.

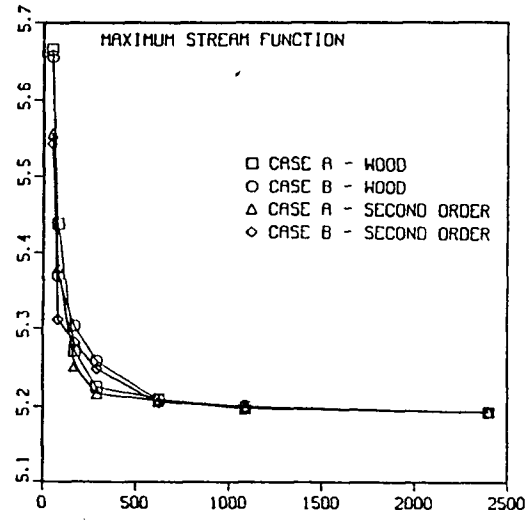

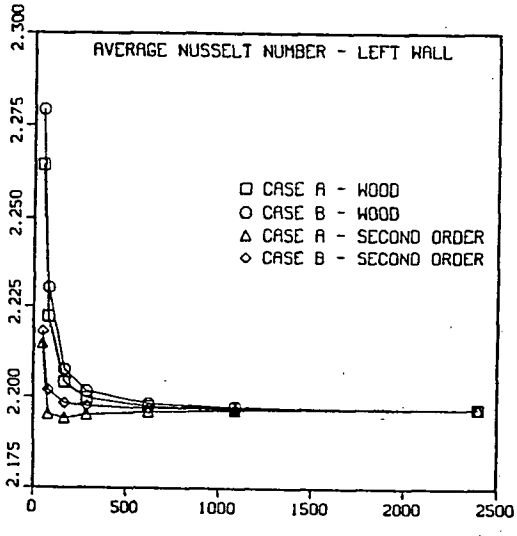

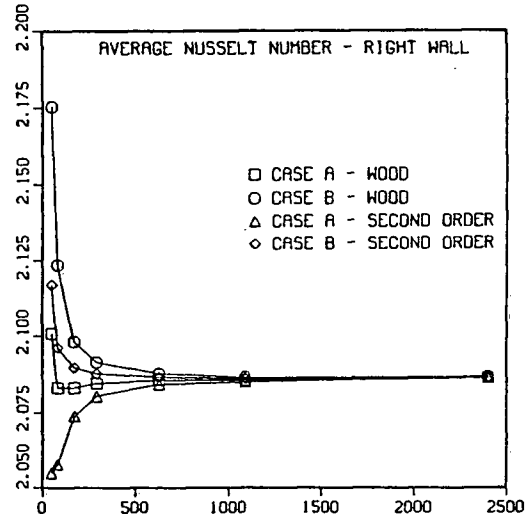

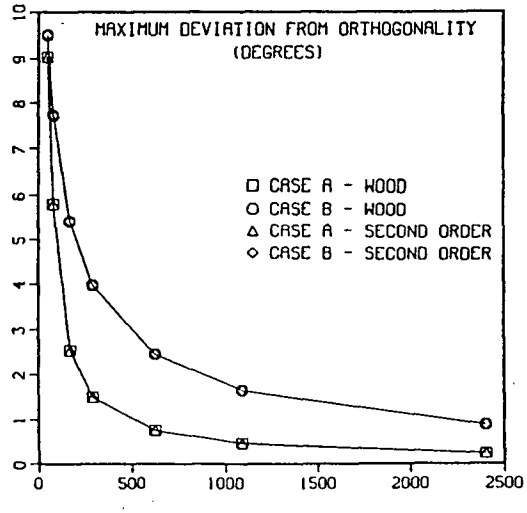

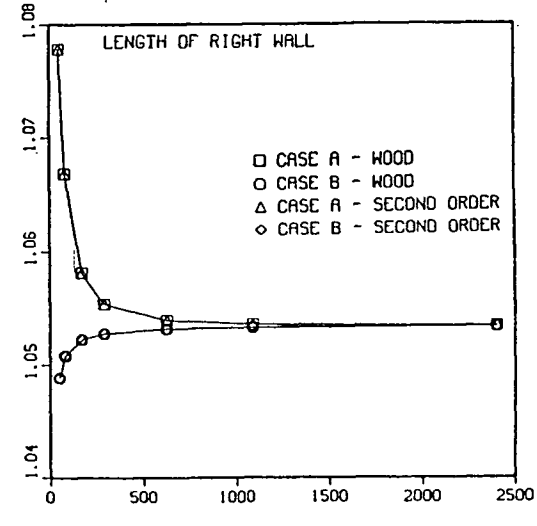

Figure 24. Plots of the monitored variables as a function of the number of discrete points for case 3.

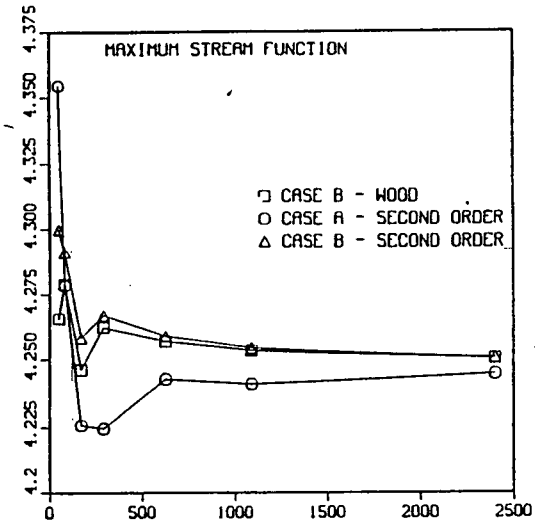

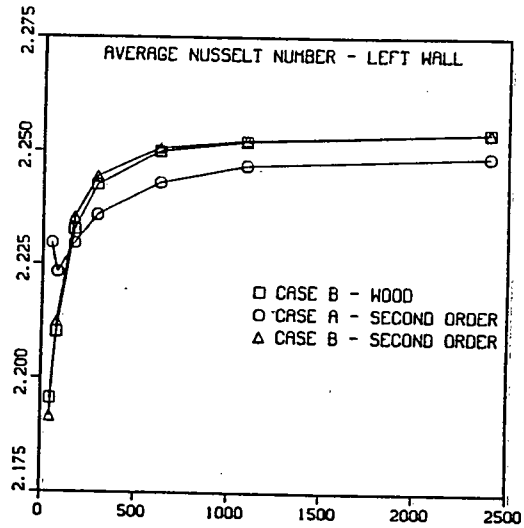

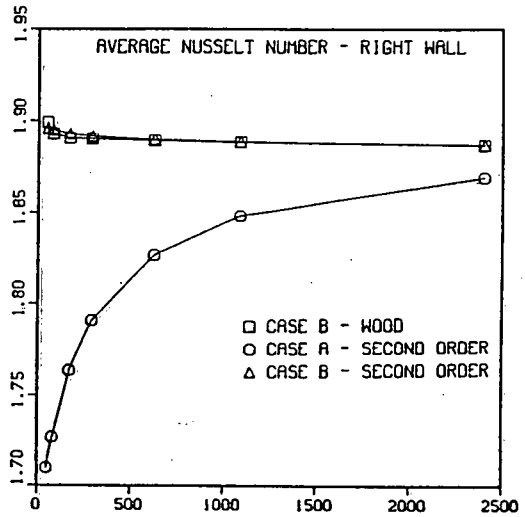

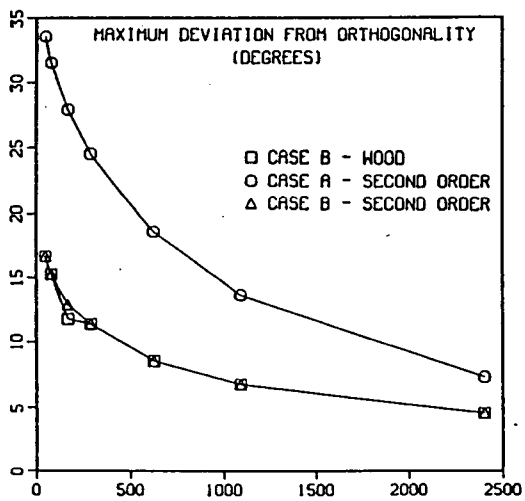

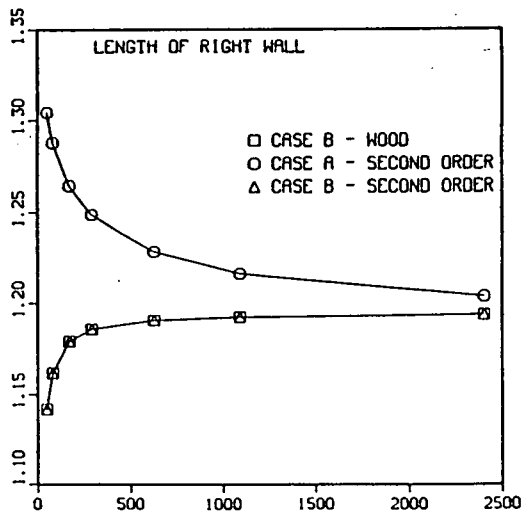

Figure 25. Plots of the monitored variables as a function of the number of discrete points for case 4.

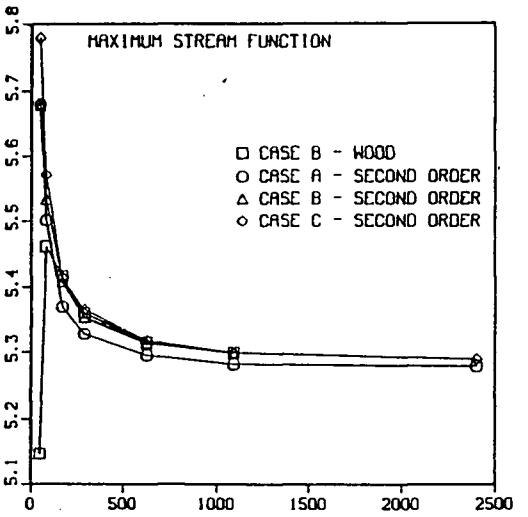

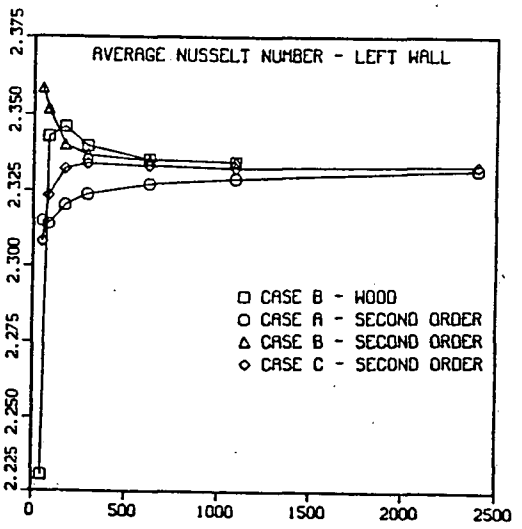

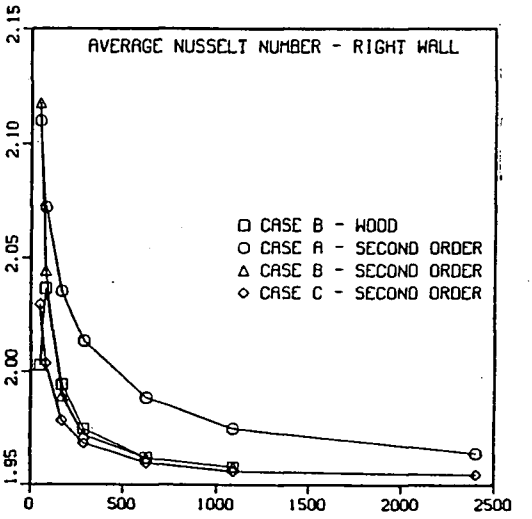

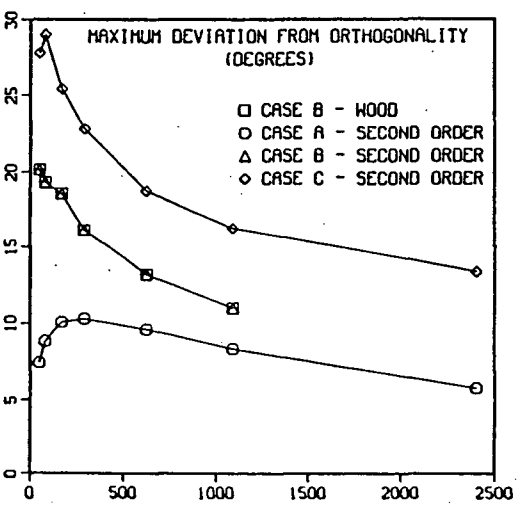

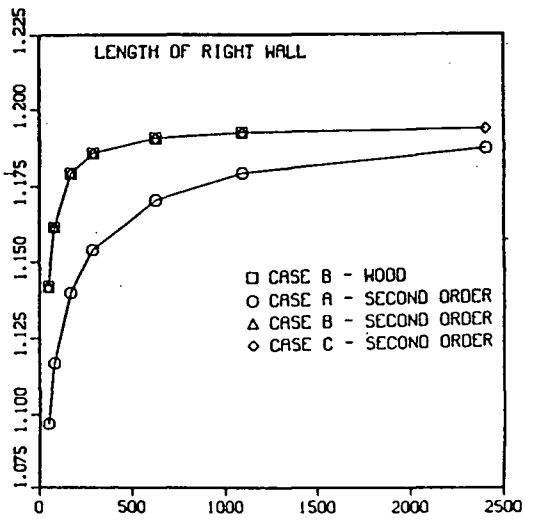

Figure 26. Plots of the monitored variables as a function of the number of discete points for case 5.

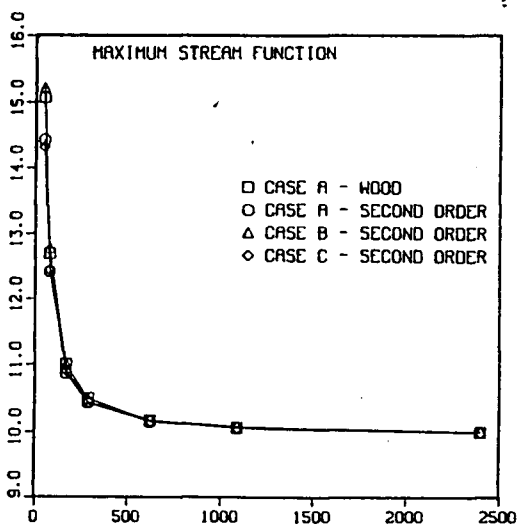

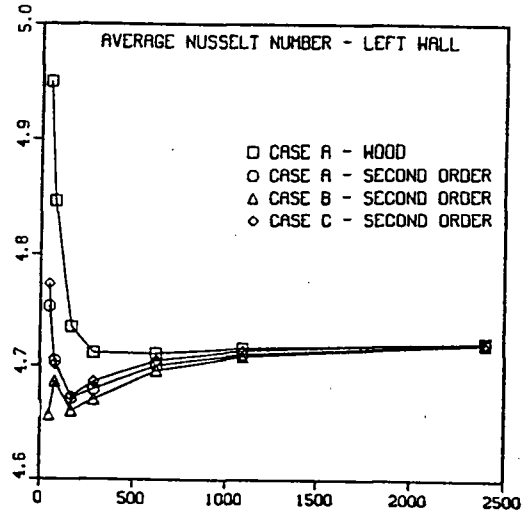

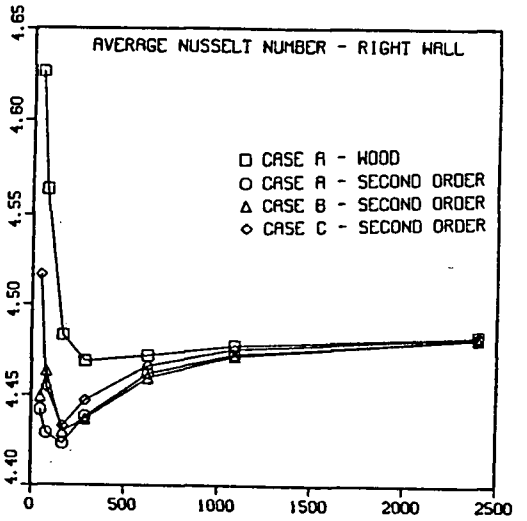

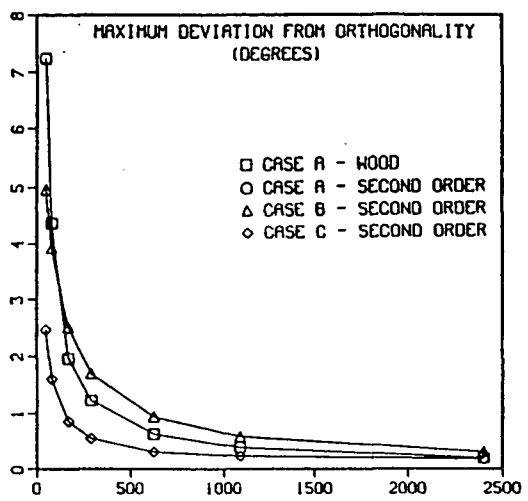

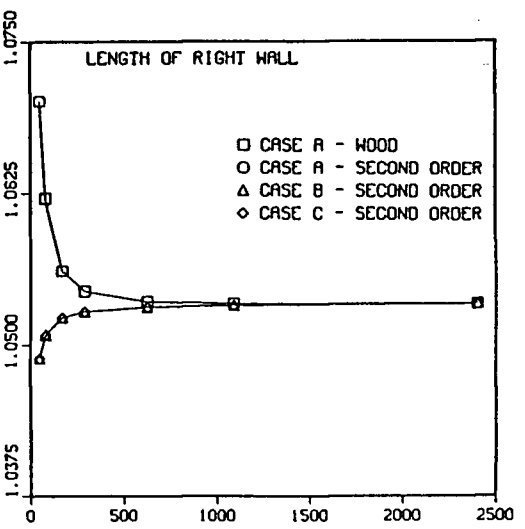

Table 13. Errors in monitored variables for cases 1 to 5 using a 33x33 grid.

Case	Grid Boundary Conditions	Vorticity Boundary Condition	Relative Error of Right Wall Length	Maximum Deviation from Orthogonality	Relative Error of Maximum Stream Function	Relative Error of Left Wall Average Nusselt Number	Relative Error of Right Wall Average Nusselt Number	Relative Error of Heat Transfer Rate
1	Case A	Wood	6.70E-5	0.386	3.75E-4	7.54E-4	9.09E-4	5.41E-5
	Case B	Wood	1.02E-4	0.588	4.18E-4	1.15E-3	1.18E-3	1.08E-4
	Case A	2nd Order	6.70E-5	0.386	5.25E-4	8.97E-4	1.05E-3	5.33E-5
	Case B	2nd Order	1.02E-4	0.588	4.18E-4	1.16E-3	1.20E-3	1.08E-4
	Case C	2nd Order	1.02E-4	0.225	5.04E-4	5.47E-4	8.01E-4	1.05E-4
2	Case A	Wood	1.47E-4	0.471	1.15E-3	6.47E-5	4.55E-4	9.06E-5
	Case B	Wood	1.17E-4	1.640	1.61E-3	2.45E-4	5.09E-5	3.54E-5
	Case A	2nd Order	1.47E-4	0.471	9.24E-4	2.17E-4	7.44E-4	9.81E-5
	Case B	2nd Order	1.17E-4	1.640	1.32E-3	1.12E-5	2.05E-4	3.42E-5
3	Case B	Wood	1.03E-3	6.74	6.23E-4	8.76E-4	7.16E-4	1.18E-4
	Case A	2nd Order	1.86E-2	13.66	2.27E-3	3.16E-3	2.06E-2	8.28E-6
	Case B	2nd Order	1.03E-3	6.74	8.58E-4	7.24E-4	8.61E-4	1.26E-4
4	Case B	Wood	1.03E-3	11.00	2.70E-3	8.16E-4	1.62E-3	1.65E-4
	Case A	2nd Order	1.20E-2	8.31	5.48E-4	1.56E-3	1.05E-2	1.44E-5
	Case B	2nd Order	1.03E-3	11.00	2.53E-3	9.08E-4	1.71E-3	1.71E-4
	Case C	2nd Order	1.03E-3	13.37	2.68E-3	4.73E-5	0.00E+0	1.59E-4
5	Case A	Wood	6.31E-5	0.386	6.79E-3	9.83E-4	1.06E-3	1.30E-5
	Case A	2nd Order	6.31E-5	0.386	5.69E-3	2.07E-3	2.15E-3	9.25E-6
	Case B	2nd Order	1.06E-4	0.588	8.19E-3	2.50E-3	2.38E-3	1.47E-5
	Case C	2nd order	1.06E-4	0.225	6.69E-3	1.42E-3	1.51E-3	2.78E-5

listed for a 33x33 grid in the same table.

C. DISCUSSION

Body-fitted orthogonal grids were generated for cases 1 to 5 considered in this exercise using all sets of grid boundary conditions defined in Table 9 with only one exception. It was not possible to generate a body-fitted orthogonal grid for case 3 with the grid boundary conditions C. It is not clear why convergence was not reached in this case, but it appears that the requirement of boundary correspondence on three faces over-constrains the problem for this particular geometry. Also, in order to obtain a converged symmetric grid for case 4 with the grid boundary conditions A, the numerical procedure had to be modified slightly. The grid boundary conditions A require the use of both Neumann and Dirichlet conditions along the entire transformed domain boundary. However, for case 4, 2 Dirichlet boundary conditions were used at, and only at, the central node of the right wall in order to obtain the symmetric mapping expected from this geometry.

To obtain an accurate numerical simulation using finite difference methods, the grid density should be highest in areas of the cavity where either the flow or the heat transfer is important, i.e. where the gradients of temperature or stream function are the greatest. It is clear from the close proximity of contour lines, that the temperature gradient is maximal in the vicinity of the

isothermal walls. The areas of highest heat transfer along the isothermal walls can be located by considering the left and right wall local Nusselt number distributions given in Figs. 17 to 21. For cavity cases 1 to 4, the top of the left wall and the bottom half of the right wall are the areas of highest heat transfer. The gradients in these areas become stronger as the Rayleigh number increases because the resulting increase in convection intensifies the local heat transfer. The fluid shear is greatest near the cavity boundary and becomes less important in the core. Again, particularly near the boundaries, the velocity gradients become steeper as the Rayleigh number increases and the flow assumes a more boundary-layer like nature.

An inspection of the numerically generated grids shown in Figs. 17 to 21 reveals that most grids have a fairly constant grid density over the entire domain. However, some grids have higher resolutions in regions where it is not justified by the gradients (eg. lower left hand corner of Fig. 17c), regions of very low grid density (eg. upper and lower right hand corners of Figs. 19a and in the middle of the right hand wall in Fig. 20a) or have problems satisfying the orthogonality condition (e.g. Fig. 20c).

The results of Figs. 22 to 26 and Table 13 also demonstrate that

1. independent of the grid and vorticity boundary conditions chosen, numerical solutions having accuracies of better than 1 percent were

obtained by using only a 22x22 grid for a Rayleigh number of 10000 with only two exceptions: cases 3 and 4 with grid boundary conditions A,

2. independent of the grid and vorticity boundary conditions chosen, numerical solutions having accuracies of better than 1 percent were obtained by using a 28x28 grid for a Rayleigh number of 100000,
3. for grids sizes larger than 30x30, the maximum stream function, average Nusselt numbers and right wall length monotically approach their asymptotic values,
4. good accuracy was obtained for the grid size of 33x33 for all cases except for cases 3 and 4 with the grid boundary conditions A,
5. it is difficult to justify which combination of grid and vorticity boundary conditions yields the most accurate results for coarser grids either because one combination of boundary conditions does not show consistent superiority over the others for all of the monitored variables or because all combinations lead to similar accuracies, and
6. the heat balance over the cavity is always well satisfied for a 33x33 grid with the present accuracy criteria.

It was somewhat surprising to discover that the different combinations of grid (with the exception of grid boundary conditions A when used with cases 3 and 4) and vorticity boundary conditions gave similar solution accuracies. The reasons why the second order vorticity boundary condition does not show any superiority to the Wood boundary condition even though the former is based on Taylor series of higher order can be explained as follows. Firstly, for the square cavity natural convection problem, Wong and Raithby [12] showed that the Wood boundary condition not only gave more accurate solutions than any of the other commonly used vorticity boundary approximations but, it yielded results which were only slightly less accurate than the second order condition. Secondly, in the present problem, the orthogonal coordinate system has to be generated numerically and hence, already contains inaccuracies. For an orthogonal system, the second order condition has more terms that require numerical manipulation of the grid characteristics than does the Wood boundary condition. Thus, it is surmised that the gain in accuracy achieved by using more terms of the Taylor series is offset, to some extent, by additional computational error associated with the numerically generated grid.

Thus, even though one of the objectives of Part I was to determine which of the grid and vorticity boundary conditions gave the most accurate numerical results for each case, there was no clear conclusion. For any given numerical

experiment, it was found that the combination of conditions which minimized the error for one dependent variable often gave poorer results for another variable. However, it was observed that, except for boundary conditions which led to undesirable grids, most combinations of grid and vorticity boundary conditions gave results of acceptable accuracy as long as a sufficient number of grid points were used. All of the natural convection results reported in Parts II and III were obtained using the Wood vorticity boundary condition, because it requires fewer numerical manipulations than does the second order boundary condition. For cavity C1, the grid boundary conditions A were chosen because the C conditions yielded high grid densities in regions which were inappropriate and the B conditions produced grids which were less orthogonal than A. For cavity C2, the grid boundary conditions B were decided upon because the A conditions lead to grids of low density in area of susceptible gradients and the C conditions result in non-orthogonal grids.

The second objective of Part I was to use the results to determine what grid size was needed to give natural convection results of acceptable accuracy. In all cases, it was found that solutions with sufficient accuracy were obtained as long as the grid size exceeded 33x33. For example, Table 13 shows that, for a 33x33 grid, the maximum error was a 0.0082 in the stream function obtained at Ra=100000 for a C1 cavity, type A grid boundary conditions and second order vorticity boundary conditions. This maximum

error is associated with the largest Rayleigh number which is in agreement with many literature observations, e.g. [12]. Therefore, the numerical natural convection results are expected to have an accuracy of better than 1 percent if a grid size of 33x33 or larger is used. As a consequence, a 35x35 grid was employed to generate all of the results in Parts II which follows. Use of a finer grid was ruled out because of the excessive computation costs.

IX. PART II

A. NUMERICAL EXPERIMENTS

The primary objective of Part II was to study the effect of the amplitude and the Rayleigh number on the natural convection flow and heat transfer in cavity types C1 and C2. The combination of the six Rayleigh numbers (0 to 100000) and five amplitudes (-0.15 to 0.15) investigated (see Table 1) yielded a total of 30 natural convection problems for each cavity. Note that these 30 experiments include several special cases. When the amplitude equals zero, the square cavity, for which there is much corroborating data in the literature, results. When the Rayleigh number equals zero, there can be no natural convection and a pure conduction problem results.

As was mentioned in the last section, the relatively simple Wood vorticity boundary condition was used in all cases since it appears to cause no loss in numerical accuracy and requires less computing time. For the cavity C1, Type A grid boundary conditions were employed while the C2 cavity used type B conditions. The different sets of grid boundary conditions are listed in Table 14. To maintain acceptable numerical accuracy for all runs, the grid size was set at 35x35.

To conserve computing time, the following procedures were utilized. Firstly, for each cavity shape, the orthogonal grid was generated only once while the Rayleigh

Table 14. Grid and vorticity boundary conditions used in Part II.

Cavity	Dimensionless Amplitude	Grid Boundary Conditions	Vorticity Boundary Condition
C1	Negative	Case A	Wood
C1	Positive	Case A	Wood
C2	Negative	Case B	Wood
C2	Positive	Case B	Wood

number was increased from 0 to 10000. Secondly, to provide better starting values each time the Rayleigh number was increased, the stream function, temperature and vorticity nodes were initialized using the final solutions obtained for the previous Rayleigh number.

B. RESULTS

The computed results for all 60 natural convection problems, including the grid, the stream function, vorticity and temperature contours as well as the local Nusselt numbers for the left and right hand walls, are presented in compact form in Appendix B. In the rest of the chapter, only the maximum stream function and the average Nusselt number of the left wall are considered further. The former characterizes the strength of the convection flow while the latter is a measure of the total heat transfer rate through the cavity. Of course, as was shown in Eq. 129, the left and right wall Nusselt numbers are simply related through the dimensionless length of the curved right wall. The maximum stream function and left wall Nusselt numbers are plotted as functions of the Rayleigh number and curved wall amplitude in Figs. 27 and 28 for cavity C1 and Figs. 29 and 30 for cavity C2. The limiting left wall Nusselt numbers for Rayleigh number equals zero (pure conduction) are presented in Table 15 and 16 for cavities C1 and C2, respectively.

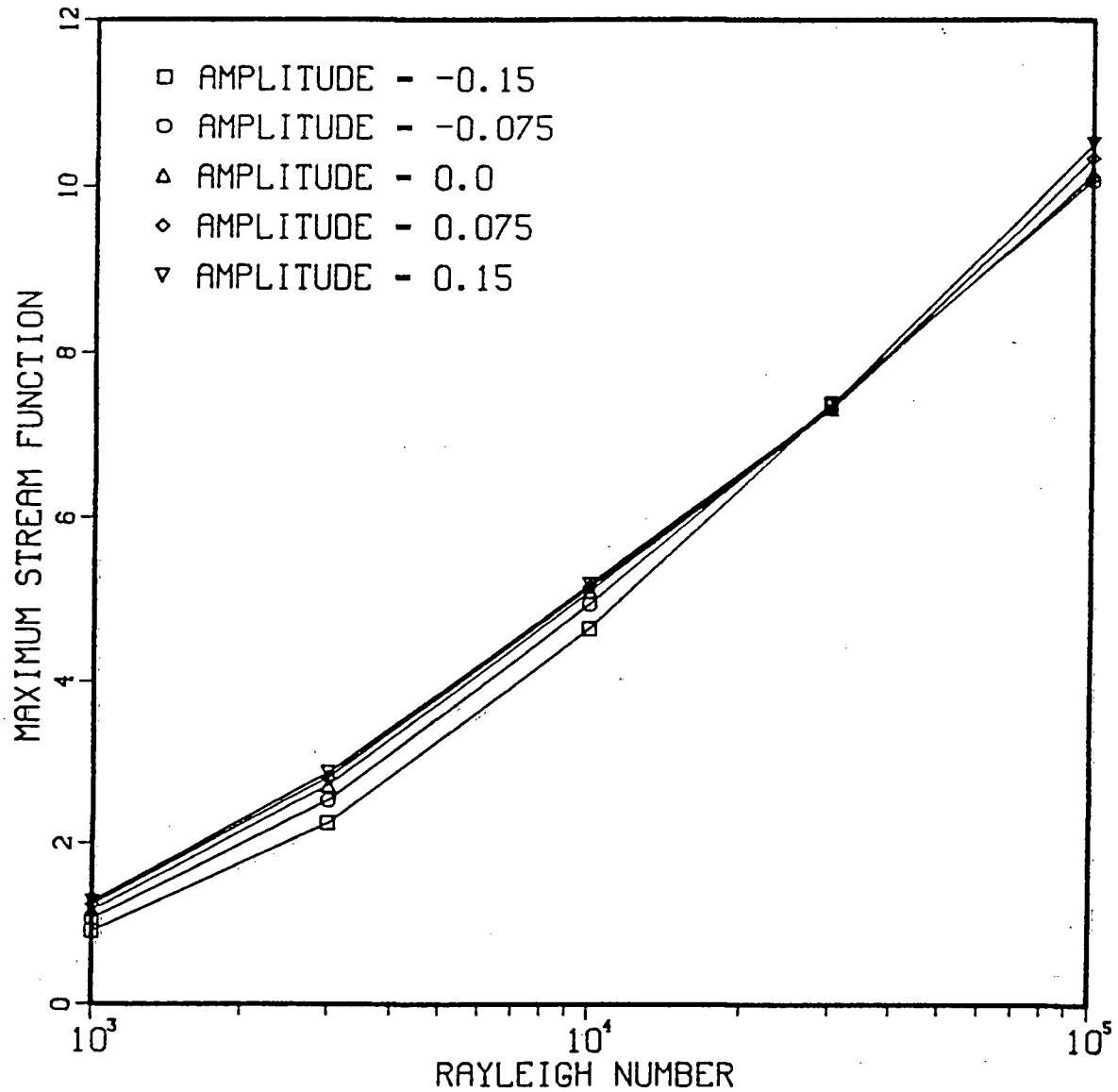

Figure 27. Plot of the maximum stream function versus the Rayleigh number for different amplitudes - cavity C1.

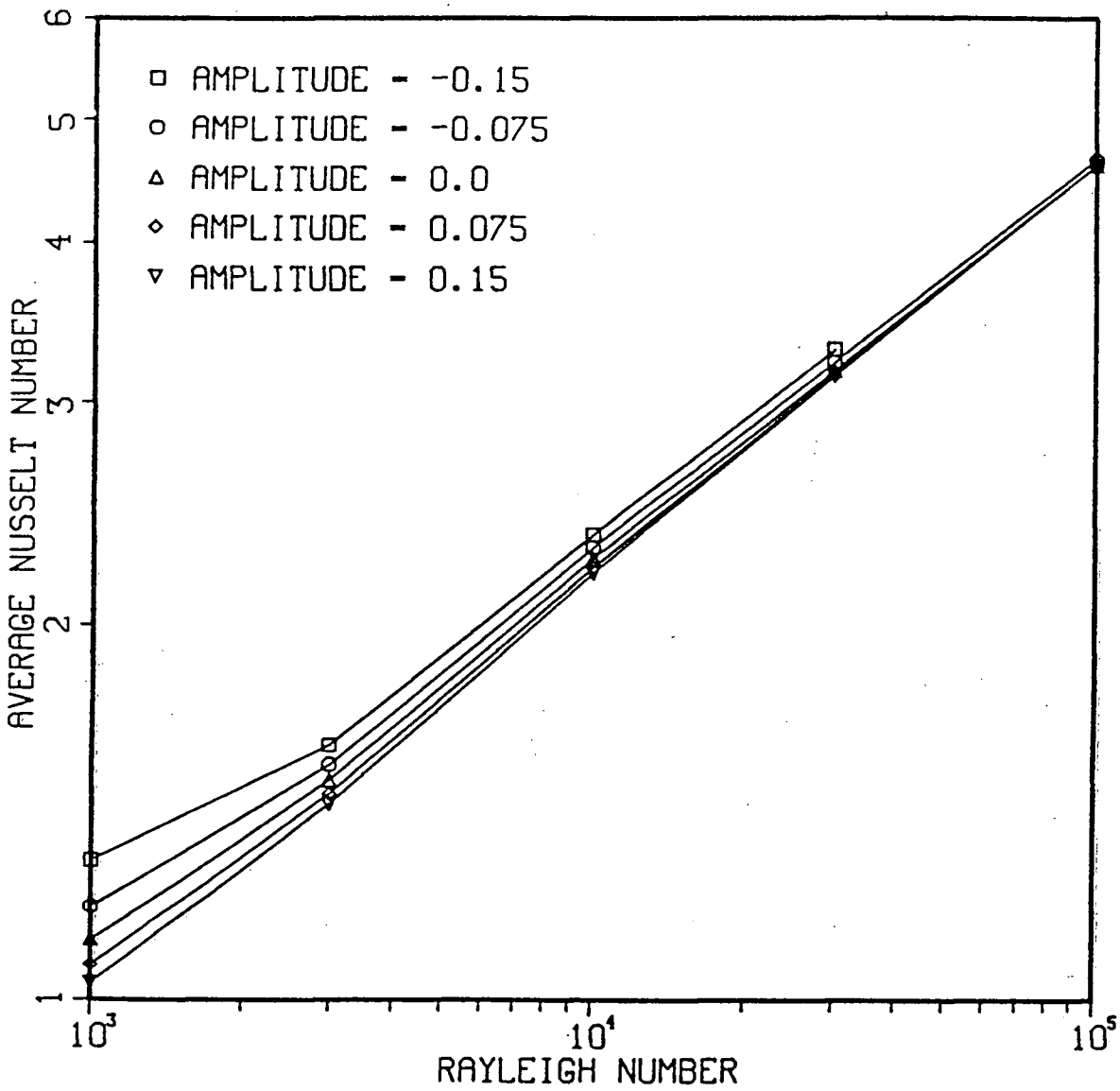

Figure 28. Plot of the average left wall Nusselt number versus the Rayleigh number for different amplitudes - cavity C1.

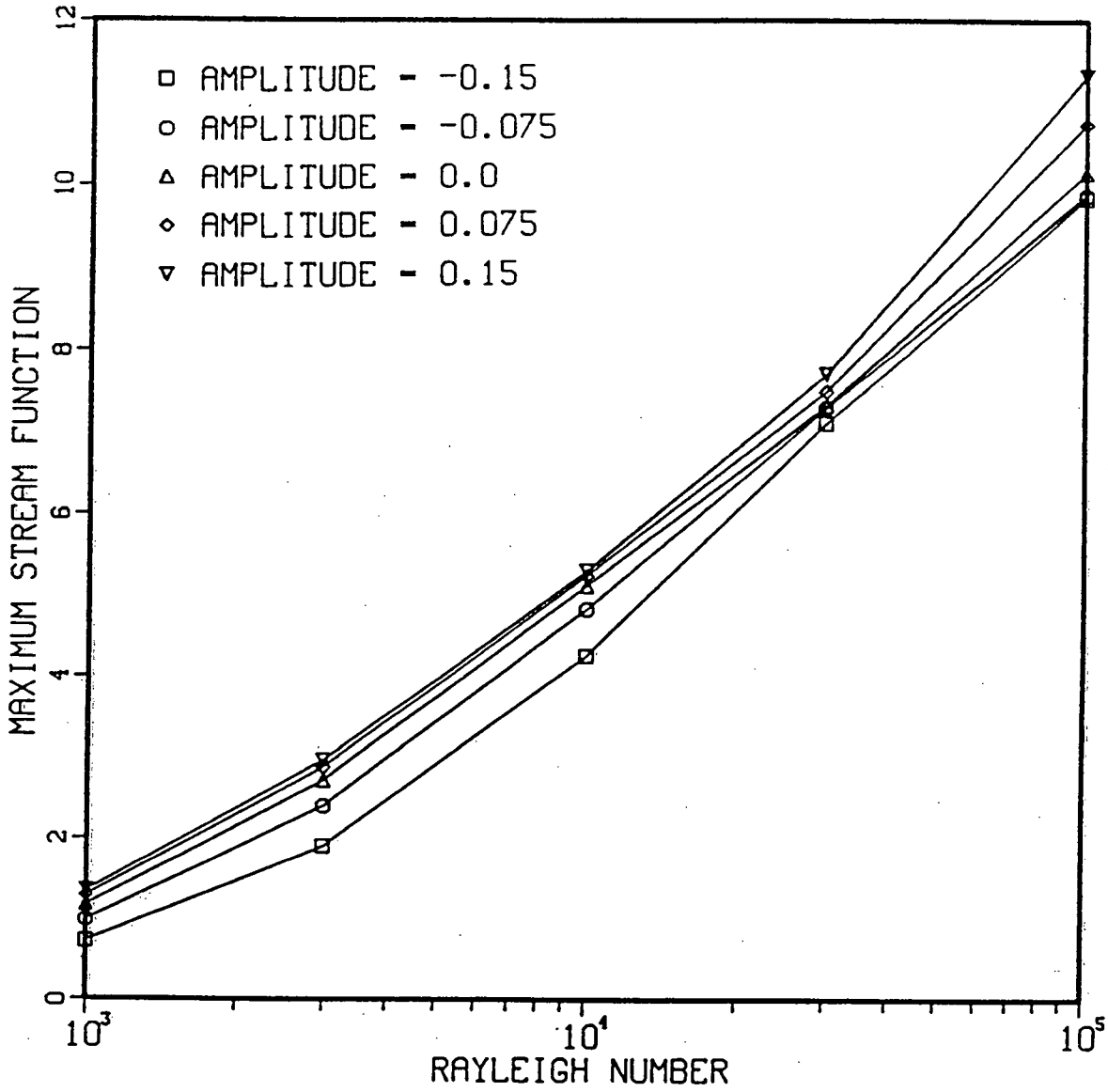

Figure 29. Plot of the maximum stream function versus the Rayleigh number and different amplitudes - cavity C2.

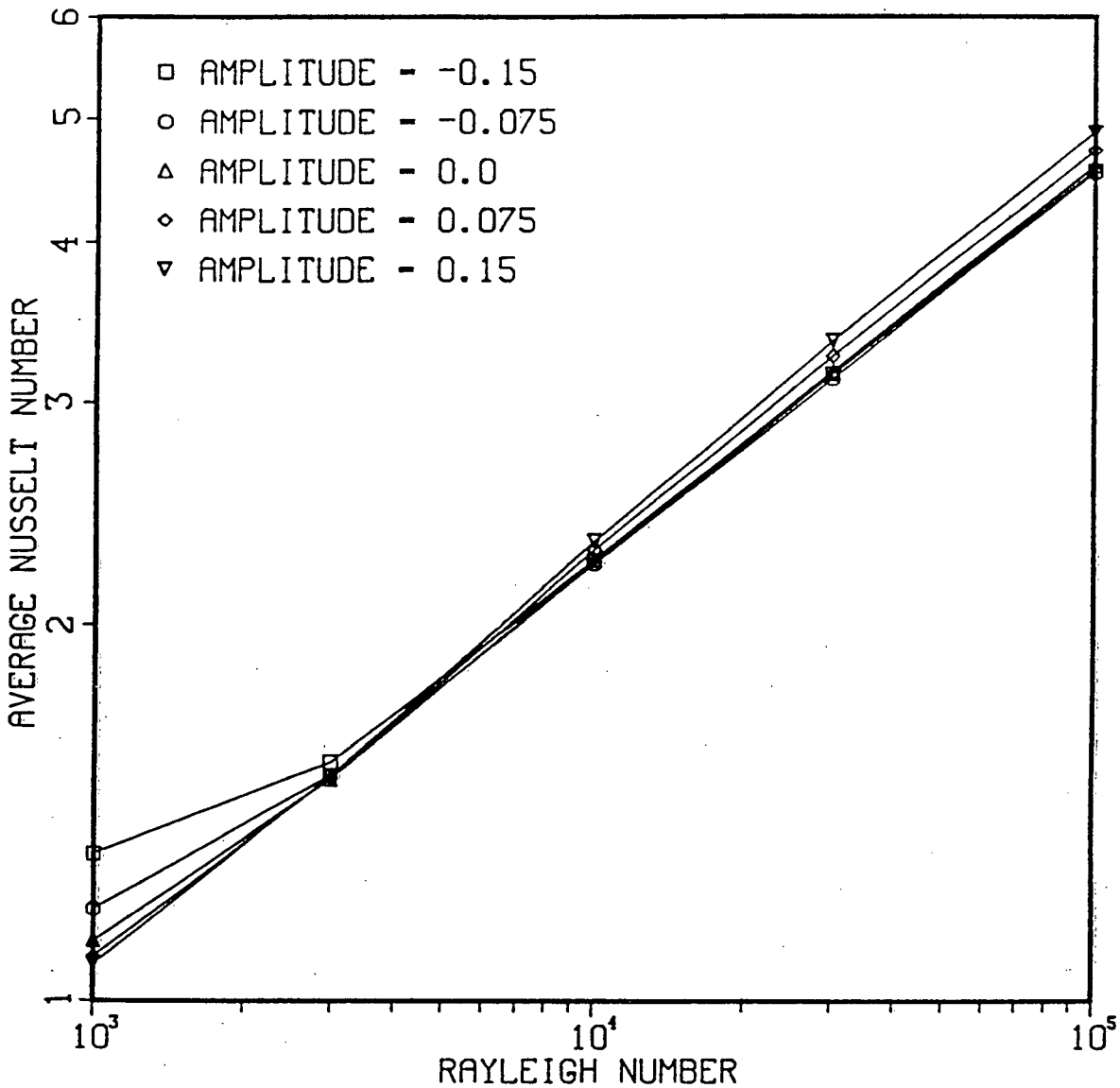

Figure 30. Plot of the average left wall Nusselt number versus the Rayleigh number and different amplitudes - cavity C2.

Table 15. Average Left wall Nusselt number as a function of amplitude for Ra=0 - cavity C1.

Dimensionless Amplitude	Average Nusselt Number
-0.150	1.224
-0.075	1.090
0.000	1.000
0.075	0.936
0.150	0.894

Table 16. Average Left wall Nusselt number as a function of amplitude for Ra=0 - cavity C2.

Dimensionless Amplitude	Average Nusselt Number
-0.150	1.262
-0.075	1.099
0.000	1.000
0.075	0.943
0.150	0.914

C. DISCUSSION

The stream function and temperature fields of the 60 natural convection problems, shown in Appendix B, are examined first. From the stream function plots, it can be seen that the "cat's-eye" flow pattern (secondary flow) occurs for both cavities C1 and C2 at a Rayleigh number of 100000 independent of the dimensionless amplitude. Apparently, for a given Rayleigh number, a similar flow pattern is obtained in all cavities regardless of their shape. Perhaps larger differences would have been observed if cavities with more extreme amplitudes had been tried. If the beginning of the laminar boundary-layer regime is considered to be reached when the derivative of the temperature with respect to the X direction is equal to zero at the middle of the cavity (even though this criterion was derived for rectangular cavity), an examination of the temperature plots shows that a boundary-layer-like regime begins to occur at a Rayleigh number of 10000 for all cavity shapes except the cavities C1 and C2 with amplitude of -0.15, which seem to require a Rayleigh number between 10000 and 30000. These results are similar to those reported in the literature for a square cavity [1,3] (Table 2).

As can be seen from Figs. 27 and 30, the maximum stream function and left wall Nusselt number are both significantly affected by the Rayleigh number and by the amplitude of the cavity. (Note that no error bars are plotted in Figs. 27 to 30; it can be assumed that the error in the maximum stream

functions and average left wall Nusselt numbers are, in all cases, less that the height of the symbols.) For both types of cavities, C1 and C2, the maximum stream function and the average Nusselt number of the left wall increase as the Rayleigh number increases. The maximum stream function also increases with increasing amplitude for both cavities C1 and C2 with one exception. For cavity C1, the amplitude has no noticeable effect on the maximum stream function at Ra=30000. The behavior of the average Nusselt number with respect to an increase of the amplitude is not so straightforward. For cavity C1, the average Nusselt number along the left wall decreases monotonically as the amplitude increases with one exception. The amplitude has a negligible effect on the average Nusselt number along the left wall at Ra=100000. However, for cavity C2, two different types of behavior are observed depending on the Rayleigh number. At low Rayleigh numbers, the average left wall Nusselt number decreases as the amplitude increases; at high Rayleigh numbers, the Nusselt number increases with increasing amplitude. For intermediate Rayleigh numbers, there is a cross-over range where the amplitude has no noticeable effect on the average Nusselt number. The trends observed for the maximum stream function and the average left wall Nusselt number as a function of amplitude are recorded in Tables 17 to 20 for each Rayleigh number.

To understand the effects of the Rayleigh number and the amplitude on the fluid flow and heat transfer in

Table 17. Percent change of the maximum stream function with increasing amplitude for a given Rayleigh number - cavity C1.

Rayleigh Number	Dimensionless Amplitude Ranges			
	-0.150 to -0.075	-0.075 to 0.000	0.000 to 0.075	0.075 to 0.150
0	-	-	-	-
1000	I	I	I	I
3000	I	I	I	I
10000	I	I	1.12	0.51
30000	0.10	-0.93	-0.09	0.57
100000	-	0.75	1.93	1.62

I: increase of 2 percent and more with an increase of the amplitude over the indicated range.
D: decrease of 2 percent and more with an increase of the amplitude over the indicated range.
-: not applicable or not defined.

Table 18. Percent change of the average left wall Nusselt number with increasing amplitude for a given Rayleigh number - cavity C1.

Rayleigh Number	Dimensionless Amplitude Ranges			
	-0.150 to -0.075	-0.075 to 0.000	0.000 to 0.075	0.075 to 0.150
0	D	D	D	D
1000	D	D	D	-1.94
3000	D	D	D	D
10000	D	D	-1.53	-1.07
30000	D	-1.53	-0.73	-0.26
100000	-	-1.02	-0.16	0.21

I: increase of 2 percent and more with an increase of the amplitude over the indicated range.
D: decrease of 2 percent and more with an increase of the amplitude over the indicated range.
-: not applicable or not defined.

Table 19. Percent change of the maximum stream function with increasing amplitude for a given Rayleigh number - cavity C2.

Rayleigh Number	Dimensionless Amplitude Ranges			
	-0.150 to -0.075	-0.075 to 0.000	0.000 to 0.075	0.075 to 0.150
0	-	-	-	-
1000	I	I	I	I
3000	I	I	I	I
10000	I	I	I	1.05
30000	I	0.43	I	I
100000	0.40	I	I	I

I: increase of 2 percent and more with an increase of the amplitude over the indicated range.
D: decrease of 2 percent and more with an increase of the amplitude over the indicated range.
-: not applicable or not defined.

Table 20. Percent change of the average left wall Nusselt number with increasing amplitude for a given Rayleigh number - cavity C2.

Rayleigh Number	Dimensionless Amplitude Ranges			
	-0.150 to -0.075	-0.075 to 0.000	0.000 to 0.075	0.075 to 0.150
0	D	D	D	D
1000	D	D	D	-1.45
3000	D	-0.65	0.23	0.26
10000	-0.62	0.77	1.79	1.66
30000	-0.92	1.37	I	I
100000	-0.36	1.29	I	I

I: increase of 2 percent and more with an increase of the amplitude over the indicated range.
D: decrease of 2 percent and more with an increase of the amplitude over the indicated range.
-: not applicable or not defined.

non-rectangular cavities, it is useful to reconsider the fundamental mechanisms involved in the natural convection phenomena.

The driving force for fluid flow in natural convection is the density difference. It results from the interaction between the gravitational body force and the hydrostatic pressure gradient and can be approximated in the present circumstances as a pure temperature effect. After dimensional analysis, the source term which drives the fluid flow is the body force term (last term on the right hand side) of Eq. 37. For a dimensionless reference temperature of 0.5, the body force term can take on positive, zero or negative values. These values correspond respectively to a body force acting upwards, a null body force or a body force acting downwards. Equation 37 shows that the body force term is the product of the Rayleigh number, the Prandtl number and the difference between the local and reference dimensionless temperatures. The dimensionless groups involved in the body force term, i.e. Ra and Pr, gather together the constant parameters affecting the natural convection problem: the values of the fluid properties evaluated at the reference temperature plus the cavity characteristic length and characteristic temperature difference. For the cavity as a whole, the strength of the natural convection flow is given by the maximum stream function and is therefore directly influenced by both Ra and Pr. The maximum stream function is also affected by the

specific geometry of the cavity. However, the relationship between the strength of the flow and the cavity geometry is, in general, far more complex.

In all convection problems, heat is transferred by both conduction and convection. Therefore, the rate of heat transfer, which is given in dimensionless terms by the average Nusselt number, is directly influenced by the following two factors:

1. the mean distance which separates the two isothermal walls, and
2. the strength of the fluid flow.

The first factor affects the amount of heat transfer through the cavity by both the conduction and convection mechanisms. If conduction dominates, the larger the distance between the two isothermal walls, the smaller will be the amount of heat transferred through the cavity. Also, when convection is the dominant mechanism, the larger the distance between the two isothermal walls, the more time the warmer stream flowing near the upper adiabatic wall has to transfer energy by conduction through the core to the cooler stream flowing along the lower adiabatic wall. Thus, the greater is the heat exchange between these two counterflowing parts of the loop, the less will be the net rate of heat transfer between the two isothermal walls.

Considering these different factors which play a role in natural convection flow and heat transfer, let's now try to interpret the results of Figs. 27 to 30, and Tables 17 to

20.

Consider cavity C1 first. There are two factors which explain why the maximum stream function increases with increasing amplitude. Regardless of the amplitude, a cold element from the bottom left corner of the cavity must move to the bottom right corner to replace a fluid element ascending because of the buoyancy induced by the hot right wall. As the amplitude decreases from 0 to -0.15, the bottom right corner of the cavity acts as a dead end to the fluid flow. Also, the fluid element which rises along the inward-sloping right wall works again it, exerting a pressure on the wall rather than accelerating the element to a higher velocity. Conversely, when the amplitude is raised from 0 to 0.15, the dead end dissappears and now an element of fluid warmed by the hot surface is free to rise unhindered to the very top of the cavity. As a consequence of these two factors, the maximum stream function generally increases as the amplitude is increased. However, for some inexplicable reason, the amplitude has no observable effect on the maximum stream function at Ra=30000.

Because the body force term of Eq. 37 is directly proportional to the Rayleigh number, the fluid flow strength, as expected, increases substantially as the Rayleigh number is raised.

Contrary to the fluid flow behavior, the heat transfer rate depends on factors which have opposing effects. Therefore, to explain the behavior of the average Nusselt

number along the left wall with respect to the dimensionless amplitude and the Rayleigh number, let's inspect the relative importance of each of these factors separately.

Without fluid flow, the average Nusselt number of the left wall decreases as the mean distance between the isothermal walls increases simply because the average length of the conduction path becomes larger. This trend is clearly indicated by Tables 15 and 16, for Ra=0. Note that when Ra=0 and A=0 (square enclosure for both cavities C1 and C2), the Nusselt number is exactly unity.

In the presence of fluid flow, the changing amplitude causes two opposing effects on the Nusselt number of the left wall. As was just observed, the strength of fluid flow increases as the amplitude increases. Thus, on the basis of this fact alone, it might be expected that the Nusselt number of the left wall would be magnified as the amplitude was increased. However, as the amplitude becomes larger, the heat transferred from the hot stream flowing along the adiabatic top wall to the cold stream flowing along the adiabatic bottom wall by conduction through the core increases. Furthermore, the average length of the conduction path between the isothermal walls also increases. These two factors would cause the average Nusselt number to diminish with increasing amplitude. Therefore, to rationalize the general trend observed, i.e. that the average Nusselt number along the left wall of the C1 cavity decreases as the amplitude increases, the effect of increasing the average

distance between the two isothermal walls must be dominating over the effect of increasing the strength of convection.

The average Nusselt number of the left wall increases substantially as the Rayleigh number increases due to the increasing strength of the flow.

Consider now the C2 cavity. There again appear to be two factors which explain why the fluid flows become stronger with increasing amplitude. First of all, for negative amplitudes, the bottom right corner of the cavity acts as a dead end to fluid flow in a similar fashion as it did for the corresponding C1 cavity. However, there is a far less abrupt change in the direction of the fluid flow in both the top and bottom right corners for positive amplitudes compared to negative amplitudes. Therefore, in the former case, less momentum is transformed into a pressure increase. Secondly, an element of warm fluid arising from the hot right wall can travel, on average, a much further distance before its upward motion is impeded by a horizontal or inward sloping wall.

The Rayleigh number affects the fluid flow strength in a similar fashion as was explained for the C1 Cavity.

Without fluid flow, the average Nusselt number of the left wall increases as the mean distance between isothermal walls increases, as expected. However, in presence of fluid flow, the effect of the amplitude on the average Nusselt number again involves the two factors with opposing effects: flow strength and distance between isothermal walls, as were

discussed for the C1 cavity. As the amplitude increases, the strength of the fluid flow increases and consequently the average Nusselt number along the left wall is expected to rise. Also, as the amplitude increases, the average length separating the two isothermal walls increases, and consequently the average Nusselt number along the left wall should decrease (due to the combined effects of increasing the conduction heat transfer resistance between the two isothermal walls and the amount of conduction heat exchange between the hot and cold streams flowing countercurrently near the two adiabatic walls). The fact that the calculated average Nusselt numbers along the left wall decrease with increasing amplitude at low Rayleigh numbers can be attributed to the dominant effect of an increasing average distance between the two isothermal walls. The reverse trend which is observed at high Rayleigh numbers suggests that the effect of fluid flow strength becomes the more important factor.

Because the increase in Rayleigh number leads to substantial increases in the strength of fluid flow, the average Nusselt number along the left wall increases directly with Rayleigh number.

D. EMPIRICAL CORRELATIONS

When the average left wall Nusselt number was plotted as a function of Rayleigh number on log-log coordinates, it was observed that a linear relationship was obtained, at

least for conditions where convection was the dominant heat transfer mechanism. Thus, for this convection dominated regime, the average Nusselt number results for each cavity shape were fitted to a simple power law relationship having the same form as Eq. 8. The empirical parameters, a and b, were obtained by a least squares linear fit of the logarithmic results and are reported in Tables 21 and 22. No statistical analysis was performed on the fitting parameters because it was recognized that an unsufficient number of points were used to obtain these results. Nonetheless, the fitting parameters determined in the present study for distorted cavities are similar in magnitude to those listed in the literature for more regular enclosures. The values of the coefficients a and b calculated from the results of the present study for a square cavity were found to differ by only 4 and 2 percent, respectively, from the coefficients obtained by De Vahl Davis and Jones [15] in their benchmark solution to this special problem. Note that for both types of cavities, the coefficient a decreases while the coefficient b increases as the amplitude is raised. A decreasing value of the coefficient a reflects the fact that the Nusselt number diminishes as the amplitude increases while an increasing value of coefficient b is indicative of the stronger flows that are possible with larger amplitudes.

Table 21. Curve fitting coefficients of the simple power law model for cavity C1 with different amplitudes.

Dimensionless Amplitude	Curve Fitting Coefficients	
	a	b
-0.150	0.138	0.307
-0.075	0.139	0.304
0.000	0.131	0.308
0.075	0.122	0.314
0.150	0.115	0.320

Table 22. Curve fitting coefficients of the simple power law model for cavity C2 with different amplitudes.

Dimensionless Amplitude	Curve Fitting Coefficients	
	a	b
-0.150	0.135	0.305
-0.075	0.133	0.306
0.000	0.131	0.308
0.075	0.128	0.312
0.150	0.122	0.320

X. PART III

A. NUMERICAL EXPERIMENTS

The primary objective of Part III was to investigate the possibility of using the present numerical approach to simulate natural convection flows in a two-dimensional non-rectangular enclosure whose shape results from a phase change process. More specifically, an attempt was made to reproduce numerically the steady-state fluid circulation pattern observed experimentally in the liquid water phase during an ice formation process. Eckert [42] carried out a number of ice forming experiments in a 5x5 cm^2 vertical square cavity. Initially, the heavily insulated cavity was filled with water whose temperature was equilibrated at the hot wall value by passing the same constant temperature fluid through the copper chambers forming the isothermal end walls. At zero time, the fluid in the right hand chamber was replaced by a second fluid from a refrigerated bath whose temperature was well below the freezing point of water. Soon thereafter, ice began to form on the cooler surface. Simultaneously, the changing flow pattern of the liquid in the cavity was visualized by a "streak photography" method. In this technique, neutrally-buoyant reflective pliolite particles suspended in the water were illuminated by a thin sheet of laser light and photographed at right angles to the main flow direction. Thus, the objective was to try and duplicate this streak pattern at a given instant in time for

a few different warm wall temperatures.

Since the present program was set up to analyze steady-state natural convection, it was necessary to assume that the process was quasi-steady, i.e., even though the ice interface is growing with time, the flow in the liquid phase is insensitive to this movement. This assumption seems quite reasonable under the present circumstances as it was observed that while the ice interface required many hours to reach its steady-state configuration, disturbances in the liquid phase took only a few minutes to become completely damped. Also the temperature boundary conditions were assumed to be as follows: left wall, hot isothermal wall; right wall, cold isothermal wall; and top and bottom walls, adiabatic walls. The growing ice surface was, of course, at 0°C. But there was likely some variation in temperature over the hotter "isothermal" wall and some heat gain through the two "adiabatic" surfaces.

Before the existing program could be used for the Part III simulations, two major modifications had to be carried out. First, the linear relationship assumed between the fluid density and the temperature does not hold for water in the temperature range from 0 to 15 degrees Celsius. In this range, the coefficient of thermal expansion is no longer constant and for the present purposes was represented by a cubic polynomial obtained by fitting the density versus temperature data given in the Handbook of Physics and Chemistry [51] for water between 0 and 20°C. A reanalysis of

the momentum equations using similar assumptions as before shows that a non-linear relation between density and temperature affects only the source term and it can be conveniently incorporated into the present program through a variable Rayleigh number which can be defined as

$$Ra=\frac{g\rho_o L_c^3 C_{p^o}(T_h-T_c)}{\mu_o k_o}\left[-\frac{\partial\rho}{\partial T}\right] \qquad (130)$$

Thus, the Rayleigh number becomes dependent on the local temperature through the relationship between $\partial\rho/\partial T$ and T. All other properties in Eq. 130 are taken to be constant and are once again evaluated at a reference temperature. These constant values are calculated using other empirical relationships obtained by fitting property data available in the literature.

The second modification concerns the method of representing the shape of the liquid-solid interface. The relationship for the interface position, X=F(Y), can no longer be given by a simple analytical formula. This problem was overcome by fitting a set of cubic spline interpolation formulae to discrete positional data taken directly from the photographs. In the cubic spline interpolation method [48,50], the variation of the dependent parameter in the interval between each pair of discrete points is represented by a cubic polynomial whose coefficients are obtained by matching conditions of continuity and smoothness at the discrete points. The extra pair of conditions needed

to evaluate the splines are obtained by using cubic equations passing through the first four and last four points to determine the initial and final slopes of the first and last splines, respectively. (Note that these end point derivatives were approximated numerically by using the divided difference technique [48-50]).

Of the many experimental results reported by Eckert [42], four cases were chosen for numerical simulation. The specific experimental and numerical parameters used in each case are reported in Table 23. In all four cases, the ice block was nearing its final steady-state shape and hence, the ice-water interface was growing only very slowly with time. The primary independent variable in these experiments was the warm wall temperature which was raised progressively from 2.5 to 15.1°C, a range which encompasses the density extremum. The reference temperature of the liquid phase, i.e. the temperature at which the constant properties were evaluated, was taken to be the average of the hot wall and the ice-water interface temperatures. The characteristic length (i.e. height or width) of the experimental chamber was 5 cm. Unfortunately, it was found that in order to obtain a converged solution with a reasonable amount of computing effort, a somewhat smaller characteristic length had to be used in two of the four numerical simulations. Reducing the characteristic length significantly reduces the range of the variable Rayleigh number (see Eq. 130). Thus, the characteristic

Table 23. Experimental and numerical conditions used for low temperature water natural convection trials.

Case	Hot Wall Temperature (Degrees Celsius)	Cold Wall Temperature (Degrees Celsius)	Characteristic Length of the Vertical Square Cavity (cm)		Liquid Phase Reference Temperature (Degrees Celsius)	Prandtl Number	Rayleigh Number Ranges	
			Experimental	Numerical simulation			Experimental	Numerical Simulation
1	2.3	-9.8	5.0	5.0	1.15	12.69	-7.90E5 to -3.45E5	-7.90E5 to -3.45E5
2	5.6	-9.8	5.0	5.0	2.8	11.94	-1.92E6 to 8.39E5	-1.92E6 to 8.39E5
3	8.6	-11.8	5.0	1.5	4.33	11.31	-2.95E6 to 3.82E6	-7.97E4 to 1.03E5
4	15.1	-11.8	5.0	1.5	7.55	10.12	-5.18E6 to 1.74E7	-1.40E5 to 4.70E5

length was reduced to 1.5 cm for the third and fourth cases (see Table 23). Although these characteristic length modifications will certainly change the strength of the flows in the distorted cavities, it was hoped that the general circulation patterns would remain qualitatively the same. This would be particularly true if, at the lower Rayleigh number range, a laminar boundary-layer regime had already been established. It was expected that the flow patterns would not change enormously with further increase in Rayleigh number once this regime has been reached.

In each simulation, the type B grid boundary conditions (boundary correspondence on the curved wall) and the Wood vorticity boundary condition were employed. A 15x33 grid was used to simulate cases 1 to 3 while a 33x33 grid was employed in case 4. These grid sizes gave similar grid densities as in Part II. The results are presented in Figs. 31 to 34 and include, for each case, the body-fitted orthogonal grid, the temperature and stream function countour plots as well as the local Nusselt number distributions along the ice-water interface and the hot wall. A reproduction of the experimental streak pattern [42] is also shown for comparison with the numerical streamline plot.

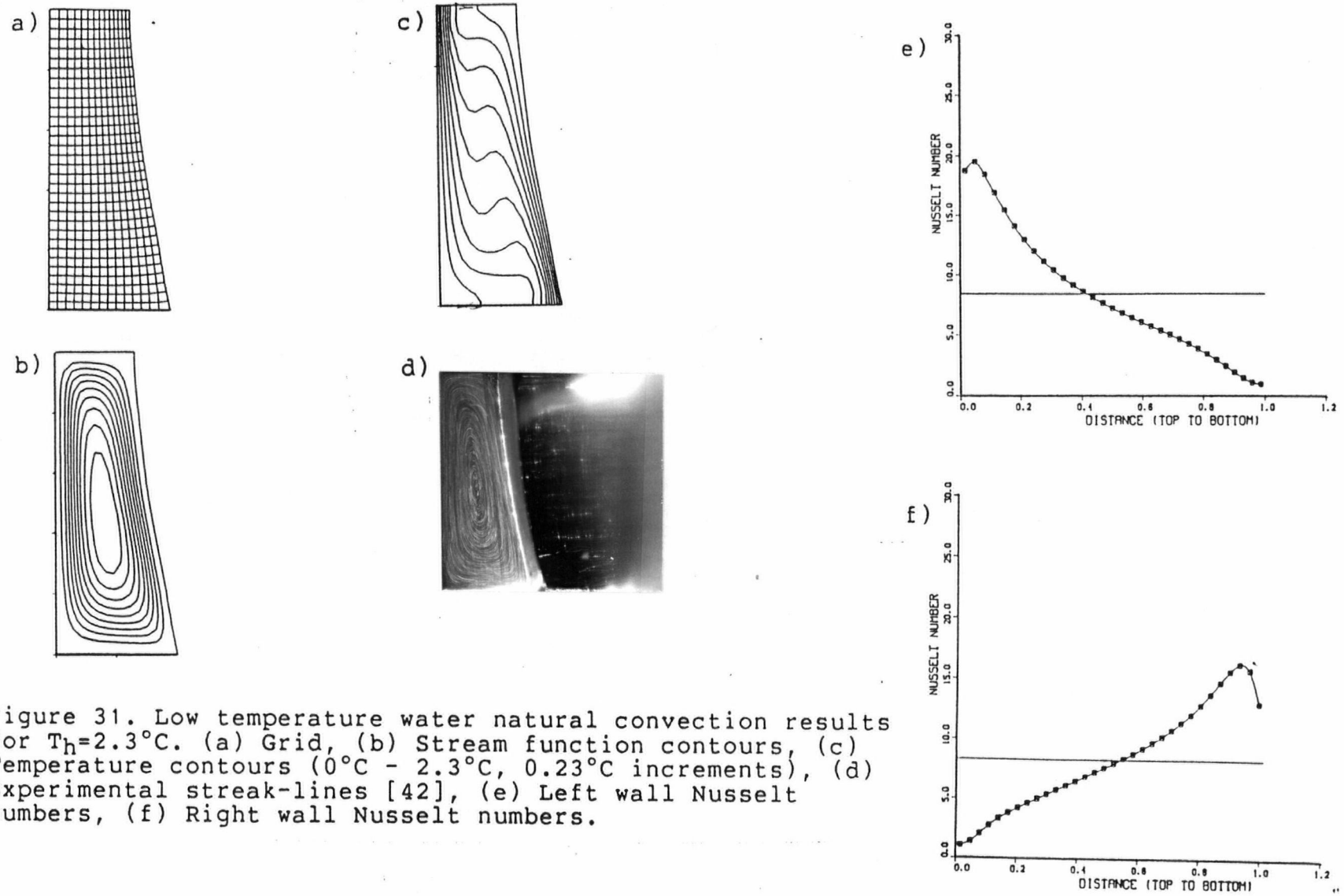

Figure 31. Low temperature water natural convection results for T_h=2.3°C. (a) Grid, (b) Stream function contours, (c) Temperature contours (0°C - 2.3°C, 0.23°C increments), (d) Experimental streak-lines [42], (e) Left wall Nusselt numbers, (f) Right wall Nusselt numbers.

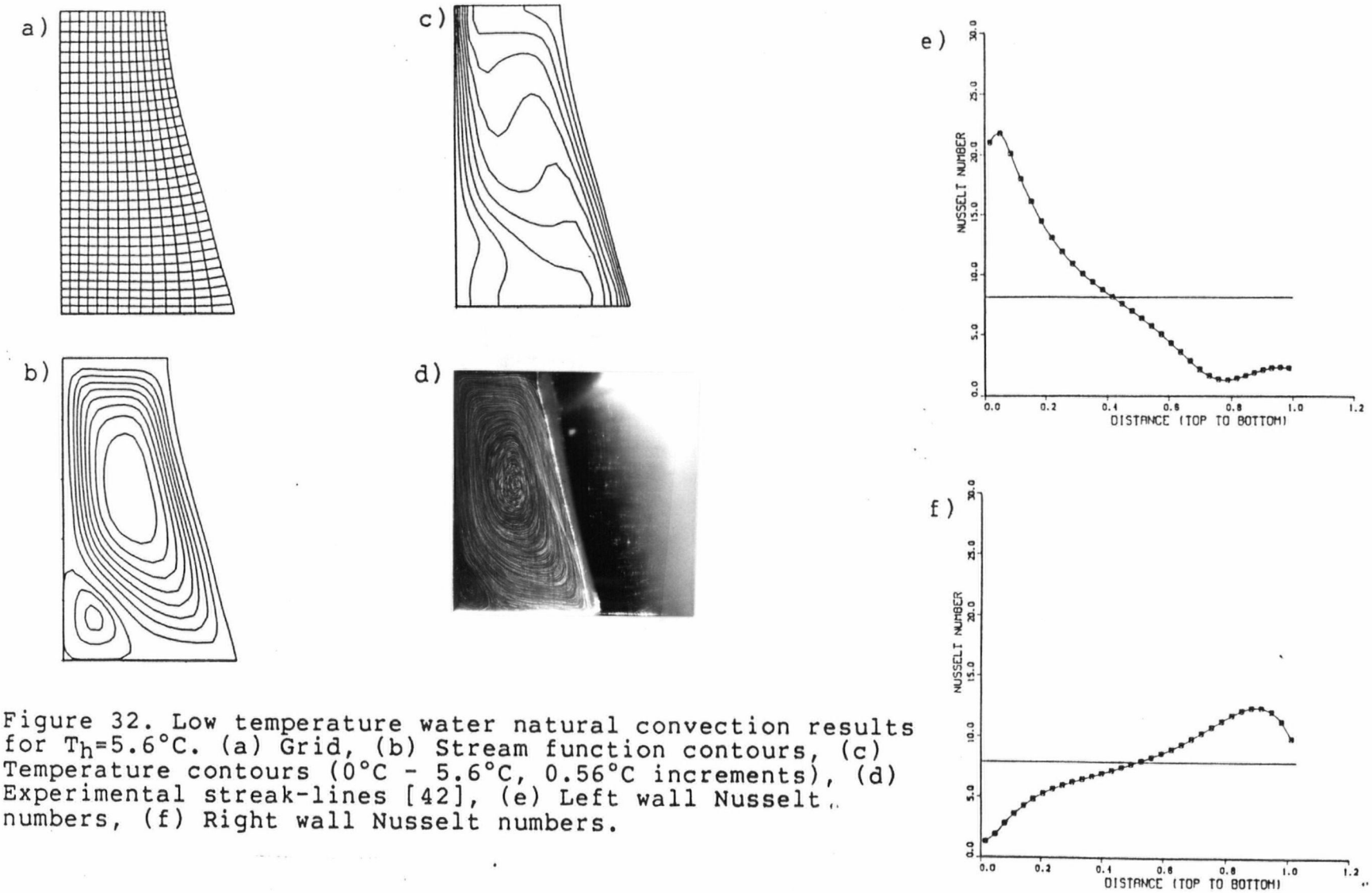

Figure 32. Low temperature water natural convection results for T_h=5.6°C. (a) Grid, (b) Stream function contours, (c) Temperature contours (0°C - 5.6°C, 0.56°C increments), (d) Experimental streak-lines [42], (e) Left wall Nusselt numbers, (f) Right wall Nusselt numbers.

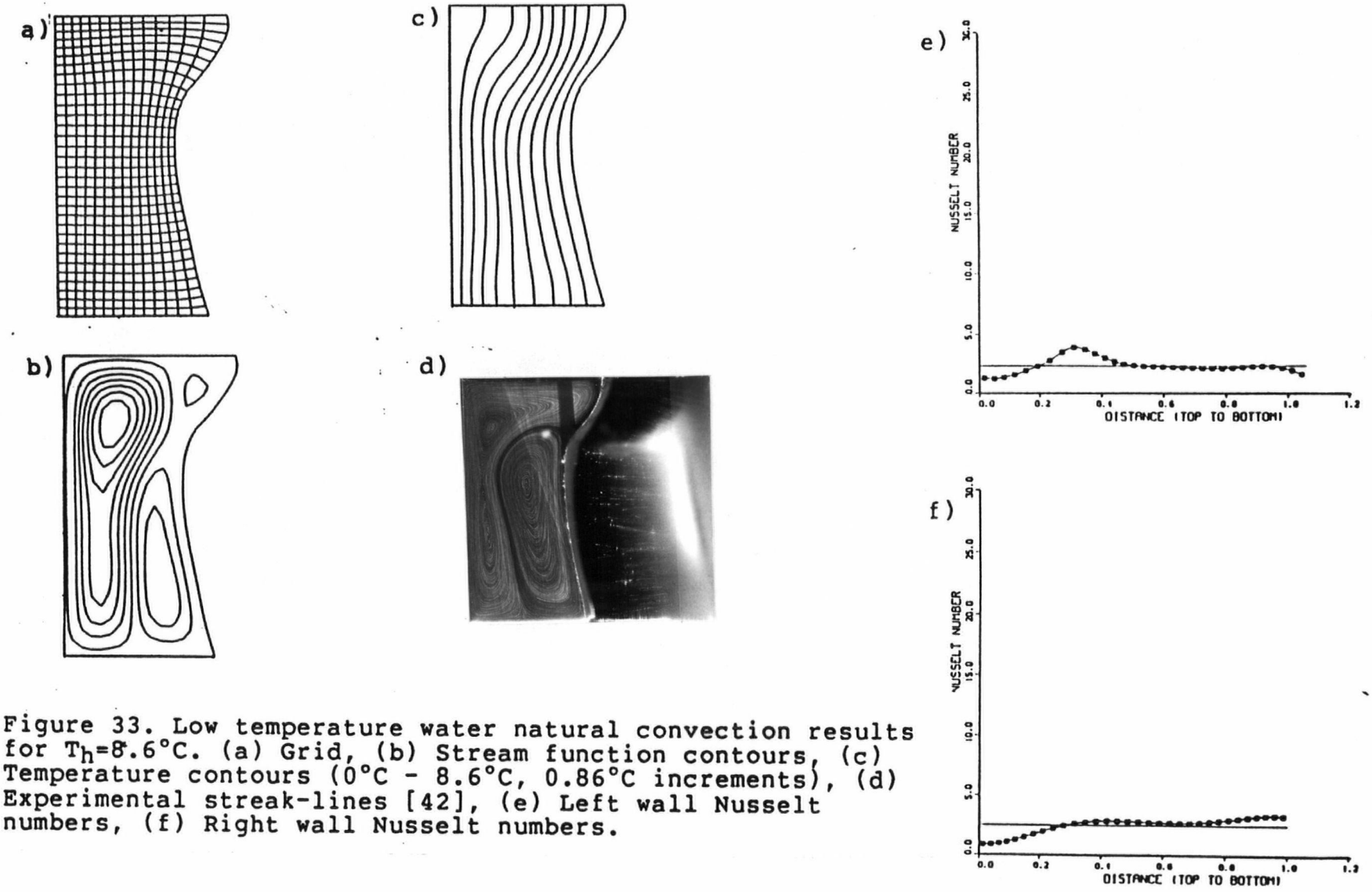

Figure 33. Low temperature water natural convection results for T_h=8.6°C. (a) Grid, (b) Stream function contours, (c) Temperature contours (0°C - 8.6°C, 0.86°C increments), (d) Experimental streak-lines [42], (e) Left wall Nusselt numbers, (f) Right wall Nusselt numbers.

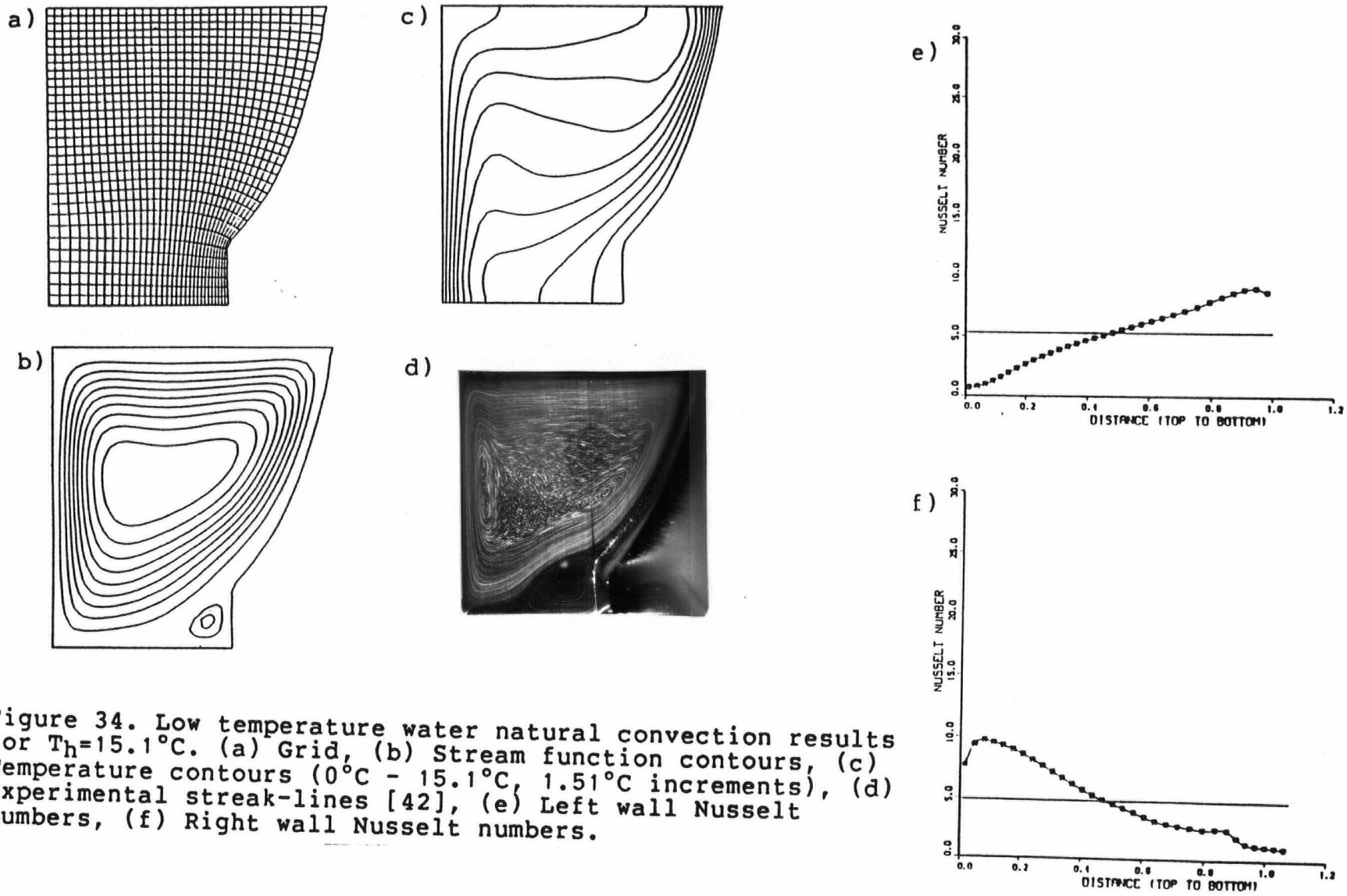

Figure 34. Low temperature water natural convection results for T_h=15.1°C. (a) Grid, (b) Stream function contours, (c) Temperature contours (0°C - 15.1°C, 1.51°C increments), (d) Experimental streak-lines [42], (e) Left wall Nusselt numbers, (f) Right wall Nusselt numbers.

B. DISCUSSION

Natural convection in the region of a density extremum has a far more complex flow behavior than any of the situations discussed earlier. Consider the changing streamline patterns revealed in Figs. 31 to 34. In case 1 (Fig. 31), the warm wall temperature is below the extremum temperature and the density increases monotonically with increasing temperature. Thus, the flow is downward along the warm left wall and upward along the cold right wall creating a unicellular anticlockwise circulation. Warm water from the left wall region impinges on the ice-water interface near the bottom and cools as it rises along this surface by natural convection. Thus, maximal heat transfer occurs near the bottom of the right wall and falls off with increasing elevation. This prediction is confirmed by the right wall local Nusselt number plot and the shape of the interface (Fig. 31). Because the heat flux into the interface is highest near the bottom, the conduction resistance (i.e. the length of the conduction path) through the ice block must be smallest in this region.

In case 2 (Fig. 32), the warm wall temperature has risen to 5.6 °C, which is slightly above the maximum density temperature of 4°C. In this case, a weaker clockwise flow can be seen to be starting in the lower left hand corner of the cavity, indicating the influence of the reversal in sign of the volumetric expansion coefficient above 4°C. However, the dominant circulation is still anticlockwise and because

the cavity temperature difference is larger, its flow strength is considerably greater than in case 1. Thus, the Nusselt number distribution over the ice interface is even more non-uniform and the interface assumes an even more noticeable slope.

At a warm wall temperature of 8.6°C (case 3, Fig. 33), numerical convergence problems were encountered. For such a temperature difference across the liquid phase, two counter-circulating loops of similar size develop. Because the two loops have almost equal strength, it is conjectured that the final flow pattern is obtained as a consequence of a very delicate momentum balance between them. Therefore, because the steady-state flow is easily destabilized, the cavity characteristic length used in the numerical investigation had to be reduced to 1.5 cm in order to ensure a converged solution within a reasonable CPU cost. As a result, the numerical stream function solution does not agree completely with the experimental streak pattern and also does not explain the shape of the ice-water interface. If the experimental pattern (Fig. 33) is examined closely, it is clear that the solidifying ice mass must be thinnest at the top because the clockwise circulating loop on the left brings heat directly from the hot wall to the cold one. Over the lower portion of the interface, the ice is partially insulated by an anticlockwise loop driven by temperatures below the density extremum. In this region, there is no direct exchange of heat between the left and

right walls. Rather, the clockwise loop must give up its heat by conduction to the anticlockwise loop which eventually transfers this heat to the ice. Because the warmest part of this latter flow loop strikes the bottom of the ice surface, the interface slopes slightly to the left.

At a temperature of 15.1°C (case 4, Fig. 34), the reversal in flow direction is almost complete with the clockwise loop originating at the wall now almost completely dominating the flow in the cavity. However, a small countercirculating flow still exists at the very bottom of the ice surface. Once again, because there is no direct heat exchange between the two walls in this region, the ice mass is much thicker at the bottom than at the top. Numerical convergence problems were also encountered in this case. In countrast to case 3, the convergence problems of case 4 were due to the large temperature difference through the liquid phase cavity which produced a convective flow which was almost turbulent in some regions of the cavity. Thus, the cavity characteristic length was once again reduced to 1.5 cm in order to achieve a converged numerical solution.

In general, the numerical predictions of the fluid circulation showed reasonably good agreement with the accompanying time-lapse streak photographs. In each case, the overall flow pattern is qualitatively reproduced. An increase in the characteristic length used in the numerical analysis would probably lead to the "cat's-eye" formation observed in case 4 and might allow the left circulation cell

to dominate near the top of the cavity in case 3. These discrepancies seem to be the only important differences between the experimental and numerical results. Unfortunately, other information, such as the experimental temperature distributions or velocity profiles were not available for additional verification of the numerical results.

The success of the present steady-state program in simulating the liquid-side natural convection flows occurring at a given instant in various ice-formation experiments, suggests that the same approach might be used to model the entire unsteady-state freezing process. This is the intended ultimate use of the numerical procedures developed in the present thesis, but time did not permit the latter simulations to be carried out. However, based on the experience gained in building up the present program, a numerical algorithm which might achieve the above-mentioned objective is presented below. First, the overall time interval of interest must be broken up into many small subintervals. These could be of increasing duration as the numerical experiment progressed, reflecting the fact that the ice grows more and more slowly with time. It would be necessary to assume that the heat transfer process in both the liquid and the solid is quasi-steady over any small subinterval in time, i.e. the flow and/or temperature are steady at each instant. Thus, starting with a finitely small, uniformly thick layer of solid phase on the cold wall

of the cavity, the solution would be extended over each subinterval by means of the following steps:

1. The irregular enclosure in which the liquid phase is trapped is transformed into a rectangular shape using the orthogonal grid generation routine. The curved ice-water interface would be represented by a set of cubic splines fitted through the boundary nodes.
2. The irregular shape bounding the solid phase is similarly transformed to a second rectangle.
3. The dependent variables (temperature, vorticity and stream function) are updated over the first transformed domain. The solution obtained at the end of the previous subinterval would be used to determine values of each dependent variables for the present subinterval. Note that the only new information supplied to the natural convection solver are the updated grid characteristics from step 1.
4. The conduction problem for the solid phase is resolved, i.e. the temperature is updated at each nodal point. Once again, initial temperature values from the previous subinterval can be used. Note that because the interface temperature is fixed at the melting temperature, the liquid and solid phase solutions are uncoupled from one another.

5. A heat balance is performed at each boundary node at the liquid-solid interface. The difference between the heat dissipated by the solid phase at that point and the heat received from the liquid phase must equal to the amount of local phase change which has taken place. Knowing the density of the solid phase and the latent heat of freezing, it then becomes possible to determine how far the interface (i.e. the nodal position) has locally advanced or receded in the normal direction to the surface during that subinterval in time. The new set of the boundary nodes thus calculated define the new ice-water interface.
6. Steps 1 to 5 are repeated until no further change in the interface position is observed. The nodal values of all dependent variables then corresponds to the final steady-state solution.

Note that each time step requires the iterative convergence of two grid generation problem (one for each phase) and two different finite difference transport problems (the diffusion and convection process taking place in the liquid phase and the conduction process in the solid phase). Thus, it is suspected that the modelling of a time dependent melting or freezing process in this manner will require such excessive amounts of computer time that the possibility of ever running it on the present computational facilities is

questionable. However, if the time subintervals are sufficiently small such the various solutions do not change significantly over that period, the starting dependent variable values may be close enough to their next steady-state answers that only a small number of iterations will be required to obtain convergence. In this case, once a solution has been generated for the first time step, it may be possible to obtain all of the succeeding ones with relatively little effort. However, if this "optimal" time subinterval proves to be too short to be practical, the simulation of an unsteady-state phase change process may have to wait until the program can be implemented on a supercomputer, preferably one with parallel processing capabilities.

XI. CONCLUSIONS

Body-fitted orthogonal grids were generated for the most distorted cavities of type C1 and C2 using three different sets of grid boundary conditions: correspondence between Cartesian and orthogonal coordinates was specified along none of the boundaries, the right wall only and the top, right and bottom walls. Most of the grid boundary conditions produced grids of reasonably constant density over the entire domain of these distorted cavities. A few boundary conditions yielded grids with very low densities in regions where gradients of stream function and temperature were substantial. With the exception of this small number of undesirable grids, it was found that, independent of the grid and vorticity boundary conditions used,

1. a grid size of 22x22 assures numerical results having accuracies better than 1 percent at a Rayleigh number of 10000,
2. a grid size of 28x28 assures numerical results with accuracies better than 1 percent for Ra=100000,
3. the maximum stream function, the average Nusselt number and the length of the right wall all monotically approach their asymptotic values for grid sizes larger than 30x30, and
4. all of the numerical results obtained for a grid size of 33x33 were accurate to better than 1 percent.

The effects of the amplitude and the Rayleigh number on the natural convection behaviour are listed below:

1. the strength of the fluid flow increases with increasing amplitude for both the C1 and C2 cavities,
2. the strength of the fluid flow increases with increasing Rayleigh number,
3. the rate of heat transfer through the cavity decreases as the amplitude increases for the C1 cavity,
4. the rate of heat transfer through the cavity decreases with increasing amplitude for the C2 cavity at low Rayleigh numbers,
5. the rate of heat transfer through the cavity increases with increasing amplitude for the C2 cavity at high Rayleigh numbers, and
6. the rate of heat transfer through the cavity increases with increasing Rayleigh number for both the C1 and C2 cavity.

The behaviour of the strength of fluid flow with respect to the amplitude and the Rayleigh number was rationalized by considering the effect of the Rayleigh number on the source term in the vorticity equation and the effect of the cavity shape in either inhibiting or enhancing fluid flow. The behaviour of the cavity Nusselt number with respect to the amplitude and Rayleigh number was interpreted by considering the opposing effects of the strength of convection and the

the average distance between the two isothermal walls on the ability of the cavity to transfer heat. Also, the average Nusselt number along the left wall was correlated with the Rayleigh number by using a power law equation of the form $Y=aX^b$ for each cavity type (C1 and C2) and for each amplitude. It was found that the coefficient a decreases while the exponent b increases as the amplitude is raised for both cavity types.

The numerical predictions of the fluid circulation for a liquid which does not have a linear density-temperature relationship showed reasonably good agreement with the flow visualisation experiments carried out by Eckert [42]. In three cases out of four, the general flow pattern was reproduced fairly accurately. Numerical convergence problems were encountered in two cases and were caused either by the very delicate balance of momentum which occurs between two counter-circulating loops of similar size or by a very large imposed temperature difference.

XII. RECOMMENDATIONS

1. Similar numerical simulations to the one presented in this thesis should be performed on other families of cavities to further investigate the merits of using body-fitted orthogonal coordinate systems to solve coupled transport phenomena problems and to learn and understand more about natural convection phenomena.
2. Cavities which are even more distorted than the ones employed here should be investigated to help differentiate between the effectiveness of the various grid and vorticity boundary conditions tried.
3. The use of a direct linear equation solver (sparse matrix solver) should be investigated to help overcome numerical convergence problems which occasionally occur when iterative procedures are used to solve coupled energy and momentum equations.
4. To further improve the convergence rate of finite difference solutions, efforts should be spent on finding a workable procedure which will optimally adjust the relaxation factors as the iterative process is being executed.

NOMENCLATURE

a,b	General coefficients
A	Cavity dimensionless amplitude
B,C	Cavity wall lengths
C_p	Fluid specific heat capacity
Dev	Deviation of the numerically generated body fitted orthogonal grid from orthogonal
$\bar{e}$	Unit vector
f	Shape factor
F	General analytical function
g,$\bar{g}$	Gravitational acceleration magnitude and vector
Gr	Grashof number
h	Convective heat transfer coefficient
H	Scale factor component
i,j	Node indices
k	Fluid thermal conductivity
L	General dimensionless length
L_c	Cavity characteristic length
M,N	Maximum values of ξ and η, respectively
Nu	Nusselt number
Nu_x	Nusselt number calculated with respect to the distance along a vertical flat plate in the flow direction
O	Order of magnitude of the remaining term in a truncated series
p	Pressure
P	Dimensionless pressure
Pe	Local Peclet number calculated with respect to the distance between two discrete points
Pr	Prandtl number

q	Heat flux component
Q	Heat transfer rate through the cavity
R	Cavity aspect ratio
Ra	Rayleigh number
Ra_x	Rayleigh number calculated with respect to the distance along a vertical flat plate in the flow direction
T	Temperature (K or otherwise specified)
v	Velocity component
V	Dimensionless velocity component
x,y	Cartesian coordinates
X,Y	Dimensionless Cartesian coordinates
Zn,Zt	Normal and tangential dimensionless general orthogonal coordinates with respect to a wall
Z1,Z2	Dimensionless general orthogonal coordinates
a	General coefficient or general vector component
$\vec{a}$	General vector
β	Fluid thermal volumetric expansion coefficient
γ	Cavity angle of tilt
Γ	General diffusion coefficient
$\Delta Zn, \Delta Z1, \Delta\eta, \Delta\xi$	Dimensionless space increments
η, ξ	Dimensionless general orthogonal coordinates
θ	Dimensionless temperature
Θ	Angle of deviation from orthogonality
μ	Viscosity
ρ	Fluid density
ϕ	General dependent variable
ψ	Dimensionless stream function

Ω	Dimensionless vorticity
$\bar{\Omega}$	Dimensionless vorticity vector

SUBSCRIPTS

ave	Average
bw,lw,rw,tw	Bottom, left, right and top cavity walls
c	Cavity cold wall (Exception: L_c)
db	Domain boundary
dyn	Dynamic
e,n,s,w	East, north, south and west control volume face indices, respectively
h	Cavity hot wall
i,j	Node indices
x,y,z	Cartesian coordinate directions (Exceptions: Nu_x and Ra_x)
w	wall or node index
zn,zt	Normal and tangential general orthogonal coordinate directions with respect to a wall
z1,z2,z3	General orthogonal coordinate directions
0	Reference temperature or position
1,2,3	Coefficient or node indices
η,ξ	General orthogonal coordinate directions
∞	Conditions far from the isothermal flat plate

REFERENCES

1. Catton, I., "Natural Convection in Enclosures", Proceeding of the Sixth International Heat Transfer Conference, Toronto, Canada, vol.6, pp.13-31, Hemisphere Publishing Corporation, Canada, 1978.

2. Ostrach, S., "Natural Convection Heat Transfer in Cavities and Cells", Proceeding of the Seventh International Heat Transfer Conference, Munchen, Fed. Rep. of Germany, vol.1, pp.365-379, Hemisphere Publishing Corporation, USA, 1982.

3. Roux, B., Grondin, J.C., Bontoux, P. and Gilly, B., "On a High-Order Accurate Method for the Numerical Study of Natural Convection in a Vertical Square Cavity", Numerical Heat Transfer, vol.1, pp.331-349, 1978.

4. Strada, M. and Heinrich, J.C., "Heat Transfer Rates in Natural Convection at High Rayleigh Numbers in Rectangular Enclosures: a Numerical Study", Numerical Heat Transfer, vol.5, pp.81-93, 1982.

5. Ozoe, H., Sayama, H. and Churchill, S. W., "Natural Convection in an Inclined Square Channel", Int. J. Heat Mass Transfer, vol.17, pp.401-406, 1974.

6. Catton, I., Ayyaswamy, P.S. and Clever, R.M., "Natural Convection Flow in a Finite, Rectangular Slot Arbitrarily Oriented with Respect to the Gravity Vector", Int. J. Heat Mass Transfer, vol.17, pp.173-184, 1974.

7. Han, J.T., "A Computational Method to Solve Nonlinear Elliptic Equations for Natural Convection in Enclosures", Numerical Heat Transfer, vol.2, pp.165-175, 1979.

8. De Vahl Davis, G., "Laminar Natural Convection in an Enclosed Rectangular Cavity", Int. J. Heat Mass Transfer, vol.11, pp.1675-1693, 1968.

9. Ropke, K.-J., and Schummer, P., "Natural Convection of a Viscoelastic Fluid in a Rectangular Enclosure", Proceeding of the Seventh International Heat Transfer Conference, Munchen, Fed. Rep. of Germany, vol.2, pp.269-273, Hemisphere Publishing Corporation, USA, 1982.

10. Zhong, Z.Y., Yang, K.T. and Lloyd, J.R., "Variable Property Effects in Laminar Natural Convection in a Square Enclosure", J. of Heat Transfer, vol.107, pp.133-138, 1985.

11. Staehle, B. and Hahne, E., "Overshooting and Damped Oscillations of Transient Natural Convection Flows in Cavities", Proceeding of the Seventh International Heat Transfer Conference, Munchen, Fed. Rep. of Germany, vol.2, pp.287-292, Hemisphere Publishing Corporation, USA, 1982.

12. Wong, H.H. and Raithby, G.D., "Improved Finite-difference Methods Based on a Critical Evaluation of the Approximation Errors", Numerical Heat Transfer, vol.2, pp.139-163, 1979.

13. Raithby, G.D., Hollands, K.G.T. and Unny, T.E., "Analysis of Heat Transfer by Natural Convection across Vertical Fluid Layers", Journal of Heat Transfer, vol.99, pp.287-292, 1977.

14. Thomas, R.W. and De Vahl Davis, G., "Natural Convection in Annular and Rectangular Cavities-A Numerical Study", Fourth Int. Congr. Heat Transfer, NC 2.4, Versailles, 1970.

15. De Vahl Davis, G. and Jones, I.P., "Natural Convection in a Square Cavity: A Comparison Exercise", Report 1982/FMT/3, ISSN 0157-5104, School of Mechanical and Industrial Engineering, The University of New South Wales, 1982.

16. Kim, D.M. and Viskanta, R., "Effect of Wall Heat Conduction on Natural Convection Heat Transfer in a Square Enclosure", Journal of Heat Transfer, vol.107, pp.139-146, 1985.

17. Chang, L.C., Lloyd, J.R. and Yang, K.T., "A Finite Difference Study of Natural Convection in Complex Enclosures", Proceeding of the Seventh International Heat Transfer Conference, Munchen, Fed. Rep. of Germany, vol.2, pp.183-188, Hemisphere Publishing Corporation, USA, 1982.

18. Ho, C.-J. and Viskanta, R., "Heat Transfer During Melting from an Isothermal Vertical Wall", Journal of Heat Transfer, vol.106, pp.12-19, 1984.

19. Gadgil, A. and Gobin, D., "Analysis of Two-dimensional Melting in Rectangular Enclosures in Presence of Convection", Journal of Heat Transfer, vol.106, pp.20-26, 1984.

20. Sparrow, E.M., Patankar, S.V. and Ramadhyani, S., "Analysis of Melting in the Presence of Natural Convection in the Melt Region", Journal of Heat Transfer, vol.99, pp.520-526, 1977.

21. Kroeger, P.G. and Ostrach, S., "The Solution of a Two-dimensional Freezing Problem Including Convection Effects in the Liquid Region", Int. J. Heat Mass Transfer, vol.17, pp.1191-1207, 1974.

22. Van Doormaal, J.P., Raithby, G.D. and Strong, A.B., "Prediction of Natural Convection in Nonrectangular Enclosures Using Orthogonal Curvilinear Coordinates", Numerical Heat Transfer, vol.4, pp.21-38, 1981.

23. Maekawa, T., and Tanasawa, I., "Natural Convection Heat Transfer in Parallelogrammic Enclosures", Proceeding of the Seventh International Heat Transfer Conference, Munchen, Fed. Rep. of Germany, vol.2, pp.227-232, Hemisphere Publishing Corporation, USA, 1982.

24. Van Doormaal, J.P., "Finite Difference Solution of Two-dimensional Natural Convection in Nonrectangular Enclosures", M.A.Sc. Thesis, University of Waterloo, Canada, 1980.

25. Thompson, J.F., Warsi, Z.U.A. and Mastin, C.W., "Boundary-fitted Coordinate Systems for Numerical Solution of Partial Differential Equations-A Review", Journal of Computational Physics, vol.47, pp.1-108, 1982.

26. Ryskin, G. and Leal, L.G., "Orthogonal Mapping", Journal of Computational Physics, vol.50, pp.71-100, 1983.

27. Chikhliwala, E.D. and Yortsos, Y.C., "Application of Orthogonal Mapping to Some Two-dimensional Domains", Journal of computational Physics, vol.57, pp.391-402, 1985.

28. Mobley, C.D. and Stewart, R.J., "On the Numerical Generation of Boundary-fitted Orthogonal Curvilinear Coordinate Systems", Journal of Computational Physics, vol.34, pp.124-135, 1980.

29. Pope, S.B., "The Calculation of Turbulent Recirculating Flows in General Orthogonal Coordinates", Journal of Computational Physics, vol.26, pp.197-217, 1978.

30. Burmeister, L.C.,"Convective Heat Transfer", John Wiley & Sons, USA, 1983.

31. Holman, J.P., "Heat Transfer", 5th edition, McGraw-Hill, USA, 1981.

32. Bird, R.B., Stewart, W.E. and Lightfoot, E.N., "Transport Phenomena", John Wiley & Sons, USA, 1960.

33. Jaluria, Y., "Natural Convection", The Science and Applications of Heat and Mass Transfer, vol.5, Pergamon Press, Great Britain, 1980.

34. Chinnappa, J.C.V., "Free Convection in Air Between a 60 Degree Vee-corrugated Plate and a Flat Plate", Int. J. Heat Mass Transfer, vol.13, pp.117-123, 1970.

35. El Sherbiny, S.M., "Free Convection in an Inclined Air Layer Contained Between V-corrugated and Flat Plates", M.A.Sc. Thesis, University of Waterloo, Canada, 1977.

36. El Sherbiny, S.M., Hollands, K.G.T. and Raithby, G.D., "Free Convection across Inclined Air Layers with One Surface V-corrugated", Journal of Heat Transfer, vol.100, pp.410-415, 1978.

37. Randall, K.R., "An Interferometric Study of Natural Convection Heat Transfer in Flat Plate and V-corrugated Enclosures", Ph.D Thesis, University of Wisconsin, USA, 1978.

38. Anderson, D.A., Tannehill, J.C. and Pletcher, R.H., "Computational Fluid Mechanics and Heat Transfer", Hemisphere Publishing Corporation, USA, 1984.

39. Patankar, S.V., "Numerical Heat Transfer and Fluid Flow", Hemisphere Publishing Corporation, USA, 1980.

40. Roache, P.J., "Computational Fluid Dynamics", Hermosa Publishers, USA, 1972.

41. Davis, H.F. and Snider, A.D., "Introduction to Vector Analysis", 4th edition, Allyn and Bacon, USA, 1979.

42. Eckert, N., "An Experimental Study of Natural Convection of Water During Ice Formation", B.A.Sc. Thesis, University of British Columbia, Canada, 1984.

43. Peyret, R. and Taylor, T.D., "Computational Methods for Fluid Flow", Springer-Verlag New York, USA, 1983.

44. Gosman, A.D., Pun, W.M., Runchal, A.K., Spalding, D.B. and Wolfshtein, M., "Heat and Mass Transfer in Recirculating Flow", Academic Press, Great Britain, 1969.

45. Aris, R., "Vectors, Tensors, and the Basic Equations of Fluid Mechanics", Prentice-Hall, USA, 1962.

46. Spiegel, M.R., "Vector Analysis", Schaum Publishing Company, USA, 1959.

47. Currie, I.G., "Fundamental Mechanics of Fluids", McGraw-Hill, USA, 1974.

48. Hornbeck, R.W., "Numerical Methods", Prentice-Hall, USA, 1975.

49. Carnahan, B., Luther, H.A. and Wilkes, J.O. "Applied Numerical Methods", John Wiley & sons, USA, 1969.

50. Forsythe, G.E., Malcolm, M.A. and Moler, C.B., "Computer Methods for Mathematical Computation", Prentice-Hall, USA, 1977.

51. Weast, R.C., "Handbook of Chemistry and Physics", 56th edition, CRC Press, USA, 1975.

APPENDIX A

The program which was used to generate the numerical results of Part I, Part II and Part III (with some minor modifications) is listed here. The listing includes descriptions of both the subroutines and the important variables.

The initialisation procedure, the discretized equations and boundary conditions and the methods used to solve them, the accuracy criteria and the divergence tests were described in previous chapters. There is only one difference between the program description given in the main body of the thesis and the program itself. This difference corcerns the way the location of the discrete grid point values are indicated on the transformed grid. In the program, the grid points are numerated using the indices I and J which are associated with the η and ξ directions, respectively. Also, the node I=1 and J=1 is associated to the top left corner of the transformed domain. The indices I and J still vary from 1 to M (M+1 for the staggered grid) and 1 to N (N+1 for the staggered grid), respectively.

Only one cavity shape can be handled at a time by the program, but many grid characteristics, vorticity boundary conditions and grid sizes can be investigated in a single execution.

```
C
C-----------------------------------------------------------------------
C
C     NAME: MAIN.
C
C     PURPOSE:
C
C     THIS SUBROUTINE READS IN DATA, MANAGES THE DIFFERENT INTERAC-
C   TION BETWEEN OTHER IMPORTANT SUBROUTINES, AND SET-UP, MAGNIFY OR
C   REDUCED ARRAYS.
C
C     CHARACTERISTIC:
C
C   - LINEAR TWO-DIMENSIONAL INTERPOLATION.
C
C-----------------------------------------------------------------------
C
C     IMPORTANT VARIABLES:
C     --------------------
C
C     - CO: CURRENT RUN NUMBER.
C     - COUL: MAXIMUM NUMBER OF RUNS.
C     - C1UL: MAXIMUM NUMBER OF ITERATION ALLOWED TO SOLVED
C           OF THE DISCRETIZED GRID DIFFERENTIAL EQUATIONS.
C     - C2UL: MAXIMUM NUMBER OF ITERATION ALLOWED TO SOLVED
C           THE DISCRETIZED CONSERVATION EQUATIONS.
C     - PTC: ARRAY CONTAINING THE CARTESIAN COORDINATE
C          OF THE PHYSICAL DOMAIN CORNER.
C     - RSF: ARRAY OF THE RATIO OF SCALE FACTORS.
C     - SF: ARRAY OF STREAM FUNCTION VALUES.
C     - T: ARRAY OF TEMPERATURE VALUES.
C     - VOR: ARRAY OF VORTICITY VALUES.
C     - XY: ARRAY OF CARTESIAN VALUES.
C     - SFN: ARRAY OF PREDICTED STREAM FUNCTION VALUES
C          FOR A NEW RUN.
C     - TN: ARRAY OF PREDICTED TEMPERATURE VALUES FOR A NEW RUN.
C     - VORN: ARRAY OF PREDICTED VORTICITY VALUES FOR A NEW RUN.
C     - XYN: ARRAY OF PREDICTED CARTESIAN COORDINATES VALUES
C          FOR A NEW RUN.
C     - BTYPE: ARRAY OF GRID BONDARY CONDITIONS.
C     - M: MAXIMUM VALUE OF THE INDICE I FOR THE NON STAGGERED
C        GRID.
C     - N: MAXIMUM VALUE OF THE INDICE J FOR THE NON STAGGERED
C        GRID.
C     - MN: MAXIMUM VALUE OF THE INDICE I (NON
C         STAGGERED GRID) FOR THE NEXT RUN.
C     - NN: MAXIMUM VALUE OF THE INDICE J (NON STAGGERED GRID)
C          FOR THE NEW RUN.
C     - EPS1: ABSOLUTE ACCURACY USED TO STOP THE GRID GENERATION.
C     - RFXY: RELAXATION FACTOR FOR THE CARTESIAN COORDINATES.
C     - EPS2: RELATIVE ACCURACY USED TO STOP THE NATURAL
C           CONVECTION CALCULATION.
C     - RFT: RELAXATION FACTOR FOR TEMPERATURE, STREAM FUNCTION
C          AND VORTICITY.
C     - VBC: VORTICITY BOUNDARY CONDITION:
C     - PR: PRANDTL NUMBER.
C     - RA: RAYLEIGH NUMBER.
C     - H: ARRAY OF SCALE FACTORS.
C     - D: ARRAY OF DERIVATIVES OF CARTESIAN COORDINATES
C         WITH RESPECT TO THE ORTHOGONAL COORDINATES.
```

```
C     - ATDMA: ARRAY OF THE TDMA COEFFICIENTS.
C     - BTDMA: ARRAY OF THE TDMA COEFFICIENTS.
C     - CTDMA: ARRAY OF THE TDMA COEFFICIENTS.
C     - DTDMA: ARRAY OF THE TDMA COEFFICIENTS.
C     - PTDMA: ARRAY OF THE TDMA COEFFICIENTS.
C     - QTDMA: ARRAY OF THE TDMA COEFFICIENTS.
C     - SLN: ARRAY OF SOLUTION VALUES.
C     - MAXSF: MAXIMUM STREAM FUNCTION VALUES.
C     - MAXVOR: MAXIMUM VORTICITY VALUES.
C     - DIST: ARRAY OF DISTANCES ALON THE BOUNDARY SHAPE
C           CALCULATED FROM THE TOP WALL.
C     - NUAV: ARRAY OF AVERAGE NUSSELT NUMBER.
C     - NUL: ARRAY OF LOCAL NUSSELT NUMBER.
C     - XYZ: ARRAY OF CONTOUR VALUES OF A SCALAR AND ITS
C          CARTESIAN COORDINATES.
C     - ZCNTR: ARRAY OF VALUES OF CONTOUR LINES.
C     - XYS: ARRAY OF CATESIAN POSITIONS OF THE STAGGERED GRID
C          NODES.
C     - COND: CONDUCTION STRENGTH THROUGH A CONTROL VOLUME FACE.
C     - CONV: CONVECTION STRENGTH THROUGH A CONTROL VOLUME VACE.
C     - DIFA: MAXIMUM GRID DEVIATION FROM ORTHOGONALITY (DEGREE).
C
C*********************************************************************
C
      IMPLICIT REAL*8(A-H,O-Z)
      INTEGER BTYPE(4),CO,COUL,C1UL,C2UL,VBC
      REAL*8 PTC(2,4),RSF(50,50)
      REAL*8 SFN(50,50),TN(50,50),XYN(50,50,2),VORN(50,50)
      REAL*8 SF(50,50),T(50,50),XY(50,50,2),VOR(50,50)
      COMMON /BLK1/ M,N
      COMMON /BLK2/ BTYPE,RSF
      COMMON /BLK3/ XY
      COMMON /BLK6/ PR,RA
      COMMON /BLK7/ T
      COMMON /BLK8/ VOR
      COMMON /BLK9/ SF
      COMMON /BLK11/ EPS1,RFXY,C1UL
      COMMON /BLK12/ EPS2,RFT,RFVOR,RFSF,C2UL,VBC
C
C*** SET UP THE GRAPHIC SOFTWARE.
C
      CALL DSPDEV ('PLOT')
C
C*** PRELIMINAIRY INPUT DATA.
C
      READ (5,360) COUL
      READ (5,370) PTC(1,1)
      READ (5,370) PTC(2,1)
      READ (5,370) PTC(1,2)
      READ (5,370) PTC(2,2)
      READ (5,370) PTC(1,3)
      READ (5,370) PTC(2,3)
      READ (5,370) PTC(1,4)
      READ (5,370) PTC(2,4)
C
C*** OVERALL LOOP.
C
C*** INPUT DATA.
C
      DO 350 CO=1,COUL
```

```
      READ (5,360) MN
      READ (5,360) NN
      READ (5,360) C1UL
      READ (5,370) EPS1
      READ (5,370) RFXY
      READ (5,360) BTYPE(1)
      READ (5,360) BTYPE(2)
      READ (5,360) BTYPE(3)
      READ (5,360) BTYPE(4)
      READ (5,370) RSF(1,1)
      READ (5,370) RSF(1,NN)
      READ (5,370) RSF(MN,NN)
      READ (5,370) RSF(MN,1)
      READ (5,370) PR
      READ (5,370) RA
      READ (5,360) C2UL
      READ (5,370) EPS2
      READ (5,370) RFT
      READ (5,370) RFVOR
      READ (5,370) RFSF
      READ (5,360) VBC
C
C*** PRINTOUT THE INPUT DATA.
C
      WRITE (6,380) CO,MN,NN,C1UL,EPS1,RFXY,(BTYPE(I),I=1,4),
     1RSF(1,1),RSF(1,NN),RSF(MN,NN),RSF(MN,1),PR,RA,C2UL,EPS2,
     2RFT,RFVOR,RFSF,VBC
C
C*** SET UP THE INITIAL CONDITION.
C
      IF (CO.NE.1) GOTO 90
      M=MN
      MP1=M+1
      MM1=M-1
      MM2=M-2
      N=NN
      NP1=N+1
      NM1=N-1
      NM2=N-2
C
C*** THE X AND Y VALUES OF BOUNDARY POINTS ARE CALCULATED USING
C*** EQUAL INTERVALS OF THE DEPENDENT VARIABLE.
C
      XY(1,1,1)=PTC(1,1)
      XY(1,1,2)=PTC(2,1)
      XY(1,N,1)=PTC(1,2)
      XY(1,N,2)=PTC(2,2)
      XY(M,N,1)=PTC(1,3)
      XY(M,N,2)=PTC(2,3)
      XY(M,1,1)=PTC(1,4)
      XY(M,1,2)=PTC(2,4)
C
C*** TOP WALL.
C
      AMO=(XY(1,N,1)-XY(1,1,1))/NM1
      DO 10 J=1,NM2
       XY(1,J+1,1)=XY(1,1,1)+J*AMO
       XY(1,J+1,2)=F(XY(1,J+1,1),1)
   10  CONTINUE
C
```

```
C*** RIGHT WALL.
C
      AMO=(XY(M,N,2)-XY(1,N,2))/MM1
      DO 20 I=1,MM2
       XY(I+1,N,2)=XY(1,N,2)+I*AMO
       XY(I+1,N,1)=F(XY(I+1,N,2),2)
  20  CONTINUE
C
C*** BOTTOM WALL.
C
      AMO=(XY(M,N,1)-XY(M,1,1))/NM1
      DO 30 J=1,NM2
       XY(M,J+1,1)=XY(M,1,1)+J*AMO
       XY(M,J+1,2)=F(XY(M,J+1,1),3)
  30  CONTINUE
C
C*** LEFT WALL.
C
      AMO=(XY(M,1,2)-XY(1,1,2))/MM1
      DO 40 I=1,MM2
       XY(I+1,1,2)=XY(1,1,2)+I*AMO
       XY(I+1,1,1)=F(XY(I+1,1,2),4)
  40  CONTINUE
C
C*** INTERNAL X AND Y VALUES.
C
      DO 60 I=2,MM1
       AMO=(XY(I,N,1)-XY(I,1,1))/NM1
       AM1=(XY(I,N,2)-XY(I,1,2))/NM1
       DO 50 J=1,NM2
        XY(I,J+1,1)=XY(I,1,1)+J*AMO
        XY(I,J+1,2)=XY(I,1,2)+J*AM1
  50   CONTINUE
  60  CONTINUE
C
C*** THE TEMPERATURE IS SET UP CONSIDERING ONLY THE CONDUCTION.
C*** SF(I,J)=0. (IMPERMEABLE WALLS) AND VOR(I,J)=0.
C
      DO 80 I=1,MP1
       DO 70 J=1,NP1
        SF(I,J)=0.D0
        T(I,J)=1.D0-(2.D0*(J-1.D0)-1.D0)/(2.D0*NM1)
        VOR(I,J)=0.D0
  70   CONTINUE
  80  CONTINUE
      GOTO 340
C
C*** MAGNIFICATION OR REDUCTION OF ARRAYS.
C
  90  IF ((MN.EQ.M).AND.(NN.EQ.N)) GOTO 340
C
C*** COORDINATES AND STREAM FUNCTION.
C
      DO 150 I=1,MN
       DO 140 J=1,NN
        DO 100 II=2,M
         IF ((II-1.)/(M-1.).GT.(I-1.)/(MN-1.)) GOTO 110
 100    CONTINUE
 110    II=II-1
        DO 120 JJ=2,N
```

```
          IF ((JJ-1.)/(N-1.).GT.(J-1.)/(NN-1.)) GOTO 130
  120     CONTINUE
  130     JJ=JJ-1
          AMO=(I-1.DO)/(MN-1.DO)-(II-1.DO)/(M-1.DO)
          AM1=(J-1.DO)/(NN-1.DO)-(JJ-1.DO)/(N-1.DO)
          AM2=1.DO/(M-1.DO)
          AM3=1.DO/(N-1.DO)
          AM4=XY(II+1,JJ,1)-XY(II,JJ,1)
          AM5=XY(II,JJ+1,1)-XY(II,JJ,1)
          AM6=XY(II+1,JJ+1,1)-XY(II+1,JJ,1)-XY(II,JJ+1,1)+XY(II,JJ,1)
          XYN(I,J,1)=XY(II,JJ,1)+AMO*AM4/AM2+AM1*AM5/AM3
     1+AMO*AM1*AM6/(AM2*AM3)
          AM4=XY(II+1,JJ,2)-XY(II,JJ,2)
          AM5=XY(II,JJ+1,2)-XY(II,JJ,2)
          AM6=XY(II+1,JJ+1,2)-XY(II+1,JJ,2)-XY(II,JJ+1,2)+XY(II,JJ,2)
          XYN(I,J,2)=XY(II,JJ,2)+AMO*AM4/AM2+AM1*AM5/AM3
     1+AMO*AM1*AM6/(AM2*AM3)
          AM4=SF(II+1,JJ)-SF(II,JJ)
          AM5=SF(II,JJ+1)-SF(II,JJ)
          AM6=SF(II+1,JJ+1)-SF(II+1,JJ)-SF(II,JJ+1)+SF(II,JJ)
          SFN(I,J)=SF(II,JJ)+AMO*AM4/AM2+AM1*AM5/AM3
     1+AMO*AM1*AM6/(AM2*AM3)
C
C*** IMPERMEABLE WALLS.
C
          IF ((I.EQ.1).OR.(I.EQ.MN)) SFN(I,J)=0.DO
          IF ((J.EQ.1).OR.(J.EQ.NN)) SFN(I,J)=0.DO
  140    CONTINUE
  150   CONTINUE
C
C*** REASSIGN THE BOUNDAIRY POINT COORDINATES.
C
C*** CORNER POINTS.
C
       XYN(1,1,1)=PTC(1,1)
       XYN(1,1,2)=PTC(2,1)
       XYN(1,NN,1)=PTC(1,2)
       XYN(1,NN,2)=PTC(2,2)
       XYN(MN,NN,1)=PTC(1,3)
       XYN(MN,NN,2)=PTC(2,3)
       XYN(MN,1,1)=PTC(1,4)
       XYN(MN,1,2)=PTC(2,4)
C
C*** TOP WALL.
C
       IF (BTYPE(1).EQ.0) GOTO 170
       AMO=(XYN(1,NN,1)-XYN(1,1,1))/(NN-1.DO)
       NNM2=NN-2
       DO 160 J=1,NNM2
        XYN(1,J+1,1)=XYN(1,1,1)+J*AMO
        XYN(1,J+1,2)=F(XYN(1,J+1,1),1)
  160   CONTINUE
C
C*** RIGHT WALL.
C
  170   IF (BTYPE(2).EQ.0) GOTO 190
       AMO=(XYN(MN,NN,2)-XYN(1,NN,2))/(MN-1.DO)
       MNM2=MN-2
       DO 180 I=1,MNM2
        XYN(I+1,NN,2)=XYN(1,NN,2)+I*AMO
```

```
        XYN(I+1,NN,1)=F(XYN(I+1,NN,2),2)
  180   CONTINUE
C
C*** BOTTOM WALL.
C
  190   IF (BTYPE(3).EQ.0) GOTO 210
        AMO=(XYN(MN,NN,1)-XYN(MN,1,1))/(NN-1.DO)
        NNM2=NN-2
        DO 200 J=1,NNM2
         XYN(MN,J+1,1)=XYN(MN,1,1)+J*AMO
         XYN(MN,J+1,2)=F(XYN(MN,J+1,1),3)
  200   CONTINUE
C
C*** LEFT WALL.
C
  210   IF (BTYPE(4).EQ.0) GOTO 230
        AMO=(XYN(MN,1,2)-XYN(1,1,2))/(MN-1.DO)
        MNM2=MN-2
        DO 220 I=1,MNM2
         XYN(I+1,1,2)=XYN(1,1,2)+I*AMO
         XYN(I+1,1,1)=F(XYN(I+1,1,2),4)
  220   CONTINUE
C
C*** TEMPERATURE AND VORTICITY.
C
  230   MP1=M+1
        NP1=N+1
        MNP1=MN+1
        NNP1=NN+1
        DO 290 I=1,MNP1
         DO 280 J=1,NNP1
          DO 240 II=2,MP1
           IF ((II-1.5)/(M-1.).GT.(I-1.5)/(MN-1.)) GOTO 250
  240     CONTINUE
  250     II=II-1
          DO 260 JJ=2,NP1
           IF ((JJ-1.5)/(N-1.).GT.(J-1.5)/(NN-1.)) GOTO 270
  260     CONTINUE
  270     JJ=JJ-1
          AMO=(I-1.5DO)/(MN-1.DO)-(II-1.5DO)/(M-1.DO)
          AM1=(J-1.5DO)/(NN-1.DO)-(JJ-1.5DO)/(N-1.DO)
          AM2=1.DO/(M-1.DO)
          AM3=1.DO/(N-1.DO)
          AM4=T(II+1,JJ)-T(II,JJ)
          AM5=T(II,JJ+1)-T(II,JJ)
          AM6=T(II+1,JJ+1)-T(II+1,JJ)-T(II,JJ+1)+T(II,JJ)
          TN(I,J)=T(II,JJ)+AMO*AM4/AM2+AM1*AM5/AM3
     1+AMO*AM1*AM6/(AM2*AM3)
          AM4=VOR(II+1,JJ)-VOR(II,JJ)
          AM5=VOR(II,JJ+1)-VOR(II,JJ)
          AM6=VOR(II+1,JJ+1)-VOR(II+1,JJ)-VOR(II,JJ+1)+VOR(II,JJ)
          VORN(I,J)=VOR(II,JJ)+AMO*AM4/AM2+AM1*AM5/AM3
     1+AMO*AM1*AM6/(AM2*AM3)
  280    CONTINUE
  290   CONTINUE
C
C*** GIVE TO XY,T,VOR AND SF ARRAYS THEIR NEW VALUES.
C
        M=MN
        N=NN
```

```
      DO 310 I=1,M
       DO 300 J=1,N
        XY(I,J,1)=XYN(I,J,1)
        XY(I,J,2)=XYN(I,J,2)
        SF(I,J)=SFN(I,J)
  300   CONTINUE
  310  CONTINUE
       MP1=M+1
       NP1=N+1
       DO 330 I=1,MP1
        DO 320 J=1,NP1
         T(I,J)=TN(I,J)
         VOR(I,J)=VORN(I,J)
  320   CONTINUE
  330  CONTINUE
C
C*** GENERATE THE ORTHOGONAL GRID.
C
  340  CALL GRIDNC
C
C*** COMPUTE THE STEADY-STATE CONDITION OF THE NATURAL CONVECTION
C*** PROBLEM.
C
       CALL NATC
C
C*** GRAPH THE RESULTS.
C
       CALL PLOT
  350 CONTINUE
C
C*** STOP THE GRAPHIC SOFTWARE.
C
      CALL DONEPL
      STOP
  360 FORMAT(I5)
  370 FORMAT(D13.3)
  380 FORMAT('1',T5,'INPUT DATA (',I3,').',2(/),
     1T5,'WOOD BOUNDARY CONDITION',/,
     2T5,'GRID SIZE IS',I3,' BY',I3,/,
     3T5,'MAX.# OF ITERATIONS= ',I3,/,
     4T5,'ACCURACY= ',D10.3,/,
     5T5,'RFXY= ',D10.3,/,
     6T5,'BTYPE(T)= ',I3,/,T5,'BTYPE(R)= ',I3,/,
     7T5,'BTYPE(B)= ',I3,/,T5,'BTYPE(L)= ',I3,/,
     8T5,'RSF(TL)= ',D10.3,/,T5,'RSF(TR)= ',D10.3,/,
     9T5,'RSF(BL)= ',D10.3,/,T5,'RSF(BR)= ',D10.3,/,
     *T5,'PR= ',D10.3,/,T5,'RA= ',D10.3,/,
     1T5,'MAX.# OF ITERATIONS= ',I3,/,
     2T5,'ACCURACY= ',D10.3,/,
     3T5,'RFT= ',D10.3,/,T5,'RFVOR= ',D10.3,/,
     4T5,'RFSF= ',D10.3,/,
     5T5,'VBC= ',I3.2(/))
      END
C
C
C
      SUBROUTINE GRIDNC
C
C*********************************************************************
C
```

```
C     NAME: GRID NON CONFORMAL.
C
C     PURPOSE:
C
C     THIS SUBROUTINE HAS BEEN BUILT TO PRODUCE AN
C   ORTHOGONAL GRID WHICH DOES NOT HAVE TO BE CONFORMAL.
C     FOR ANY OF BOUNDARY THE GRID POINT POSITIONS COULD
C   BE PRESCRIBED (BTYPE=1). IN THAT CASE THE INITIAL POINT
C   POSITIONS WILL BE USED.
C     THE RATIO OF SCALE FACTORS IN EACH CORNER COULD BE
C   SPECIFIED ALSO. THE RATIO AT A SPECIFIC CORNER WILL BE CONSIDERED
C   ONLY IF THE GRID POINT POSITIONS ARE NOT SPECIFIED ON THE
C   WALL JOINING AT THE CORNER.
C
C     CHARACTERISTIC:
C
C     - LINE BY LINE SOLVER.
C     - SECOND ORDER ACCURACY NEUMANN BOUNDARY CONDITION.
C     - ABSOLUTE ACCURACY CRITERION.
C     - MAXIMUM NUMBER OF ITERATION.
C     - RELAXATION FACTOR.
C
C*********************************************************************
C
      IMPLICIT REAL*8(A-H,O-Z)
      INTEGER BTYPE(4),C1,C1UL
      REAL*8 D(50,50,4),H(50,50,2),RSF(50,50),XY(50,50,2)
      REAL*8 ATDMA(50),BTDMA(50),CTDMA(50),DTDMA(50),SLN(50)
      COMMON /BLK1/ M,N
      COMMON /BLK2/ BTYPE,RSF
      COMMON /BLK3/ XY
      COMMON /BLK4/ H
      COMMON /BLK5/ D
      COMMON /BLK10/ ATDMA,BTDMA,CTDMA,DTDMA,SLN
      COMMON /BLK11/ EPS1,RFXY,C1UL
C
C*** SET UP VARIABLES.
C
      C1=0
      MM1=M-1
      MM2=M-2
      NM1=N-1
      NM2=N-2
C
C*** OVERALL LOOP.
C
C*** CALCULATE THE RATIO OF SCALE FACTORS.
C
   10 CALL DISF
      DIFX=0.D0
      DIFY=0.D0
C
C*** MOVE ROWS.
C
      DO 120 I=2,MM1
C
C*** SOLVE FOR Y.
C
C*** SET UP THE TDMA COEFFICIENTS.
C
```

```
      DO 20 J=2,NM1
       AT=2.DO/(RSF(I,J)+RSF(I-1,J))
       AR=(RSF(I,J)+RSF(I,J+1))/2.DO
       AB=2.DO/(RSF(I,J)+RSF(I+1,J))
       AL=(RSF(I,J)+RSF(I,J-1))/2.DO
       ATDMA(J)=AT+AR+AB+AL
       BTDMA(J)=AR
       CTDMA(J)=AL
       DTDMA(J)=AT*XY(I-1,J,2)+AB*XY(I+1,J,2)
  20   CONTINUE
C
C*** SET UP THE BOUNDARY CONDITION (NEUMAN OR DIRICHLET).
C
      IF (BTYPE(4).EQ.1) GOTO 30
      ATDMA(1)=3.DO
      BTDMA(1)=4.DO
      CTDMA(1)=0.DO
      AMO=3.DO*XY(I,1,1)-4.DO*XY(I,2,1)+XY(I,3,1)
      DTDMA(1)=-AMO*F(XY(I,1,2),8)
      ACRI1=-1.DO
      GOTO 40
  30  ATDMA(1)=1.DO
      BTDMA(1)=0.DO
      CTDMA(1)=0.DO
      DTDMA(1)=XY(I,1,2)
      ACRI1=0.DO
  40  IF (BTYPE(2).EQ.1) GOTO 50
      ATDMA(N)=3.DO
      BTDMA(N)=0.DO
      CTDMA(N)=4.DO
      AMO=3.DO*XY(I,N,1)-4.DO*XY(I,NM1,1)+XY(I,NM2,1)
      DTDMA(N)=-AMO*F(XY(I,N,2),6)
      ACRIM=-1.DO
      GOTO 60
  50  ATDMA(N)=1.DO
      BTDMA(N)=0.DO
      CTDMA(N)=0.DO
      DTDMA(N)=XY(I,N,2)
      ACRIM=0.DO
C
C*** REVISED TRIDIAGONAL-MATRIX ALGORITHM.
C
  60  CALL RTDMA (N,ACRI1,ACRIM)
C
C*** STORE THE VECTOR SOLUTION.
C
      DO 70 J=1,N
       AMO=XY(I,J,2)+RFXY*(SLN(J)-XY(I,J,2))
       DIFY=DMAX1(DIFY,DABS(AMO-XY(I,J,2)))
       XY(I,J,2)=AMO
  70  CONTINUE
C
C*** DIRICHLET CONDITIONS.
C
C*** RIGHT WALL.
C
      IF (BTYPE(2).EQ.1) GOTO 80
      AMO=F(XY(I,N,2),2)
      DIFX=DMAX1(DIFX,DABS(AMO-XY(I,N,1)))
      XY(I,N,1)=AMO
```

```
C
C*** LEFT WALL.
C
  80  IF (BTYPE(4).EQ.1) GOTO 90
      AMO=F(XY(I,1,2),4)
      DIFX=DMAX1(DIFX,DABS(AMO-XY(I,1,1)))
      XY(I,1,1)=AMO
C
C*** SOLVE FOR X.
C
C*** SET UP THE TDMA COEFFICIENTS.
C
  90  DO 100 J=2,NM1
       AT=2.DO/(RSF(I,J)+RSF(I-1,J))
       AR=(RSF(I,J)+RSF(I,J+1))/2.DO
       AB=2.DO/(RSF(I,J)+RSF(I+1,J))
       AL=(RSF(I,J)+RSF(I,J-1))/2.DO
       ATDMA(J)=AT+AR+AB+AL
       BTDMA(J)=AR
       CTDMA(J)=AL
       DTDMA(J)=AT*XY(I-1,J,1)+AB*XY(I+1,J,1)
 100  CONTINUE
C
C*** SET UP THE BOUNDARY CONDITIONS (DIRICHLET).
C
      DTDMA(2)=DTDMA(2)+CTDMA(2)*XY(I,1,1)
      CTDMA(2)=0.DO
      DTDMA(NM1)=DTDMA(NM1)+BTDMA(NM1)*XY(I,N,1)
      BTDMA(NM1)=0.DO
C
C*** TRIDIAGONAL-MATRIX ALGORITHM.
C
      CALL TDMA (2,NM1)
C
C*** STORE THE SOLUTION VECTOR.
C
      DO 110 J=2,NM1
       AMO=XY(I,J,1)+RFXY*(SLN(J)-XY(I,J,1))
       DIFX=DMAX1(DIFX,DABS(AMO-XY(I,J,1)))
       XY(I,J,1)=AMO
 110  CONTINUE
 120 CONTINUE
C
C*** MOVE COLUMNS.
C
     DO 230 J=2,NM1
C
C*** SOLVE FOR X.
C
C*** SET UP THE TDMA COEFFICIENTS.
C
      DO 130 I=2,MM1
       AT=2.DO/(RSF(I,J)+RSF(I-1,J))
       AR=(RSF(I,J)+RSF(I,J+1))/2.DO
       AB=2.DO/(RSF(I,J)+RSF(I+1,J))
       AL=(RSF(I,J)+RSF(I,J-1))/2.DO
       ATDMA(I)=AT+AR+AB+AL
       BTDMA(I)=AB
       CTDMA(I)=AT
       DTDMA(I)=AR*XY(I,J+1,1)+AL*XY(I,J-1,1)
```

```
 130  CONTINUE
C
C*** SET UP THE BOUNDARY CONDITIONS (NEWMAN OR DIRICHLET).
C
      IF (BTYPE(1).EQ.1) GOTO 140
      ATDMA(1)=3.DO
      BTDMA(1)=4.DO
      CTDMA(1)=0.DO
      AMO=3.DO*XY(1,J,2)-4.DO*XY(2,J,2)+XY(3,J,2)
      DTDMA(1)=-AMO*F(XY(1,J,1),5)
      ACRI1=-1.DO
      GOTO 150
 140  ATDMA(1)=1.DO
      BTDMA(1)=0.DO
      CTDMA(1)=0.DO
      DTDMA(1)=XY(1,J,1)
      ACRI1=0.DO
 150  IF (BTYPE(3).EQ.1) GOTO 160
      ATDMA(M)=3.DO
      BTDMA(M)=0.DO
      CTDMA(M)=4.DO
      AMO=3.DO*XY(M,J,2)-4.DO*XY(MM1,J,2)+XY(MM2,J,2)
      DTDMA(M)=-AMO*F(XY(M,J,1),7)
      ACRIM=-1.DO
      GOTO 170
 160  ATDMA(M)=1.DO
      BTDMA(M)=0.DO
      CTDMA(M)=0.DO
      DTDMA(M)=XY(M,J,1)
      ACRIM=0.DO
C
C*** REVISED TRIDIAGONAL-MATRIX ALGORITHM.
C
 170  CALL RTDMA (M,ACRI1,ACRIM)
C
C*** STORE THE VECTOR SOLUTION.
C
      DO 180 I=1,M
       AMO=XY(I,J,1)+RFXY*(SLN(I)-XY(I,J,1))
       DIFX=DMAX1(DIFX,DABS(AMO-XY(I,J,1)))
       XY(I,J,1)=AMO
 180  CONTINUE
C
C*** DIRICHLET CONDITIONS.
C
C*** TOP WALL.
C
      IF (BTYPE(1).EQ.1) GOTO 190
      AMO=F(XY(1,J,1),1)
      DIFY=DMAX1(DIFY,DABS(AMO-XY(1,J,2)))
      XY(1,J,2)=AMO
C
C*** BOTTOM WALL.
C
 190  IF (BTYPE(3).EQ.1) GOTO 200
      AMO=F(XY(M,J,1),3)
      DIFY=DMAX1(DIFY,DABS(AMO-XY(M,J,2)))
      XY(M,J,2)=AMO
C
C*** SOLVE FOR Y.
```

```
C
C*** SET UP THE TDMA COEFFICIENTS.
C
 200  DO 210 I=2,MM1
       AT=2.DO/(RSF(I,J)+RSF(I-1,J))
       AR=(RSF(I,J)+RSF(I,J+1))/2.DO
       AB=2.DO/(RSF(I,J)+RSF(I+1,J))
       AL=(RSF(I,J)+RSF(I,J-1))/2.DO
       ATDMA(I)=AT+AR+AB+AL
       BTDMA(I)=AB
       CTDMA(I)=AT
       DTDMA(I)=AR*XY(I,J+1,2)+AL*XY(I,J-1,2)
 210  CONTINUE
C
C*** SET THE BOUNDARY CONDITIONS (DIRICHLET).
C
      DTDMA(2)=DTDMA(2)+CTDMA(2)*XY(1,J,2)
      CTDMA(2)=0.DO
      DTDMA(MM1)=DTDMA(MM1)+BTDMA(MM1)*XY(M,J,2)
      BTDMA(MM1)=0.DO
C
C*** TRIDIAGONAL-MATRIX ALGORITHM.
C
      CALL TDMA (2,MM1)
C
C*** STORE THE VECTOR SOLUTION.
C
      DO 220 I=2,MM1
       AMO=XY(I,J,2)+RFXY*(SLN(I)-XY(I,J,2))
       DIFY=DMAX1(DIFY,DABS(AMO-XY(I,J,2)))
       XY(I,J,2)=AMO
 220  CONTINUE
 230 CONTINUE
C
C*** ACCURACY AND PRINTOUT.
C
     C1=C1+1
     WRITE (6,240) C1,DIFX,DIFY
     IF ((DIFX.GE.2.DO).OR.(DIFY.GE.2.DO)) STOP
     IF (((DIFX.GT.EPS1).OR.(DIFY.GT.EPS1)).AND.(C1.LT.C1UL))
    1GOTO 10
C
C*** CALCULATION OF THE DERIVATIVES AND SCALE FACTORS.
C
     CALL DSF
C
C*** ORTHOGONALITY TEST.
C
     CALL ORTHO
     RETURN
 240 FORMAT(/,T5,'(',I3,')',3X,'DIFX= ',D11.5,3X,'DIFY= ',D11.5)
     END
C
C
C
     SUBROUTINE NATC
C
C**********************************************************************
C
C    NAME: NATURAL CONVECTION.
```

```
C
C     PURPOSE:
C
C     THIS SUBROUTINE COMPUTES THE SOLUTION OF A STEADY-STATE
C   NATURAL CONVECTION IN A NON-RECTANGULAR CAVITY.
C
C     CHARACTERISTIC:
C
C     - LINE BY LINE SOLVER.
C     - WOOD VORTICITY BOUNDARY CONDITION.
C     - EXPONENTIAL SCHEME.
C     - GRID IS ORTHOGONAL AND NOT NECESSAIRLY CONFORMAL.
C     - GRID IS UNIFORMLY SPACE IN THE NEW DOMAIN.
C     - RELAXATION FACTOR.
C     - STAGGERED GRID.
C     - RELATIVE ACCURACY CRITERION.
C     - DIVERGENCE TEST.
C     - MAXIMUM NUMBER OF ITERATIONS.
C     - WALLS ARE IMPERMEABLE.
C     - TOP AND BOTTOM WALLS ARE ADIABATIC.
C     - RIGHT AND LEFT WALLS ARE ISOTHERMS.
C
C*********************************************************************
C
      IMPLICIT REAL*8(A-H,O-Z)
      INTEGER C2,C2UL,VBC
      REAL*8 ATDMA(50),BTDMA(50),CTDMA(50),DTDMA(50),SLN(50)
      REAL*8 SF(50,50),T(50,50),VOR(50,50)
      REAL*8 D(50,50,4),H(50,50,2),MAXSF,MAXVOR
      COMMON /BLK1/ M,N
      COMMON /BLK4/ H
      COMMON /BLK5/ D
      COMMON /BLK6/ PR,RA
      COMMON /BLK7/ T
      COMMON /BLK8/ VOR
      COMMON /BLK9/ SF
      COMMON /BLK10/ ATDMA,BTDMA,CTDMA,DTDMA,SLN
      COMMON /BLK12/ EPS2,RFT,RFVOR,RFSF,C2UL,VBC
C
C*** SET UP VARIABLES.
C
      C2=0
      MM1=M-1
      MM2=M-2
      MP1=M+1
      NM1=N-1
      NM2=N-2
      NP1=N+1
C
C*** OVERALL LOOP.
C
   10 MAXVOR=0.D0
      MAXSF=0.D0
      DIFT=0.D0
      DIFVOR=0.D0
      DIFSF=0.D0
C
C*** MOVE ROWS.
C
      DO 100 I=2,M
```

```
C
C*** ENERGY EQUATION.
C
C*** COMPUTATION OF ENERGY EQUATION COEFFICIENTS.
C
      DO 20 J=2,N
       COND=(H(I-1,J-1,1)+H(I-1,J,1))/(H(I-1,J-1,2)+H(I-1,J,2))
       CONV=SF(I-1,J-1)-SF(I-1,J)
       AT=COND*COEFF(COND,CONV)+DMAX1(0.DO,-CONV)
       COND=(H(I-1,J,2)+H(I,J,2))/(H(I-1,J,1)+H(I,J,1))
       CONV=SF(I-1,J)-SF(I,J)
       AR=COND*COEFF(COND,CONV)+DMAX1(0.DO,-CONV)
       COND=(H(I,J-1,1)+H(I,J,1))/(H(I,J-1,2)+H(I,J,2))
       CONV=SF(I,J-1)-SF(I,J)
       AB=COND*COEFF(COND,CONV)+DMAX1(0.DO,CONV)
       COND=(H(I-1,J-1,2)+H(I,J-1,2))/(H(I-1,J-1,1)+H(I,J-1,1))
       CONV=SF(I-1,J-1)-SF(I,J-1)
       AL=COND*COEFF(COND,CONV)+DMAX1(0.DO,CONV)
       ATDMA(J)=AT+AR+AB+AL
       BTDMA(J)=AR
       CTDMA(J)=AL
       DTDMA(J)=AT*T(I-1,J)+AB*T(I+1,J)
  20  CONTINUE
C
C*** SET UP THE BOUNDARY CONDITIONS (CONSTANT TEMPERATURE WALLS).
C
      ATDMA(1)=1.DO
      BTDMA(1)=-1.DO
      CTDMA(1)=0.DO
      DTDMA(1)=0.DO
      ATDMA(NP1)=1.DO
      BTDMA(NP1)=0.DO
      CTDMA(NP1)=-1.DO
      DTDMA(NP1)=2.DO
C
C*** TRIDIAGONAL-MATRIX ALGORITHM.
C
      CALL TDMA (1,NP1)
C
C*** STORE THE SOLUTION VECTOR.
C
      DO 30 J=1,NP1
       AMO=T(I,J)+RFT*(SLN(J)-T(I,J))
       DIFT=DMAX1(DIFT,DABS(AMO-T(I,J)))
       T(I,J)=AMO
  30  CONTINUE
C
C*** VORTICITY EQUATION.
C
C*** COMPUTATION OF VORTICITY EQUATION COEFFICIENTS.
C
      DO 40 J=2,N
       COND=PR*(H(I-1,J-1,1)+H(I-1,J,1))/(H(I-1,J-1,2)+H(I-1,J,2))
       CONV=SF(I-1,J-1)-SF(I-1,J)
       AT=COND*COEFF(COND,CONV)+DMAX1(0.DO,-CONV)
       COND=PR*(H(I-1,J,2)+H(I,J,2))/(H(I-1,J,1)+H(I,J,1))
       CONV=SF(I-1,J)-SF(I,J)
       AR=COND*COEFF(COND,CONV)+DMAX1(0.DO,-CONV)
       COND=PR*(H(I,J-1,1)+H(I,J,1))/(H(I,J-1,2)+H(I,J,2))
       CONV=SF(I,J-1)-SF(I,J)
```

```
        AB=COND*COEFF(COND,CONV)+DMAX1(0.DO,CONV)
        COND=PR*(H(I-1,J-1,2)+H(I,J-1,2))/(H(I-1,J-1,1)+H(I,J-1,1))
        CONV=SF(I-1,J-1)-SF(I,J-1)
        AL=COND*COEFF(COND,CONV)+DMAX1(0.DO,CONV)
        AMO=(D(I-1,J-1,2)+D(I-1,J,2)+D(I,J-1,2)+D(I,J,2))/4.DO
        AM1=(D(I-1,J-1,4)+D(I-1,J,4)+D(I,J-1,4)+D(I,J,4))/4.DO
        AM2=(T(I,J+1)-T(I,J-1))/2.DO
        AM3=(T(I-1,J)-T(I+1,J))/2.DO
        B=(AM1*AM2-AMO*AM3)*PR*RA
        ATDMA(J)=AT+AR+AB+AL
        BTDMA(J)=AR
        CTDMA(J)=AL
        DTDMA(J)=AT*VOR(I-1,J)+AB*VOR(I+1,J)+B
  40    CONTINUE
C
C*** SET UP THE VORTICITY BOUNDARY CONDITION.
C*** WALLS ARE IMPERMEABLE.
C
        IF (VBC.EQ.1) GOTO 50
C
C*** WOOD.
C
        AMO=(H(I-1,1,1)+H(I,1,1))/2.DO
        AM1=(H(I-1,1,2)+H(I,1,2))/2.DO
        AM2=(H(I-1,2,1)+H(I,2,1))/2.DO
        AM3=(H(I-1,2,2)+H(I,2,2))/2.DO
        AM4=(H(I-1,3,1)+H(I,3,1))/2.DO
        AM5=(H(I-1,3,2)+H(I,3,2))/2.DO
        AM6=(-3.DO*AMO*AM1+4.DO*AM2*AM3-AM4*AM5)/2.DO
        AM7=(-3.DO*AM1/AMO+4.DO*AM3/AM2-AM5/AM4)/2.DO
        AM8=(AMO**2)/2.DO
        AM9=AMO*AM6/(6.DO*AM1)
        AM10=-(AMO**3)*AM7/(3.DO*AM1)
        AM11=-(AMO**2)/4.DO
        AM12=-AMO*AM6/(12.DO*AM1)
        AM13=(AMO**2)/6.DO
        AM14=(AMO**3)*AM7/(6.DO*AM1)
        AM15=AM8+AM9+AM10
        AM16=AM11+AM12+AM13+AM14
        ATDMA(1)=AM16
        BTDMA(1)=AM15+AM16
        CTDMA(1)=0.DO
        DTDMA(1)=(SF(I-1,2)+SF(I,2))/2.DO
        AMO=(H(I-1,N,1)+H(I,N,1))/2.DO
        AM1=(H(I-1,N,2)+H(I,N,2))/2.DO
        AM2=(H(I-1,NM1,1)+H(I,NM1,1))/2.DO
        AM3=(H(I-1,NM1,2)+H(I,NM1,2))/2.DO
        AM4=(H(I-1,NM2,1)+H(I,NM2,1))/2.DO
        AM5=(H(I-1,NM2,2)+H(I,NM2,2))/2.DO
        AM6=(-3.DO*AMO*AM1+4.DO*AM2*AM3-AM4*AM5)/2.DO
        AM7=(-3.DO*AM1/AMO+4.DO*AM3/AM2-AM5/AM4)/2.DO
        AM8=(AMO**2)/2.DO
        AM9=AMO*AM6/(6.DO*AM1)
        AM10=-(AMO**3)*AM7/(3.DO*AM1)
        AM11=-(AMO**2)/4.DO
        AM12=-AMO*AM6/(12.DO*AM1)
        AM13=(AMO**2)/6.DO
        AM14=(AMO**3)*AM7/(6.DO*AM1)
        AM15=AM8+AM9+AM10
        AM16=AM11+AM12+AM13+AM14
```

```
      ATDMA(NP1)=AM16
      BTDMA(NP1)=0.DO
      CTDMA(NP1)=AM15+AM16
      DTDMA(NP1)=(SF(I-1,NM1)+SF(I,NM1))/2.DO
      ACRI1=0.DO
      ACRIM=0.DO
      GOTO 60
C
C*** SECOND ORDER.
C
   50 AMO=(H(I-1,1,1)+H(I,1,1))/2.DO
      AM1=(H(I-1,1,2)+H(I,1,2))/2.DO
      AM2=(H(I-1,2,1)+H(I,2,1))/2.DO
      AM3=(H(I-1,2,2)+H(I,2,2))/2.DO
      AM4=(H(I-1,3,1)+H(I,3,1))/2.DO
      AM5=(H(I-1,3,2)+H(I,3,2))/2.DO
      AM6=(-3.DO*AMO*AM1+4.DO*AM2*AM3-AM4*AM5)/2.DO
      AM7=(-3.DO*AM1/AMO+4.DO*AM3/AM2-AM5/AM4)/2.DO
      AM8=27.DO*(AMO**2)/4.DO
      AM9=3.DO*AMO*AM6/(2.DO*AM1)
      AM10=-3.DO*(AMO**3)*AM7/AM1
      AM11=-3.DO*(AMO**2)/4.DO
      AM12=-AMO*AM6/(6.DO*AM1)
      AM13=(AMO**3)*AM7/(3.DO*AM1)
      AM14=-9.DO*(AMO**2)/4.DO
      AM15=-AMO*AM6/(2.DO*AM1)
      AM16=4.DO*(AMO**2)/3.DO
      AM17=(AMO**3)*AM7/AM1
      AM18=AM8+AM9+AM10
      AM19=AM11+AM12+AM13
      AM20=AM14+AM15+AM16+AM17
      ATDMA(1)=AM20
      BTDMA(1)=AM18+AM20
      CTDMA(1)=0.DO
      DTDMA(1)=(16.DO*(SF(I-1,2)+SF(I,2))-(SF(I-1,3)+SF(I,3)))/2.DO
      ACRI1=AM19
      AMO=(H(I-1,N,1)+H(I,N,1))/2.DO
      AM1=(H(I-1,N,2)+H(I,N,2))/2.DO
      AM2=(H(I-1,NM1,1)+H(I,NM1,1))/2.DO
      AM3=(H(I-1,NM1,2)+H(I,NM1,2))/2.DO
      AM4=(H(I-1,NM2,1)+H(I,NM2,1))/2.DO
      AM5=(H(I-1,NM2,2)+H(I,NM2,2))/2.DO
      AM6=(-3.DO*AMO*AM1+4.DO*AM2*AM3-AM4*AM5)/2.DO
      AM7=(-3.DO*AM1/AMO+4.DO*AM3/AM2-AM5/AM4)/2.DO
      AM8=27.DO*(AMO**2)/4.DO
      AM9=3.DO*AMO*AM6/(2.DO*AM1)
      AM10=-3.DO*(AMO**3)*AM7/AM1
      AM11=-3.DO*(AMO**2)/4.DO
      AM12=-AMO*AM6/(6.DO*AM1)
      AM13=(AMO**3)*AM7/(3.DO*AM1)
      AM14=-9.DO*(AMO**2)/4.DO
      AM15=-AMO*AM6/(2.DO*AM1)
      AM16=4.DO*(AMO**2)/3.DO
      AM17=(AMO**3)*AM7/AM1
      AM18=AM8+AM9+AM10
      AM19=AM11+AM12+AM13
      AM20=AM14+AM15+AM16+AM17
      ATDMA(NP1)=AM20
      BTDMA(NP1)=0.DO
      CTDMA(NP1)=AM18+AM20
```

```
      DTDMA(NP1)=(16.DO*(SF(I-1,NM1)+SF(I,NM1))-(SF(I-1,NM2)
     1+SF(I,NM2)))/2.DO
      ACRIM=AM19
C
C*** REVISED TRIDIAGONAL-MATRIX ALGORITHM.
C
   60 CALL RTDMA (NP1,ACRI1,ACRIM)
C
C*** STORE THE SOLUTION VECTOR.
C
      DO 70 J=1,NP1
       AMO=VOR(I,J)+RFVOR*(SLN(J)-VOR(I,J))
       DIFVOR=DMAX1(DIFVOR,DABS(AMO-VOR(I,J)))
       MAXVOR=DMAX1(MAXVOR,DABS(AMO))
       VOR(I,J)=AMO
   70 CONTINUE
      IF (I.EQ.M) GOTO 100
C
C*** STREAM FUNCTION EQUATION.
C
C*** COMPUTATION OF THE STREAM FUNCTION EQUATION COEFFICIENTS.
C
      DO 80 J=2,NM1
       AT=(H(I-1,J,1)+H(I,J,1))/(H(I-1,J,2)+H(I,J,2))
       AR=(H(I,J,2)+H(I,J+1,2))/(H(I,J,1)+H(I,J+1,1))
       AB=(H(I,J,1)+H(I+1,J,1))/(H(I,J,2)+H(I+1,J,2))
       AL=(H(I,J-1,2)+H(I,J,2))/(H(I,J-1,1)+H(I,J,1))
       AMO=(VOR(I,J)+VOR(I,J+1)+VOR(I+1,J)+VOR(I+1,J+1))/4.DO
       B=AMO*H(I,J,1)*H(I,J,2)
       ATDMA(J)=AT+AR+AB+AL
       BTDMA(J)=AR
       CTDMA(J)=AL
       DTDMA(J)=AT*SF(I-1,J)+AB*SF(I+1,J)+B
   80 CONTINUE
C
C*** SET UP THE BOUNDARY CONDITIONS.
C
      DTDMA(2)=DTDMA(2)+CTDMA(2)*SF(I,1)
      CTDMA(2)=0.DO
      DTDMA(NM1)=DTDMA(NM1)+BTDMA(NM1)*SF(I,N)
      BTDMA(NM1)=0.DO
C
C*** TRIDIAGONAL-MATRIX ALGORITHM.
C
      CALL TDMA (2,NM1)
C
C*** STORE THE SOLUTION VECTOR.
C
      DO 90 J=2,NM1
       AMO=SF(I,J)+RFSF*(SLN(J)-SF(I,J))
       DIFSF=DMAX1(DIFSF,DABS(AMO-SF(I,J)))
       MAXSF=DMAX1(MAXSF,DABS(AMO))
       SF(I,J)=AMO
   90 CONTINUE
  100 CONTINUE
C
C*** MOVE COLUMNS
C
      DO 190 J=2,N
C
```

```
C*** ENERGY EQUATION.
C
C*** COMPUTATION OF ENERGY EQUATION COEFFICIENTS.
C
      DO 110 I=2,M
       COND=(H(I-1,J-1,1)+H(I-1,J,1))/(H(I-1,J-1,2)+H(I-1,J,2))
       CONV=SF(I-1,J-1)-SF(I-1,J)
       AT=COND*COEFF(COND,CONV)+DMAX1(0.DO,-CONV)
       COND=(H(I-1,J,2)+H(I,J,2))/(H(I-1,J,1)+H(I,J,1))
       CONV=SF(I-1,J)-SF(I,J)
       AR=COND*COEFF(COND,CONV)+DMAX1(0.DO,-CONV)
       COND=(H(I,J-1,1)+H(I,J,1))/(H(I,J-1,2)+H(I,J,2))
       CONV=SF(I,J-1)-SF(I,J)
       AB=COND*COEFF(COND,CONV)+DMAX1(0.DO,CONV)
       COND=(H(I-1,J-1,2)+H(I,J-1,2))/(H(I-1,J-1,1)+H(I,J-1,1))
       CONV=SF(I-1,J-1)-SF(I,J-1)
       AL=COND*COEFF(COND,CONV)+DMAX1(0.DO,CONV)
       ATDMA(I)=AT+AR+AB+AL
       BTDMA(I)=AB
       CTDMA(I)=AT
       DTDMA(I)=AR*T(I,J+1)+AL*T(I,J-1)
 110  CONTINUE
C
C*** SET UP THE BOUNDARY CONDITIONS (ADIABATIC WALLS).
C
      ATDMA(1)=1.DO
      BTDMA(1)=1.DO
      CTDMA(1)=0.DO
      DTDMA(1)=0.DO
      ATDMA(MP1)=1.DO
      BTDMA(MP1)=0.DO
      CTDMA(MP1)=1.DO
      DTDMA(MP1)=0.DO
C
C*** TRIDIAGONAL-MATRIX ALGORITHM.
C
      CALL TDMA (1,MP1)
C
C*** STORE THE SOLUTION VECTOR.
C
      DO 120 I=1,MP1
       AMO=T(I,J)+RFT*(SLN(I)-T(I,J))
       DIFT=DMAX1(DIFT,DABS(AMO-T(I,J)))
       T(I,J)=AMO
 120  CONTINUE
C
C*** VORTICITY EQUATION.
C
C*** COMPUTATION OF VORTICITY EQUATION COEFFICIENTS.
C
      DO 130 I=2,M
       COND=PR*(H(I-1,J-1,1)+H(I-1,J,1))/(H(I-1,J-1,2)+H(I-1,J,2))
       CONV=SF(I-1,J-1)-SF(I-1,J)
       AT=COND*COEFF(COND,CONV)+DMAX1(0.DO,-CONV)
       COND=PR*(H(I-1,J,2)+H(I,J,2))/(H(I-1,J,1)+H(I,J,1))
       CONV=SF(I-1,J)-SF(I,J)
       AR=COND*COEFF(COND,CONV)+DMAX1(0.DO,-CONV)
       COND=PR*(H(I,J-1,1)+H(I,J,1))/(H(I,J-1,2)+H(I,J,2))
       CONV=SF(I,J-1)-SF(I,J)
       AB=COND*COEFF(COND,CONV)+DMAX1(0.DO,CONV)
```

```
        COND=PR*(H(I-1,J-1,2)+H(I,J-1,2))/(H(I-1,J-1,1)+H(I,J-1,1))
        CONV=SF(I-1,J-1)-SF(I,J-1)
        AL=COND*COEFF(COND,CONV)+DMAX1(0.D0,CONV)
        AM0=(D(I-1,J-1,2)+D(I-1,J,2)+D(I,J-1,2)+D(I,J,2))/4.D0
        AM1=(D(I-1,J-1,4)+D(I-1,J,4)+D(I,J-1,4)+D(I,J,4))/4.D0
        AM2=(T(I,J+1)-T(I,J-1))/2.D0
        AM3=(T(I-1,J)-T(I+1,J))/2.D0
        B=(AM1*AM2-AM0*AM3)*PR*RA
        ATDMA(I)=AT+AR+AB+AL
        BTDMA(I)=AB
        CTDMA(I)=AT
        DTDMA(I)=AR*VOR(I,J+1)+AL*VOR(I,J-1)+B
  130   CONTINUE
C
C***  SET UP THE VORTICITY BOUNDARY CONDITION.
C***  WALLS ARE IMPERMEABLE.
C
        IF (VBC.EQ.1) GOTO 140
C
C***  WOOD.
C
        AM0=(H(1,J-1,2)+H(1,J,2))/2.D0
        AM1=(H(1,J-1,1)+H(1,J,1))/2.D0
        AM2=(H(2,J-1,2)+H(2,J,2))/2.D0
        AM3=(H(2,J-1,1)+H(2,J,1))/2.D0
        AM4=(H(3,J-1,2)+H(3,J,2))/2.D0
        AM5=(H(3,J-1,1)+H(3,J,1))/2.D0
        AM6=(-3.D0*AM0*AM1+4.D0*AM2*AM3-AM4*AM5)/2.D0
        AM7=(-3.D0*AM1/AM0+4.D0*AM3/AM2-AM5/AM4)/2.D0
        AM8=(AM0**2)/2.D0
        AM9=AM0*AM6/(6.D0*AM1)
        AM10=-(AM0**3)*AM7/(3.D0*AM1)
        AM11=-(AM0**2)/4.D0
        AM12=-AM0*AM6/(12.D0*AM1)
        AM13=(AM0**2)/6.D0
        AM14=(AM0**3)*AM7/(6.D0*AM1)
        AM15=AM8+AM9+AM10
        AM16=AM11+AM12+AM13+AM14
        ATDMA(1)=AM16
        BTDMA(1)=AM15+AM16
        CTDMA(1)=0.D0
        DTDMA(1)=(SF(2,J-1)+SF(2,J))/2.D0
        AM0=(H(M,J-1,2)+H(M,J,2))/2.D0
        AM1=(H(M,J-1,1)+H(M,J,1))/2.D0
        AM2=(H(MM1,J-1,2)+H(MM1,J,2))/2.D0
        AM3=(H(MM1,J-1,1)+H(MM1,J,1))/2.D0
        AM4=(H(MM2,J-1,2)+H(MM2,J,2))/2.D0
        AM5=(H(MM2,J-1,1)+H(MM2,J,1))/2.D0
        AM6=(-3.D0*AM0*AM1+4.D0*AM2*AM3-AM4*AM5)/2.D0
        AM7=(-3.D0*AM1/AM0+4.D0*AM3/AM2-AM5/AM4)/2.D0
        AM8=(AM0**2)/2.D0
        AM9=AM0*AM6/(6.D0*AM1)
        AM10=-(AM0**3)*AM7/(3.D0*AM1)
        AM11=-(AM0**2)/4.D0
        AM12=-AM0*AM6/(12.D0*AM1)
        AM13=(AM0**2)/6.D0
        AM14=(AM0**3)*AM7/(6.D0*AM1)
        AM15=AM8+AM9+AM10
        AM16=AM11+AM12+AM13+AM14
        ATDMA(MP1)=AM16
```

```
      BTDMA(MP1)=0.DO
      CTDMA(MP1)=AM15+AM16
      DTDMA(MP1)=(SF(MM1,J-1)+SF(MM1,J))/2.DO
      ACRI1=0.DO
      ACRIM=0.DO
      GOTO 150
C
C*** SECOND ORDER.
C
  140 AMO=(H(1,J-1,2)+H(1,J,2))/2.DO
      AM1=(H(1,J-1,1)+H(1,J,1))/2.DO
      AM2=(H(2,J-1,2)+H(2,J,2))/2.DO
      AM3=(H(2,J-1,1)+H(2,J,1))/2.DO
      AM4=(H(3,J-1,2)+H(3,J,2))/2.DO
      AM5=(H(3,J-1,1)+H(3,J,1))/2.DO
      AM6=(-3.DO*AMO*AM1+4.DO*AM2*AM3-AM4*AM5)/2.DO
      AM7=(-3.DO*AM1/AMO+4.DO*AM3/AM2-AM5/AM4)/2.DO
      AM8=27.DO*(AMO**2)/4.DO
      AM9=3.DO*AMO*AM6/(2.DO*AM1)
      AM10=-3.DO*(AMO**3)*AM7/AM1
      AM11=-3.DO*(AMO**2)/4.DO
      AM12=-AMO*AM6/(6.DO*AM1)
      AM13=(AMO**3)*AM7/(3.DO*AM1)
      AM14=-9.DO*(AMO**2)/4.DO
      AM15=-AMO*AM6/(2.DO*AM1)
      AM16=4.DO*(AMO**2)/3.DO
      AM17=(AMO**3)*AM7/AM1
      AM18=AM8+AM9+AM10
      AM19=AM11+AM12+AM13
      AM20=AM14+AM15+AM16+AM17
      ATDMA(1)=AM20
      BTDMA(1)=AM18+AM20
      CTDMA(1)=0.DO
      DTDMA(1)=(16.DO*(SF(2,J-1)+SF(2,J))-(SF(3,J-1)+SF(3,J)))/2.DO
      ACRI1=AM19
      AMO=(H(M,J-1,2)+H(M,J,2))/2.DO
      AM1=(H(M,J-1,1)+H(M,J,1))/2.DO
      AM2=(H(MM1,J-1,2)+H(MM1,J,2))/2.DO
      AM3=(H(MM1,J-1,1)+H(MM1,J,1))/2.DO
      AM4=(H(MM2,J-1,2)+H(MM2,J,2))/2.DO
      AM5=(H(MM2,J-1,1)+H(MM2,J,1))/2.DO
      AM6=(-3.DO*AMO*AM1+4.DO*AM2*AM3-AM4*AM5)/2.DO
      AM7=(-3.DO*AM1/AMO+4.DO*AM3/AM2-AM5/AM4)/2.DO
      AM8=27.DO*(AMO**2)/4.DO
      AM9=3.DO*AMO*AM6/(2.DO*AM1)
      AM10=-3.DO*(AMO**3)*AM7/AM1
      AM11=-3.DO*(AMO**2)/4.DO
      AM12=-AMO*AM6/(6.DO*AM1)
      AM13=(AMO**3)*AM7/(3.DO*AM1)
      AM14=-9.DO*(AMO**2)/4.DO
      AM15=-AMO*AM6/(2.DO*AM1)
      AM16=4.DO*(AMO**2)/3.DO
      AM17=(AMO**3)*AM7/AM1
      AM18=AM8+AM9+AM10
      AM19=AM11+AM12+AM13
      AM20=AM14+AM15+AM16+AM17
      ATDMA(MP1)=AM20
      BTDMA(MP1)=0.DO
      CTDMA(MP1)=AM18+AM20
      DTDMA(MP1)=(16.DO*(SF(MM1,J-1)+SF(MM1,J))-(SF(MM2,J-1)
```

```
     1+SF(MM2,J)))/2.DO
       ACRIM=AM19
C
C*** REVISED TRIDIAGONAL-MATRIX ALGORITHM.
C
  150  CALL RTDMA (MP1,ACRI1,ACRIM)
C
C*** STORE THE SOLUTION VECTOR.
C
       DO 160 I=1,MP1
        AMO=VOR(I,J)+RFVOR*(SLN(I)-VOR(I,J))
        DIFVOR=DMAX1(DIFVOR,DABS(AMO-VOR(I,J)))
        MAXVOR=DMAX1(MAXVOR,DABS(AMO))
        VOR(I,J)=AMO
  160  CONTINUE
       IF (J.EQ.N) GOTO 190
C
C*** STREAM FUNCTION EQUATION.
C
C*** COMPUTATION OF THE STREAM FUNCTION EQUATION COEFFICIENTS.
C
       DO 170 I=2,MM1
        AT=(H(I-1,J,1)+H(I,J,1))/(H(I-1,J,2)+H(I,J,2))
        AR=(H(I,J,2)+H(I,J+1,2))/(H(I,J,1)+H(I,J+1,1))
        AB=(H(I,J,1)+H(I+1,J,1))/(H(I,J,2)+H(I+1,J,2))
        AL=(H(I,J-1,2)+H(I,J,2))/(H(I,J-1,1)+H(I,J,1))
        AMO=(VOR(I,J)+VOR(I,J+1)+VOR(I+1,J)+VOR(I+1,J+1))/4.DO
        B=AMO*H(I,J,1)*H(I,J,2)
        ATDMA(I)=AT+AR+AB+AL
        BTDMA(I)=AB
        CTDMA(I)=AT
        DTDMA(I)=AR*SF(I,J+1)+AL*SF(I,J-1)+B
  170  CONTINUE
C
C*** SET UP THE BOUNDARY CONDITIONS.
C
       DTDMA(2)=DTDMA(2)+CTDMA(2)*SF(1,J)
       CTDMA(2)=0.DO
       DTDMA(MM1)=DTDMA(MM1)+BTDMA(MM1)*SF(M,J)
       BTDMA(MM1)=0.DO
C
C*** TRIDIAGONAL-MATRIX ALGORITHM.
C
       CALL TDMA (2,MM1)
C
C*** STORE THE SOLUTION VECTOR.
C
       DO 180 I=2,MM1
        AMO=SF(I,J)+RFSF*(SLN(I)-SF(I,J))
        DIFSF=DMAX1(DIFSF,DABS(AMO-SF(I,J)))
        MAXSF=DMAX1(MAXSF,DABS(AMO))
        SF(I,J)=AMO
  180  CONTINUE
  190 CONTINUE
C
C*** ACCURACY, TEST AND PRINTOUT.
C
      C2=C2+1
      AMO=DIFT
      AM1=DIFVOR/MAXVOR
```

```
      AM2=DIFSF/MAXSF
      WRITE (6,200) C2,DIFT,DIFVOR,DIFSF,MAXVOR,MAXSF,AM0,AM1,
     1AM2
      IF (MAXVOR.GE.1.D10) STOP
      IF (((AM0.GT.EPS2).OR.(AM1.GT.EPS2).OR.(AM2.GT.EPS2))
     1.AND.          (C2.LT.C2UL)) GOTO 10
C
C*** CALCULATION OF NUSSELT NUMBERS.
C
      CALL NU
      RETURN
  200 FORMAT(/,T5,'(',I3,')',T15,'ENERGY',T26,'VORTICITY',
     1T38,'STREAM FUNCTION',/,T5,48('-'),/,T5,'DIF',
     2T13,D11.5,T26,D11.5,T40,D11.5,/,T5,'MAX',
     3T26,D11.5,T40,D11.5,/,T5,'RATIO',T13,D11.5,
     4T26,D11.5,T40,D11.5)
      END
C
C
C
      SUBROUTINE PLOT
C
C**********************************************************************
C
C     NAME: PLOT.
C
C     PURPOSE:
C
C     THIS SUBROUTINE PRODUCES THE PLOT OF THE GRID,
C   THE TEMPERATURE, THE STREAM FUNCTION, AND
C   VORTICITY DISTRIBUTIONS AND THE
C   THE LOCAL NUSSELT NUMBER PLOTS.
C
C     NB. THIS SUBROUTINE IS NOT GENERAL BUT SPECIFIC TO A GIVEN
C   PROBLEM. IT ALSO REQUIRED THE SOFTWARE "DISSPLA"
C
C**********************************************************************
C
      IMPLICIT REAL*8(A-H,O-Z)
      REAL*8 XY(50,50,2),T(50,50),SF(50,50),VOR(50,50)
      REAL*8 DIST(50,4),NUAV(4),NUL(50,4)
      REAL X(100),Y(100),XYS(50,50,2),XYZ(50,50,3),ZCNTR(50)
      REAL MAXSF,MINSF,MAXVOR,MINVOR
      COMMON /BLK1/ M,N
      COMMON /BLK3/ XY
      COMMON /BLK6/ PR,RA
      COMMON /BLK7/ T
      COMMON /BLK8/ VOR
      COMMON /BLK9/ SF
      COMMON /BLK13/ DIST,NUAV,NUL
      COMMON /BLKA/ XYZ,ZCNTR
C
C*** GRID TO COARSE.
C
      IF ((M.LT.20).AND.(N.LT.20)) RETURN
C
C*** SET UP VARIABLES.
C
      MM1=M-1
      MP1=M+1
```

```
      MP2=M+2
      NP1=N+1
C
C*** GRAPH THE GRID.
C
      CALL BGNPL (-1)
      CALL TITLE ('GRID',-4,'X AXIS',6,'Y AXIS',6,7.,6.)
      CALL GRAPH (0.,.2,0.,.2)
      CALL FRAME
      DO 20 I=1,M
       DO 10 J=1,N
        X(J)=XY(I,J,1)
        Y(J)=XY(I,J,2)
   10  CONTINUE
       CALL CURVE (X,Y,N,0)
   20 CONTINUE
      DO 40 J=1,N
       DO 30 I=1,M
        X(I)=XY(I,J,1)
        Y(I)=XY(I,J,2)
   30  CONTINUE
       CALL CURVE (X,Y,M,0)
   40 CONTINUE
      CALL ENDPL (-1)
C
C*** GRAPH THE LOCAL NUSSELT NUMBERS (RIGHT WALL).
C
      CALL BGNPL (-2)
      CALL TITLE ('NUSSELT NUMBER AT RIGHT WALL (VS) DISTANCE$',-100,
     1'DISTANCE (TOP TO BOTTOM)',24,'NUSSELT NUMBER',14,7.,6.)
      AMO=10./6.
      CALL GRAF (0.,.2,1.4,0.,.1.,10.)
      CALL FRAME
      CALL GRACE (0.)
      CALL MESSAG ('PR=',3,4.,5.7)
      CALL REALNO (PR,2,'ABUT','ABUT')
      CALL MESSAG ('RA=',3,4.,5.4)
      CALL REALNO (RA,-2,'ABUT','ABUT')
      CALL MARKER (13)
      CALL SPLINE
      DO 50 I=1,MM1
       X(I)=(DIST(I,2)+DIST(I+1,2))/2.
       Y(I)=NUL(I+1,2)
   50 CONTINUE
      CALL CURVE (X,Y,MM1,1)
      X(1)=0.
      Y(1)=NUAV(2)
      X(2)=DIST(M,2)
      Y(2)=NUAV(2)
      CALL RESET ('SPLINE')
      CALL CURVE (X,Y,2,0)
      YPOS=NUAV(2)*6./10.+.02
      CALL MESSAG ('AVERAGE',7,0.5,YPOS)
      CALL ENDPL (-2)
C
C*** GRAPH THE LOCAL NUSSELT NUMBER (LEFT WALL).
C
      CALL BGNPL (-3)
      CALL TITLE ('NUSSELT NUMBER AT LEFT WALL (VS) DISTANCE$',-100,
     1'DISTANCE (TOP TO BOTTOM)',24,'NUSSELT NUMBER',14,7.,6.)
```

```
      CALL GRAF (0.,.2,1.4,0.,.1.,10.)
      CALL FRAME
      CALL GRACE (0.)
      CALL MESSAG ('PR=',3,4.,5.7)
      CALL REALNO (PR,2,'ABUT','ABUT')
      CALL MESSAG ('RA=',3,4.,5.4)
      CALL REALNO (RA,-2,'ABUT','ABUT')
      CALL MARKER (13)
      CALL SPLINE
      DO 60 I=1,MM1
       X(I)=(DIST(I,4)+DIST(I+1,4))/2.
       Y(I)=NUL(I+1,4)
   60 CONTINUE
      CALL CURVE (X,Y,MM1,1)
      X(1)=0.
      Y(1)=NUAV(4)
      X(2)=DIST(M,4)
      Y(2)=NUAV(4)
      CALL RESET ('SPLINE')
      CALL CURVE (X,Y,2,0)
      YPOS=NUAV(4)*6./10.+.02
      CALL MESSAG ('AVERAGE',7,3.75,YPOS)
      CALL ENDPL (-3)
C
C*** THE TEMPERATURE
C*** IS NOT DEFINED AT THE GRID INTERSECTIONS
C*** BUT AT THE CENTER OF EACH SQUARE DEFINE BY THE GRID.
C*** CALCULATION OF THE COORDINATES OF THE CENTER.
C
C*** CORNER POINTS.
C
      XYS(1,1,1)=XY(1,1,1)
      XYS(1,1,2)=XY(1,1,2)
      XYS(1,NP1,1)=XY(1,N,1)
      XYS(1,NP1,2)=XY(1,N,2)
      XYS(MP1,1,1)=XY(M,1,1)
      XYS(MP1,1,2)=XY(M,1,2)
      XYS(MP1,NP1,1)=XY(M,N,1)
      XYS(MP1,NP1,2)=XY(M,N,2)
C
C*** BOUNDARY POINTS.
C
      DO 70 J=2,N
       XYS(1,J,1)=(XY(1,J,1)+XY(1,J-1,1))/2.DO
       XYS(1,J,2)=(XY(1,J,2)+XY(1,J-1,2))/2.DO
       XYS(MP1,J,1)=(XY(M,J,1)+XY(M,J-1,1))/2.DO
       XYS(MP1,J,2)=(XY(M,J,2)+XY(M,J-1,2))/2.DO
   70 CONTINUE
      DO 80 I=2,M
       XYS(I,1,1)=(XY(I,1,1)+XY(I-1,1,1))/2.DO
       XYS(I,1,2)=(XY(I,1,2)+XY(I-1,1,2))/2.DO
       XYS(I,NP1,1)=(XY(I,N,1)+XY(I-1,N,1))/2.DO
       XYS(I,NP1,2)=(XY(I,N,2)+XY(I-1,N,2))/2.DO
   80 CONTINUE
C
C*** INTERNAL POINTS.
C
      DO 100 I=2,M
       DO 90 J=2,N
      XYS(I,J,1)=(XY(I,J,1)+XY(I-1,J,1)+XY(I,J-1,1)+XY(I-1,J-1,1))
```

```
     1/4.DO
      XYS(I,J,2)=(XY(I,J,2)+XY(I-1,J,2)+XY(I,J-1,2)+XY(I-1,J-1,2))
     1/4.DO
   90  CONTINUE
  100 CONTINUE
C
C*** GRAPH THE TEMPERATURE FIELD.
C
      DO 120 I=1,MP1
       DO 110 J=1,NP1
        XYZ(I,J,1)=XYS(I,J,1)
        XYZ(I,J,2)=XYS(I,J,2)
        IF (J.EQ.1) XYZ(I,J,3)=0.
        IF (J.EQ.NP1) XYZ(I,J,3)=1.
        IF ((J.NE.1).AND.(J.NE.NP1)) XYZ(I,J,3)=T(I,J)
  110  CONTINUE
  120 CONTINUE
      CALL BGNPL (-4)
      CALL TITLE ('TEMPERATURE FIELDS',-100,
     1'X AXIS',6,'Y AXIS',6,7.,6.)
      CALL GRAPH (0.,.2,0.,.2)
      CALL FRAME
      CALL GRACE (0.)
      CALL MESSAG ('PR=',3,4.,5.7)
      CALL REALNO (PR,2,'ABUT','ABUT')
      CALL MESSAG ('RA=',3,4.,5.4)
      CALL REALNO (RA,-2,'ABUT','ABUT')
      WRITE (6,270)
      AM0=0.
      AM1=1.
      WRITE (6,300) AM0,AM1
      DO 130 I=1,9
       ZCNTR(I)=I/10.
       WRITE (6,310) I,ZCNTR(I)
  130 CONTINUE
      CALL CNTR (MP1,NP1,9)
      X(1)=0.
      Y(1)=1.
      DO 140 I=1,MP1
       X(I+1)=XYS(I,NP1,1)
       Y(I+1)=XYS(I,NP1,2)
  140 CONTINUE
      CALL CURVE (X,Y,MP2,0)
      CALL ENDPL (-4)
C
C*** GRAPH THE VORTICITY FIELD.
C
      XYZ(1,1,3)=(VOR(1,2)+VOR(2,1)+VOR(2,2))/3.
      XYZ(1,NP1,3)=(VOR(1,N)+VOR(2,N)+VOR(2,NP1))/3.
      XYZ(MP1,1,3)=(VOR(M,1)+VOR(M,2)+VOR(MP1,2))/3.
      XYZ(MP1,NP1,3)=(VOR(M,N)+VOR(M,NP1)+VOR(MP1,N))/3.
      DO 150 I=2,M
       XYZ(I,1,3)=(VOR(I,1)+VOR(I,2))/2.
       XYZ(I,NP1,3)=(VOR(I,N)+VOR(I,NP1))/2.
  150 CONTINUE
      DO 160 J=2,N
       XYZ(1,J,3)=(VOR(1,J)+VOR(2,J))/2.
       XYZ(MP1,J,3)=(VOR(M,J)+VOR(MP1,J))/2.
  160 CONTINUE
      DO 180 I=2,M
```

```
      DO 170 J=2,N
       XYZ(I,J,3)=VOR(I,J)
  170  CONTINUE
  180 CONTINUE
      CALL BGNPL (-5)
      CALL TITLE ('VORTICITY FIELD$',-100,
     1'X AXIS',6,'Y AXIS',6,7.,6.)
      CALL GRAPH (0.,.2,0.,.2)
      CALL FRAME
      CALL GRACE (0.)
      CALL MESSAG ('PR=',3,4.,5.7)
      CALL REALNO (PR,2,'ABUT','ABUT')
      CALL MESSAG ('RA=',3,4.,5.4)
      CALL REALNO (RA,-2,'ABUT','ABUT')
      WRITE (6,280)
      MAXVOR=XYZ(1,1,3)
      MINVOR=XYZ(1,1,3)
      DO 200 I=1,MP1
       DO 190 J=1,NP1
        MINVOR=AMIN1(MINVOR,XYZ(I,J,3))
        MAXVOR=AMAX1(MAXVOR,XYZ(I,J,3))
  190  CONTINUE
  200 CONTINUE
      WRITE (6,300) MINVOR,MAXVOR
      DO 210 I=1,9
       ZCNTR(I)=(MAXVOR-MINVOR)*I/10.+MINVOR
       WRITE (6,310) I,ZCNTR(I)
  210 CONTINUE
      CALL CNTR (MP1,NP1,9)
      X(1)=0.
      Y(1)=1.
      DO 220 I=1,MP1
       X(I+1)=XYS(I,NP1,1)
       Y(I+1)=XYS(I,NP1,2)
  220 CONTINUE
      CALL CURVE (X,Y,MP2,0)
      CALL ENDPL (-5)
C
C*** GRAPH THE STREAM FUNCTION FIELD.
C
      MAXSF=SF(1,1)
      MINSF=SF(1,1)
      DO 240 I=1,M
       DO 230 J=1,N
        XYZ(I,J,1)=XY(I,J,1)
        XYZ(I,J,2)=XY(I,J,2)
        XYZ(I,J,3)=SF(I,J)
        MAXSF=AMAX1(MAXSF,XYZ(I,J,3))
        MINSF=AMIN1(MINSF,XYZ(I,J,3))
  230  CONTINUE
  240 CONTINUE
      CALL BGNPL (-6)
      CALL TITLE ('STREAM FUNCTION FIELD$',-100
     1,'X AXIS',6,'Y AXIS',6,7.,6.)
      CALL GRAPH (0.,.2,0.,.2)
      CALL FRAME
      CALL GRACE (0.)
      CALL MESSAG ('PR=',3,4.,5.7)
      CALL REALNO (PR,2,'ABUT','ABUT')
      CALL MESSAG ('RA=',3,4.,5.4)
```

```
      CALL REALNO (RA,-2,'ABUT','ABUT')
      WRITE (6,290)
      WRITE (6,300) MINSF,MAXSF
      DO 250 I=1,9
       ZCNTR(I)=(MAXSF-MINSF)*I/10.+MINSF
       WRITE (6,310) I,ZCNTR(I)
  250 CONTINUE
      CALL CNTR (M,N,9)
      X(1)=0.
      Y(1)=1.
      DO 260 I=1,M
       X(I+1)=XY(I,N,1)
       Y(I+1)=XY(I,N,2)
  260 CONTINUE
      CALL CURVE (X,Y,MP1,0)
      CALL ENDPL (-6)
      RETURN
  270 FORMAT(/,T5,'TEMPERATURE CONTOUR VALUES.')
  280 FORMAT(/,T5,'VORTICITY COUNTOUR VALUES.')
  290 FORMAT(/,T5,'STREAM FUNCTION CONTOUR VALUES.')
  300 FORMAT(T5,'MIN= ',E15.7,/,T5,'MAX= ',E15.7)
  310 FORMAT(T5,'CONTOUR #',I5,5X,E15.7)
      END
C
C
C
      SUBROUTINE TDMA (IMIN,IMAX)
C
C*********************************************************************
C
C     NAME: TRIDIAGONAL MATRIX ALGORITHM.
C
C     PURPOSE:
C
C     THIS SUBROUTINE SOLVES A TRIDIAGONAL MATRIX.
C
C     INPUT DATA:
C
C     - IMIN: MINIMUM INDEX.
C     - IMAX: MAXIMUM INDEX.
C
C*********************************************************************
C
      IMPLICIT REAL*8(A-H,O-Z)
      REAL*8 ATDMA(50),BTDMA(50),CTDMA(50),DTDMA(50)
      REAL*8 PTDMA(50),QTDMA(50),SLN(50)
      COMMON /BLK10/ ATDMA,BTDMA,CTDMA,DTDMA,SLN
C
C*** SET UP VARIABLES.
C
      IMINP1=IMIN+1
      IMAXM1=IMAX-1
      N=IMAX-IMIN
C
C*** SOLVE THE ARRAY.
C
      PTDMA(IMIN)=BTDMA(IMIN)/ATDMA(IMIN)
      QTDMA(IMIN)=DTDMA(IMIN)/ATDMA(IMIN)
      DO 10 I=IMINP1,IMAX
       DEN=ATDMA(I)-CTDMA(I)*PTDMA(I-1)
```

```
      PTDMA(I)=BTDMA(I)/DEN
      QTDMA(I)=(DTDMA(I)+CTDMA(I)*QTDMA(I-1))/DEN
   10 CONTINUE
      SLN(IMAX)=QTDMA(IMAX)
      DO 20 I=1,N
      J=IMAX-I
      SLN(J)=PTDMA(J)*SLN(J+1)+QTDMA(J)
   20 CONTINUE
      RETURN
      END
C
C
C
      SUBROUTINE RTDMA (IMAX,ACRI1,ACRIM)
C
C*********************************************************************
C
C     NAME: REVISED TRIDIAGONAL MATRIX ALGORITHM.
C
C     PURPOSE:
C
C     THIS PROGRAM SOLVES A TRIDIAGONAL-MATRIX WHICH HAS TWO ELEMENTS
C   OUTSIDE OF THE TRIDIAGONAL. THE FIRST ONE IS LOCATED ROW 1 AND
C   COLUMN 3, AND THE SECOND IS LOCATED ROW IMAX AND COLUMN IMAX-2.
C
C     INPUT DATA:
C
C     - IMAX: NUMBER OF ROW AND COLUMN IN THE ARRAY.
C     - ACRI1: ADDITIONAL COEFFICIENT RELATED TO THE ROW 1.
C     - ACRIM: ADDITIONAL COEFFICIENT RELATED TO THE ROW IMAX.
C
C*********************************************************************
C
      IMPLICIT REAL*8(A-H,O-Z)
      REAL*8 ATDMA(50),BTDMA(50),CTDMA(50),DTDMA(50),SLN(50)
      COMMON /BLK10/ ATDMA,BTDMA,CTDMA,DTDMA,SLN
C
C*** SET UP VARIABLES.
C
      IMAXM1=IMAX-1
C
C*** MODIFIED THE TDMA COEFFICIENTS.
C
      ATDMA(2)=ATDMA(2)-CTDMA(2)*BTDMA(1)/ATDMA(1)
      BTDMA(2)=BTDMA(2)+CTDMA(2)*ACRI1/ATDMA(1)
      DTDMA(2)=DTDMA(2)+CTDMA(2)*DTDMA(1)/ATDMA(1)
      ATDMA(IMAXM1)=ATDMA(IMAXM1)-BTDMA(IMAXM1)*CTDMA(IMAX)
     1/ATDMA(IMAX)
      CTDMA(IMAXM1)=CTDMA(IMAXM1)+BTDMA(IMAXM1)*ACRIM/ATDMA(IMAX)
      DTDMA(IMAXM1)=DTDMA(IMAXM1)+BTDMA(IMAXM1)*DTDMA(IMAX)
     1/ATDMA(IMAX)
      CTDMA(2)=0.D0
      BTDMA(IMAXM1)=0.D0
C
C*** TDMA.
C
      CALL TDMA (2,IMAXM1)
C
C*** CALCULATE VALUES FOR 1 AND IMAX.
C
```

```
      SLN(1)=(BTDMA(1)*SLN(2)+ACRI1*SLN(3)+DTDMA(1))/ATDMA(1)
      SLN(IMAX)=(ACRIM*SLN(IMAX-2)+CTDMA(IMAX)*SLN(IMAXM1)
     1+DTDMA(IMAX))/ATDMA(IMAX)
      RETURN
      END
C
C
C
      DOUBLE PRECISION FUNCTION COEFF (COND,CONV)
C
C*********************************************************************
C
C     NAME: COEFFICIENT.
C
C     PURPOSE:
C
C     THIS SUBROUTINE CALCULATES THE COEFFICIENT A(P)
C   OF THE POWER LAW SCHEME AS PRESENTED BY PATANKAR.D
C
C     NB. THE POWER LAW IS USED BELOW, BUT OTHER SCHEMES AS CENTRAL
C   DIFFERENCE SCHEME, UPWIND SCHEME OR HYBRID SCHEME COULD BE
C   USED AS WELL.
C
C     INPUT DATA:
C
C     - COND: CONDUTION STRENGTH.
C     - CONV: CONVECTION STRENGTH.
C
C*********************************************************************
C
      IMPLICIT REAL*8(A-H,O-Z)
      COEFF=DMAX1(0.D0,(1.D0-0.1D0*DABS(CONV/COND))**5)
      RETURN
      END
C
C
C
      SUBROUTINE DISF
C
C*****************************************************************
C
C     NAME: DISTORTION FUNCTION.
C
C     PURPOSE:
C
C     THIS PROGRAM COMPUTES THE FIRST ORDER DERIVATIVES OF THE
C   CARTESIAN COORDINATES WITH RESPECT TO THE ORTHOGONAL
C   COORDINATES AND THE SCALE FACTORS ALONG BOUNDARIES
C   WHERE TWO DIRICHLET BOUNDARY CONDITIONS ARE USED.
C   ALONG BOUNDARIES WHERE THE POINT
C   POSITIONS ARE NOT GIVEN THE RATIOS OF SCALE FACTORS ARE
C   SPECIFIED BY LINEARLY INTERPOLATING THE CORNER VALUES.
C   THE RATIO OF SCALE FACTORS FOR THE INTERNAL GRID POINTS
C   ARE COMPUTE USING THE FORMULA PROPOSED BY G. RYSKIN AND
C   L.G. LEAL.
C
C     CHARACTERISTIC:
C
C     - FINITE DIFFERENCES FORMULA OF SECOND ORDER.
C
```

```
C*************************************************************
C
      IMPLICIT REAL*8(A-H,O-Z)
      INTEGER BTYPE(4)
      REAL*8 D(50,50,4),H(50,50,2),RSF(50,50),XY(50,50,2)
      COMMON /BLK1/ M,N
      COMMON /BLK2/ BTYPE,RSF
      COMMON /BLK3/ XY
      COMMON /BLK4/ H
      COMMON /BLK5/ D
C
C*** SET UP VARIABLES.
C
      MM1=M-1
      MM2=M-2
      NM1=N-1
      NM2=N-2
C
C*** ASSIGN RATIO OF SCALE FACTORS AT BOUNDARIES.
C
C*** TOP LEFT CORNER.
C
      IF ((BTYPE(1).EQ.0).AND.(BTYPE(4).EQ.0)) GOTO 10
      D(1,1,1)=(-3.D0*XY(1,1,1)+4.D0*XY(1,2,1)-XY(1,3,1))/2.D0
      D(1,1,2)=(-3.D0*XY(1,1,2)+4.D0*XY(1,2,2)-XY(1,3,2))/2.D0
      D(1,1,3)=(3.D0*XY(1,1,1)-4.D0*XY(2,1,1)+XY(3,1,1))/2.D0
      D(1,1,4)=(3.D0*XY(1,1,2)-4.D0*XY(2,1,2)+XY(3,1,2))/2.D0
      H(1,1,1)=(D(1,1,1)**2+D(1,1,2)**2)**0.5D0
      H(1,1,2)=(D(1,1,3)**2+D(1,1,4)**2)**0.5D0
      RSF(1,1)=H(1,1,2)/H(1,1,1)
C
C*** TOP RIGHT CORNER.
C
   10 IF ((BTYPE(1).EQ.0).AND.(BTYPE(2).EQ.0)) GOTO 20
      D(1,N,1)=(3.D0*XY(1,N,1)-4.D0*XY(1,NM1,1)+XY(1,NM2,1))/2.D0
      D(1,N,2)=(3.D0*XY(1,N,2)-4.D0*XY(1,NM1,2)+XY(1,NM2,2))/2.D0
      D(1,N,3)=(3.D0*XY(1,N,1)-4.D0*XY(2,N,1)+XY(3,N,1))/2.D0
      D(1,N,4)=(3.D0*XY(1,N,2)-4.D0*XY(2,N,2)+XY(3,N,2))/2.D0
      H(1,N,1)=(D(1,N,1)**2+D(1,N,2)**2)**0.5D0
      H(1,N,2)=(D(1,N,3)**2+D(1,N,4)**2)**0.5D0
      RSF(1,N)=H(1,N,2)/H(1,N,1)
C
C*** BOTTOM LEFT CORNER.
C
   20 IF ((BTYPE(4).EQ.0).AND.(BTYPE(3).EQ.0)) GOTO 30
      D(M,1,1)=(-3.D0*XY(M,1,1)+4.D0*XY(M,2,1)-XY(M,3,1))/2.D0
      D(M,1,2)=(-3.D0*XY(M,1,2)+4.D0*XY(M,2,2)-XY(M,3,2))/2.D0
      D(M,1,3)=(-3.D0*XY(M,1,1)+4.D0*XY(MM1,1,1)-XY(MM2,1,1))/2.D0
      D(M,1,4)=(-3.D0*XY(M,1,2)+4.D0*XY(MM1,1,2)-XY(MM2,1,2))/2.D0
      H(M,1,1)=(D(M,1,1)**2+D(M,1,2)**2)**0.5D0
      H(M,1,2)=(D(M,1,3)**2+D(M,1,4)**2)**0.5D0
      RSF(M,1)=H(M,1,2)/H(M,1,1)
C
C*** BOTTOM RIGHT CORNER.
C
   30 IF ((BTYPE(2).EQ.0).AND.(BTYPE(3).EQ.0)) GOTO 40
      D(M,N,1)=(3.D0*XY(M,N,1)-4.D0*XY(M,NM1,1)+XY(M,NM2,1))/2.D0
      D(M,N,2)=(3.D0*XY(M,N,2)-4.D0*XY(M,NM1,2)+XY(M,NM2,2))/2.D0
      D(M,N,3)=(-3.D0*XY(M,N,1)+4.D0*XY(MM1,N,1)-XY(MM2,N,1))/2.D0
      D(M,N,4)=(-3.D0*XY(M,N,2)+4.D0*XY(MM1,N,2)-XY(MM2,N,2))/2.D0
```

```
      H(M,N,1)=(D(M,N,1)**2+D(M,N,2)**2)**0.5DO
      H(M,N,2)=(D(M,N,3)**2+D(M,N,4)**2)**0.5DO
      RSF(M,N)=H(M,N,2)/H(M,N,1)
C
C*** TOP WALL.
C
   40 IF (BTYPE(1).EQ.0) GOTO 60
      DO 50 J=2,NM1
       D(1,J,1)=(XY(1,J+1,1)-XY(1,J-1,1))/2.DO
       D(1,J,2)=(XY(1,J+1,2)-XY(1,J-1,2))/2.DO
       D(1,J,3)=(3.DO*XY(1,J,1)-4.DO*XY(2,J,1)+XY(3,J,1))/2.DO
       D(1,J,4)=(3.DO*XY(1,J,2)-4.DO*XY(2,J,2)+XY(3,J,2))/2.DO
       H(1,J,1)=(D(1,J,1)**2+D(1,J,2)**2)**0.5DO
       H(1,J,2)=(D(1,J,3)**2+D(1,J,4)**2)**0.5DO
       RSF(1,J)=H(1,J,2)/H(1,J,1)
   50 CONTINUE
C
C*** BOTTOM WALL.
C
   60 IF (BTYPE(3).EQ.0) GOTO 80
      DO 70 J=2,NM1
       D(M,J,1)=(XY(M,J+1,1)-XY(M,J-1,1))/2.DO
       D(M,J,2)=(XY(M,J+1,2)-XY(M,J-1,2))/2.DO
       D(M,J,3)=(-3.DO*XY(M,J,1)+4.DO*XY(MM1,J,1)-XY(MM2,J,1))/2.DO
       D(M,J,4)=(-3.DO*XY(M,J,2)+4.DO*XY(MM1,J,2)-XY(MM2,J,2))/2.DO
       H(M,J,1)=(D(M,J,1)**2+D(M,J,2)**2)**0.5DO
       H(M,J,2)=(D(M,J,3)**2+D(M,J,4)**2)**0.5DO
       RSF(M,J)=H(M,J,2)/H(M,J,1)
   70 CONTINUE
C
C*** LEFT WALL.
C
   80 IF (BTYPE(4).EQ.0) GOTO 100
      DO 90 I=2,MM1
       D(I,1,1)=(-3.DO*XY(I,1,1)+4.DO*XY(I,2,1)-XY(I,3,1))/2.DO
       D(I,1,2)=(-3.DO*XY(I,1,2)+4.DO*XY(I,2,2)-XY(I,3,2))/2.DO
       D(I,1,3)=(XY(I-1,1,1)-XY(I+1,1,1))/2.DO
       D(I,1,4)=(XY(I-1,1,2)-XY(I+1,1,2))/2.DO
       H(I,1,1)=(D(I,1,1)**2+D(I,1,2)**2)**0.5DO
       H(I,1,2)=(D(I,1,3)**2+D(I,1,4)**2)**0.5DO
       RSF(I,1)=H(I,1,2)/H(I,1,1)
   90 CONTINUE
C
C*** RIGHT WALL.
C
  100 IF (BTYPE(2).EQ.0) GOTO 120
      DO 110 I=2,MM1
       D(I,N,1)=(3.DO*XY(I,N,1)-4.DO*XY(I,NM1,1)+XY(I,NM2,1))/2.DO
       D(I,N,2)=(3.DO*XY(I,N,2)-4.DO*XY(I,NM1,2)+XY(I,NM2,2))/2.DO
       D(I,N,3)=(XY(I-1,N,1)-XY(I+1,N,1))/2.DO
       D(I,N,4)=(XY(I-1,N,2)-XY(I+1,N,2))/2.DO
       H(I,N,1)=(D(I,N,1)**2+D(I,N,2)**2)**0.5DO
       H(I,N,2)=(D(I,N,3)**2+D(I,N,4)**2)**0.5DO
       RSF(I,N)=H(I,N,2)/H(I,N,1)
  110 CONTINUE
C
C*** EVALUATION OF RATIO OF SCALE FACTOR AT BOUNDARIES WHERE
C*** POINTS ARE NOT FIXED, USING A LINEAR INTERPOLATION
C*** OF CORNER POINTS.
C
```

```
C*** TOP WALL.
C
 120 IF (BTYPE(1).EQ.1) GOTO 140
     DO 130 J=2,NM1
      RSF(1,J)=RSF(1,1)+(J-1.DO)*(RSF(1,N)-RSF(1,1))/NM1
 130 CONTINUE
C
C*** RIGHT WALL.
 140 IF (BTYPE(2).EQ.1) GOTO 160
     DO 150 I=2,MM1
      RSF(I,N)=RSF(1,N)+(I-1.DO)*(RSF(M,N)-RSF(1,N))/MM1
 150 CONTINUE
C
C*** BOTTOM WALL.
C
 160 IF (BTYPE(3).EQ.1) GOTO 180
     DO 170 J=2,NM1
      RSF(M,J)=RSF(M,1)+(J-1.DO)*(RSF(M,N)-RSF(M,1))/NM1
 170 CONTINUE
C
C*** LEFT WALL.
C
 180 IF (BTYPE(4).EQ.1) GOTO 200
     DO 190 I=2,MM1
      RSF(I,1)=RSF(1,1)+(I-1.DO)*(RSF(M,1)-RSF(1,1))/MM1
 190 CONTINUE
C
C*** COMPUTATION OF THE RATIO OF SCALE FACTORS FOR THE
C*** INTERIOR POINTS USING THE RELATION PROPOSED
C*** BY G. RYSKIN AND L.G. LEAL.
C
 200 DO 220 I=2,MM1
      DO 210 J=2,NM1
       AMO=(I-1.DO)/MM1
       AM1=(J-1.DO)/NM1
       RSF(I,J)=(1.DO-AMO)*RSF(1,J)+AMO*RSF(M,J)
    1+(1.DO-AM1)*RSF(I,1)+AM1*RSF(I,N)
    2-((1.DO-AMO)*(1.DO-AM1)*RSF(1,1)
    3+(1.DO-AMO)*AM1*RSF(1,N)
    4+AMO*(1.DO-AM1)*RSF(M,1)+AMO*AM1*RSF(M,N))
 210  CONTINUE
 220 CONTINUE
     RETURN
     END
C
C
C
     SUBROUTINE DSF
C
C*****************************************************************
C
C    NAME: DERIVATIVES AND SCALE FACTORS.
C
C    PURPOSE:
C
C    THIS SUBROUTINE COMPUTES THE FIRST ORDER DERIVATIVES OF THE
C  CARTESIAN COORDINATES WITH RESPECT TO THE ORTHOGONAL
C  COORDINATES AND CALCULATES THE SCALE FACTORS.
C
C    CHARACTERISTIC:
```

```
C
C     - FINITE DIFFERENCES FORMULA OF SECOND ORDER.
C
C*************************************************************
C
      IMPLICIT REAL*8(A-H,O-Z)
      REAL*8 D(50,50,4),H(50,50,2),XY(50,50,2)
      COMMON /BLK1/ M,N
      COMMON /BLK3/ XY
      COMMON /BLK4/ H
      COMMON /BLK5/ D
C
C*** SET UP VARIABLES.
C
      MM1=M-1
      MM2=M-2
      NM1=N-1
      NM2=N-2
C
C*** DERIVATIVES AT CORNER.
C
C*** TOP LEFT CORNER.
C
      D(1,1,1)=(-3.DO*XY(1,1,1)+4.DO*XY(1,2,1)-XY(1,3,1))/2.DO
      D(1,1,2)=(-3.DO*XY(1,1,2)+4.DO*XY(1,2,2)-XY(1,3,2))/2.DO
      D(1,1,3)=(3.DO*XY(1,1,1)-4.DO*XY(2,1,1)+XY(3,1,1))/2.DO
      D(1,1,4)=(3.DO*XY(1,1,2)-4.DO*XY(2,1,2)+XY(3,1,2))/2.DO
C
C*** TOP RIGHT CORNER.
C
      D(1,N,1)=(3.DO*XY(1,N,1)-4.DO*XY(1,NM1,1)+XY(1,NM2,1))/2.DO
      D(1,N,2)=(3.DO*XY(1,N,2)-4.DO*XY(1,NM1,2)+XY(1,NM2,2))/2.DO
      D(1,N,3)=(3.DO*XY(1,N,1)-4.DO*XY(2,N,1)+XY(3,N,1))/2.DO
      D(1,N,4)=(3.DO*XY(1,N,2)-4.DO*XY(2,N,2)+XY(3,N,2))/2.DO
C
C*** BOTTOM LEFT CORNER.
C
      D(M,1,1)=(-3.DO*XY(M,1,1)+4.DO*XY(M,2,1)-XY(M,3,1))/2.DO
      D(M,1,2)=(-3.DO*XY(M,1,2)+4.DO*XY(M,2,2)-XY(M,3,2))/2.DO
      D(M,1,3)=(-3.DO*XY(M,1,1)+4.DO*XY(MM1,1,1)-XY(MM2,1,1))/2.DO
      D(M,1,4)=(-3.DO*XY(M,1,2)+4.DO*XY(MM1,1,2)-XY(MM2,1,2))/2.DO
C
C*** BOTTOM RIGHT CORNER.
C
      D(M,N,1)=(3.DO*XY(M,N,1)-4.DO*XY(M,NM1,1)+XY(M,NM2,1))/2.DO
      D(M,N,2)=(3.DO*XY(M,N,2)-4.DO*XY(M,NM1,2)+XY(M,NM2,2))/2.DO
      D(M,N,3)=(-3.DO*XY(M,N,1)+4.DO*XY(MM1,N,1)-XY(MM2,N,1))/2.DO
      D(M,N,4)=(-3.DO*XY(M,N,2)+4.DO*XY(MM1,N,2)-XY(MM2,N,2))/2.DO
C
C*** DERIVATIVES AT THE BOUNDARIES.
C
      DO 10 J=2,NM1
C
C*** TOP WALL.
C
       D(1,J,1)=(XY(1,J+1,1)-XY(1,J-1,1))/2.DO
       D(1,J,2)=(XY(1,J+1,2)-XY(1,J-1,2))/2.DO
       D(1,J,3)=(3.DO*XY(1,J,1)-4.DO*XY(2,J,1)+XY(3,J,1))/2.DO
       D(1,J,4)=(3.DO*XY(1,J,2)-4.DO*XY(2,J,2)+XY(3,J,2))/2.DO
C
```

```
C*** BOTTOM WALL.
C
      D(M,J,1)=(XY(M,J+1,1)-XY(M,J-1,1))/2.DO
      D(M,J,2)=(XY(M,J+1,2)-XY(M,J-1,2))/2.DO
      D(M,J,3)=(-3.DO*XY(M,J,1)+4.DO*XY(MM1,J,1)-XY(MM2,J,1))/2.DO
      D(M,J,4)=(-3.DO*XY(M,J,2)+4.DO*XY(MM1,J,2)-XY(MM2,J,2))/2.DO
   10 CONTINUE
      DO 20 I=2,MM1
C
C*** LEFT WALL.
C
      D(I,1,1)=(-3.DO*XY(I,1,1)+4.DO*XY(I,2,1)-XY(I,3,1))/2.DO
      D(I,1,2)=(-3.DO*XY(I,1,2)+4.DO*XY(I,2,2)-XY(I,3,2))/2.DO
      D(I,1,3)=(XY(I-1,1,1)-XY(I+1,1,1))/2.DO
      D(I,1,4)=(XY(I-1,1,2)-XY(I+1,1,2))/2.DO
C
C*** RIGHT WALL.
C
      D(I,N,1)=(3.DO*XY(I,N,1)-4.DO*XY(I,NM1,1)+XY(I,NM2,1))/2.DO
      D(I,N,2)=(3.DO*XY(I,N,2)-4.DO*XY(I,NM1,2)+XY(I,NM2,2))/2.DO
      D(I,N,3)=(XY(I-1,N,1)-XY(I+1,N,1))/2.DO
      D(I,N,4)=(XY(I-1,N,2)-XY(I+1,N,2))/2.DO
   20 CONTINUE
C
C*** DERIVATIVES FOR THE INNER GRID POINTS.
C
      DO 40 I=2,MM1
       DO 30 J=2,NM1
        D(I,J,1)=(XY(I,J+1,1)-XY(I,J-1,1))/2.DO
        D(I,J,2)=(XY(I,J+1,2)-XY(I,J-1,2))/2.DO
        D(I,J,3)=(XY(I-1,J,1)-XY(I+1,J,1))/2.DO
        D(I,J,4)=(XY(I-1,J,2)-XY(I+1,J,2))/2.DO
   30  CONTINUE
   40 CONTINUE
C
C*** CALCULATION OF THE SCALE FACTOR.
C
      DO 60 I=1,M
       DO 50 J=1,N
        H(I,J,1)=(D(I,J,1)**2+D(I,J,2)**2)**0.5DO
        H(I,J,2)=(D(I,J,3)**2+D(I,J,4)**2)**0.5DO
   50  CONTINUE
   60 CONTINUE
      RETURN
      END
C
C
C
      DOUBLE PRECISION FUNCTION F(Z,I)
C
C*********************************************************************
C
C     NAME: FUNCTION.
C
C     PURPOSE:
C
C     THIS SUBPROGRAM SPECIFIED THE DIRICHLET BOUNDARY CONDITIONS
C   OR RETURN THE NORMAL DERIVATIVE AT THE WALLS.
C
C     INPUT DATA:
```

```
C
C     - Z: INDEPENDENT VARIABLE.
C     - I: FUNCTION NUMBER (1 TO 8).
C          WHERE   I=1: FUNCTION TOP      Y=F(X)
C                  I=2: FUNCTION RIGHT    X=F(Y)
C                  I=3: FUNCTION BOTTOM   Y=F(X)
C                  I=4: FUNCTION LEFT     X=F(Y)
C                  I=5: DERIVATIVE TOP.
C                  I=6: DERIVATIVE RIGHT.
C                  I=7: DERIVATIVE BOTTOM.
C                  I=8: DERIVATIVE LEFT.
C
C*********************************************************************
C
      IMPLICIT REAL*8(A-H,O-Z)
      AMP=0.075D0
C
C*** FUNCTION TOP WALL.
C
      IF (I.EQ.1) F=1.D0
C
C*** FUNCTION RIGHT WALL.
C
      IF (I.EQ.2) F=1.D0
C      IF (I.EQ.2) F=1.D0-AMP+AMP*DCOS(4.D0*DATAN(1.D0)*Z)
C      IF (I.EQ.2) F=1.D0+AMP-AMP*DCOS(4.D0*DATAN(1.D0)*Z)
C      IF (I.EQ.2) F=1.D0-AMP+AMP*DCOS(8.D0*DATAN(1.D0)*Z)
C      IF (I.EQ.2) F=1.D0+AMP-AMP*DCOS(8.D0*DATAN(1.D0)*Z)
C
C*** FUNCTION BOTTOM WALL.
C
      IF (I.EQ.3) F=0.D0
C
C*** FUNCTION LEFT WALL.
C
      IF (I.EQ.4) F=0.D0
C
C*** DERIVATIVE TOP WALL.
C
      IF (I.EQ.5) F=0.D0
C
C*** DERIVATIVE RIGHT WALL.
C
      IF (I.EQ.6) F=0.D0
C      IF (I.EQ.6) F=-4.D0*DATAN(1.D0)*AMP*DSIN(4.D0*DATAN(1.D0)*Z)
C      IF (I.EQ.6) F=4.D0*DATAN(1.D0)*AMP*DSIN(4.D0*DATAN(1.D0)*Z)
C      IF (I.EQ.6) F=-8.D0*DATAN(1.D0)*AMP*DSIN(8.D0*DATAN(1.D0)*Z)
C      IF (I.EQ.6) F=8.D0*DATAN(1.D0)*AMP*DSIN(8.D0*DATAN(1.D0)*Z)
C
C*** DERIVATIVE BOTTOM WALL.
C
      IF (I.EQ.7) F=0.D0
C
C*** DERIVATIVE LEFT WALL.
C
      IF (I.EQ.8) F=0.D0
      RETURN
      END
C
C
```

```
C
      SUBROUTINE NU
C
C*********************************************************************
C
C     NAME: NUSSELT.
C
C     PURPOSE:
C
C     THIS SUBROUTINE COMPUTES THE DISTANCE ALONG THE WALLS, THE
C   LOCAL NUSSELT NUMBERS AND THE AVERAGE NUSSELT NUMBERS.
C
C     CHARACTERISTIC:
C
C     - INTEGRATION BY TRAPEZE.
C
C*********************************************************************
C
      IMPLICIT REAL*8(A-H,O-Z)
      REAL*8 H(50,50,2)
      REAL*8 DIST(50,4),NUAV(4),NUL(50,4)
      REAL*8 T(50,50)
      COMMON /BLK1/ M,N
      COMMON /BLK4/ H
      COMMON /BLK7/ T
      COMMON /BLK13/ DIST,NUAV,NUL
C
C*** SET UP VARIABLES
C
      NP1=N+1
      DIST(1,2)=0.D0
      DIST(1,4)=0.D0
      NUAV(2)=0.D0
      NUAV(4)=0.D0
C
C*** RIGHT WALL.
C*** CALCULATE THE DISTANCE (TOP TO BOTTOM) AND THE LOCAL NUSSELT
C*** NUMBER.
C
      DO 10 I=2,M
       DIST(I,2)=DIST(I-1,2)+(H(I,N,2)+H(I-1,N,2))/2.D0
       NUL(I,2)=2.D0*(T(I,NP1)-T(I,N))/(H(I-1,N,1)+H(I,N,1))
       NUAV(2)=NUAV(2)+NUL(I,2)*(DIST(I,2)-DIST(I-1,2))
   10 CONTINUE
      NUAV(2)=NUAV(2)/DIST(M,2)
C
C*** LEFT WALL.
C*** CALCULATE THE DISTANCES (TOP TO BOTTOM) AND THE LOCAL NUSSELT
C*** NUMBER.
C
      DO 20 I=2,M
       DIST(I,4)=DIST(I-1,4)+(H(I,1,2)+H(I-1,1,2))/2.D0
       NUL(I,4)=2.D0*(T(I,2)-T(I,1))/(H(I-1,1,1)+H(I,1,1))
       NUAV(4)=NUAV(4)+NUL(I,4)*(DIST(I,4)-DIST(I-1,4))
   20 CONTINUE
      NUAV(4)=NUAV(4)/DIST(M,4)
C
C*** PRINTOUT.
C
      WRITE (6,30) NUAV(2),NUAV(4),DIST(M,2),DIST(M,4)
```

```
      RETURN
   30 FORMAT(/,T5,'AVERAGE NUSSELT NUMBER (RIGHT WALL)= ',D15.7./,
     1T5,'AVERAGE NUSSELT NUMBER (LEFT WALL)= ',D15.7./,
     2T5,'LENGTH OF THE WALL(RIGHT)= ',D15.7./,
     3T5,'LENGTH OF THE WALL(LEFT)= ',D15.7)
      END
C
C
C
      SUBROUTINE ORTHO
C
C*********************************************************************
C
C     NAME: ORTHOGONAL.
C
C     PURPOSE:
C
C     THIS PROGRAM CALCULATES THE INTERSECTING ANGLE OF TWO
C   COORDINATE LINES AT ALL POINTS OF THE GRID.
C
C     NB. THE FORMULA USED HERE IS TAKEN IN THE CHIKHLIWALA AND YOHSOS
C   ARTICLE.
C
C*********************************************************************
C
      IMPLICIT REAL*8(A-H,O-Z)
      REAL*8 D(50,50,4)
      COMMON /BLK1/ M,N
      COMMON /BLK5/ D
C
C*** SET UP DATA.
C
      DIFA=0.DO
      SUM=0.ODO
      MI=1
      MJ=1
C
C*** ORTHOGONALITY TEST.
C
      DO 20 I=1,M
       DO 10 J=1,N
         AMO=D(I,J,1)*D(I,J,3)+D(I,J,2)*D(I,J,4)
         AM1=((D(I,J,1)**2+D(I,J,2)**2)**0.5DO)*((D(I,J,3)**2
     1+D(I,J,4)**2)**0.5DO)
         ANGLE=DARCOS(AMO/AM1)*180.DO/(4.DO*DATAN(1.DO))
         SUM=SUM+DABS(90.ODO-ANGLE)
         AMO=OMAX1(DIFA,DABS(90.DO-ANGLE))
         IF ((AMO-DIFA).LT.1.OD-6) GOTO 10
         MI=I
         MJ=J
         DIFA=AMO
   10  CONTINUE
   20 CONTINUE
C
C*** AVERAGE DEVIATION OF ORTHOGONALITY.
C
      SUM=SUM/(M*N)
C
C*** PRINTOUT.
C
```

```
      WRITE (6,30) DIFA,MI,MJ
      WRITE (6,40) SUM
      RETURN
   30 FORMAT(/,T5,'MAX. DEVIATION OF ORTHOGONALITY '.
     1'(ALL POINTS, DEGREE)= '.
     2D15.7,/,T5,'POSITION: I= ',I2,' ,J= ',I2)
   40 FORMAT(/,T5,'AVERAGE DEVIATION OF ORTHOGONALITY '.
     1'(ALL POINTS, DEGREE)= ',D15.7)
      END
C
C
C
      SUBROUTINE CNTR (IMAX,JMAX,NCNTR)
C
C**********************************************************************
C
C     NAME: CONTOUR.
C
C     PURPOSE:
C
C     THIS SUBROUTINE DRAWS THE CONTOUR LINES OF A SCALAR
C   DEPENDENT VARIABLE
C   WHICH IS KNOWN OVER A NON RECTANGULAR GRID.
C
C     INPUT DATA:
C
C     - IMAX: MAXIMUM VALUE OF THE INDEX I IN XYZ(I,J,K).
C     - JMAX: MAXIMUM VALUE OF THE INDEX J IN XYZ(I,J,K).
C     - NCNTR: NUMBER OF CONTOUR LINES.
C
C     CHARACTERISTIC:
C
C     - LINEAR INTERPOLATION IS USED.
C
C**********************************************************************
C
      REAL XYZ(50,50,3),XCNTR(10),YCNTR(10),ZCNTR(50)
      COMMON /BLKA/ XYZ,ZCNTR
C
C*** SET UP VARIABLES.
C
      IMAXM1=IMAX-1
      JMAXM1=JMAX-1
C
C*** OVERALL LOOP.
C
      DO 80 K=1,NCNTR
       DO 70 I=1,IMAXM1
        DO 60 J=1,JMAXM1
          ZMAX=AMAX1(XYZ(I,J,3),XYZ(I+1,J,3),XYZ(I,J+1,3),
     1XYZ(I+1,J+1,3))
          ZMIN=AMIN1(XYZ(I,J,3),XYZ(I+1,J,3),XYZ(I,J+1,3),
     1XYZ(I+1,J+1,3))
          IF ((ZCNTR(K).LT.ZMIN).OR.(ZCNTR(K).GT.ZMAX)) GOTO 60
          L=0
          ZMAX=AMAX1(XYZ(I,J,3),XYZ(I,J+1,3))
          ZMIN=AMIN1(XYZ(I,J,3),XYZ(I,J+1,3))
          IF ((ZCNTR(K).LT.ZMIN).OR.(ZCNTR(K).GT.ZMAX)) GOTO 10
          L=L+1
          XCNTR(L)=XLINT(I,J,I,J+1,K)
```

```
      YCNTR(L)=YLINT(I,J,I,J+1,K)
10    ZMAX=AMAX1(XYZ(I,J+1,3),XYZ(I+1,J+1,3))
      ZMIN=AMIN1(XYZ(I,J+1,3),XYZ(I+1,J+1,3))
      IF ((ZCNTR(K).LT.ZMIN).OR.(ZCNTR(K).GT.ZMAX)) GOTO 20
      L=L+1
      XCNTR(L)=XLINT(I,J+1,I+1,J+1,K)
      YCNTR(L)=YLINT(I,J+1,I+1,J+1,K)
20    ZMAX=AMAX1(XYZ(I+1,J,3),XYZ(I+1,J+1,3))
      ZMIN=AMIN1(XYZ(I+1,J,3),XYZ(I+1,J+1,3))
      IF ((ZCNTR(K).LT.ZMIN).OR.(ZCNTR(K).GT.ZMAX)) GOTO 30
      L=L+1
      XCNTR(L)=XLINT(I+1,J,I+1,J+1,K)
      YCNTR(L)=YLINT(I+1,J,I+1,J+1,K)
30    ZMAX=AMAX1(XYZ(I,J,3),XYZ(I+1,J,3))
      ZMIN=AMIN1(XYZ(I,J,3),XYZ(I+1,J,3))
      IF ((ZCNTR(K).LT.ZMIN).OR.(ZCNTR(K).GT.ZMAX)) GOTO 40
      L=L+1
      XCNTR(L)=XLINT(I,J,I+1,J,K)
      YCNTR(L)=YLINT(I,J,I+1,J,K)
40    IF (L.EQ.2) GOTO 50
       XCNTR(1)=XYZ(I,J,1)
       YCNTR(1)=XYZ(I,J,2)
       XCNTR(2)=XYZ(I,J+1,1)
       YCNTR(2)=XYZ(I,J+1,2)
       XCNTR(3)=XYZ(I+1,J+1,1)
       YCNTR(3)=XYZ(I+1,J+1,2)
       XCNTR(4)=XYZ(I+1,J,1)
       YCNTR(4)=XYZ(I+1,J,2)
       XCNTR(5)=XYZ(I,J,1)
       YCNTR(5)=XYZ(I,J,2)
       XCNTR(6)=XYZ(I+1,J+1,1)
       YCNTR(6)=XYZ(I+1,J+1,2)
       CALL CURVE (XCNTR,YCNTR,6,0)
       XCNTR(1)=XYZ(I+1,J,1)
       YCNTR(1)=XYZ(I+1,J,2)
       XCNTR(2)=XYZ(I,J+1,1)
       YCNTR(2)=XYZ(I,J+1,2)
       CALL CURVE (XCNTR,YCNTR,2,0)
       GOTO 60
50     CALL CURVE (XCNTR,YCNTR,2,0)
60   CONTINUE
70  CONTINUE
80 CONTINUE
   RETURN
   END
C
C
C
   REAL FUNCTION XLINT (I1,J1,I2,J2,K)
   REAL XYZ(50,50,3),ZCNTR(50)
   COMMON /BLKA/ XYZ,ZCNTR
   AM0=ZCNTR(K)-XYZ(I1,J1,3)
   AM1=XYZ(I2,J2,3)-XYZ(I1,J1,3)
   AM2=XYZ(I2,J2,1)-XYZ(I1,J1,1)
   XLINT=AM0*AM2/AM1+XYZ(I1,J1,1)
   RETURN
   END
C
C
C
```

```
REAL FUNCTION YLINT (I1,J1,I2,J2,K)
REAL XYZ(50,50,3),ZCNTR(50)
COMMON /BLKA/ XYZ,ZCNTR
AMO=ZCNTR(K)-XYZ(I1,J1,3)
AM1=XYZ(I2,J2,3)-XYZ(I1,J1,3)
AM2=XYZ(I2,J2,2)-XYZ(I1,J1,2)
YLINT=AMO*AM2/AM1+XYZ(I1,J1,2)
RETURN
END
```

APPENDIX B

The numerical results of Part II are presented in this appendix. Plots of the grid; the temperature, stream function and vorticity distributions; and the local Nusselt number distributions along the left and right wall are presented here for each cavity type, dimensionless amplitude and Rayleigh number. The results of cavity C1 are presented first. For each cavity, the results are presented in order of increasing amplitude, and for each amplitude, they are given in order of increasing Rayleigh number.

Each of the following pages contains the information listed below:

1. The values of the Prandtl number, Rayleigh number and dimensionless amplitude are written at the top of the left column. Directly below, in the same column, the average Nusselt numbers of the isothermal walls, the vorticity countour line values and the stream function countour line values are listed. The values of the isotherms are not included because they always range from 0 (cavity left wall) to 1 (cavity right wall) in increments of 0.1.
2. Plots of local Nusselt number along the right and left walls versus the distances calculated from the top of the cavity are presented at the middle and the bottom of the left column,

respectively.

3. Plots of the grid and the temperature, stream function and vorticity contours are presented in order from the top to the bottom of the right column. The minimum contour line value for the steam function is always the one corresponding to the wall. The maximum positive contour line value for the vorticity is always the one closest to the center.

PR= 1.0
RA= 0.0
DIMENSIONLESS AMPLITUDE= -0.150
AVERAGE NUSSELT NUMBER (RIGHT WALL)= 0.1164160E+01
AVERAGE NUSSELT NUMBER (LEFT WALL)= 0.1224422E+01
LENGTH OF THE WALL(RIGHT)= 0.1053394E+01
LENGTH OF THE WALL(LEFT)= 0.1000000E+01

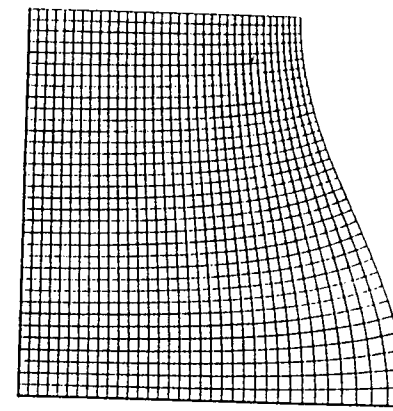

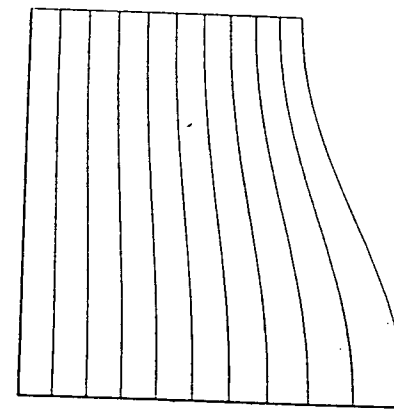

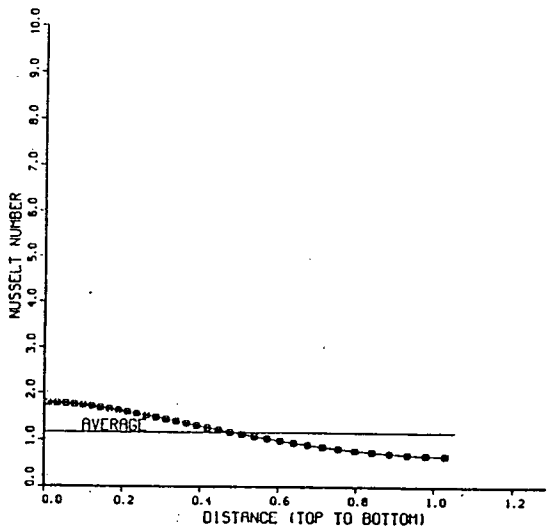

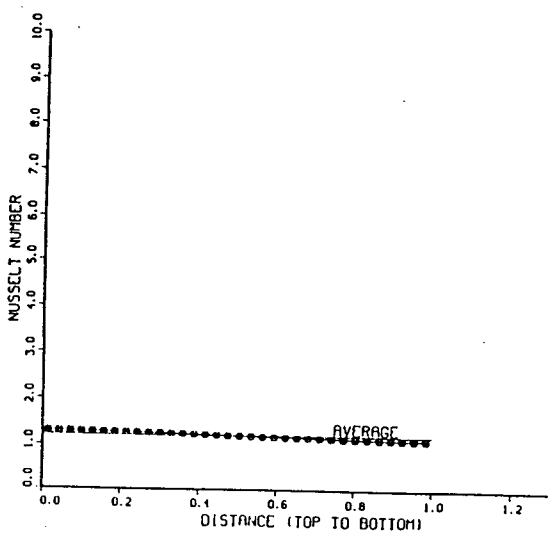

PR= 1.0
RA= 1000.0
DIMENSIONLESS AMPLITUDE= -0.150
AVERAGE NUSSELT NUMBER (RIGHT WALL)= 0.1231642E+01
AVERAGE NUSSELT NUMBER (LEFT WALL)= 0.1287287E+01
LENGTH OF THE WALL(RIGHT)= 0.1053372E+01
LENGTH OF THE WALL(LEFT)= 0.1000000E+01

VORTICITY COUNTOUR VALUES.
MIN= -0.5339651E+02
MAX= 0.3067580E+02

CONTOUR #	1	-0.4498927E+02
CONTOUR #	2	-0.3658206E+02
CONTOUR #	3	-0.2817484E+02
CONTOUR #	4	-0.1976761E+02
CONTOUR #	5	-0.1136038E+02
CONTOUR #	6	-0.2953140E+01
CONTOUR #	7	0.5454086E+01
CONTOUR #	8	0.1386131E+02
CONTOUR #	9	0.2226854E+02

STREAM FUNCTION CONTOUR VALUES.
MIN= 0.0
MAX= 0.9066495E+00

CONTOUR #	1	0.9066492E-01
CONTOUR #	2	0.1813298E+00
CONTOUR #	3	0.2719948E+00
CONTOUR #	4	0.3626597E+00
CONTOUR #	5	0.4533247E+00
CONTOUR #	6	0.5439897E+00
CONTOUR #	7	0.6346546E+00
CONTOUR #	8	0.7253196E+00
CONTOUR #	9	0.8159845E+00

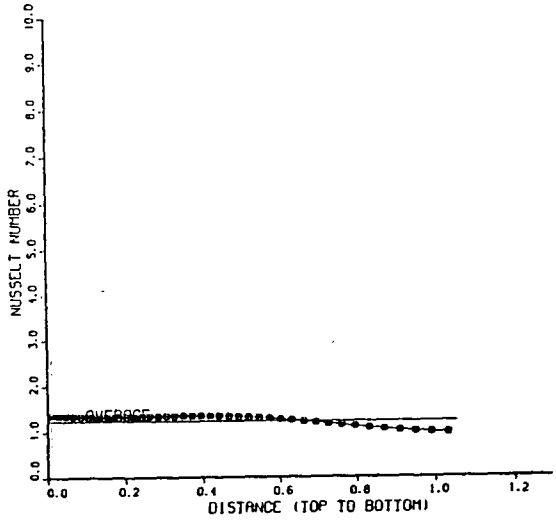

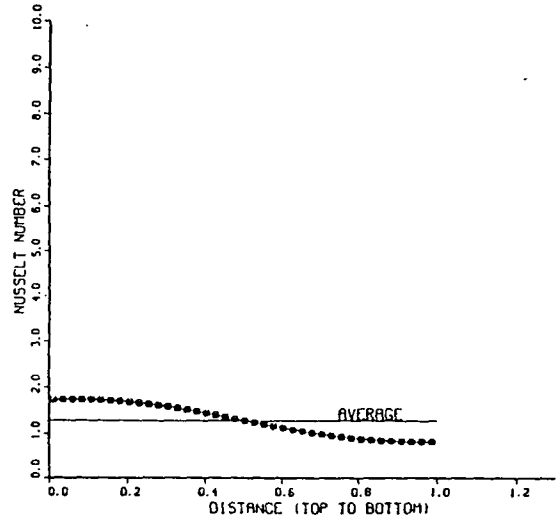

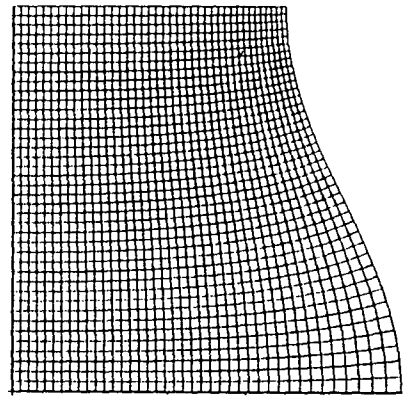

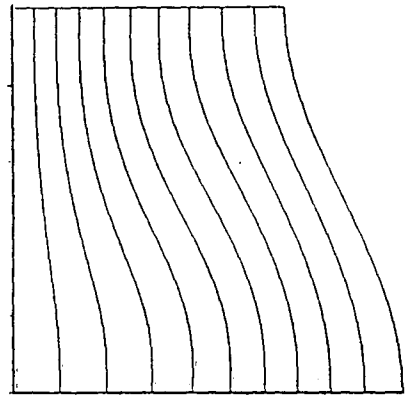

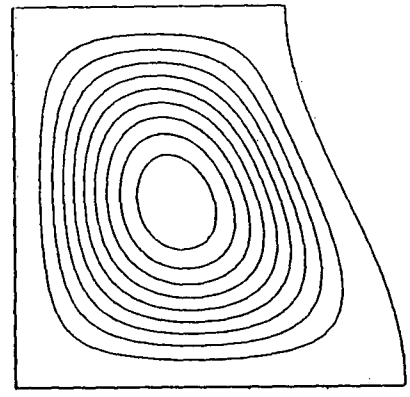

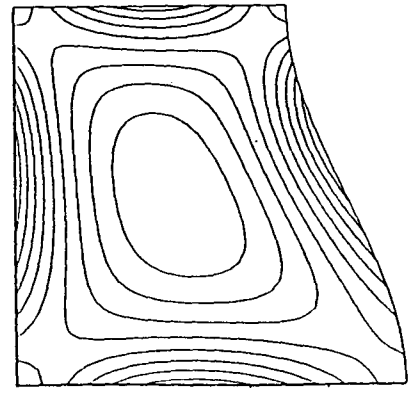

PR= 1.0
RA= 3000.0
DIMENSIONLESS AMPLITUDE= -0.150
AVERAGE NUSSELT NUMBER (RIGHT WALL)= 0.1523848E+01
AVERAGE NUSSELT NUMBER (LEFT WALL)= 0.1605338E+01
LENGTH OF THE WALL(RIGHT)= 0.1053372E+01
LENGTH OF THE WALL(LEFT)= 0.1000000E+01

VORTICITY COUNTOUR VALUES.
MIN= -0.1504148E+03
MAX= 0.7222437E+02

CONTOUR #	1	-0.1281509E+03
CONTOUR #	2	-0.1058870E+03
CONTOUR #	3	-0.8362305E+02
CONTOUR #	4	-0.6135913E+02
CONTOUR #	5	-0.3909521E+02
CONTOUR #	6	-0.1683130E+02
CONTOUR #	7	0.5432617E+01
CONTOUR #	8	0.2769653E+02
CONTOUR #	9	0.4996042E+02

STREAM FUNCTION CONTOUR VALUES.
MIN= 0.0
MAX= 0.2244084E+01

CONTOUR #	1	0.2244084E+00
CONTOUR #	2	0.4488168E+00
CONTOUR #	3	0.6732253E+00
CONTOUR #	4	0.8976337E+00
CONTOUR #	5	0.1122042E+01
CONTOUR #	6	0.1346450E+01
CONTOUR #	7	0.1570859E+01
CONTOUR #	8	0.1795266E+01
CONTOUR #	9	0.2019674E+01

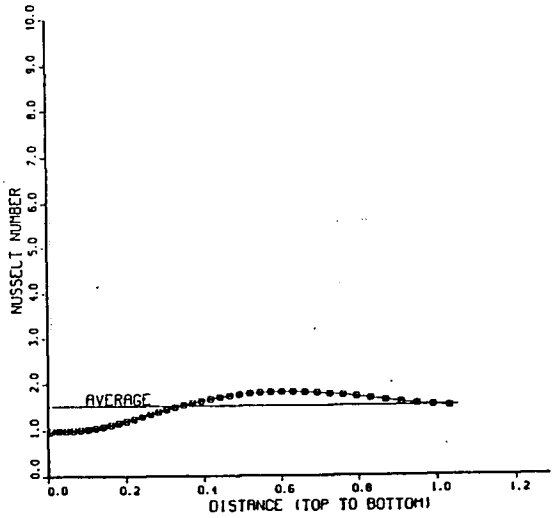

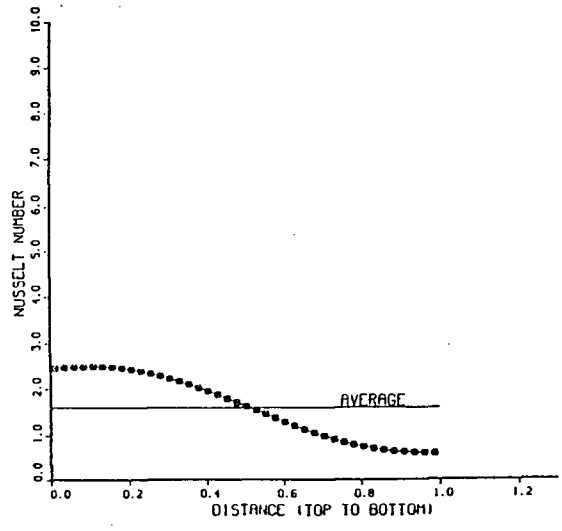

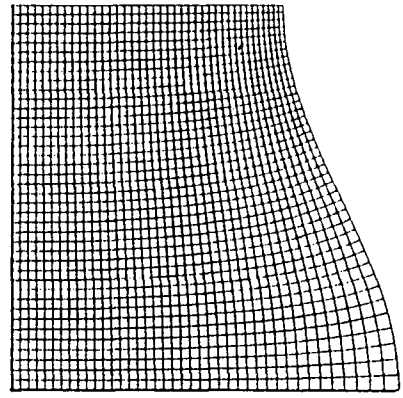

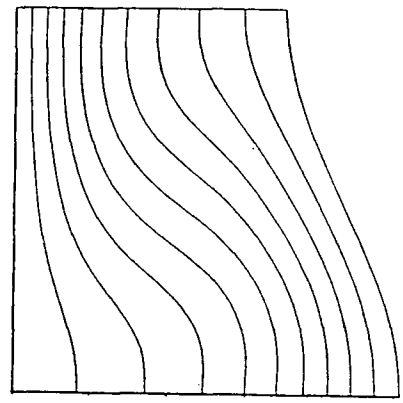

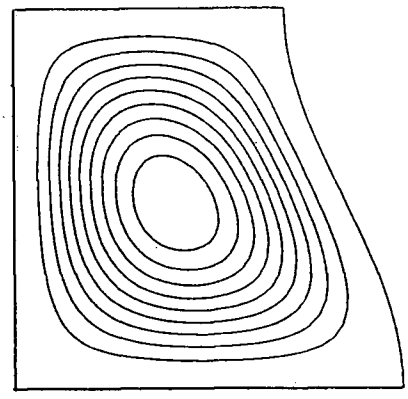

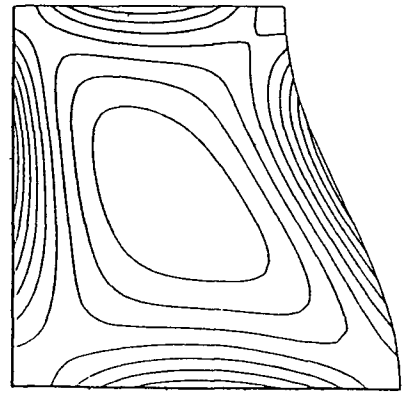

PR= 1.0
RA= 10000.0
DIMENSIONLESS AMPLITUDE= -0.150
AVERAGE NUSSELT NUMBER (RIGHT WALL)= 0.2236863E+01
AVERAGE NUSSELT NUMBER (LEFT WALL)= 0.2355938E+01
LENGTH OF THE WALL(RIGHT)= 0.1053372E+01
LENGTH OF THE WALL(LEFT)= 0.1000000E+01

VORTICITY COUNTOUR VALUES.
MIN= -0.4391618E+03
MAX= 0.1388923E+03

CONTOUR #	1	-0.3813564E+03
CONTOUR #	2	-0.3235510E+03
CONTOUR #	3	-0.2657456E+03
CONTOUR #	4	-0.2079403E+03
CONTOUR #	5	-0.1501350E+03
CONTOUR #	6	-0.9232959E+02
CONTOUR #	7	-0.3452417E+02
CONTOUR #	8	0.2328101E+02
CONTOUR #	9	0.8106643E+02

STREAM FUNCTION CONTOUR VALUES.
MIN= 0.0
MAX= 0.4654137E+01

CONTOUR #	1	0.4654136E+00
CONTOUR #	2	0.9308273E+00
CONTOUR #	3	0.1396240E+01
CONTOUR #	4	0.1861654E+01
CONTOUR #	5	0.2327067E+01
CONTOUR #	6	0.2792481E+01
CONTOUR #	7	0.3257895E+01
CONTOUR #	8	0.3723309E+01
CONTOUR #	9	0.4188722E+01

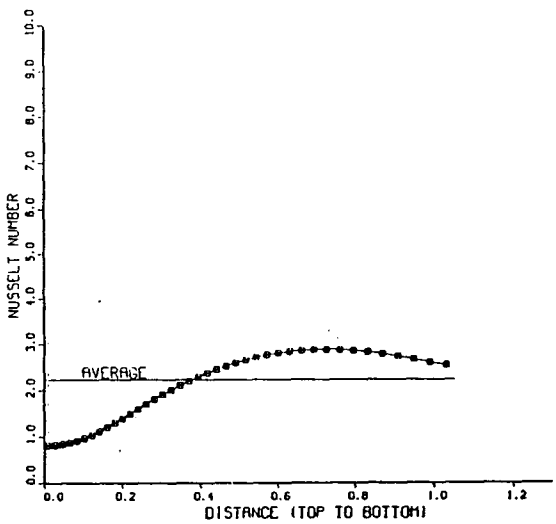

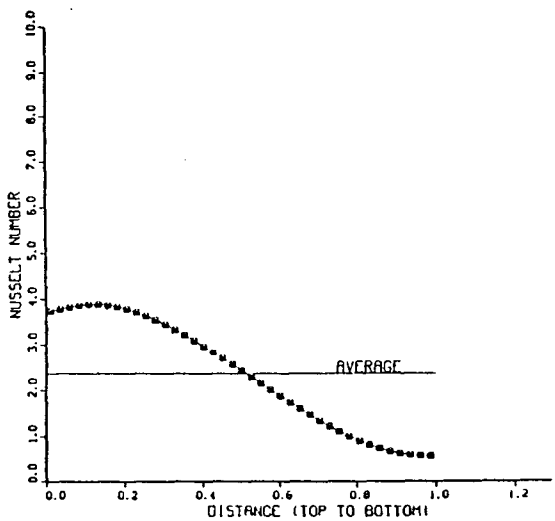

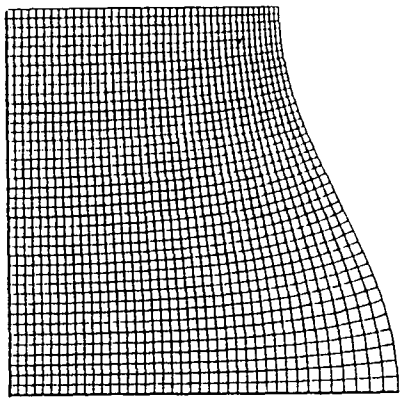

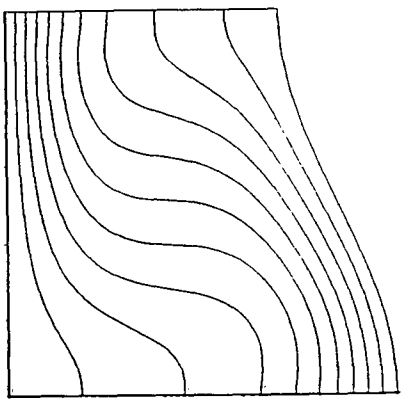

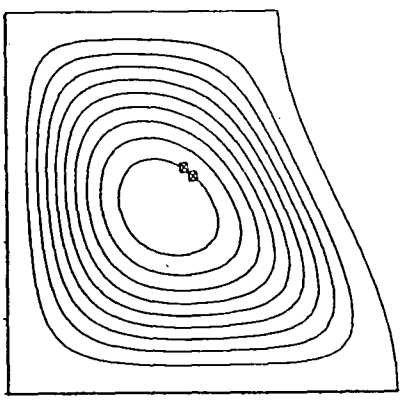

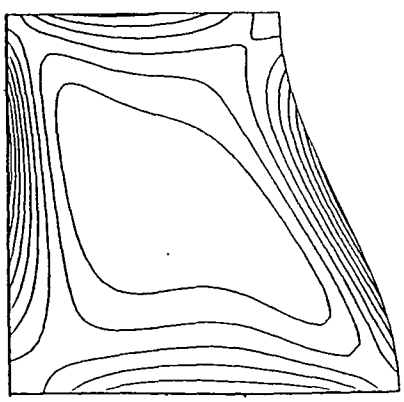

PR= 1.0
RA= 30000.0
DIMENSIONLESS AMPLITUDE= -0.150
AVERAGE NUSSELT NUMBER (RIGHT WALL)= 0.3135803E+01
AVERAGE NUSSELT NUMBER (LEFT WALL)= 0.3303327E+01
LENGTH OF THE WALL(RIGHT)= 0.1053372E+01
LENGTH OF THE WALL(LEFT)= 0.1000000E+01

VORTICITY COUNTOUR VALUES.
MIN= -0.1060230E+04
MAX= 0.2697053E+03

CONTOUR #	1	-0.9272361E+03
CONTOUR #	2	-0.7842429E+03
CONTOUR #	3	-0.6612493E+03
CONTOUR #	4	-0.5282561E+03
CONTOUR #	5	-0.3952627E+03
CONTOUR #	6	-0.2622688E+03
CONTOUR #	7	-0.1292756E+03
CONTOUR #	8	0.3718262E+01
CONTOUR #	9	0.1367117E+03

STREAM FUNCTION CONTOUR VALUES.
MIN= 0.0
MAX= 0.7396093E+01

CONTOUR #	1	0.7396093E+00
CONTOUR #	2	0.1478218E+01
CONTOUR #	3	0.2218827E+01
CONTOUR #	4	0.2958436E+01
CONTOUR #	5	0.3698045E+01
CONTOUR #	6	0.4437655E+01
CONTOUR #	7	0.5177264E+01
CONTOUR #	8	0.5916874E+01
CONTOUR #	9	0.6656483E+01

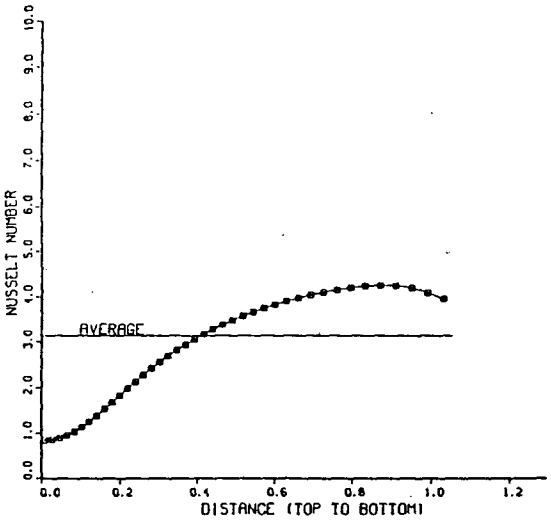

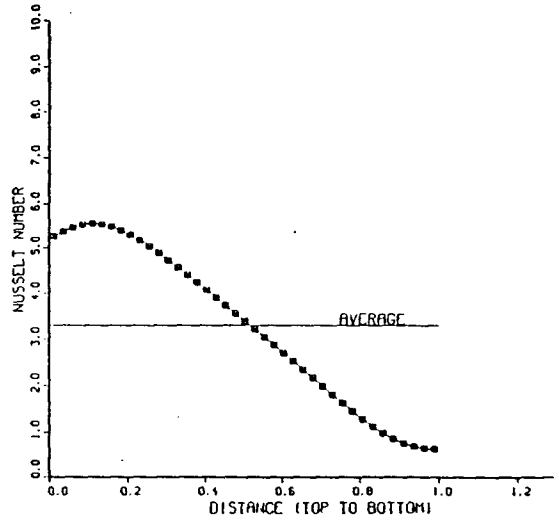

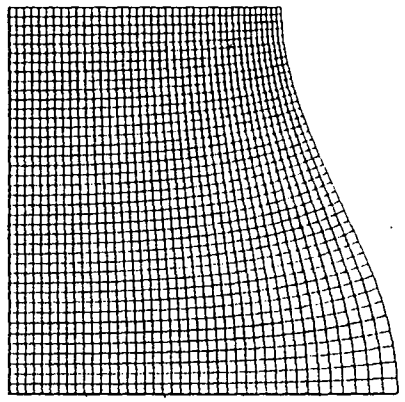

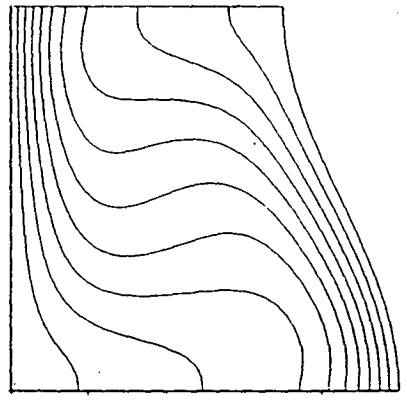

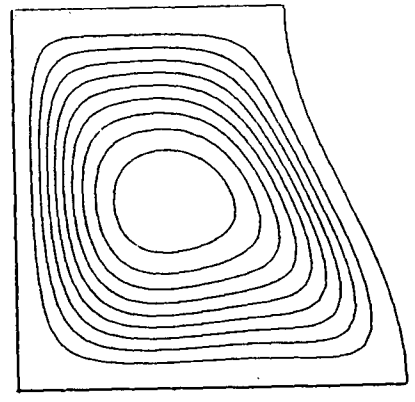

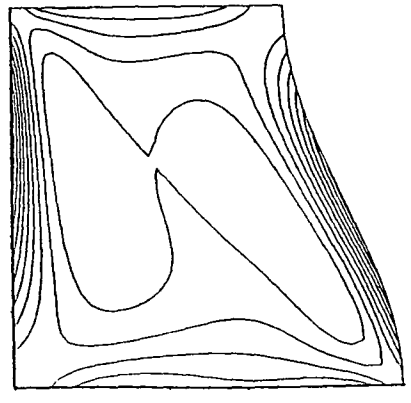

PR= 1.0
RA= 100000.0
DIMENSIONLESS AMPLITUDE= -0.150
AVERAGE NUSSELT NUMBER (RIGHT WALL)= 0.4477163E+01
AVERAGE NUSSELT NUMBER (LEFT WALL)= 0.4716380E+01
LENGTH OF THE WALL(RIGHT)= 0.1063410E+01
LENGTH OF THE WALL(LEFT)= 0.1000000E+01

VORTICITY COUNTOUR VALUES.
MIN= -0.2680707E+04
MAX= 0.6641846E+03

CONTOUR #	1	-0.2347218E+04
CONTOUR #	2	-0.2013729E+04
CONTOUR #	3	-0.1680240E+04
CONTOUR #	4	-0.1346750E+04
CONTOUR #	5	-0.1013261E+04
CONTOUR #	6	-0.6797722E+03
CONTOUR #	7	-0.3462833E+03
CONTOUR #	8	-0.1278370E+02
CONTOUR #	9	0.3206953E+03

STREAM FUNCTION CONTOUR VALUES.
MIN= 0.0
MAX= 0.1006742E+02

CONTOUR #	1	0.1006742E+01
CONTOUR #	2	0.2013484E+01
CONTOUR #	3	0.3020226E+01
CONTOUR #	4	0.4026968E+01
CONTOUR #	5	0.5033710E+01
CONTOUR #	6	0.6040452E+01
CONTOUR #	7	0.7047194E+01
CONTOUR #	8	0.8053936E+01

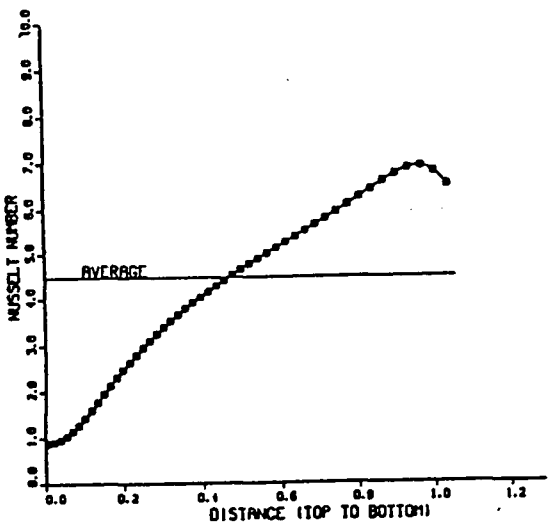

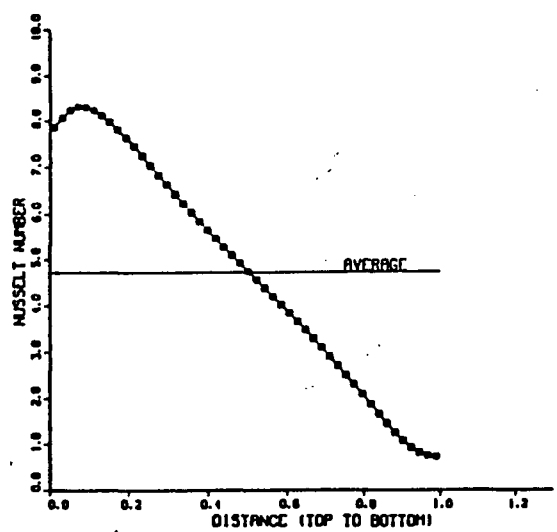

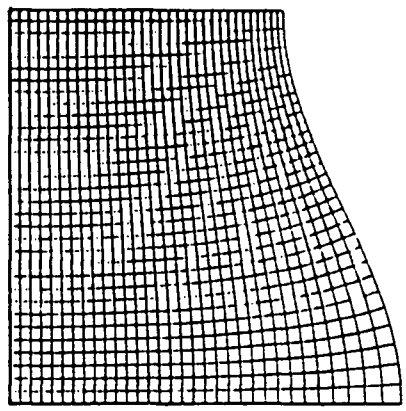

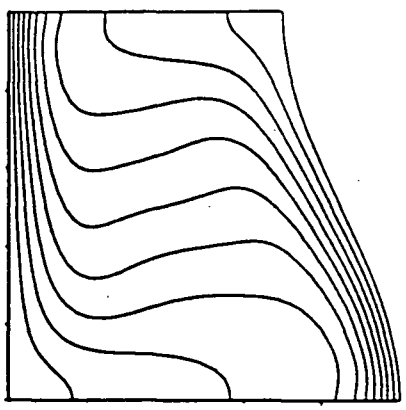

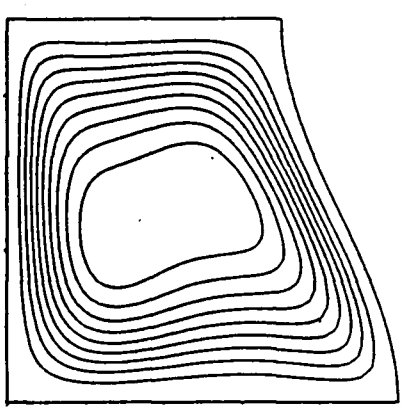

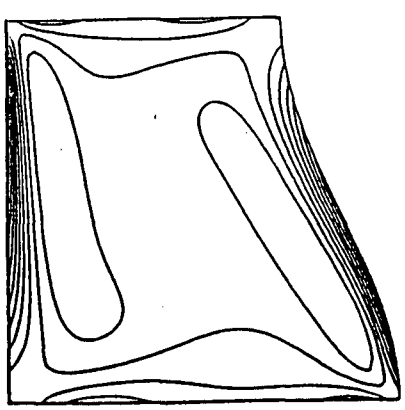

PR= 1.0
RA= 0.0
DIMENSIONLESS AMPLITUDE= -0.075
AVERAGE NUSSELT NUMBER (RIGHT WALL)= 0.1077903E+01
AVERAGE NUSSELT NUMBER (LEFT WALL)= 0.1080488E+01
LENGTH OF THE WALL(RIGHT)= 0.1013727E+01
LENGTH OF THE WALL(LEFT)= 0.1000000E+01

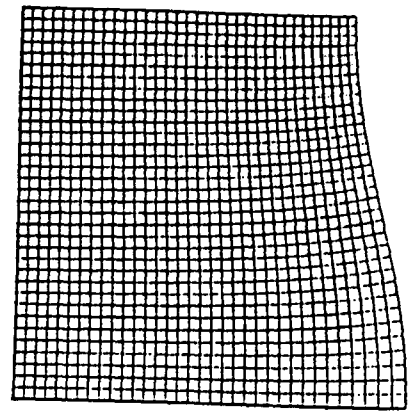

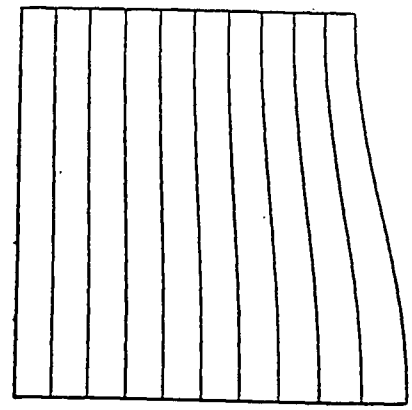

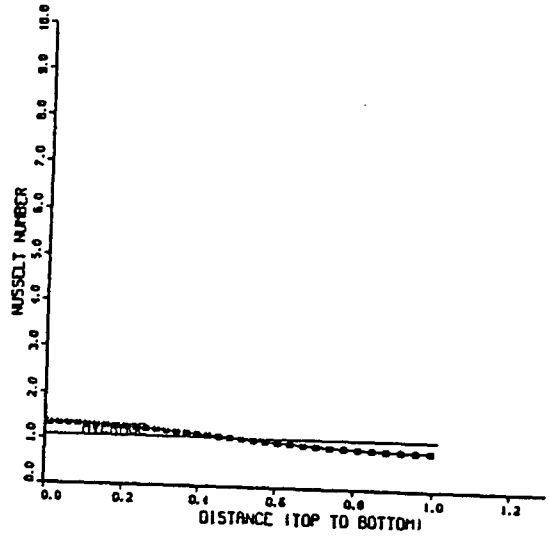

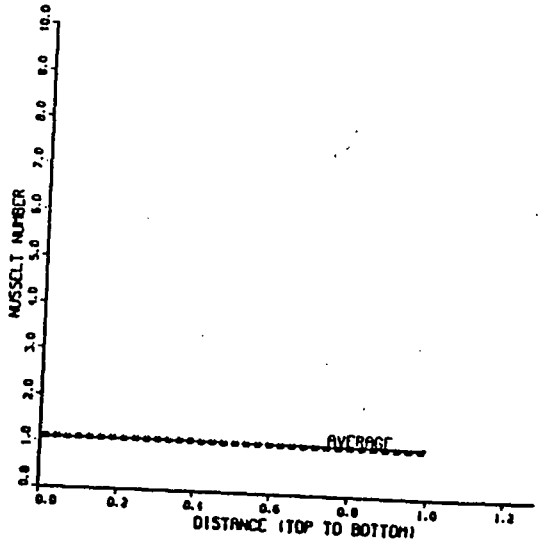

PR= 1.0
RA= 1000.0
DIMENSIONLESS AMPLITUDE= -0.075
AVERAGE NUSSELT NUMBER (RIGHT WALL)= 0.1173338E+01
AVERAGE NUSSELT NUMBER (LEFT WALL)= 0.1189285E+01
LENGTH OF THE WALL(RIGHT)= 0.1013727E+01
LENGTH OF THE WALL(LEFT)= 0.1000000E+01

VORTICITY COUNTOUR VALUES.
MIN= -0.5208338E+02
MAX= 0.3180869E+02

CONTOUR #	1	-0.4369417E+02
CONTOUR #	2	-0.3530498E+02
CONTOUR #	3	-0.2691577E+02
CONTOUR #	4	-0.1852658E+02
CONTOUR #	5	-0.1013737E+02
CONTOUR #	6	-0.1748169E+01
CONTOUR #	7	0.6641037E+01
CONTOUR #	8	0.1503026E+02
CONTOUR #	9	0.2341946E+02

STREAM FUNCTION CONTOUR VALUES.
MIN= 0.0
MAX= 0.1062971E+01

CONTOUR #	1	0.1062971E+00
CONTOUR #	2	0.2125942E+00
CONTOUR #	3	0.3188913E+00
CONTOUR #	4	0.4251884E+00
CONTOUR #	5	0.5314856E+00
CONTOUR #	6	0.6377826E+00
CONTOUR #	7	0.7440798E+00
CONTOUR #	8	0.8503768E+00
CONTOUR #	9	0.9566740E+00

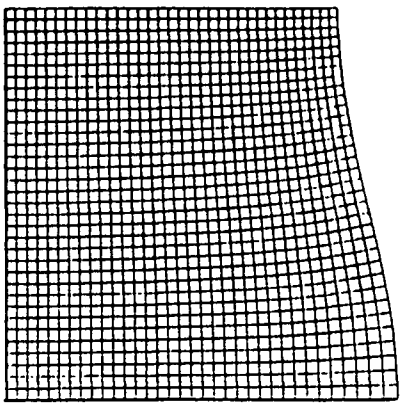

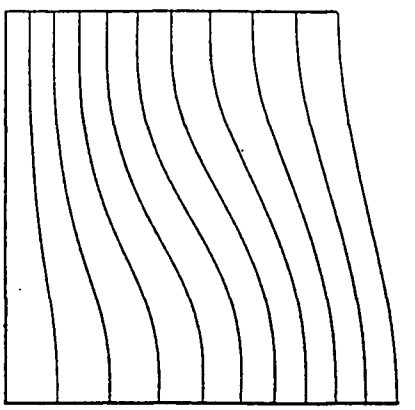

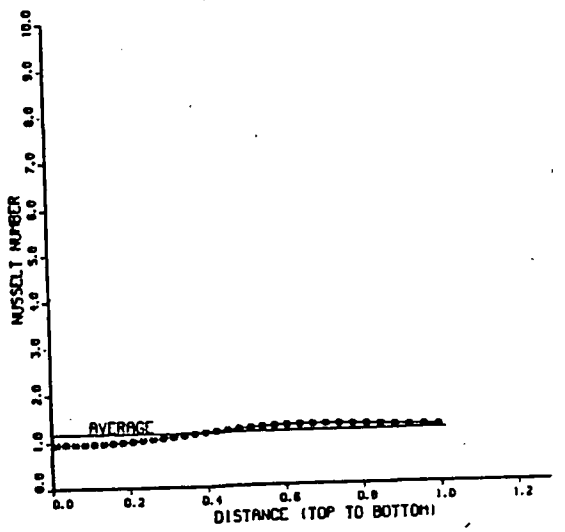

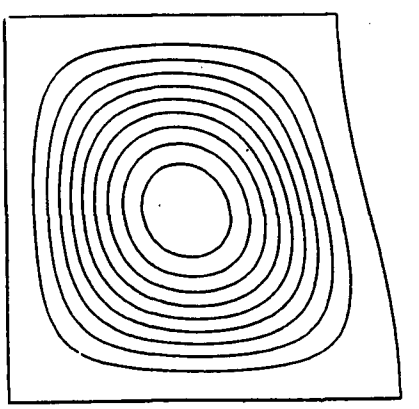

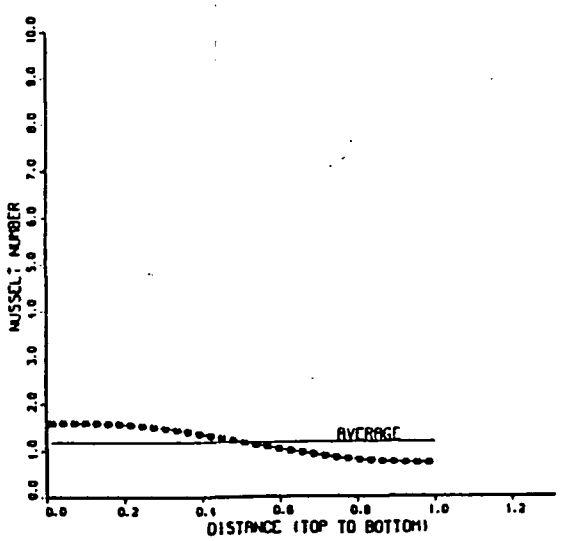

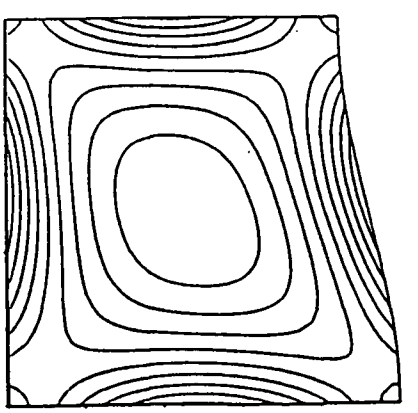

PR= 1.0
RA= 3000.0
DIMENSIONLESS AMPLITUDE= -0.075
AVERAGE NUSSELT NUMBER (RIGHT WALL)= 0.1527188E+01
AVERAGE NUSSELT NUMBER (LEFT WALL)= 0.1548141E+01
LENGTH OF THE WALL(RIGHT)= 0.1013727E+01
LENGTH OF THE WALL(LEFT)= 0.1000000E+01

VORTICITY COUNTOUR VALUES.
MIN= -0.1496883E+03
MAX= 0.7050732E+02

CONTOUR #	1	-0.1276687E+03
CONTOUR #	2	-0.1056492E+03
CONTOUR #	3	-0.8362961E+02
CONTOUR #	4	-0.6161005E+02
CONTOUR #	5	-0.3959048E+02
CONTOUR #	6	-0.1757094E+02
CONTOUR #	7	0.4448624E+01
CONTOUR #	8	0.2646820E+02
CONTOUR #	9	0.4848776E+02

STREAM FUNCTION CONTOUR VALUES.
MIN= 0.0
MAX= 0.2525986E+01

CONTOUR #	1	0.2525985E+00
CONTOUR #	2	0.5051871E+00
CONTOUR #	3	0.7577957E+00
CONTOUR #	4	0.1010394E+01
CONTOUR #	5	0.1262893E+01
CONTOUR #	6	0.1515591E+01
CONTOUR #	7	0.1768189E+01
CONTOUR #	8	0.2020788E+01
CONTOUR #	9	0.2273387E+01

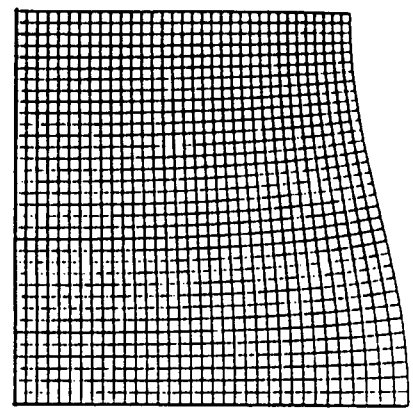

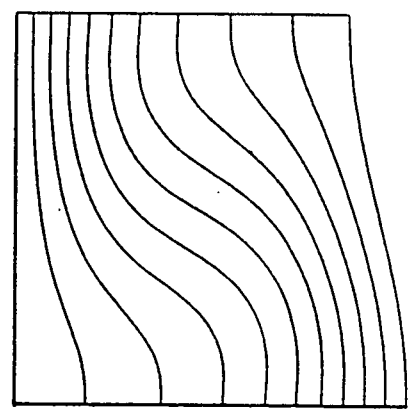

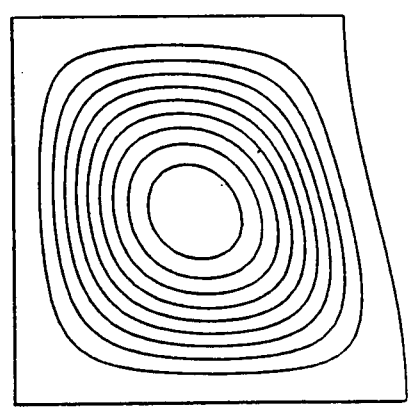

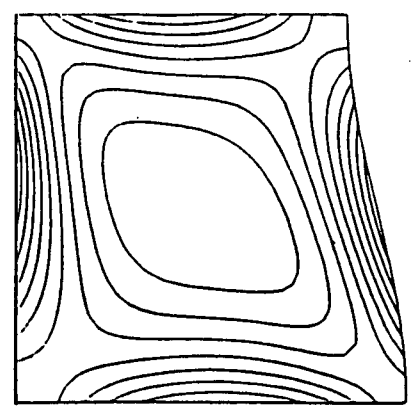

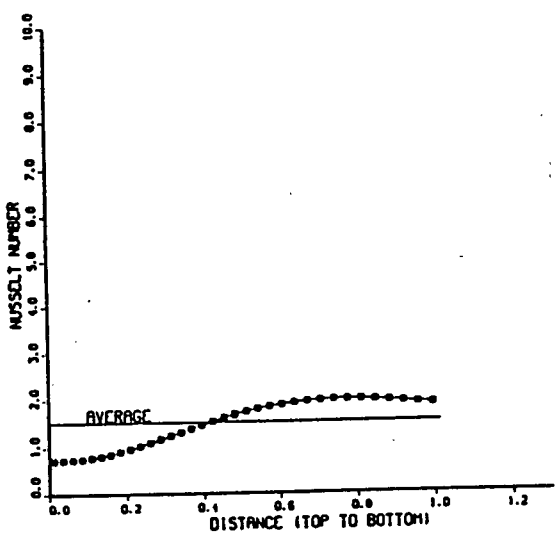

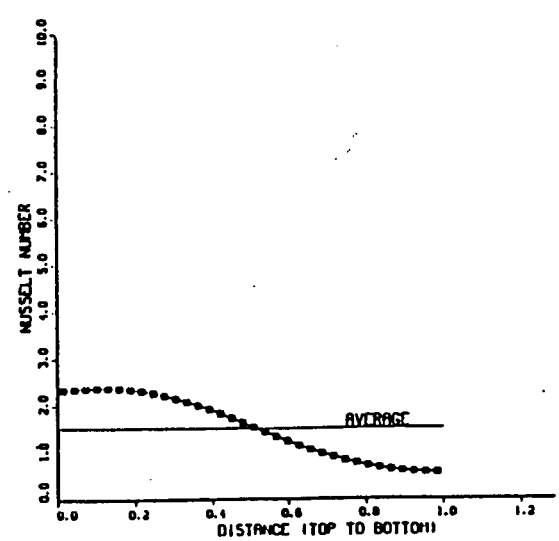

PR= 1.0
RA= 10000.0
DIMENSIONLESS AMPLITUDE= -0.075
AVERAGE NUSSELT NUMBER (RIGHT WALL)= 0.2271343E+01
AVERAGE NUSSELT NUMBER (LEFT WALL)= 0.2302238E+01
LENGTH OF THE WALL(RIGHT)= 0.1013727E+01
LENGTH OF THE WALL(LEFT)= 0.1000000E+01

VORTICITY COUNTOUR VALUES.
MIN= -0.4328752E+03
MAX= 0.1211660E+03

CONTOUR #	1	-0.3764708E+03
CONTOUR #	2	-0.3200668E+03
CONTOUR #	3	-0.2636628E+03
CONTOUR #	4	-0.2072587E+03
CONTOUR #	5	-0.1508547E+03
CONTOUR #	6	-0.9445068E+02
CONTOUR #	7	-0.3804639E+02
CONTOUR #	8	0.1835742E+02
CONTOUR #	9	0.7476172E+02

STREAM FUNCTION CONTOUR VALUES.
MIN= 0.0
MAX= 0.4956753E+01

CONTOUR #	1	0.4956753E+00
CONTOUR #	2	0.9913505E+00
CONTOUR #	3	0.1487025E+01
CONTOUR #	4	0.1982700E+01
CONTOUR #	5	0.2478374E+01
CONTOUR #	6	0.2974051E+01
CONTOUR #	7	0.3469727E+01
CONTOUR #	8	0.3965402E+01
CONTOUR #	9	0.4461076E+01

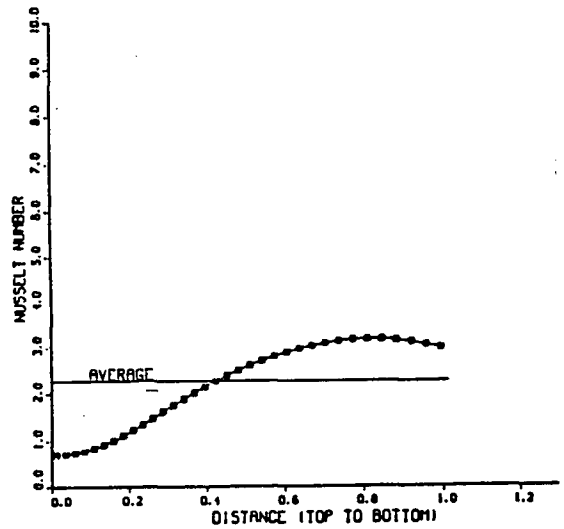

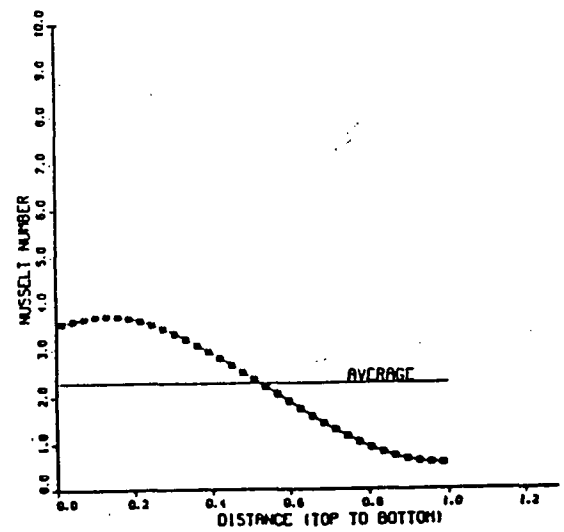

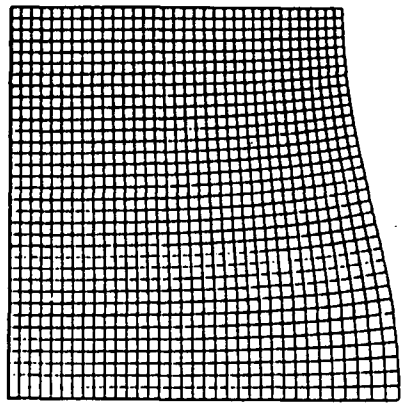

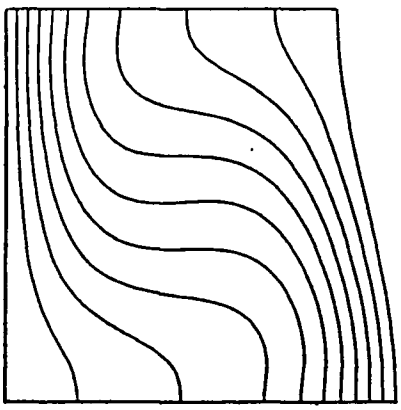

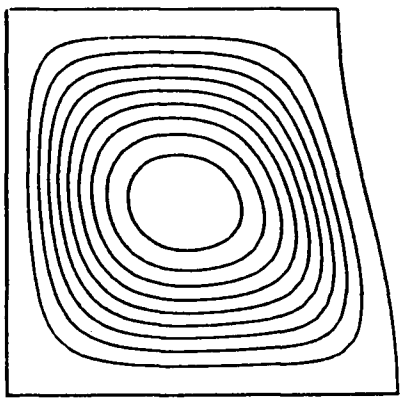

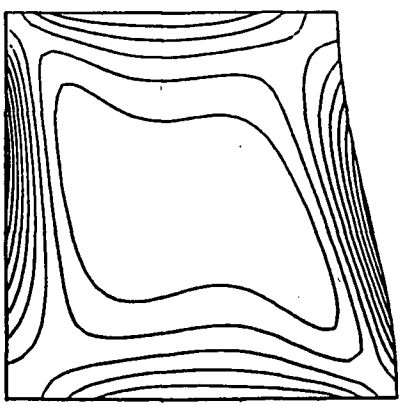

PR= 1.0
RA= 30000.0
DIMENSIONLESS AMPLITUDE= -0.075
AVERAGE NUSSELT NUMBER (RIGHT WALL)= 0.3184918E+01
AVERAGE NUSSELT NUMBER (LEFT WALL)= 0.3228787E+01
LENGTH OF THE WALL(RIGHT)= 0.1013727E+01
LENGTH OF THE WALL(LEFT)= 0.1000000E+01

VORTICITY COUNTOUR VALUES.
MIN= -0.1047068E+04
MAX= 0.2668937E+03

CONTOUR #	1	-0.8156802E+03
CONTOUR #	2	-0.7842722E+03
CONTOUR #	3	-0.6528640E+03
CONTOUR #	4	-0.5214558E+03
CONTOUR #	5	-0.3900476E+03
CONTOUR #	6	-0.2586394E+03
CONTOUR #	7	-0.1272312E+03
CONTOUR #	8	0.4177002E+01
CONTOUR #	9	0.1355852E+03

STREAM FUNCTION CONTOUR VALUES.
MIN= 0.0
MAX= 0.7403912E+01

CONTOUR #	1	0.7403911E+00
CONTOUR #	2	0.1480782E+01
CONTOUR #	3	0.2221172E+01
CONTOUR #	4	0.2961564E+01
CONTOUR #	5	0.3701954E+01
CONTOUR #	6	0.4442346E+01
CONTOUR #	7	0.5182737E+01
CONTOUR #	8	0.5923129E+01
CONTOUR #	9	0.6663518E+01

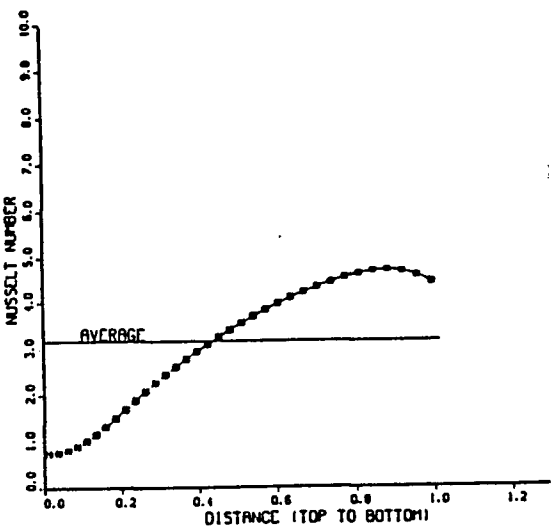

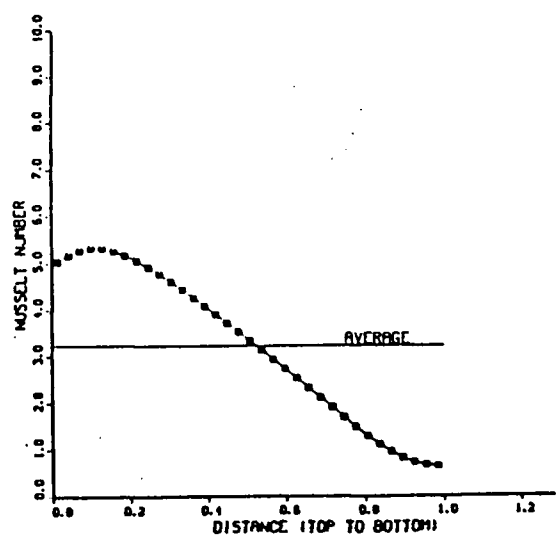

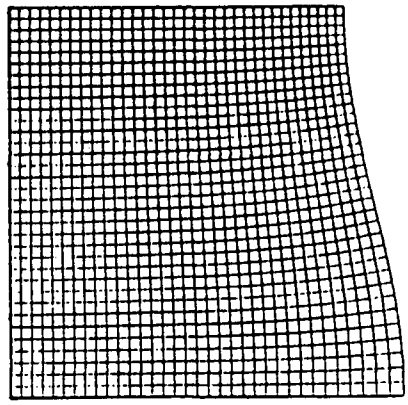

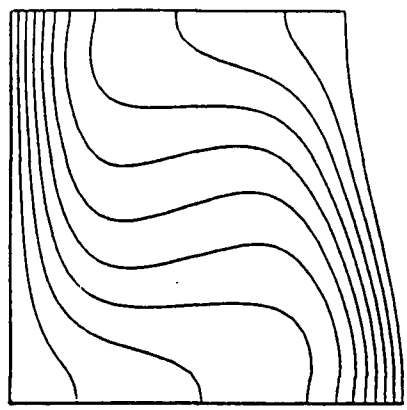

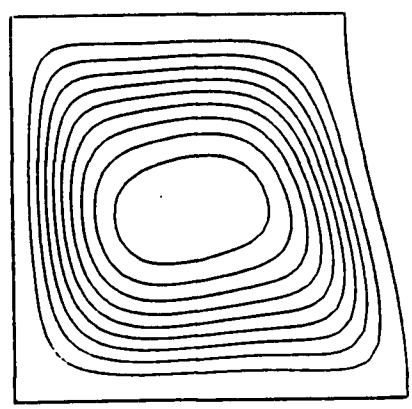

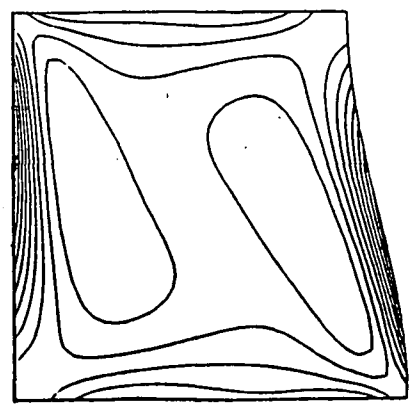

PR= 1.0
RA= 100000.0
DIMENSIONLESS AMPLITUDE= -0.075
AVERAGE NUSSELT NUMBER (RIGHT WALL)= 0.4877280E+01
AVERAGE NUSSELT NUMBER (LEFT WALL)= 0.4640108E+01
LENGTH OF THE WALL(RIGHT)= 0.1013727E+01
LENGTH OF THE WALL(LEFT)= 0.1000000E+01

VORTICITY COUNTOUR VALUES.
MIN= -0.2678384E+04
MAX= 0.6526648E+03

CONTOUR #	1	-0.2345280E+04
CONTOUR #	2	-0.2012175E+04
CONTOUR #	3	-0.1678070E+04
CONTOUR #	4	-0.1345965E+04
CONTOUR #	5	-0.1012860E+04
CONTOUR #	6	-0.6797551E+03
CONTOUR #	7	-0.3466504E+03
CONTOUR #	8	-0.1354541E+02
CONTOUR #	9	0.3195598E+03

STREAM FUNCTION CONTOUR VALUES.
MIN= 0.0
MAX= 0.1006550E+02

CONTOUR #	1	0.1006550E+01
CONTOUR #	2	0.2013100E+01
CONTOUR #	3	0.3019650E+01
CONTOUR #	4	0.4026200E+01
CONTOUR #	5	0.5032751E+01
CONTOUR #	6	0.6039300E+01
CONTOUR #	7	0.7045851E+01
CONTOUR #	8	0.8052402E+01
CONTOUR #	9	0.9058952E+01

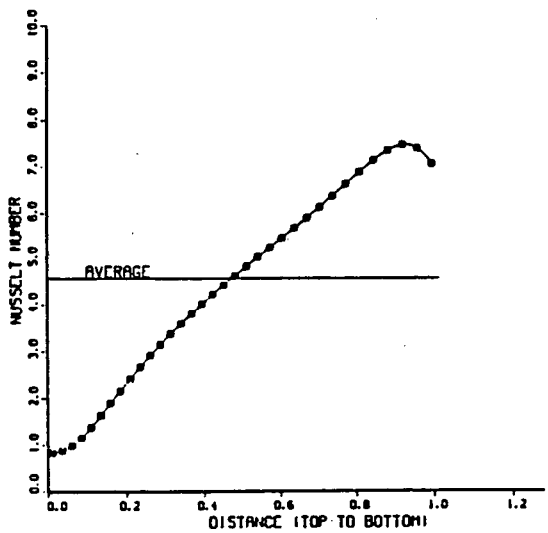

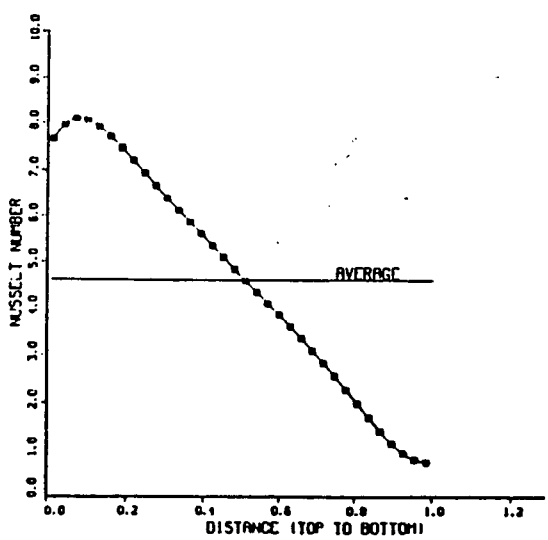

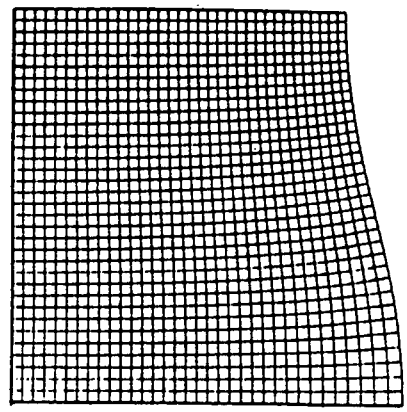

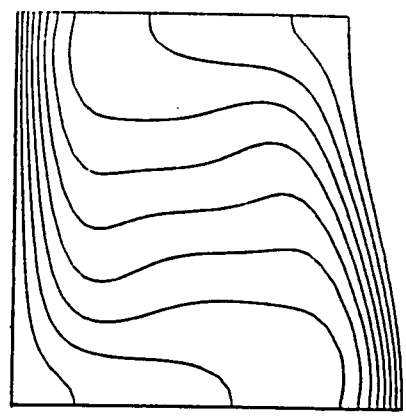

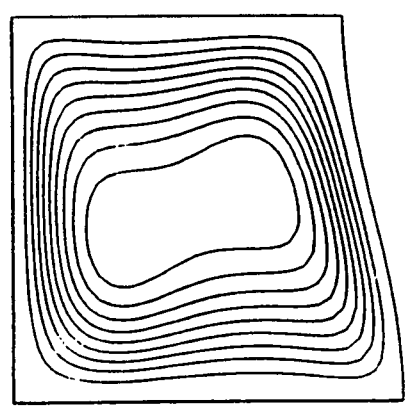

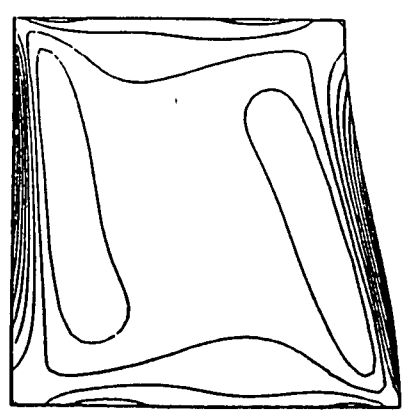

PR= 1.0
RA= 0.0
DIMENSIONLESS AMPLITUDE= 0.0
AVERAGE NUSSELT NUMBER (RIGHT WALL)= 0.10007138+01
AVERAGE NUSSELT NUMBER (LEFT WALL)= 0.99999428+00
LENGTH OF THE WALL(RIGHT)= 0.10000000E+01
LENGTH OF THE WALL(LEFT)= 0.10000000E+01

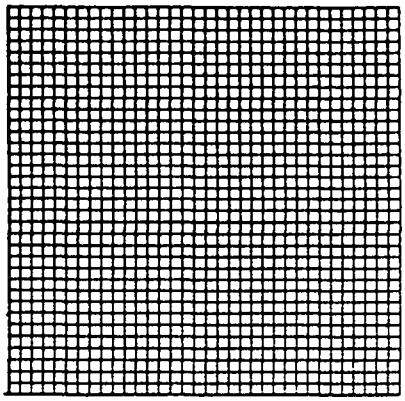

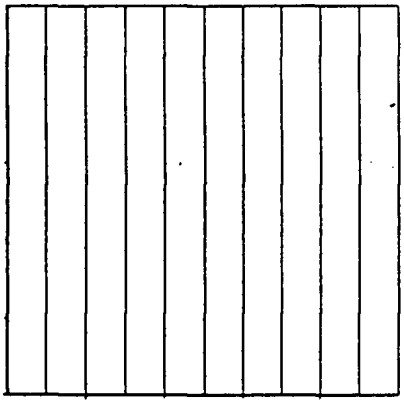

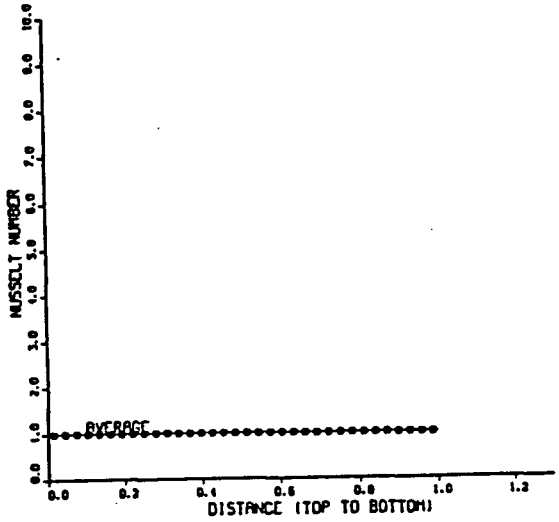

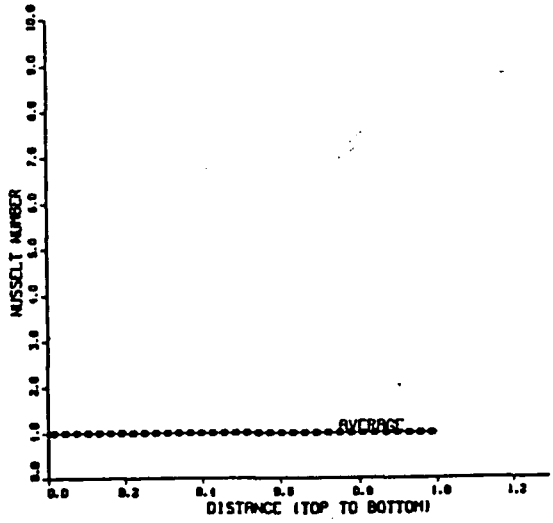

```
PR= 1.0
RA= 1000
DIMENSIONLESS AMPLITUDE= 0.0
AVERAGE NUSSELT NUMBER (RIGHT WALL)=   0.1117314E+01
AVERAGE NUSSELT NUMBER (LEFT WALL)=    0.1117116E+01
LENGTH OF THE WALL(RIGHT)=   0.1000000E+01
LENGTH OF THE WALL(LEFT)=    0.1000000E+01

VORTICITY COUNTOUR VALUES.
MIN=   -0.8111407E+02
MAX=    0.3103278E+02
CONTOUR #     1       -0.4280838E+01
CONTOUR #     2       -0.3450471E+02
CONTOUR #     3       -0.2620003E+02
CONTOUR #     4       -0.1789536E+02
CONTOUR #     5       -0.9590668E+01
CONTOUR #     6       -0.1285980E+01
CONTOUR #     7        0.7018707E+01
CONTOUR #     8        0.1832338E+02
CONTOUR #     9        0.2962806E+02

STREAM FUNCTION CONTOUR VALUES.
MIN=    0.0
MAX=    0.1172150E+01
CONTOUR #     1        0.1172149E+00
CONTOUR #     2        0.2344298E+00
CONTOUR #     3        0.3516449E+00
CONTOUR #     4        0.4688599E+00
CONTOUR #     5        0.5860748E+00
CONTOUR #     6        0.7032897E+00
CONTOUR #     7        0.8205047E+00
CONTOUR #     8        0.9377197E+00
CONTOUR #     9        0.1054935E+01
```

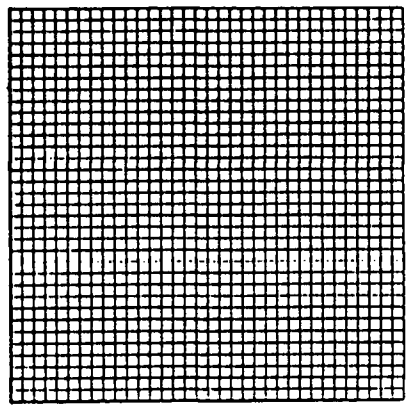

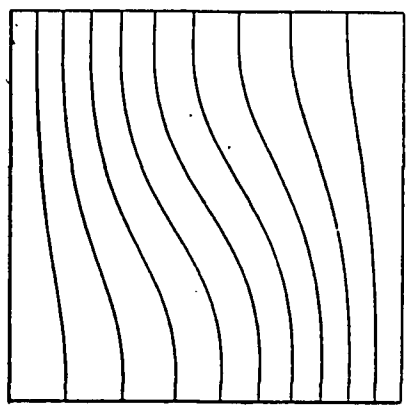

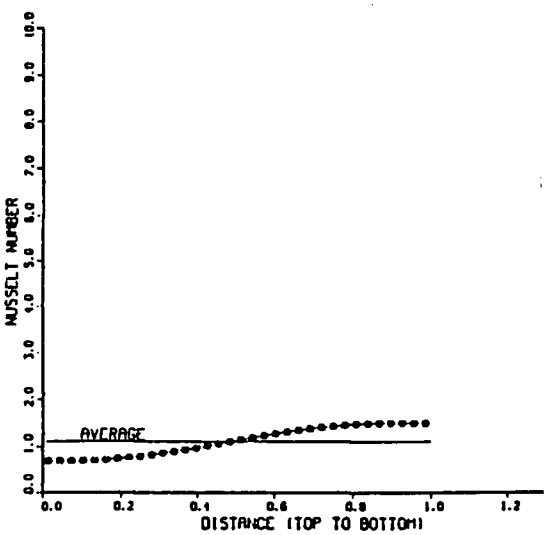

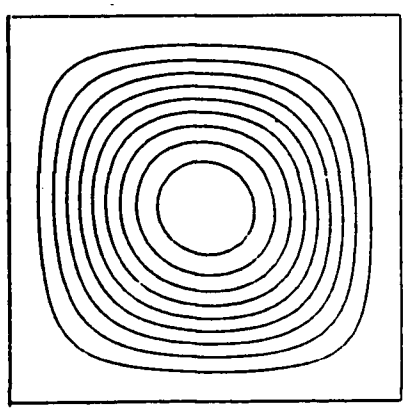

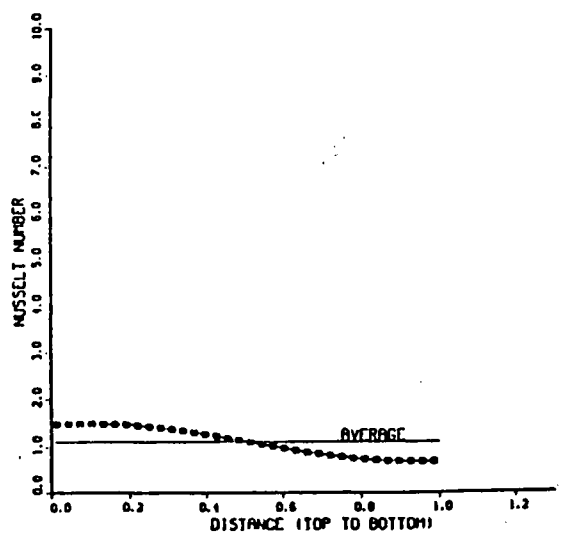

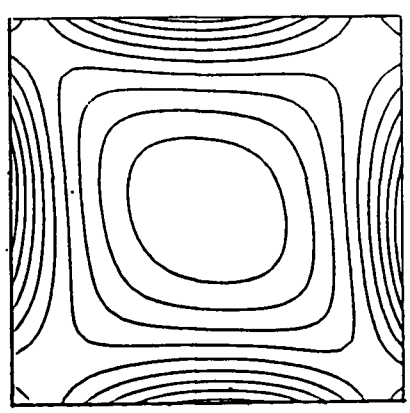

PR= 1.0
RA= 3000.0
DIMENSIONLESS AMPLITUDE= 0.0
AVERAGE NUSSELT NUMBER (RIGHT WALL)= 0.1603907E+01
AVERAGE NUSSELT NUMBER (LEFT WALL)= 0.1603778E+01
LENGTH OF THE WALL(RIGHT)= 0.1000000E+01
LENGTH OF THE WALL(LEFT)= 0.1000000E+01

VORTICITY CONTOUR VALUES.
MIN= -0.1473278E+03
MAX= 0.6775168E+02

CONTOUR #	1	-0.1258196E+03
CONTOUR #	2	-0.1043117E+03
CONTOUR #	3	-0.8280374E+02
CONTOUR #	4	-0.6129584E+02
CONTOUR #	5	-0.3978792E+02
CONTOUR #	6	-0.1827998E+02
CONTOUR #	7	0.3227921E+01
CONTOUR #	8	0.2473582E+02
CONTOUR #	9	0.4624374E+02

STREAM FUNCTION CONTOUR VALUES.
MIN= 0.0
MAX= 0.2709788E+01

CONTOUR #	1	0.2709788E+00
CONTOUR #	2	0.5419585E+00
CONTOUR #	3	0.8129393E+00
CONTOUR #	4	0.1083919E+01
CONTOUR #	5	0.1354898E+01
CONTOUR #	6	0.1625877E+01
CONTOUR #	7	0.1896858E+01
CONTOUR #	8	0.2167837E+01
CONTOUR #	9	0.2438816E+01

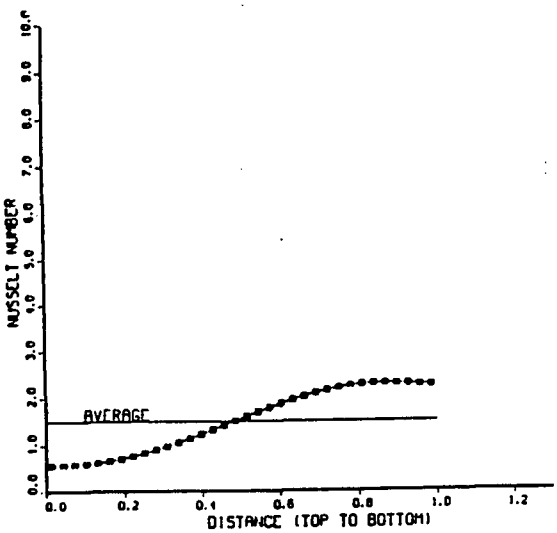

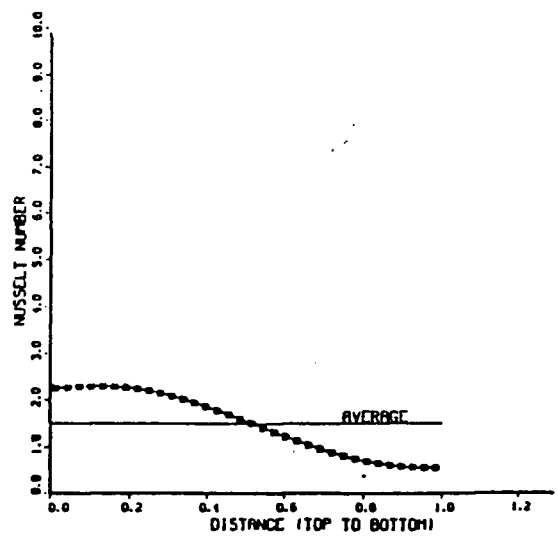

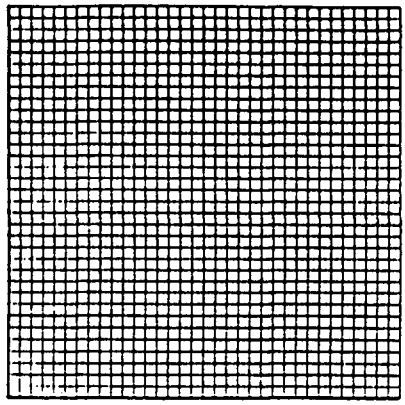

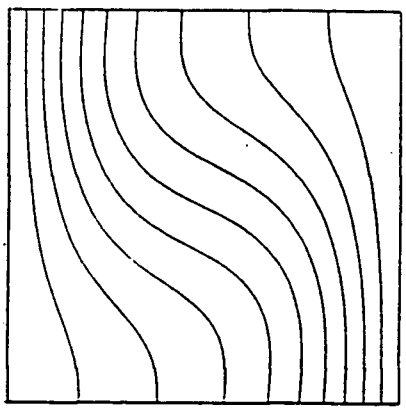

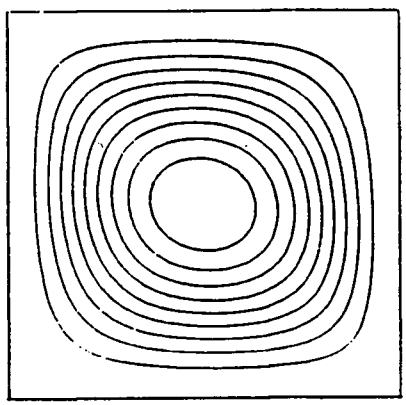

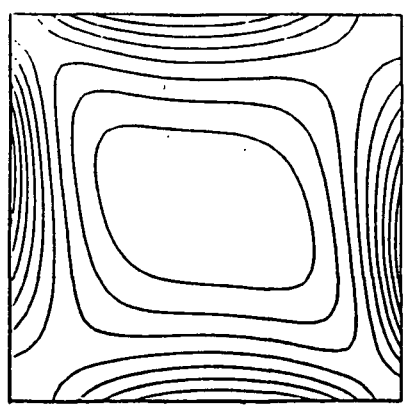

PR= 1.0
RA= 10000.0
DIMENSIONLESS AMPLITUDE= 0.0
AVERAGE NUSSELT NUMBER (RIGHT WALL)= 0.2255568E+01
AVERAGE NUSSELT NUMBER (LEFT WALL)= 0.2255677E+01
LENGTH OF THE WALL(RIGHT)= 0.1000000E+01
LENGTH OF THE WALL(LEFT)= 0.1000000E+01

VORTICITY COUNTOUR VALUES.
MIN= -0.4267256E+03
MAX= 0.1278877E+03

CONTOUR #	1	-0.3713642E+03
CONTOUR #	2	-0.3158030E+03
CONTOUR #	3	-0.2603416E+03
CONTOUR #	4	-0.2048804E+03
CONTOUR #	5	-0.1494192E+03
CONTOUR #	6	-0.9395776E+02
CONTOUR #	7	-0.3849658E+02
CONTOUR #	8	0.1696460E+02
CONTOUR #	9	0.7242578E+02

STREAM FUNCTION CONTOUR VALUES.
MIN= 0.0
MAX= 0.5112517E+01

CONTOUR #	1	0.5112517E+00
CONTOUR #	2	0.1022503E+01
CONTOUR #	3	0.1533754E+01
CONTOUR #	4	0.2045006E+01
CONTOUR #	5	0.2556257E+01
CONTOUR #	6	0.3067509E+01
CONTOUR #	7	0.3578761E+01
CONTOUR #	8	0.4090013E+01
CONTOUR #	9	0.4601265E+01

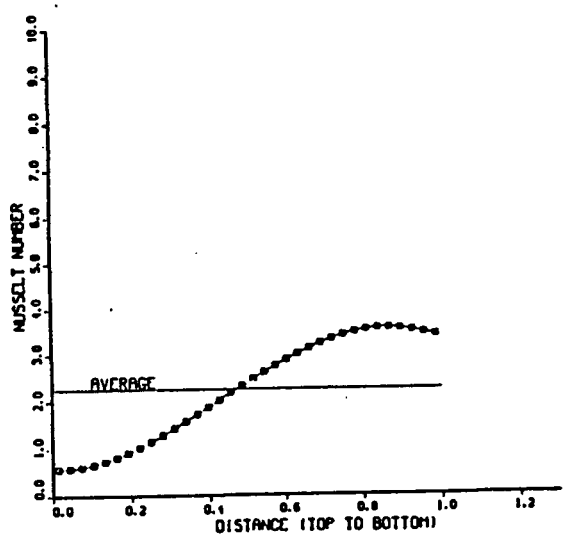

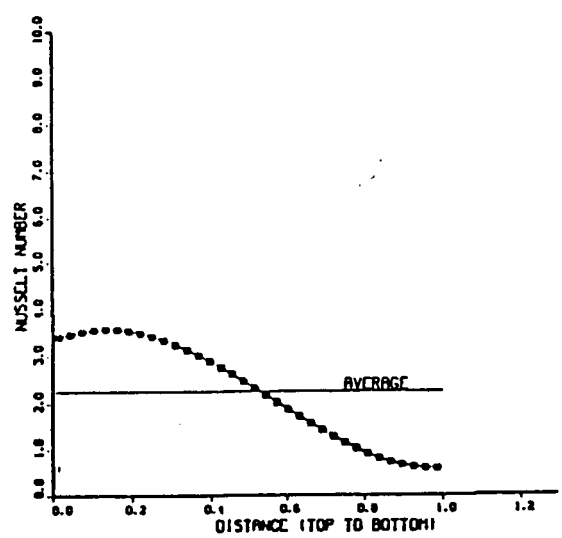

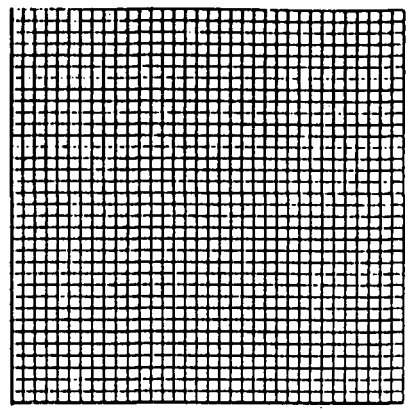

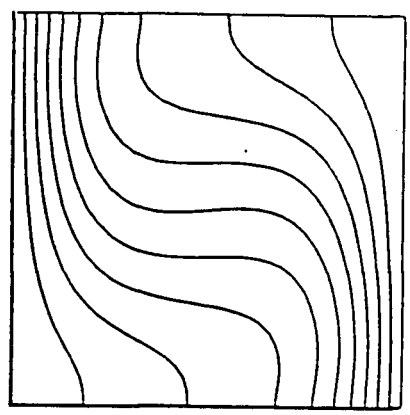

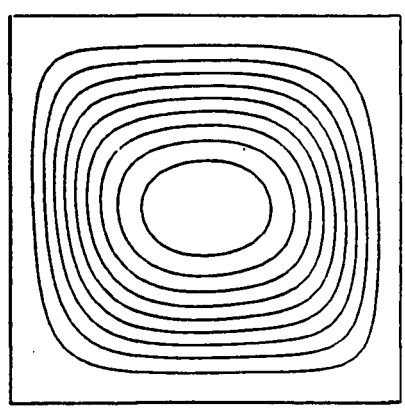

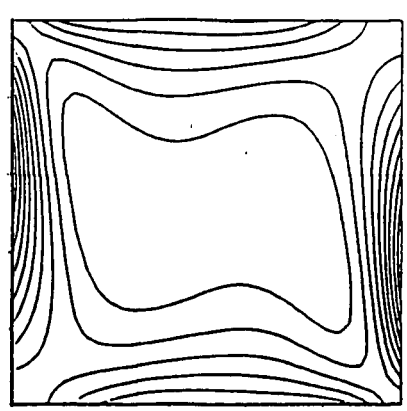

PR= 1.0
RA= 30000.0
DIMENSIONLESS AMPLITUDE= 0.0
AVERAGE NUSSELT NUMBER (RIGHT WALL)= 0.3178228E+01
AVERAGE NUSSELT NUMBER (LEFT WALL)= 0.3178228E+01
LENGTH OF THE WALL(RIGHT)= 0.1000000E+01
LENGTH OF THE WALL(LEFT)= 0.1000000E+01

VORTICITY COUNTOUR VALUES.
MIN= -0.1042258E+04
MAX= 0.2597678E+03

CONTOUR #	1	-0.9120558E+03
CONTOUR #	2	-0.7818533E+03
CONTOUR #	3	-0.6516506E+03
CONTOUR #	4	-0.5214480E+03
CONTOUR #	5	-0.3912454E+03
CONTOUR #	6	-0.2610430E+03
CONTOUR #	7	-0.1308403E+03
CONTOUR #	8	-0.6374512E+00
CONTOUR #	9	0.1286647E+03

STREAM FUNCTION CONTOUR VALUES.
MIN= 0.0
MAX= 0.7335073E+01

CONTOUR #	1	0.7335073E+00
CONTOUR #	2	0.1467014E+01
CONTOUR #	3	0.2200521E+01
CONTOUR #	4	0.2934028E+01
CONTOUR #	5	0.3667535E+01
CONTOUR #	6	0.4401043E+01
CONTOUR #	7	0.5134550E+01
CONTOUR #	8	0.5868058E+01
CONTOUR #	9	0.6601565E+01

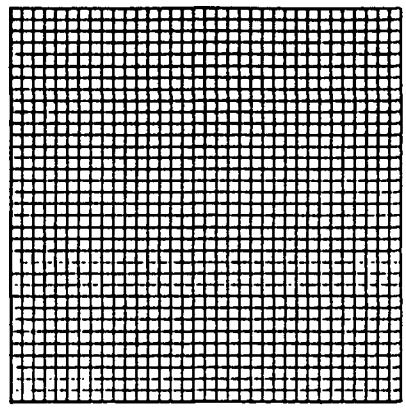

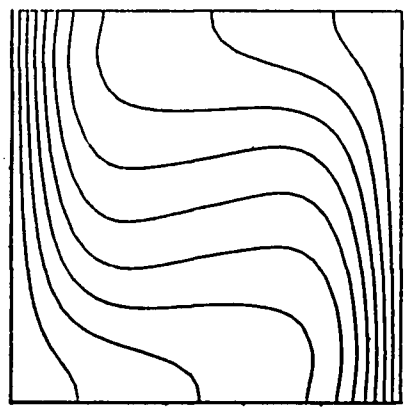

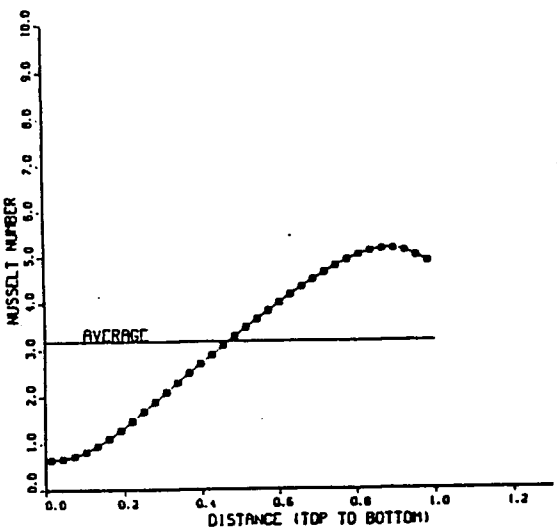

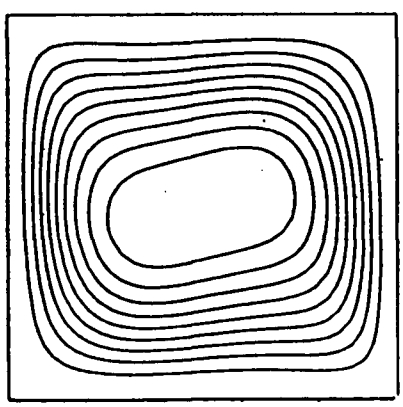

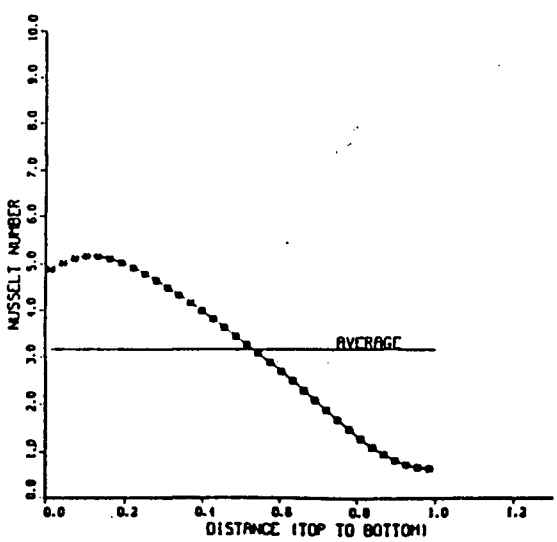

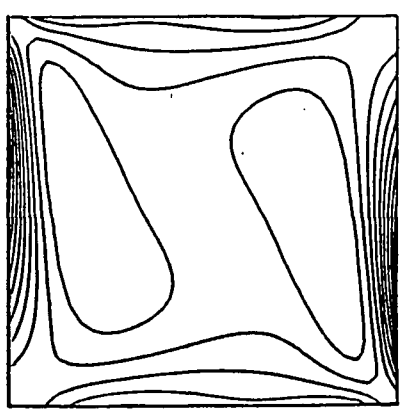

```
PR= 1.0
RA= 100000.0
DIMENSIONLESS AMPLITUDE= 0.0
AVERAGE NUSSELT NUMBER (RIGHT WALL)=   0.4582916E+01
AVERAGE NUSSELT NUMBER (LEFT WALL)=    0.4582480E+01
LENGTH OF THE WALL(RIGHT)=    0.1000000E+01
LENGTH OF THE WALL(LEFT)=     0.1000000E+01

VORTICITY COUNTOUR VALUES.
MIN=  -0.3694243E+04
MAX=   0.6211931E+03
CONTOUR #    1        -0.2362700E+04
CONTOUR #    2        -0.2031186E+04
CONTOUR #    3        -0.1699612E+04
CONTOUR #    4        -0.1368069E+04
CONTOUR #    5        -0.1036525E+04
CONTOUR #    6        -0.7049614E+03
CONTOUR #    7        -0.3734382E+03
CONTOUR #    8        -0.4189453E+02
CONTOUR #    9         0.2896494E+03

STREAM FUNCTION CONTOUR VALUES.
MIN=   0.0
MAX=   0.1014151E+02
CONTOUR #    1         0.1014151E+01
CONTOUR #    2         0.2028301E+01
CONTOUR #    3         0.3042453E+01
CONTOUR #    4         0.4056603E+01
CONTOUR #    5         0.5070755E+01
CONTOUR #    6         0.6084906E+01
CONTOUR #    7         0.7099056E+01
CONTOUR #    8         0.8113208E+01
CONTOUR #    9         0.9127358E+01
```

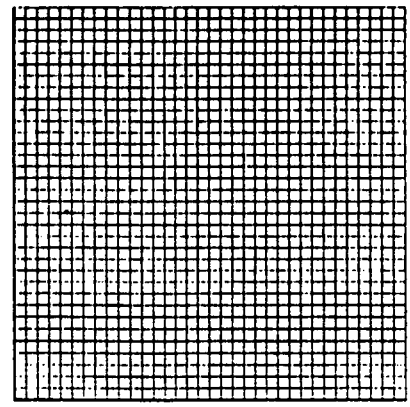

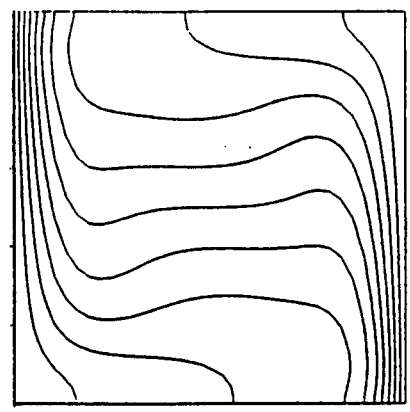

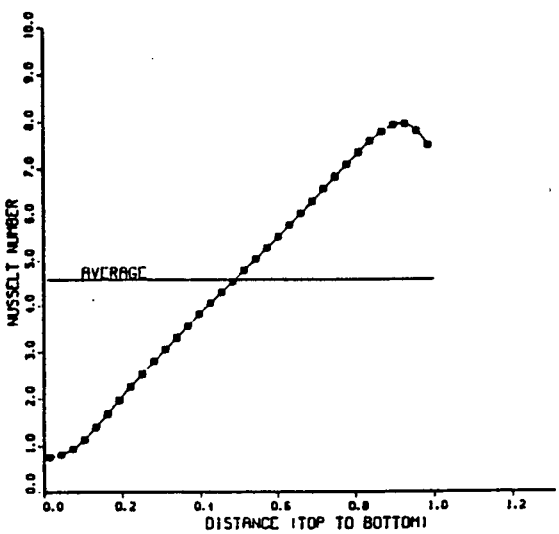

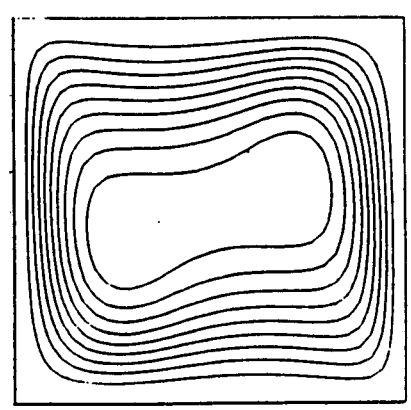

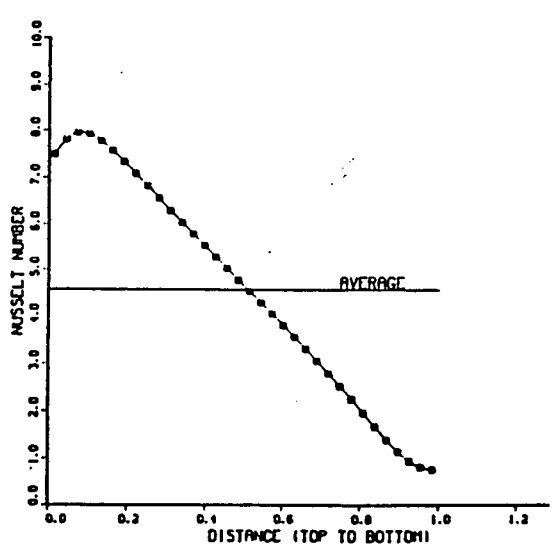

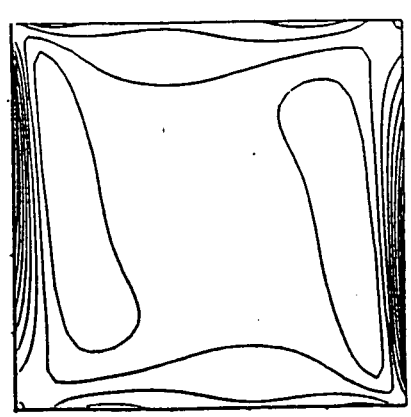

PR= 1.0
RA= 0.0
DIMENSIONLESS AMPLITUDE= 0.075
AVERAGE NUSSELT NUMBER (RIGHT WALL)= 0.8288885E+00
AVERAGE NUSSELT NUMBER (LEFT WALL)= 0.8368884E+00
LENGTH OF THE WALL(RIGHT)= 0.1013733E+01
LENGTH OF THE WALL(LEFT)= 0.1000000E+01

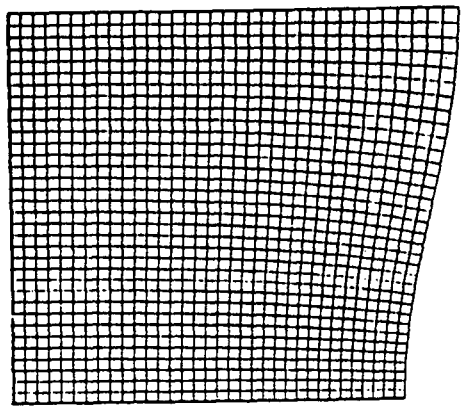

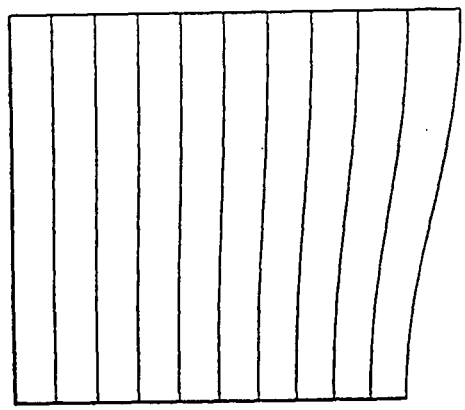

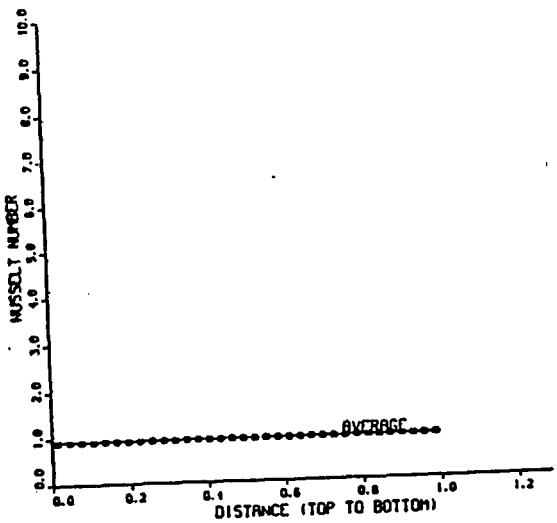

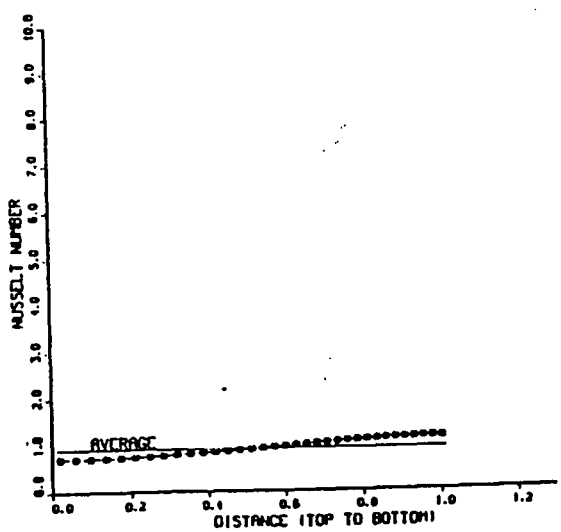

PR= 1.0
RA= 1000.0
DIMENSIONLESS AMPLITUDE= 0.075
AVERAGE NUSSELT NUMBER (RIGHT WALL)= 0.1052864E+01
AVERAGE NUSSELT NUMBER (LEFT WALL)= 0.1066817E+01
LENGTH OF THE WALL(RIGHT)= 0.1013732E+01
LENGTH OF THE WALL(LEFT)= 0.1000000E+01

VORTICITY COUNTOUR VALUES.
MIN= -0.8269403E+02
MAX= 0.3165074E+02

CONTOUR #	1	-0.4425955E+02
CONTOUR #	2	-0.3582509E+02
CONTOUR #	3	-0.2738961E+02
CONTOUR #	4	-0.1895615E+02
CONTOUR #	5	-0.1052167E+02
CONTOUR #	6	-0.2087173E+01
CONTOUR #	7	0.6347280E+01
CONTOUR #	8	0.1478177E+02
CONTOUR #	9	0.2321625E+02

STREAM FUNCTION CONTOUR VALUES.
MIN= 0.0
MAX= 0.1236493E+01

CONTOUR #	1	0.1236493E+00
CONTOUR #	2	0.2472986E+00
CONTOUR #	3	0.3709478E+00
CONTOUR #	4	0.4945972E+00
CONTOUR #	5	0.6182466E+00
CONTOUR #	6	0.7418958E+00
CONTOUR #	7	0.8655452E+00
CONTOUR #	8	0.9891945E+00
CONTOUR #	9	0.1112844E+01

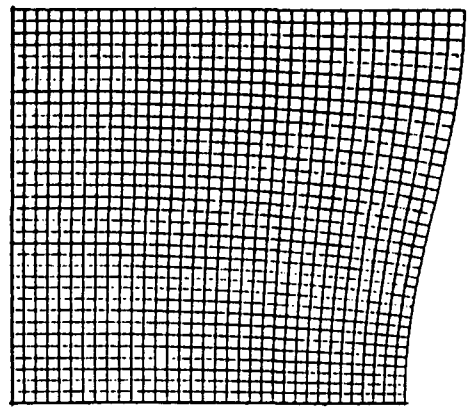

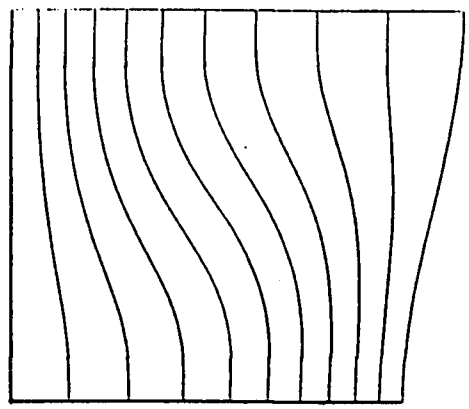

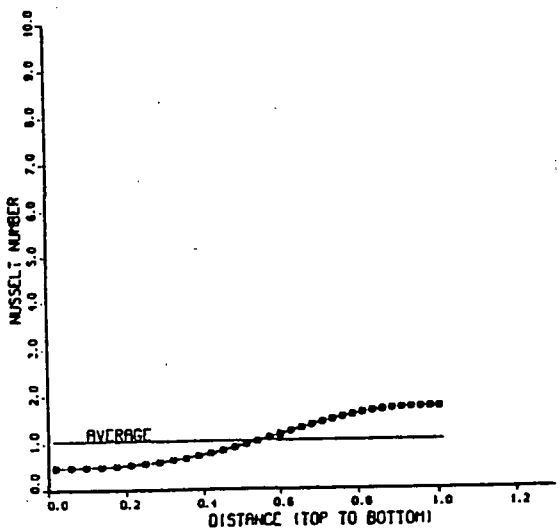

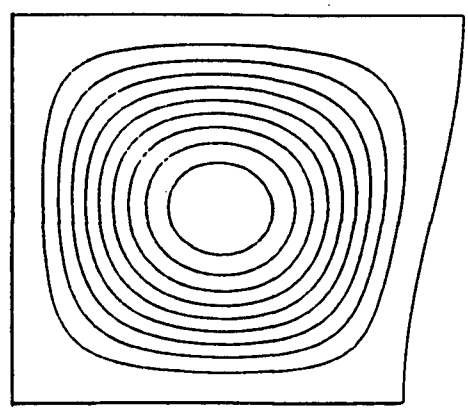

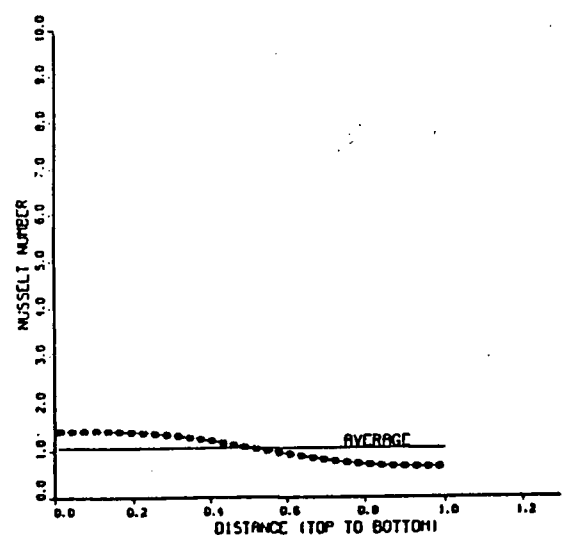

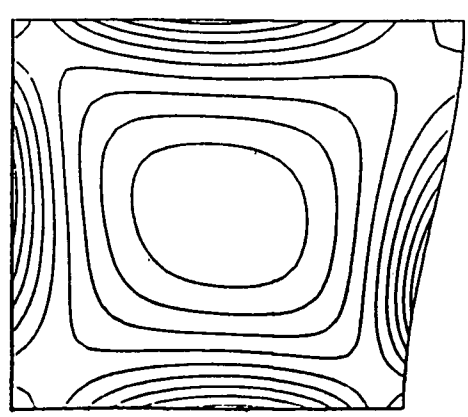

PR= 1.0
RA= 3000.0
DIMENSIONLESS AMPLITUDE= 0.075
AVERAGE NUSSELT NUMBER (RIGHT WALL)= 0.1447768E+01
AVERAGE NUSSELT NUMBER (LEFT WALL)= 0.1467836E+01
LENGTH OF THE WALL(RIGHT)= 0.1013732E+01
LENGTH OF THE WALL(LEFT)= 0.1000000E+01

VORTICITY COUNTOUR VALUES.
MIN= -0.1534630E+03
MAX= 0.6552072E+02

CONTOUR #	1	-0.1318646E+03
CONTOUR #	2	-0.1096662E+03
CONTOUR #	3	-0.8776787E+02
CONTOUR #	4	-0.6586951E+02
CONTOUR #	5	-0.4397113E+02
CONTOUR #	6	-0.2207277E+02
CONTOUR #	7	-0.1744080E+00
CONTOUR #	8	0.2172388E+02
CONTOUR #	9	0.4362234E+02

STREAM FUNCTION CONTOUR VALUES.
MIN= 0.0
MAX= 0.2811059E+01

CONTOUR #	1	0.2811059E+00
CONTOUR #	2	0.5622118E+00
CONTOUR #	3	0.8433177E+00
CONTOUR #	4	0.1124423E+01
CONTOUR #	5	0.1405529E+01
CONTOUR #	6	0.1686634E+01
CONTOUR #	7	0.1967739E+01
CONTOUR #	8	0.2248846E+01
CONTOUR #	9	0.2529953E+01

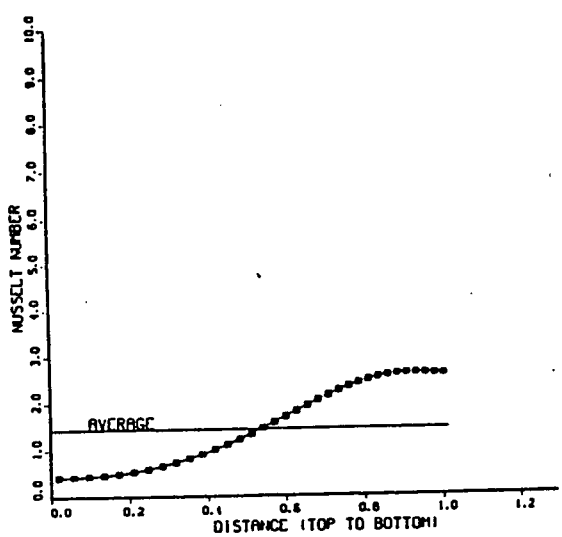

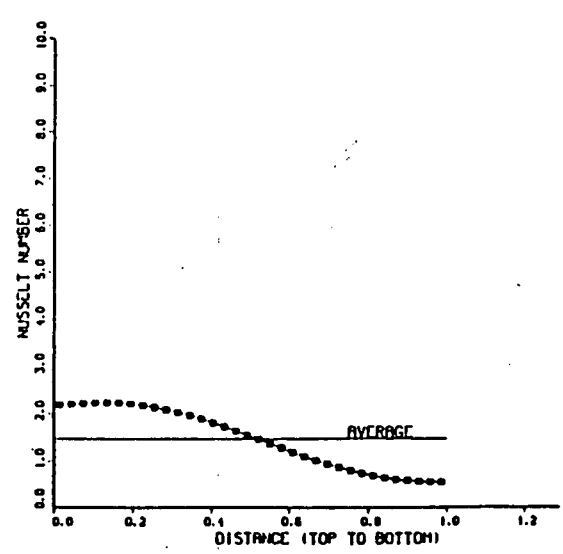

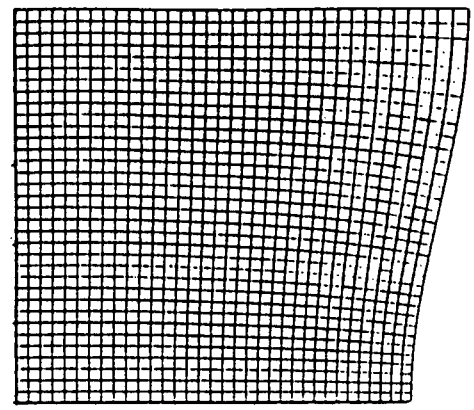

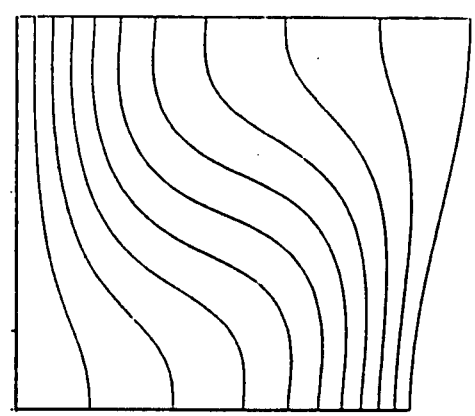

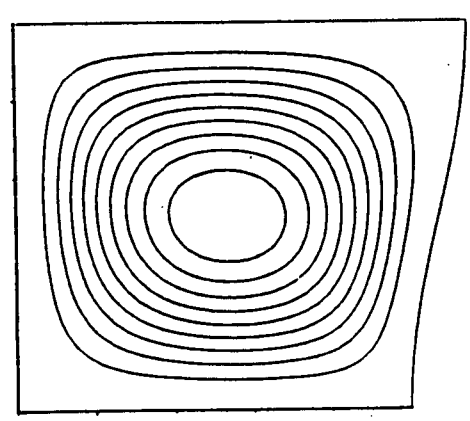

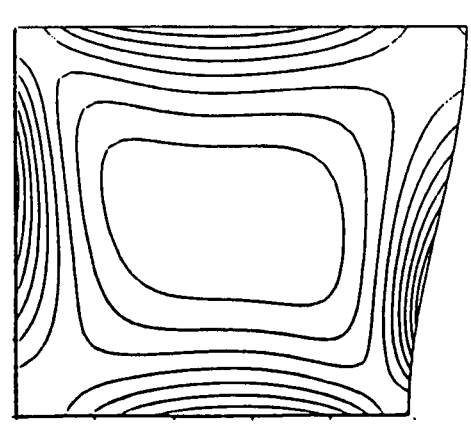

PR= 1.0
RA= 10000.0
DIMENSIONLESS AMPLITUDE= 0.075
AVERAGE NUSSELT NUMBER (RIGHT WALL)= 0.2190764E+01
AVERAGE NUSSELT NUMBER (LEFT WALL)= 0.2231014E+01
LENGTH OF THE WALL(RIGHT)= 0.1013732E+01
LENGTH OF THE WALL(LEFT)= 0.1000000E+01

VORTICITY COUNTOUR VALUES.
MIN= -0.4412958E+03
MAX= 0.1268161E+03

CONTOUR #	1	-0.3844846E+03
CONTOUR #	2	-0.3276733E+03
CONTOUR #	3	-0.2708623E+03
CONTOUR #	4	-0.2140512E+03
CONTOUR #	5	-0.1572400E+03
CONTOUR #	6	-0.1004290E+03
CONTOUR #	7	-0.4361768E+02
CONTOUR #	8	0.1319336E+02
CONTOUR #	9	0.7000439E+02

STREAM FUNCTION CONTOUR VALUES.
MIN= 0.0
MAX= 0.5170072E+01

CONTOUR #	1	0.5170071E+00
CONTOUR #	2	0.1034014E+01
CONTOUR #	3	0.1551021E+01
CONTOUR #	4	0.2068027E+01
CONTOUR #	5	0.2585035E+01
CONTOUR #	6	0.3102041E+01
CONTOUR #	7	0.3619048E+01
CONTOUR #	8	0.4136056E+01
CONTOUR #	9	0.4653064E+01

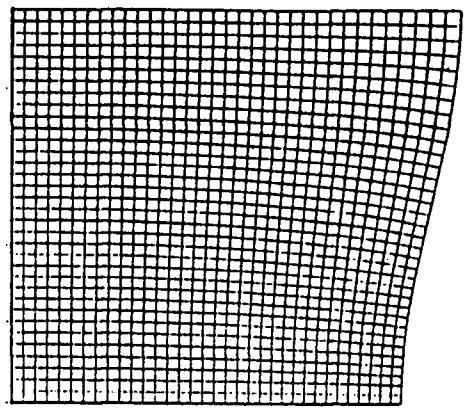

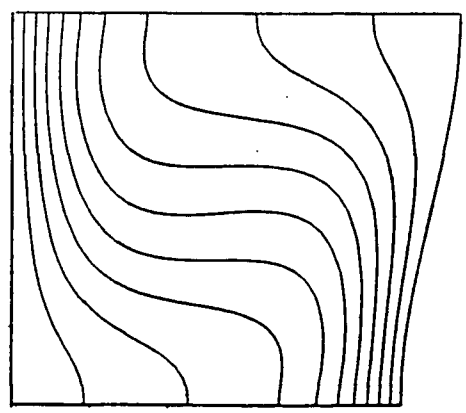

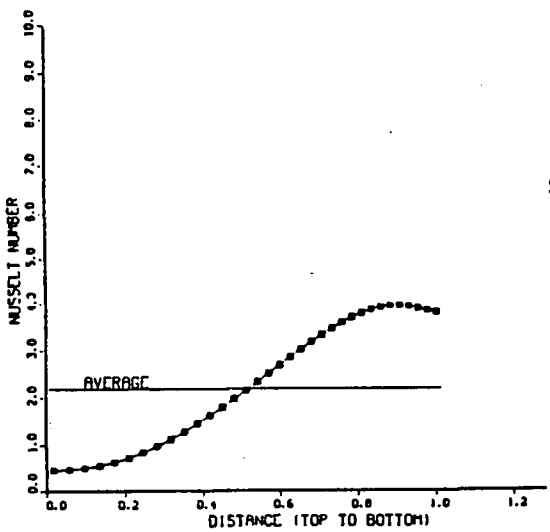

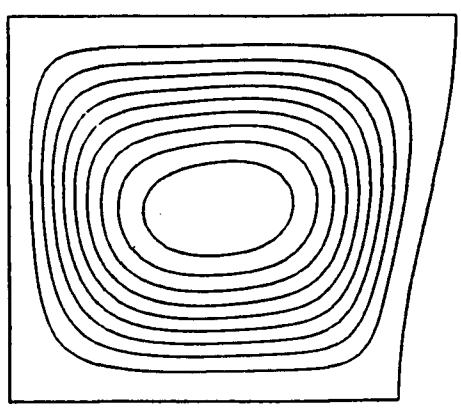

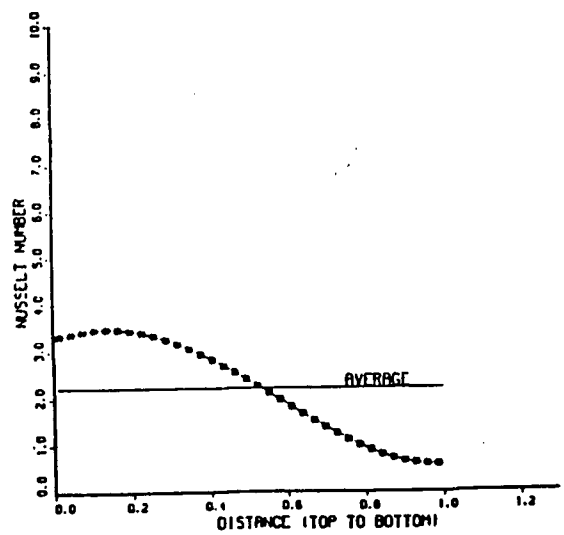

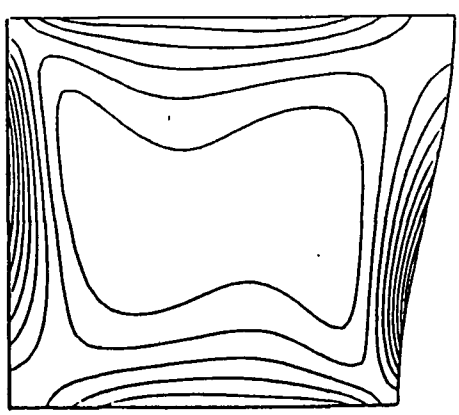

PR= 1.0
RA= 30000.0
DIMENSIONLESS AMPLITUDE= 0.075
AVERAGE NUSSELT NUMBER (RIGHT WALL)= 0.3113428E+01
AVERAGE NUSSELT NUMBER (LEFT WALL)= 0.3155944E+01
LENGTH OF THE WALL(RIGHT)= 0.1013732E+01
LENGTH OF THE WALL(LEFT)= 0.1000000E+01

VORTICITY COUNTOUR VALUES.
MIN= -0.1067888E+04
MAX= 0.2634832E+03

CONTOUR #	1	-0.8344897E+03
CONTOUR #	2	-0.8013818E+03
CONTOUR #	3	-0.6662737E+03
CONTOUR #	4	-0.5351655E+03
CONTOUR #	5	-0.4020578E+03
CONTOUR #	6	-0.2689495E+03
CONTOUR #	7	-0.1358413E+03
CONTOUR #	8	-0.2733184E+01
CONTOUR #	9	0.1303748E+03

STREAM FUNCTION CONTOUR VALUES.
MIN= 0.0
MAX= 0.7327776E+01

CONTOUR #	1	0.7327776E+00
CONTOUR #	2	0.1465555E+01
CONTOUR #	3	0.2198332E+01
CONTOUR #	4	0.2931109E+01
CONTOUR #	5	0.3663887E+01
CONTOUR #	6	0.4396664E+01
CONTOUR #	7	0.5129441E+01
CONTOUR #	8	0.5862221E+01
CONTOUR #	9	0.6594997E+01

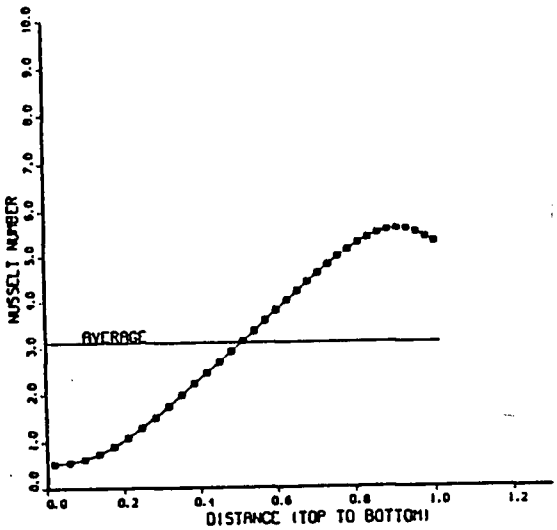

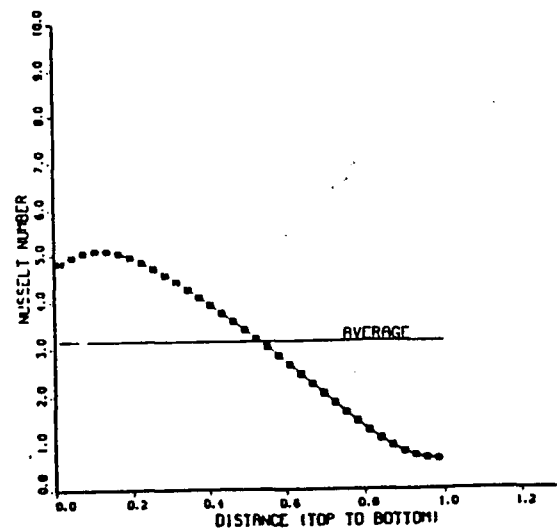

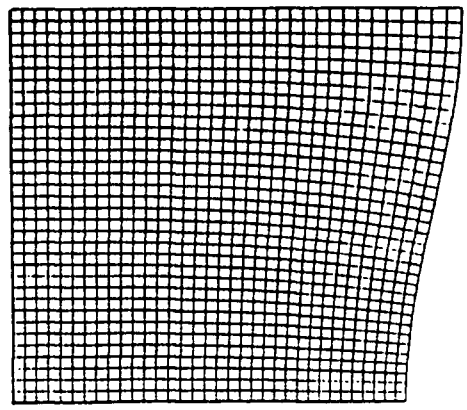

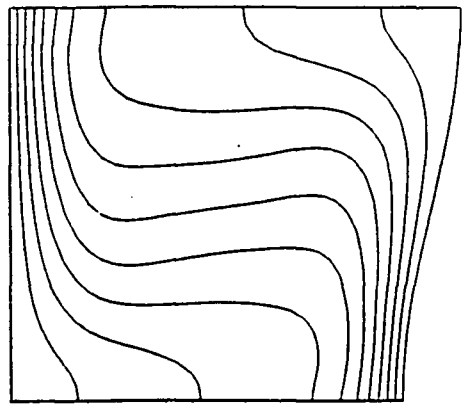

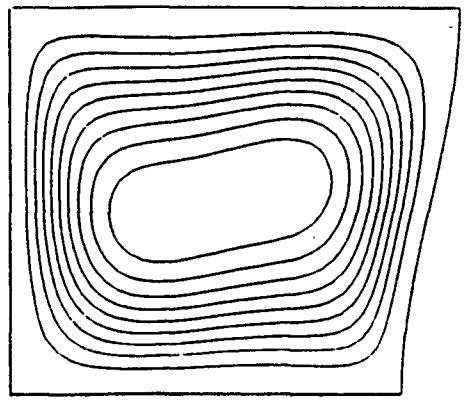

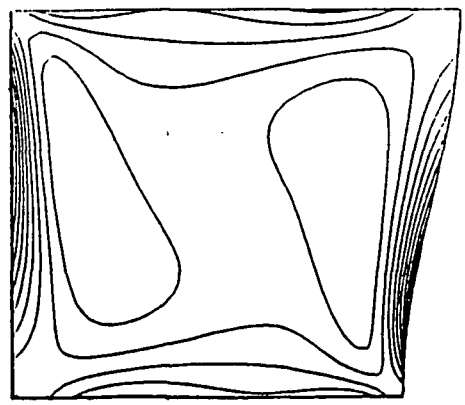

PR= 1.0
RA= 0.0
DIMENSIONLESS AMPLITUDE= 0.150
AVERAGE NUSSELT NUMBER (RIGHT WALL)= 0.8611182E+00
AVERAGE NUSSELT NUMBER (LEFT WALL)= 0.8947178E+00
LENGTH OF THE WALL(RIGHT)= 0.1053476E+01
LENGTH OF THE WALL(LEFT)= 0.1000000E+01

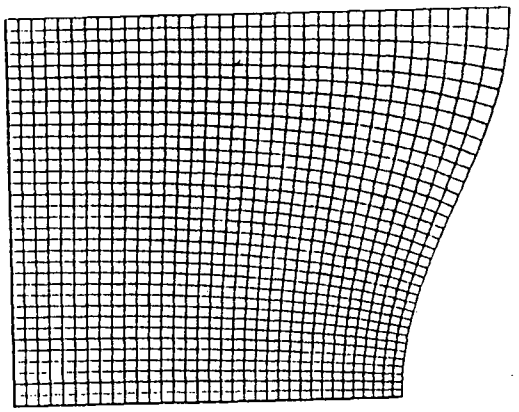

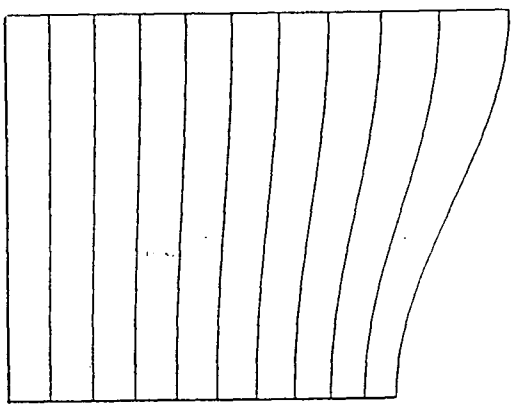

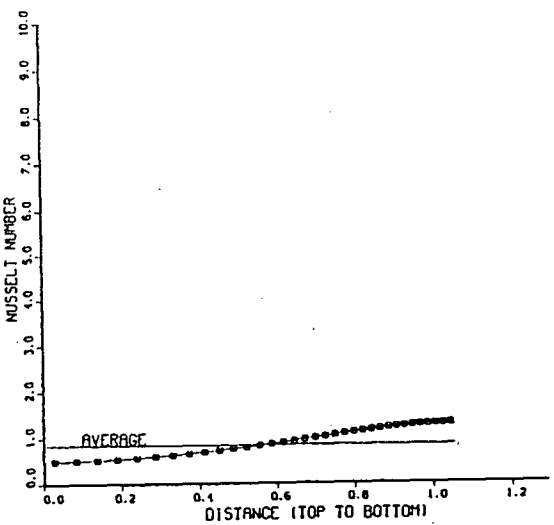

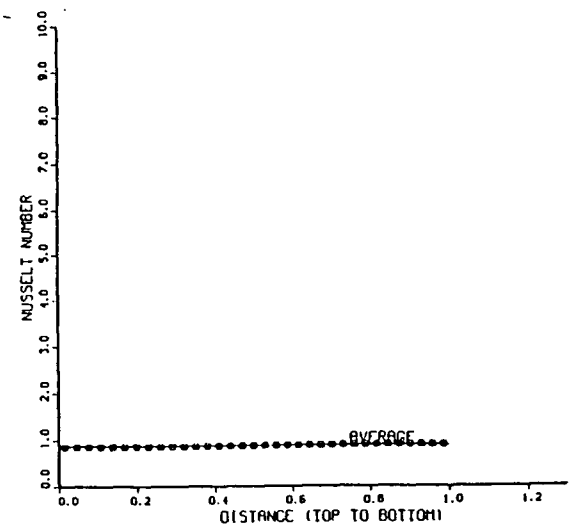

PR= 1.0
RA= 1000.0
DIMENSIONLESS AMPLITUDE= 0.150
AVERAGE NUSSELT NUMBER (RIGHT WALL)= 0.9791071E+00
AVERAGE NUSSELT NUMBER (LEFT WALL)= 0.1031256E+01
LENGTH OF THE WALL(RIGHT)= 0.1053476E+01
LENGTH OF THE WALL(LEFT)= 0.1000000E+01

VORTICITY COUNTOUR VALUES.
MIN= -0.6488451E+02
MAX= 0.3114812E+02

CONTOUR #	1	-0.4628123E+02
CONTOUR #	2	-0.3767798E+02
CONTOUR #	3	-0.2907475E+02
CONTOUR #	4	-0.2047148E+02
CONTOUR #	5	-0.1186821E+02
CONTOUR #	6	-0.3264954E+01
CONTOUR #	7	0.5338318E+01
CONTOUR #	8	0.1394159E+02
CONTOUR #	9	0.2254483E+02

STREAM FUNCTION CONTOUR VALUES.
MIN= 0.0
MAX= 0.1274205E+01

CONTOUR #	1	0.1274205E+00
CONTOUR #	2	0.2548410E+00
CONTOUR #	3	0.3822615E+00
CONTOUR #	4	0.5096821E+00
CONTOUR #	5	0.6371026E+00
CONTOUR #	6	0.7645231E+00
CONTOUR #	7	0.8919436E+00
CONTOUR #	8	0.1019363E+01
CONTOUR #	9	0.1146784E+01

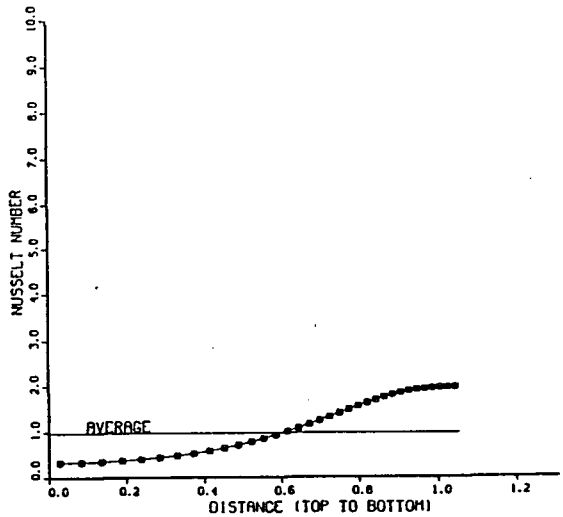

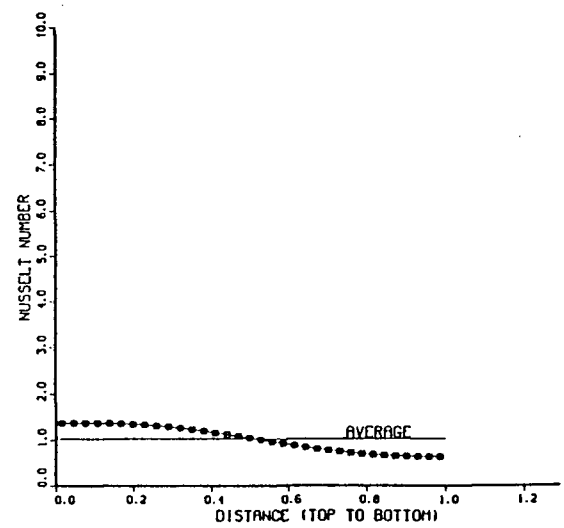

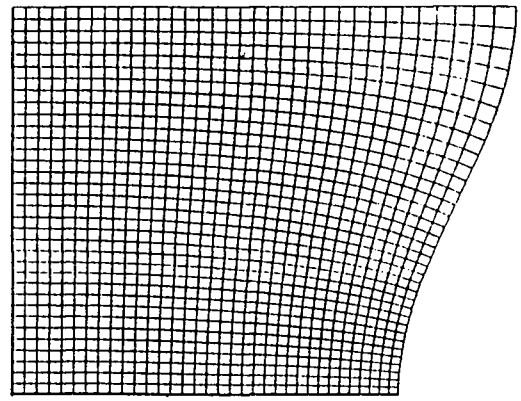

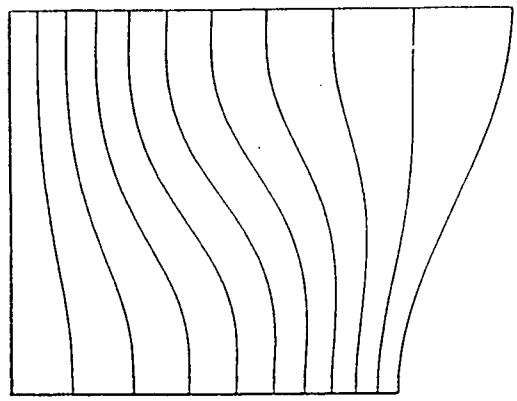

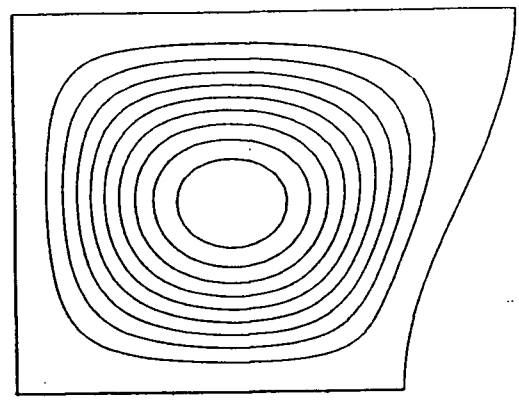

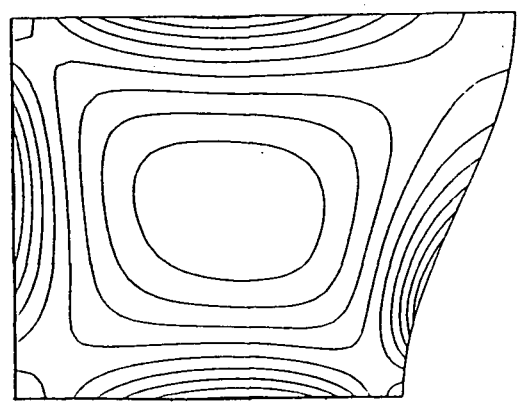

PR= 1.0
RA= 3000.0
DIMENSIONLESS AMPLITUDE= 0.150
AVERAGE NUSSELT NUMBER (RIGHT WALL)= 0.1366085E+01
AVERAGE NUSSELT NUMBER (LEFT WALL)= 0.1439019E+01
LENGTH OF THE WALL(RIGHT)= 0.1053476E+01
LENGTH OF THE WALL(LEFT)= 0.1000000E+01

VORTICITY COUNTOUR VALUES.
MIN= -0.1595408E+03
MAX= 0.6383082E+02

CONTOUR #	1	-0.1371837E+03
CONTOUR #	2	-0.1148466E+03
CONTOUR #	3	-0.9248940E+02
CONTOUR #	4	-0.7015224E+02
CONTOUR #	5	-0.4780507E+02
CONTOUR #	6	-0.2545789E+02
CONTOUR #	7	-0.3110718E+01
CONTOUR #	8	0.1823645E+02
CONTOUR #	9	0.4158362E+02

STREAM FUNCTION CONTOUR VALUES.
MIN= 0.0
MAX= 0.2869203E+01

CONTOUR #	1	0.2869202E+00
CONTOUR #	2	0.5738405E+00
CONTOUR #	3	0.8607607E+00
CONTOUR #	4	0.1147680E+01
CONTOUR #	5	0.1434601E+01
CONTOUR #	6	0.1721520E+01
CONTOUR #	7	0.2008441E+01
CONTOUR #	8	0.2295361E+01
CONTOUR #	9	0.2582281E+01

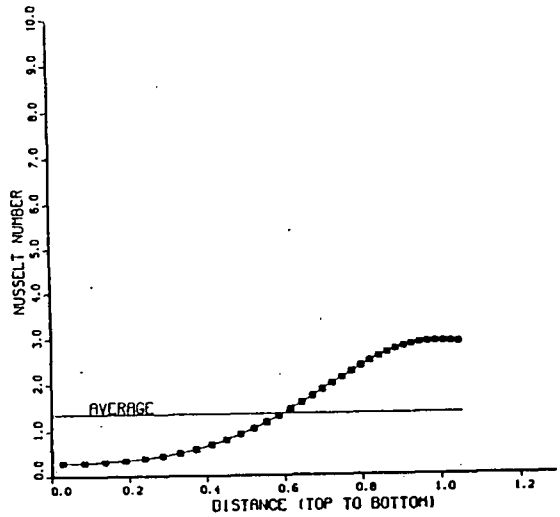

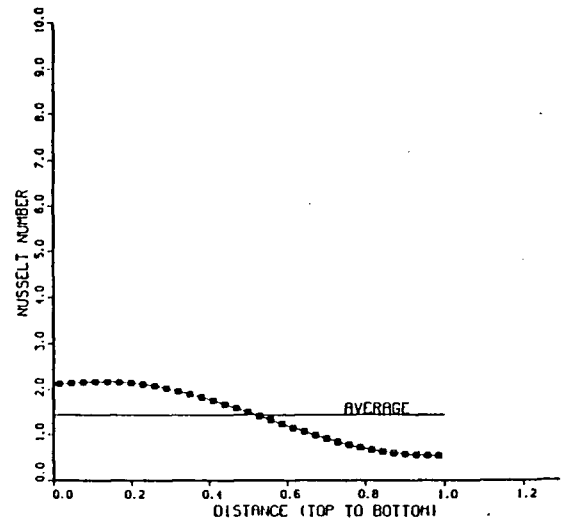

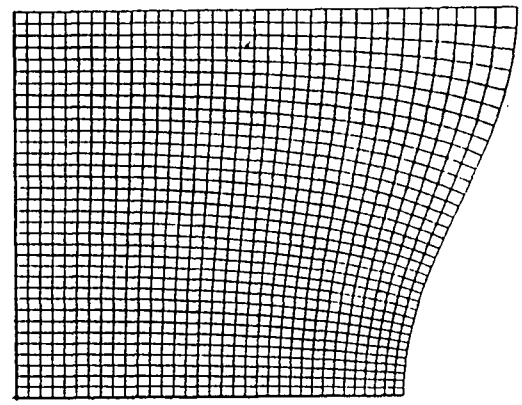

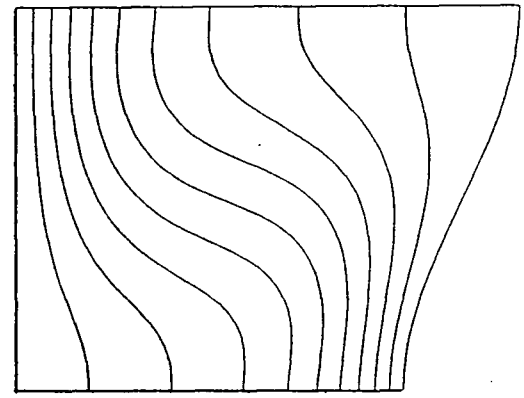

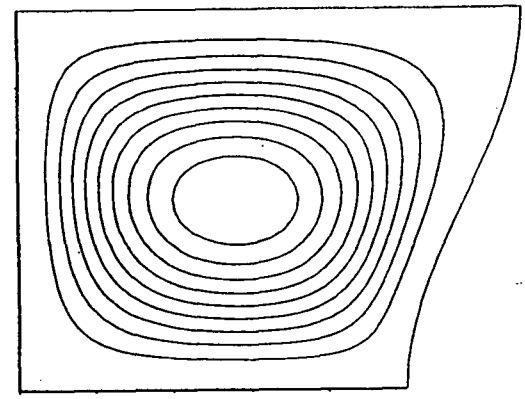

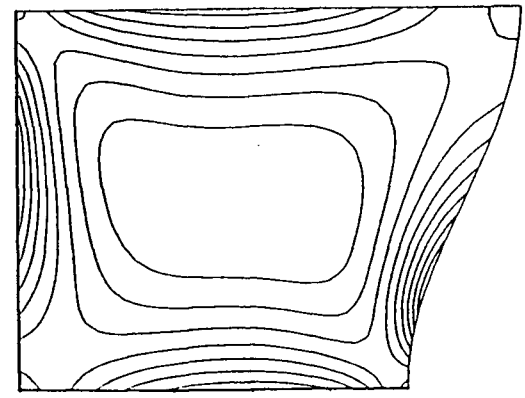

PR= 1.0
RA= 10000.0
DIMENSIONLESS AMPLITUDE= 0.150
AVERAGE NUSSELT NUMBER (RIGHT WALL)= 0.2085385E+01
AVERAGE NUSSELT NUMBER (LEFT WALL)= 0.2187152E+01
LENGTH OF THE WALL(RIGHT)= 0.1053476E+01
LENGTH OF THE WALL(LEFT)= 0.1000000E+01

VORTICITY COUNTOUR VALUES.
MIN= -0.4531328E+03
MAX= 0.1267906E+03

CONTOUR #	1	-0.3951404E+03
CONTOUR #	2	-0.3371479E+03
CONTOUR #	3	-0.2791558E+03
CONTOUR #	4	-0.2211635E+03
CONTOUR #	5	-0.1631711E+03
CONTOUR #	6	-0.1051790E+03
CONTOUR #	7	-0.4718652E+02
CONTOUR #	8	0.1080566E+02
CONTOUR #	9	0.6879785E+02

STREAM FUNCTION CONTOUR VALUES.
MIN= 0.0
MAX= 0.5196774E+01

CONTOUR #	1	0.5196773E+00
CONTOUR #	2	0.1039354E+01
CONTOUR #	3	0.1559031E+01
CONTOUR #	4	0.2078709E+01
CONTOUR #	5	0.2598385E+01
CONTOUR #	6	0.3118063E+01
CONTOUR #	7	0.3637741E+01
CONTOUR #	8	0.4157418E+01
CONTOUR #	9	0.4677094E+01

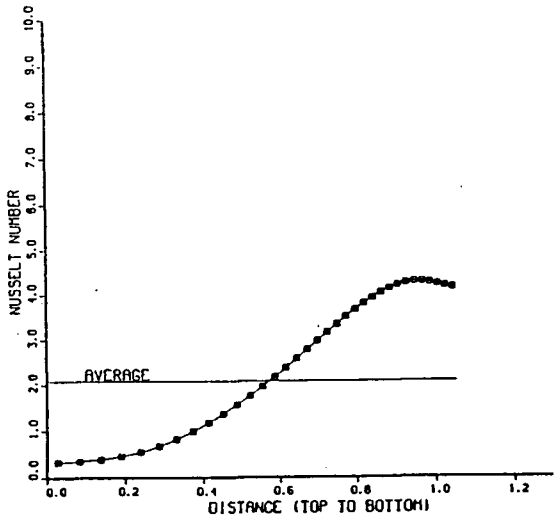

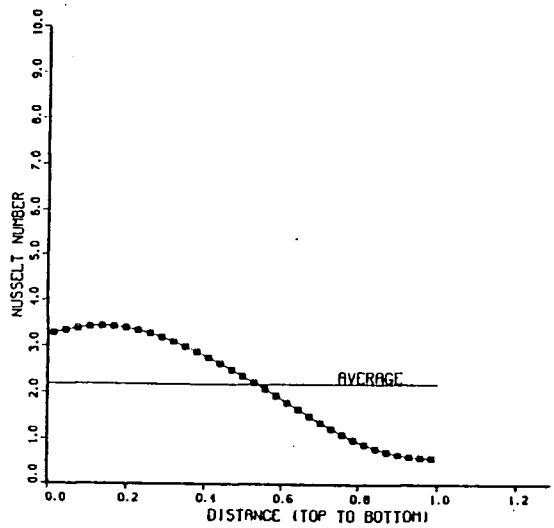

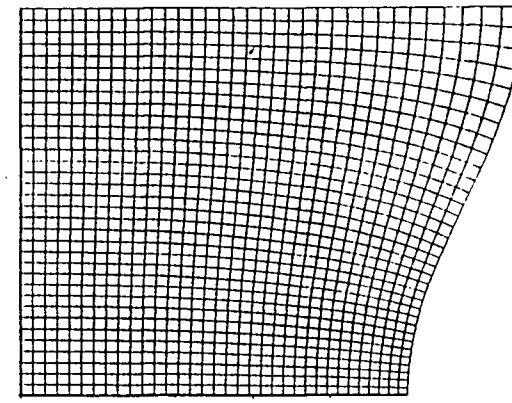

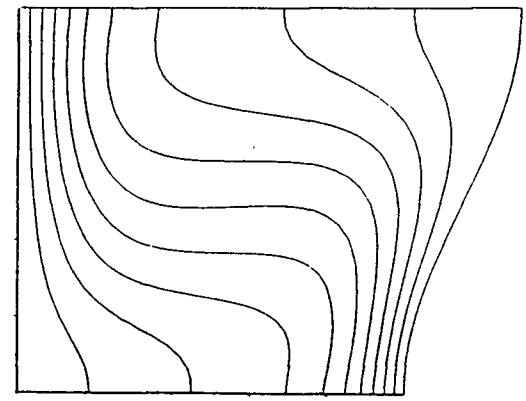

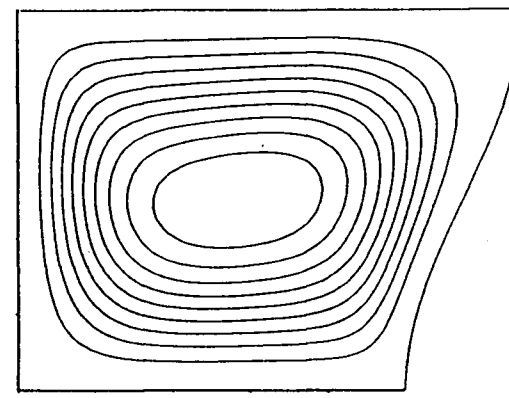

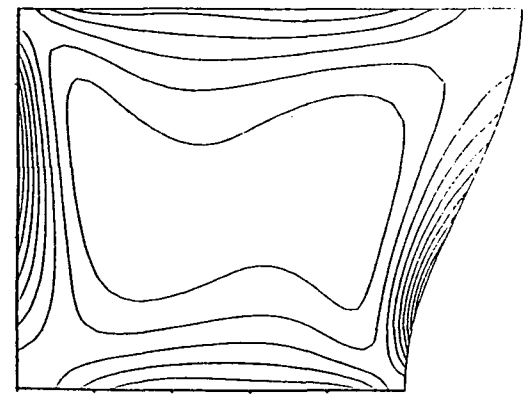

PR= 1.0
RA= 30000.0
DIMENSIONLESS AMPLITUDE= 0.150
AVERAGE NUSSELT NUMBER (RIGHT WALL)= 0.2988174E+01
AVERAGE NUSSELT NUMBER (LEFT WALL)= 0.3147563E+01
LENGTH OF THE WALL(RIGHT)= 0.1053476E+01
LENGTH OF THE WALL(LEFT)= 0.1000000E+01

VORTICITY COUNTOUR VALUES.
MIN= -0.1084109E+04
MAX= 0.2651633E+03

CONTOUR #	1	-0.9491818E+03
CONTOUR #	2	-0.8142546E+03
CONTOUR #	3	-0.6793274E+03
CONTOUR #	4	-0.5444001E+03
CONTOUR #	5	-0.4094734E+03
CONTOUR #	6	-0.2745458E+03
CONTOUR #	7	-0.1396187E+03
CONTOUR #	8	-0.4691162E+01
CONTOUR #	9	0.1302356E+03

STREAM FUNCTION CONTOUR VALUES.
MIN= 0.0
MAX= 0.7370053E+01

CONTOUR #	1	0.7370053E+00
CONTOUR #	2	0.1474010E+01
CONTOUR #	3	0.2211015E+01
CONTOUR #	4	0.2948021E+01
CONTOUR #	5	0.3685026E+01
CONTOUR #	6	0.4422030E+01
CONTOUR #	7	0.5159036E+01
CONTOUR #	8	0.5896042E+01
CONTOUR #	9	0.6633047E+01

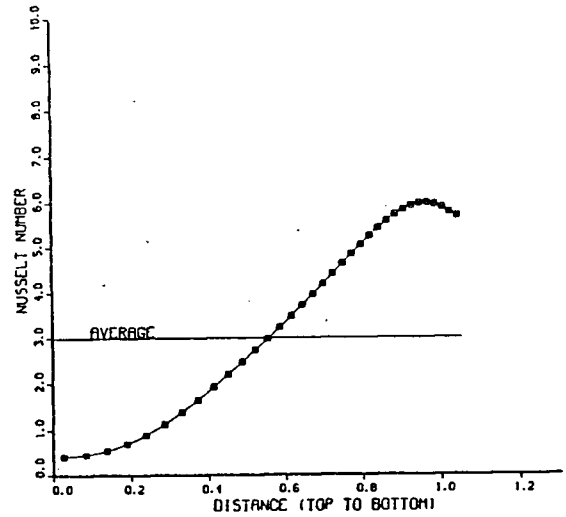

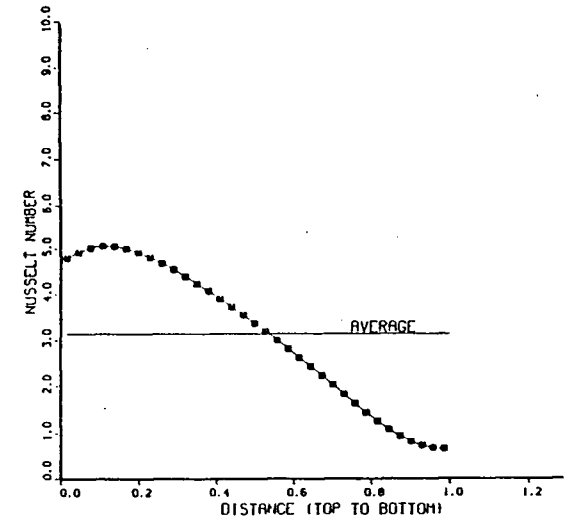

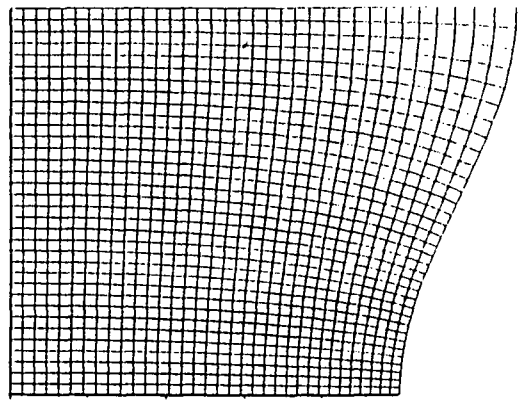

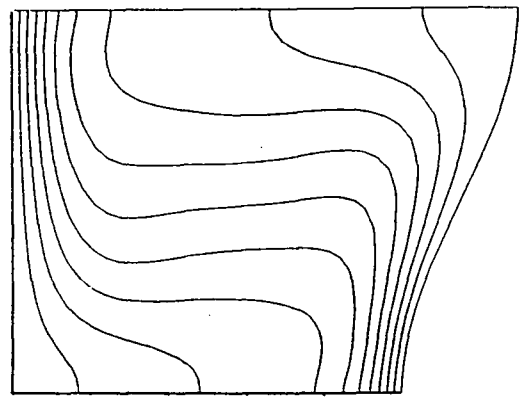

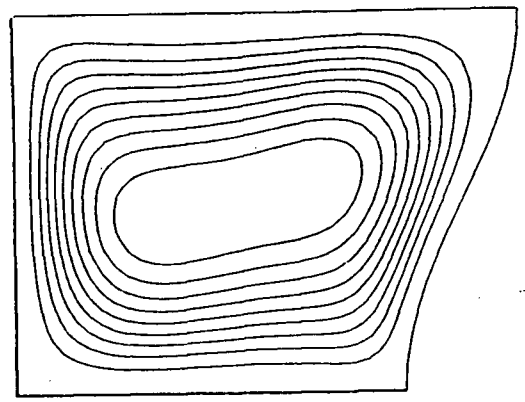

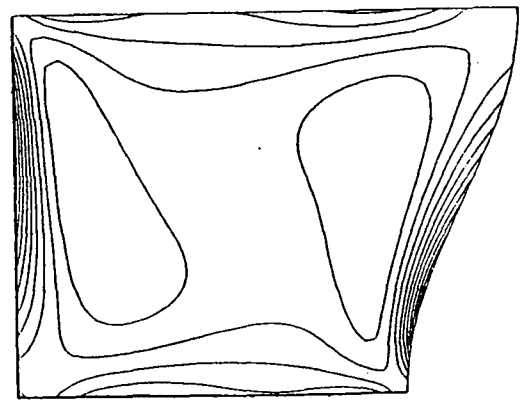

PR= 1.0
RA= 100000.0
DIMENSIONLESS AMPLITUDE= 0.150
AVERAGE NUSSELT NUMBER (RIGHT WALL)= 0.4361712E+01
AVERAGE NUSSELT NUMBER (LEFT WALL)= 0.4594788E+01
LENGTH OF THE WALL(RIGHT)= 0.1053476E+01
LENGTH OF THE WALL(LEFT)= 0.1000000E+01

VORTICITY COUNTOUR VALUES.
MIN= -0.2748340E+04
MAX= 0.6252297E+03

CONTOUR #	1	-0.2411883E+04
CONTOUR #	2	-0.2074427E+04
CONTOUR #	3	-0.1736969E+04
CONTOUR #	4	-0.1399512E+04
CONTOUR #	5	-0.1062055E+04
CONTOUR #	6	-0.7245984E+03
CONTOUR #	7	-0.3871414E+03
CONTOUR #	8	-0.4968433E+02
CONTOUR #	9	0.2877722E+03

STREAM FUNCTION CONTOUR VALUES.
MIN= 0.0
MAX= 0.1050607E+02

CONTOUR #	1	0.1050607E+01
CONTOUR #	2	0.2101213E+01
CONTOUR #	3	0.3151818E+01
CONTOUR #	4	0.4202426E+01
CONTOUR #	5	0.5253033E+01
CONTOUR #	6	0.6303638E+01
CONTOUR #	7	0.7354246E+01
CONTOUR #	8	0.8404854E+01
CONTOUR #	9	0.9455460E+01

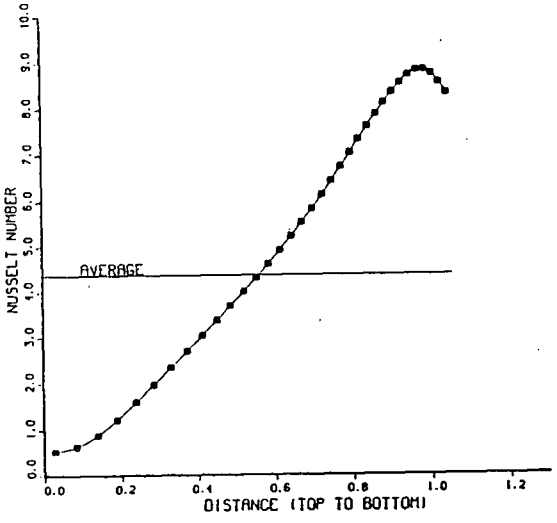

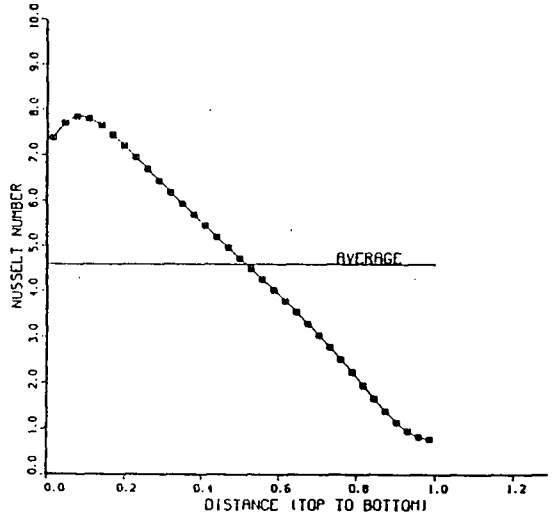

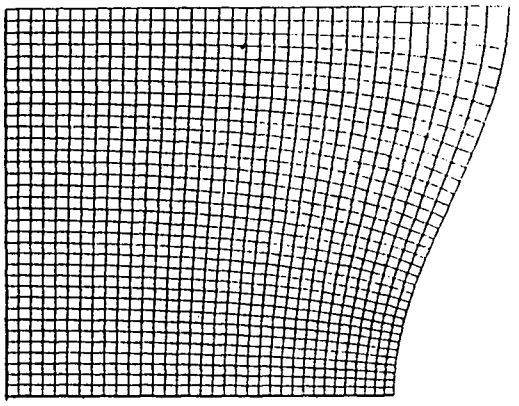

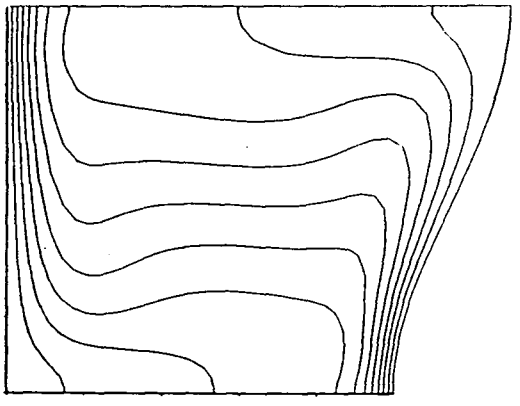

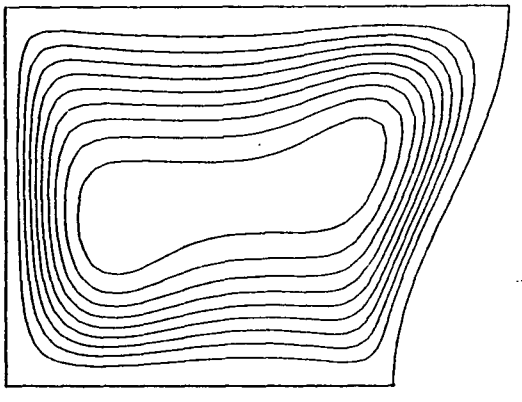

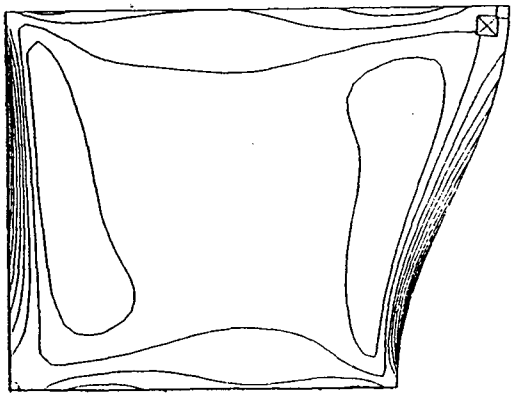

PR= 1.0
RA= 0.0
DIMENSIONLESS AMPLITUDE= -0.150
AVERAGE NUSSELT NUMBER (RIGHT WALL)= 0.1060091E+01
AVERAGE NUSSELT NUMBER (LEFT WALL)= 0.1262015E+01
LENGTH OF THE WALL(RIGHT)= 0.1192486E+01
LENGTH OF THE WALL(LEFT)= 0.9999378E+00

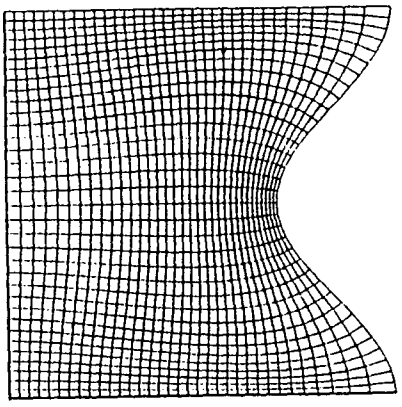

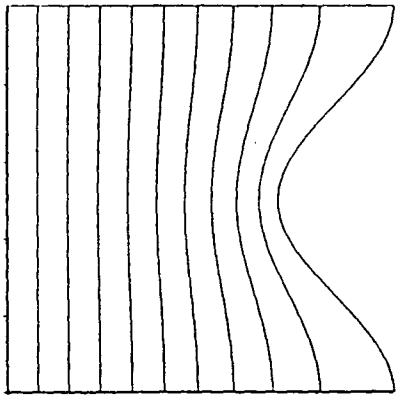

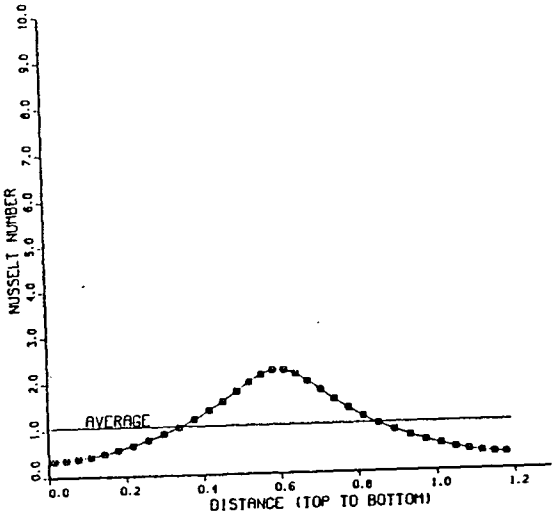

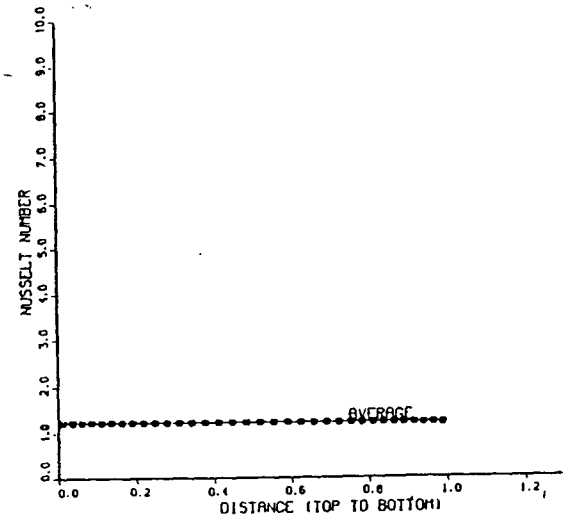

PR= 1.0
RA= 1000.0
DIMENSIONLESS AMPLITUDE= -0.150
AVERAGE NUSSELT NUMBER (RIGHT WALL)= 0.1098053E+01
AVERAGE NUSSELT NUMBER (LEFT WALL)= 0.1310722E+01
LENGTH OF THE WALL(RIGHT)= 0.1192486E+01
LENGTH OF THE WALL(LEFT)= 0.9988378E+00

VORTICITY COUNTOUR VALUES.
MIN= -0.7787270E+02
MAX= 0.2656781E+02

CONTOUR #	1	-0.6722864E+02
CONTOUR #	2	-0.5658459E+02
CONTOUR #	3	-0.4594057E+02
CONTOUR #	4	-0.3529651E+02
CONTOUR #	5	-0.2465247E+02
CONTOUR #	6	-0.1400842E+02
CONTOUR #	7	-0.3364349E+01
CONTOUR #	8	0.7279694E+01
CONTOUR #	9	0.1792374E+02

STREAM FUNCTION CONTOUR VALUES.
MIN= 0.0
MAX= 0.7184311E+00

CONTOUR #	1	0.7184309E-01
CONTOUR #	2	0.1436862E+00
CONTOUR #	3	0.2155292E+00
CONTOUR #	4	0.2873724E+00
CONTOUR #	5	0.3592154E+00
CONTOUR #	6	0.4310586E+00
CONTOUR #	7	0.5029016E+00
CONTOUR #	8	0.5747448E+00
CONTOUR #	9	0.6465878E+00

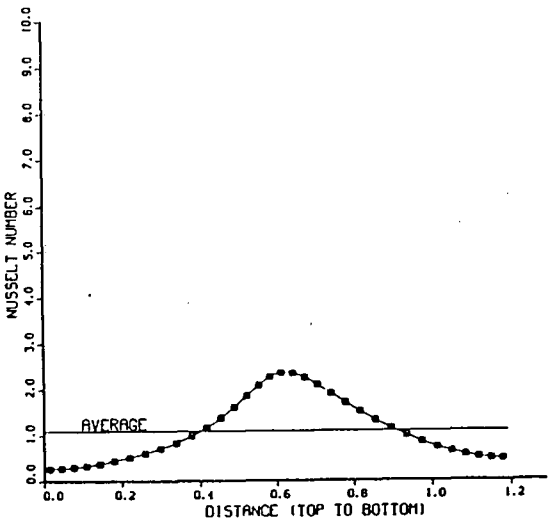

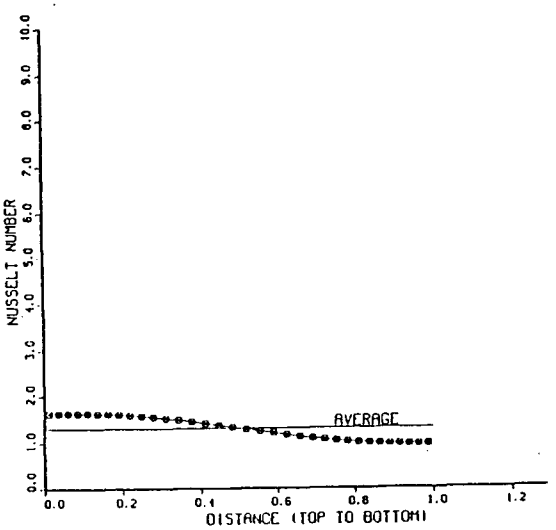

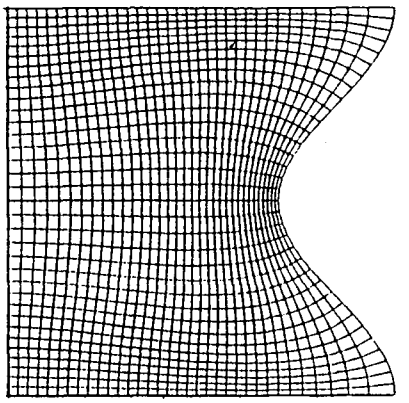

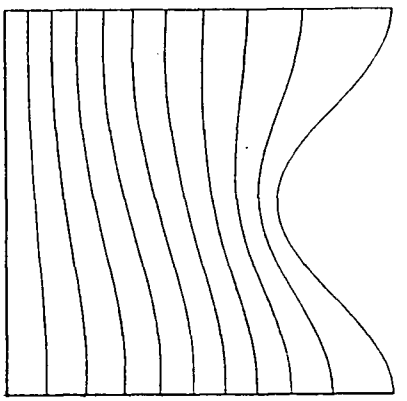

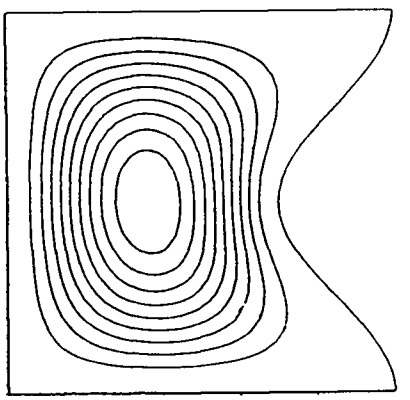

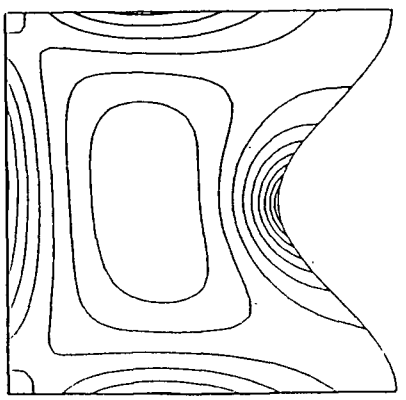

PR= 1.0
RA= 3000.0
DIMENSIONLESS AMPLITUDE= -0.150
AVERAGE NUSSELT NUMBER (RIGHT WALL)= 0.1301820E+01
AVERAGE NUSSELT NUMBER (LEFT WALL)= 0.1552536E+01
LENGTH OF THE WALL(RIGHT)= 0.1192486E+01
LENGTH OF THE WALL(LEFT)= 0.9999378E+00

VORTICITY COUNTOUR VALUES.
MIN= -0.2202487E+03
MAX= 0.7359808E+02

CONTOUR #	1	-0.1908640E+03
CONTOUR #	2	-0.1614793E+03
CONTOUR #	3	-0.1320947E+03
CONTOUR #	4	-0.1027100E+03
CONTOUR #	5	-0.7332532E+02
CONTOUR #	6	-0.4394066E+02
CONTOUR #	7	-0.1455598E+02
CONTOUR #	8	0.1482867E+02
CONTOUR #	9	0.4421326E+02

STREAM FUNCTION CONTOUR VALUES.
MIN= 0.0
MAX= 0.1900163E+01

CONTOUR #	1	0.1900163E+00
CONTOUR #	2	0.3800325E+00
CONTOUR #	3	0.5700488E+00
CONTOUR #	4	0.7600651E+00
CONTOUR #	5	0.9500813E+00
CONTOUR #	6	0.1140098E+01
CONTOUR #	7	0.1330113E+01
CONTOUR #	8	0.1520130E+01
CONTOUR #	9	0.1710145E+01

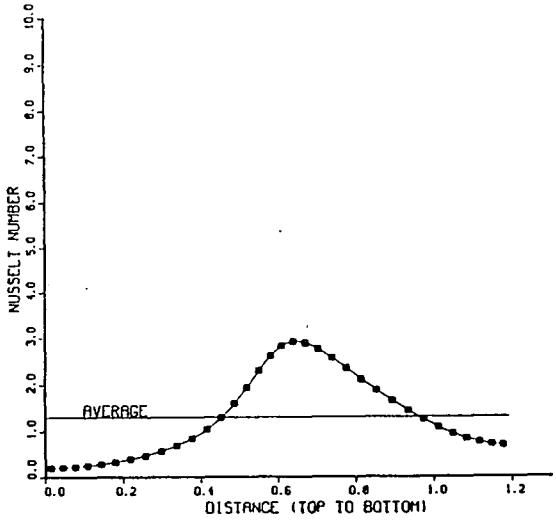

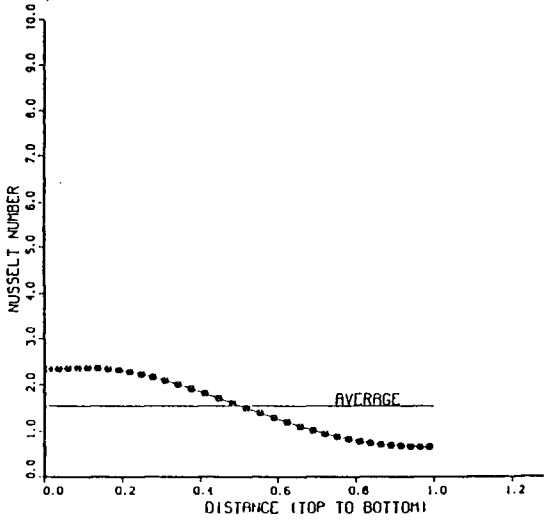

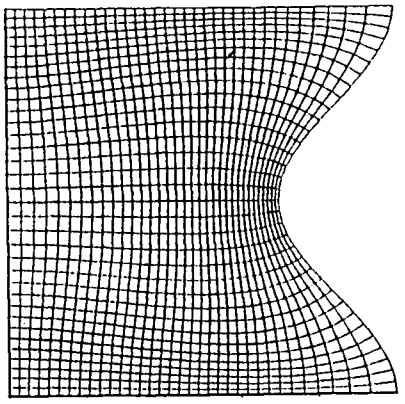

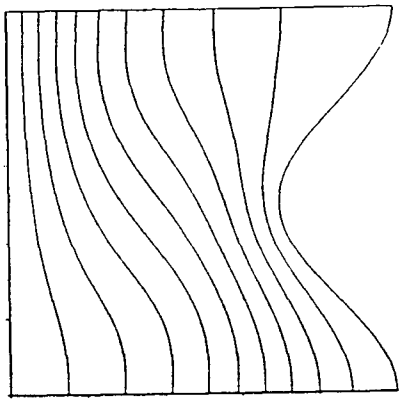

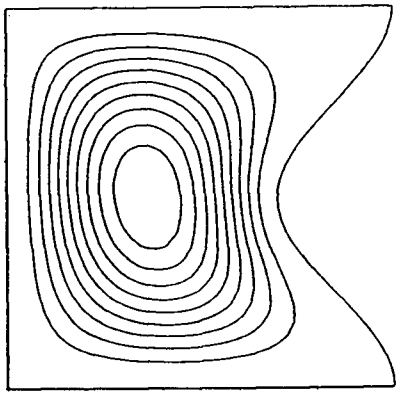

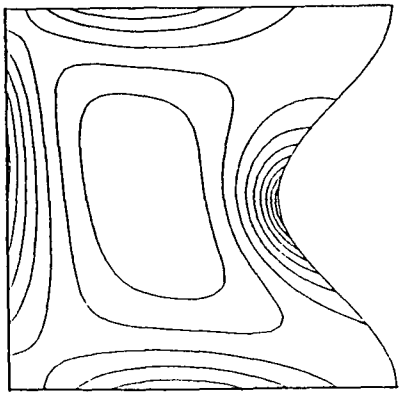

PR= 1.0
RA= 10000.0
DIMENSIONLESS AMPLITUDE= -0.150
AVERAGE NUSSELT NUMBER (RIGHT WALL)= 0.1888602E+01
AVERAGE NUSSELT NUMBER (LEFT WALL)= 0.2252446E+01
LENGTH OF THE WALL(RIGHT)= 0.1182486E+01
LENGTH OF THE WALL(LEFT)= 0.9998378E+00

VORTICITY COUNTOUR VALUES.
MIN= -0.6052932E+03
MAX= 0.1476740E+03

CONTOUR #	1	-0.5299963E+03
CONTOUR #	2	-0.4546997E+03
CONTOUR #	3	-0.3794031E+03
CONTOUR #	4	-0.3041064E+03
CONTOUR #	5	-0.2288098E+03
CONTOUR #	6	-0.1535132E+03
CONTOUR #	7	-0.7821680E+02
CONTOUR #	8	-0.2919922E+01
CONTOUR #	9	0.7237695E+02

STREAM FUNCTION CONTOUR VALUES.
MIN= 0.0
MAX= 0.4249744E+01

CONTOUR #	1	0.4249744E+00
CONTOUR #	2	0.8499489E+00
CONTOUR #	3	0.1274923E+01
CONTOUR #	4	0.1699898E+01
CONTOUR #	5	0.2124871E+01
CONTOUR #	6	0.2549846E+01
CONTOUR #	7	0.2974819E+01
CONTOUR #	8	0.3399796E+01
CONTOUR #	9	0.3824769E+01

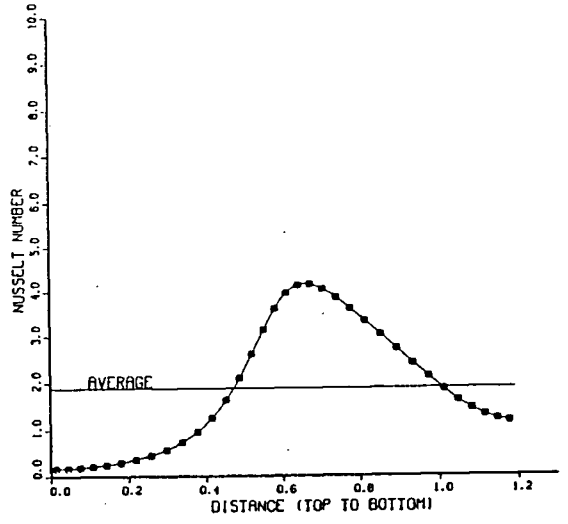

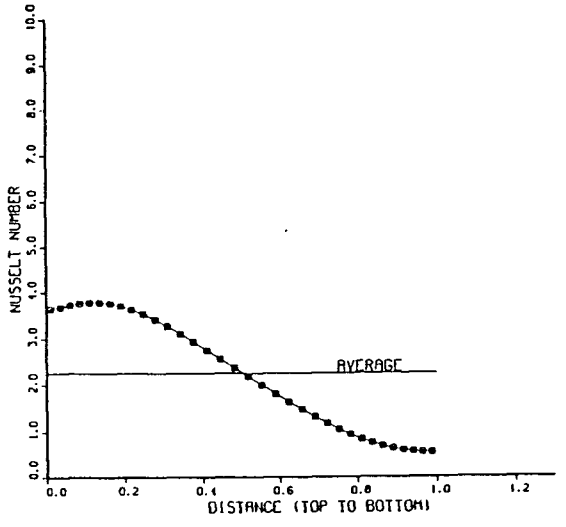

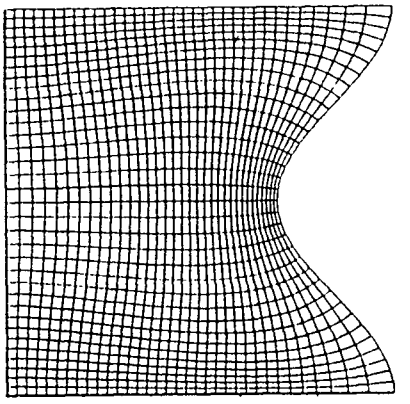

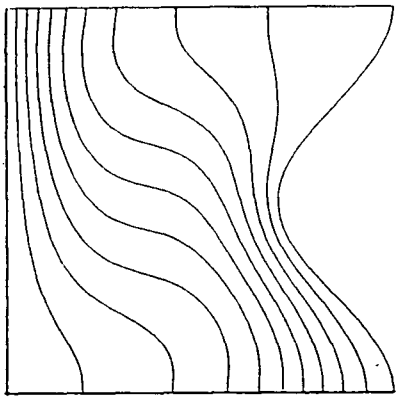

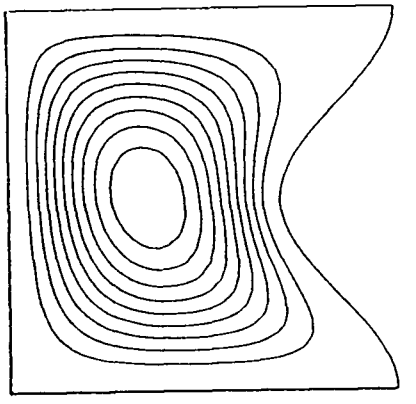

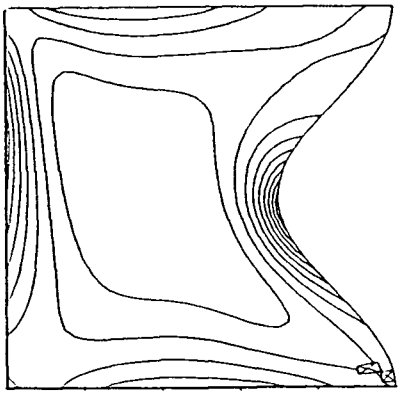

PR= 1.0
RA= 30000.0
DIMENSIONLESS AMPLITUDE= -0.150
AVERAGE NUSSELT NUMBER (RIGHT WALL)= 0.2654413E+01
AVERAGE NUSSELT NUMBER (LEFT WALL)= 0.3165359E+01
LENGTH OF THE WALL(RIGHT)= 0.1192486E+01
LENGTH OF THE WALL(LEFT)= 0.9999379E+00

VORTICITY COUNTOUR VALUES.
MIN= -0.1387027E+04
MAX= 0.2566150E+03

CONTOUR #	1	-0.1222663E+04
CONTOUR #	2	-0.1058289E+04
CONTOUR #	3	-0.8939348E+03
CONTOUR #	4	-0.7295708E+03
CONTOUR #	5	-0.5652063E+03
CONTOUR #	6	-0.4008423E+03
CONTOUR #	7	-0.2364778E+03
CONTOUR #	8	-0.7211377E+02
CONTOUR #	9	0.9226024E+02

STREAM FUNCTION CONTOUR VALUES.
MIN= 0.0
MAX= 0.7117961E+01

CONTOUR #	1	0.7117960E+00
CONTOUR #	2	0.1423592E+01
CONTOUR #	3	0.2135387E+01
CONTOUR #	4	0.2847183E+01
CONTOUR #	5	0.3558978E+01
CONTOUR #	6	0.4270776E+01
CONTOUR #	7	0.4982571E+01
CONTOUR #	8	0.5694367E+01
CONTOUR #	9	0.6406164E+01

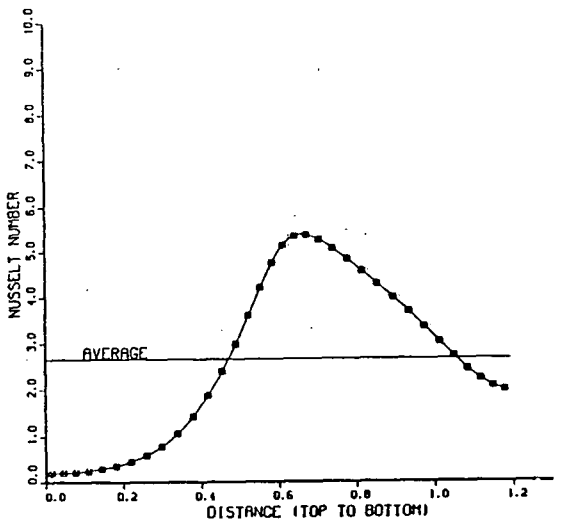

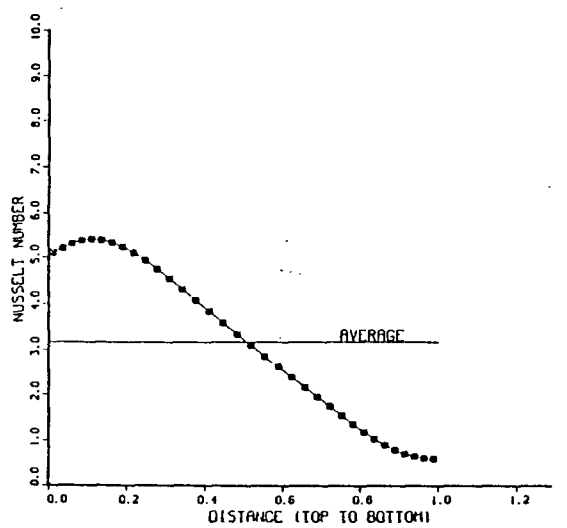

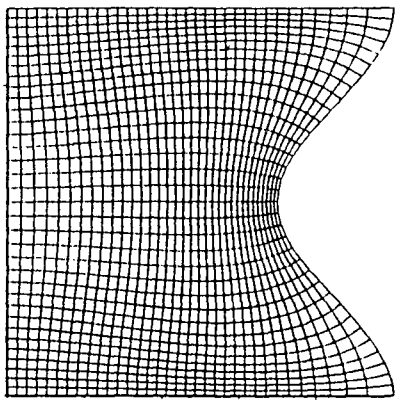

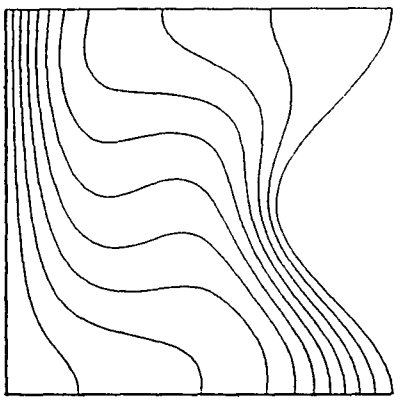

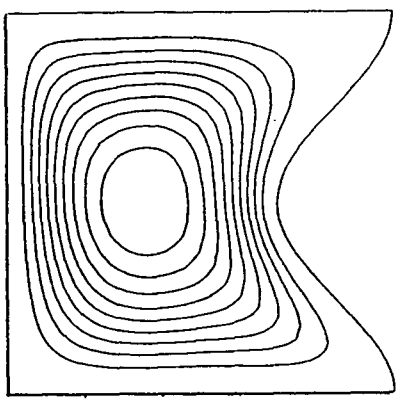

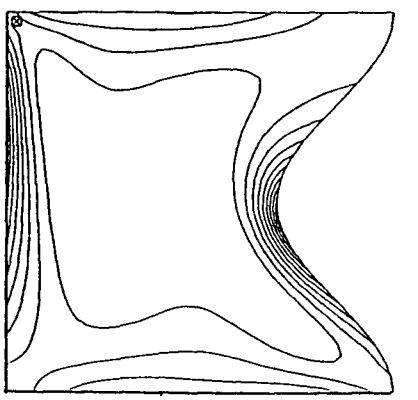

PR= 1.0
RA= 100000.0
DIMENSIONLESS AMPLITUDE= -0.150
AVERAGE NUSSELT NUMBER (RIGHT WALL)= 0.3815717E+01
AVERAGE NUSSELT NUMBER (LEFT WALL)= 0.4550381E+01
LENGTH OF THE WALL(RIGHT)= 0.1192486E+01
LENGTH OF THE WALL(LEFT)= 0.9999378E+00

VORTICITY COUNTOUR VALUES.
MIN= -0.3236859E+04
MAX= 0.6098074E+03

CONTOUR #	1	-0.2852193E+04
CONTOUR #	2	-0.2467526E+04
CONTOUR #	3	-0.2082859E+04
CONTOUR #	4	-0.1698193E+04
CONTOUR #	5	-0.1313526E+04
CONTOUR #	6	-0.9288594E+03
CONTOUR #	7	-0.5441931E+03
CONTOUR #	8	-0.1595264E+03
CONTOUR #	9	0.2251406E+03

STREAM FUNCTION CONTOUR VALUES.
MIN= 0.0
MAX= 0.9830267E+01

CONTOUR #	1	0.9830267E+00
CONTOUR #	2	0.1966052E+01
CONTOUR #	3	0.2949080E+01
CONTOUR #	4	0.3932106E+01
CONTOUR #	5	0.4915132E+01
CONTOUR #	6	0.5898159E+01
CONTOUR #	7	0.6881186E+01
CONTOUR #	8	0.7864213E+01
CONTOUR #	9	0.8847239E+01

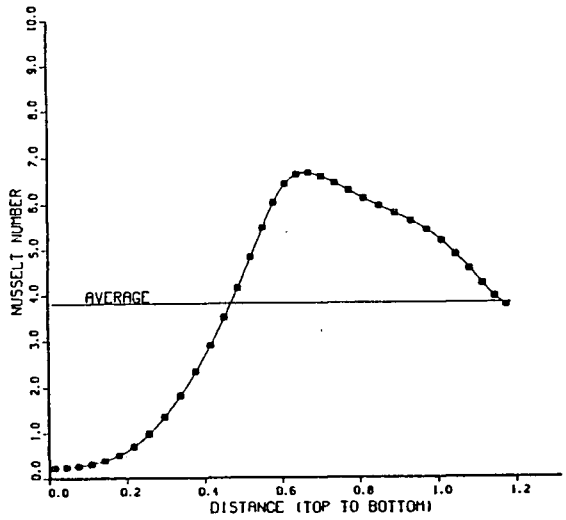

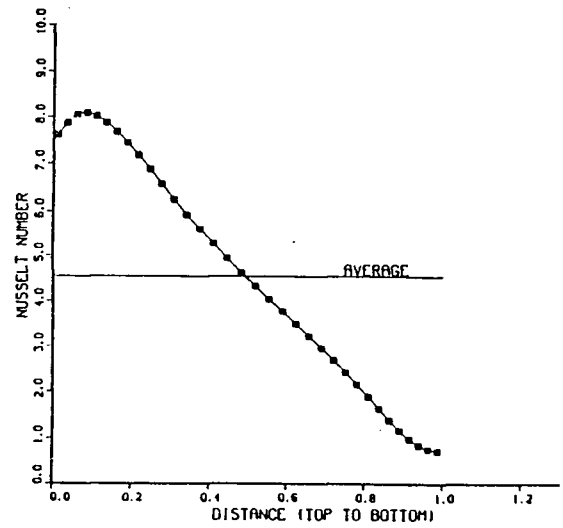

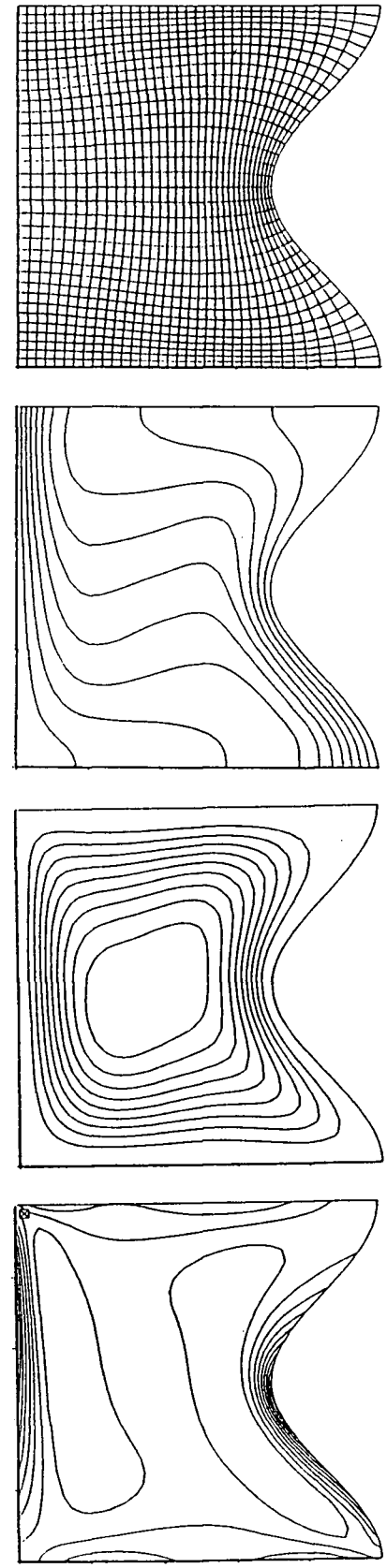

PR= 1.0
RA= 0.0
DIMENSIONLESS AMPLITUDE= -0.075
AVERAGE NUSSELT NUMBER (RIGHT WALL)= 0.1046563E+01
AVERAGE NUSSELT NUMBER (LEFT WALL)= 0.1099328E+01
LENGTH OF THE WALL(RIGHT)= 0.1052813E+01
LENGTH OF THE WALL(LEFT)= 0.9999620E+00

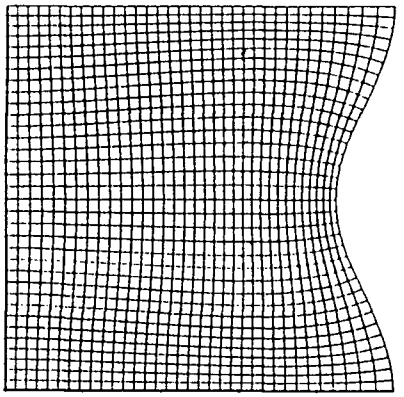

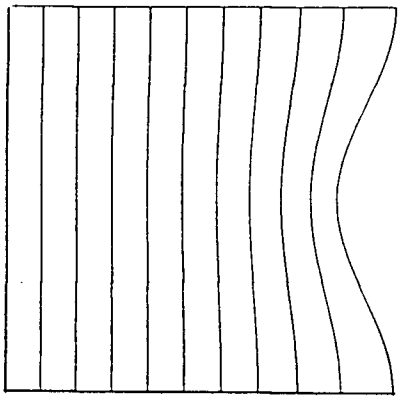

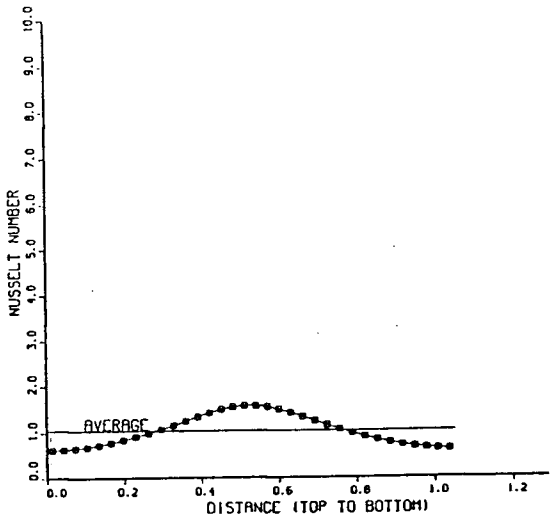

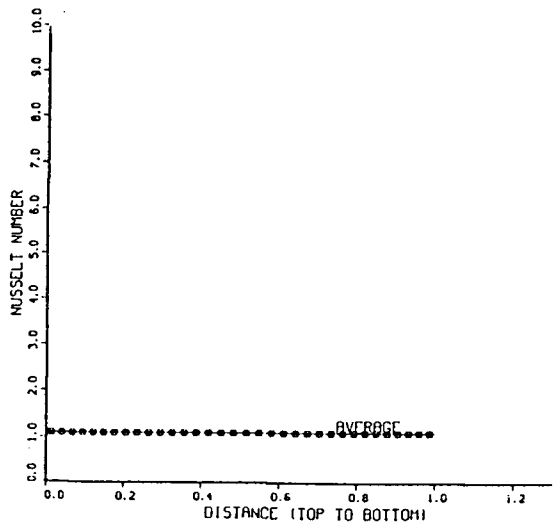

PR= 1.0
RA= 1000.0
DIMENSIONLESS AMPLITUDE= -0.075
AVERAGE NUSSELT NUMBER (RIGHT WALL)= 0.1124238E+01
AVERAGE NUSSELT NUMBER (LEFT WALL)= 0.1183972E+01
LENGTH OF THE WALL(RIGHT)= 0.1052813E+01
LENGTH OF THE WALL(LEFT)= 0.9999620E+00

VORTICITY COUNTOUR VALUES.
MIN= -0.6886629E+02
MAX= 0.3121031E+02

CONTOUR #	1	-0.5887662E+02
CONTOUR #	2	-0.4886697E+02
CONTOUR #	3	-0.3885732E+02
CONTOUR #	4	-0.2884767E+02
CONTOUR #	5	-0.1883801E+02
CONTOUR #	6	-0.8828339E+01
CONTOUR #	7	0.1181305E+01
CONTOUR #	8	0.1118088E+02
CONTOUR #	9	0.2120064E+02

STREAM FUNCTION CONTOUR VALUES.
MIN= 0.0
MAX= 0.9785647E+00

CONTOUR #	1	0.9785646E-01
CONTOUR #	2	0.1957128E+00
CONTOUR #	3	0.2935693E+00
CONTOUR #	4	0.3914258E+00
CONTOUR #	5	0.4892823E+00
CONTOUR #	6	0.5871387E+00
CONTOUR #	7	0.6849952E+00
CONTOUR #	8	0.7828517E+00
CONTOUR #	9	0.8807081E+00

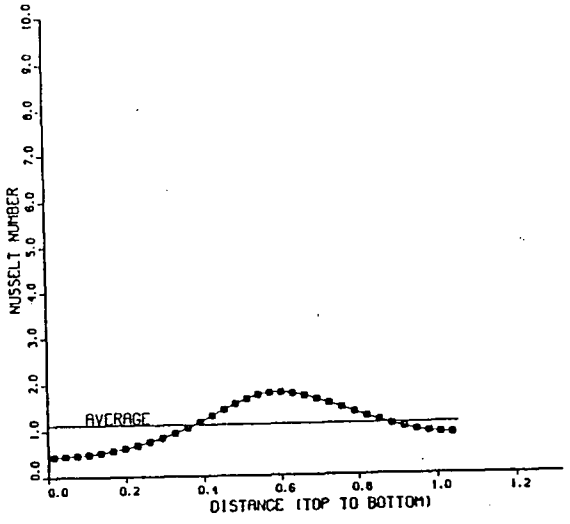

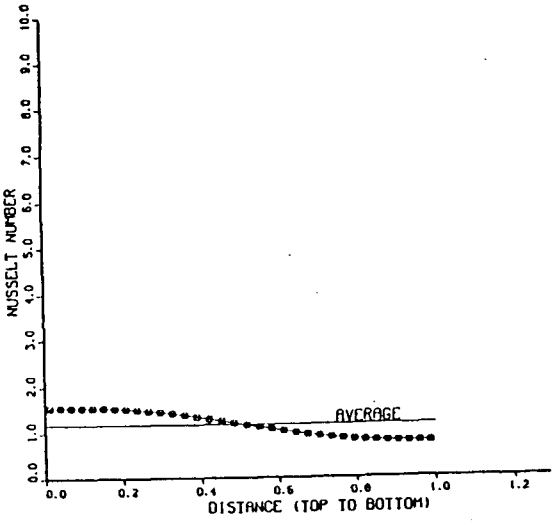

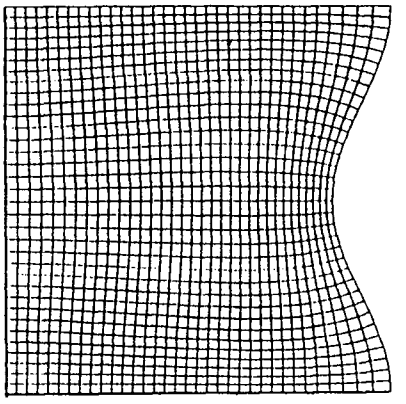

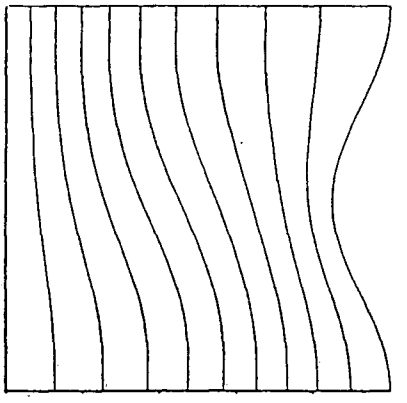

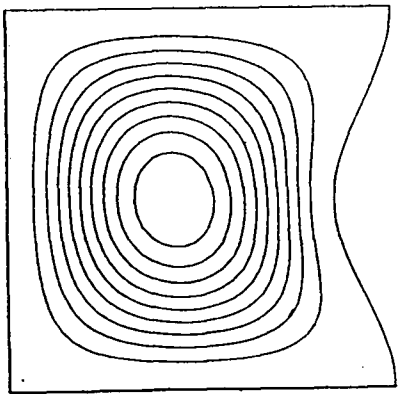

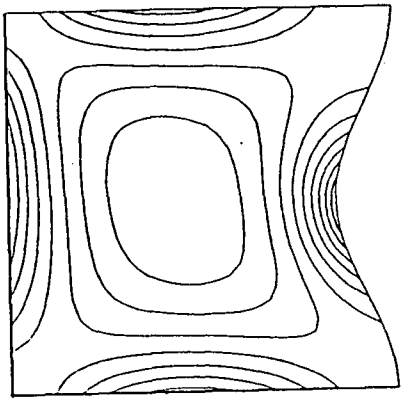

PR= 1.0
RA= 3000.0
DIMENSIONLESS AMPLITUDE= -0.075
AVERAGE NUSSELT NUMBER (RIGHT WALL)= 0.1437706E+01
AVERAGE NUSSELT NUMBER (LEFT WALL)= 0.1513598E+01
LENGTH OF THE WALL(RIGHT)= 0.1052813E+01
LENGTH OF THE WALL(LEFT)= 0.9999620E+00

VORTICITY COUNTOUR VALUES.
MIN= -0.1021734E+03
MAX= 0.7216054E+02

CONTOUR #	1	-0.1657400E+03
CONTOUR #	2	-0.1393067E+03
CONTOUR #	3	-0.1128733E+03
CONTOUR #	4	-0.8643991E+02
CONTOUR #	5	-0.6000653E+02
CONTOUR #	6	-0.3357317E+02
CONTOUR #	7	-0.7139786E+01
CONTOUR #	8	0.1929358E+02
CONTOUR #	9	0.4572696E+02

STREAM FUNCTION CONTOUR VALUES.
MIN= 0.0
MAX= 0.2394137E+01

CONTOUR #	1	0.2394137E+00
CONTOUR #	2	0.4788275E+00
CONTOUR #	3	0.7182412E+00
CONTOUR #	4	0.9576550E+00
CONTOUR #	5	0.1197068E+01
CONTOUR #	6	0.1436482E+01
CONTOUR #	7	0.1675896E+01
CONTOUR #	8	0.1915309E+01
CONTOUR #	9	0.2154722E+01

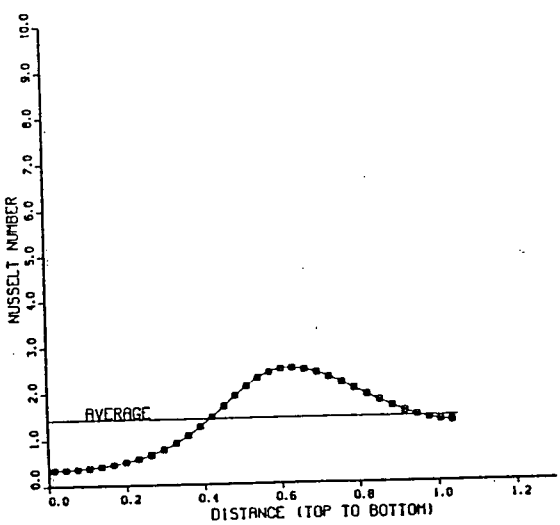

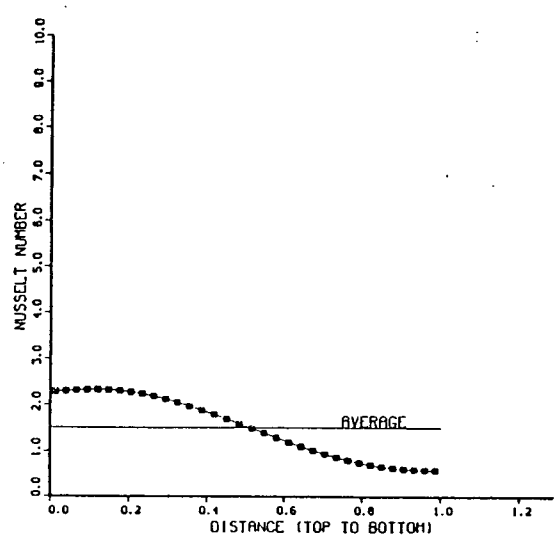

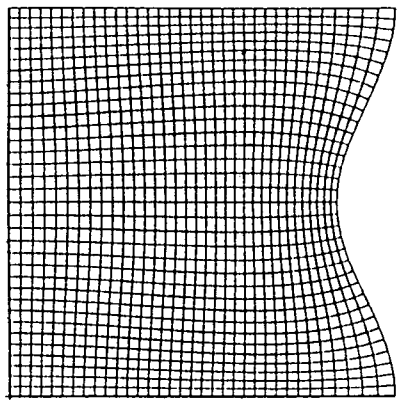

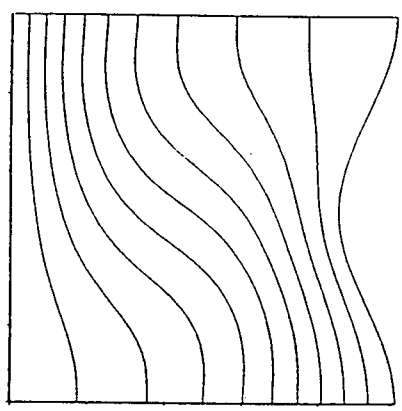

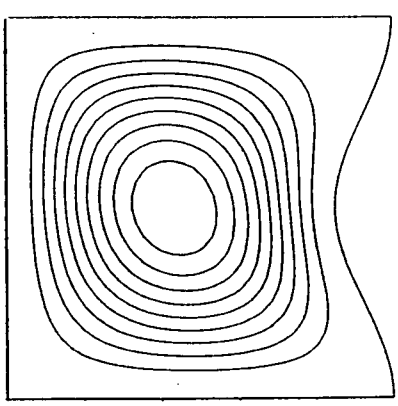

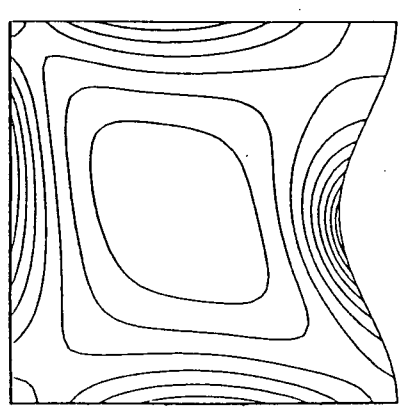

PR= 1.0
RA= 10000.0
DIMENSIONLESS AMPLITUDE= -0.075
AVERAGE NUSSELT NUMBER (RIGHT WALL)= 0.2126877E+01
AVERAGE NUSSELT NUMBER (LEFT WALL)= 0.2238398E+01
LENGTH OF THE WALL(RIGHT)= 0.1052813E+01
LENGTH OF THE WALL(LEFT)= 0.9998620E+00

VORTICITY COUNTOUR VALUES:
MIN= -0.5304016E+03
MAX= 0.1318391E+03

CONTOUR #	1	-0.4641675E+03
CONTOUR #	2	-0.3979333E+03
CONTOUR #	3	-0.3316992E+03
CONTOUR #	4	-0.2654656E+03
CONTOUR #	5	-0.1992314E+03
CONTOUR #	6	-0.1329973E+03
CONTOUR #	7	-0.6676343E+02
CONTOUR #	8	-0.5295410E+00
CONTOUR #	9	0.6570459E+02

STREAM FUNCTION CONTOUR VALUES.
MIN= 0.0
MAX= 0.4824135E+01

CONTOUR #	1	0.4824136E+00
CONTOUR #	2	0.9648269E+00
CONTOUR #	3	0.1447240E+01
CONTOUR #	4	0.1929653E+01
CONTOUR #	5	0.2412066E+01
CONTOUR #	6	0.2894481E+01
CONTOUR #	7	0.3376893E+01
CONTOUR #	8	0.3859307E+01
CONTOUR #	9	0.4341721E+01

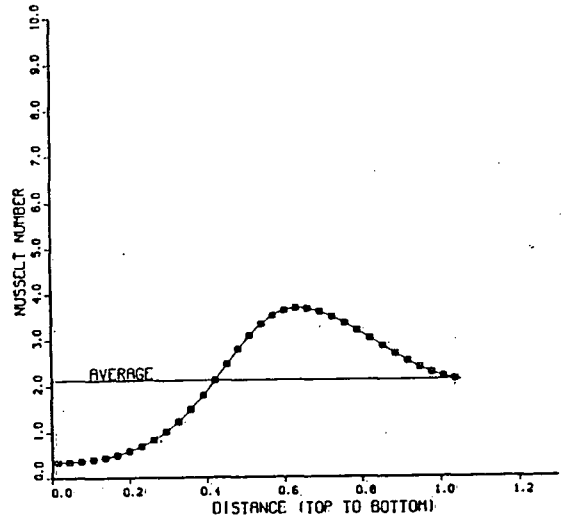

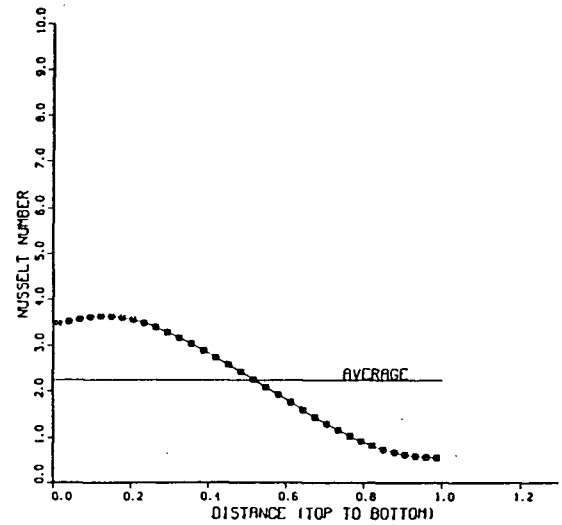

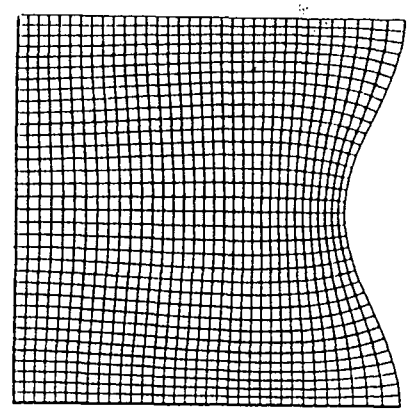

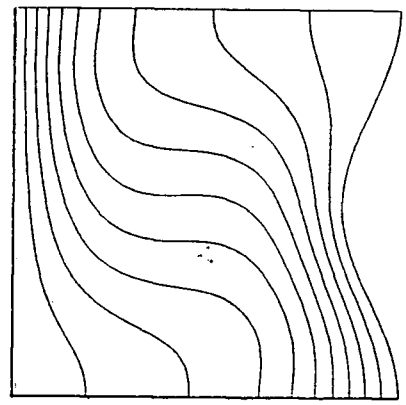

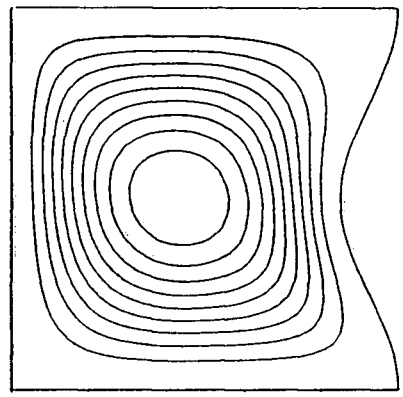

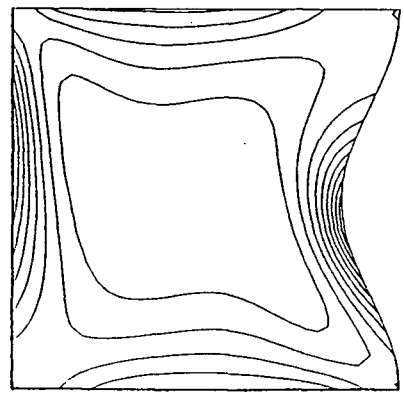

PR= 1.0
RA= 30000.0
DIMENSIONLESS AMPLITUDE= -0.075
AVERAGE NUSSELT NUMBER (RIGHT WALL)= 0.2978904E+01
AVERAGE NUSSELT NUMBER (LEFT WALL)= 0.3136203E+01
LENGTH OF THE WALL(RIGHT)= 0.1052813E+01
LENGTH OF THE WALL(LEFT)= 0.9999620E+00

VORTICITY COUNTOUR VALUES.
MIN= -0.1225978E+04
MAX= 0.2537362E+03

CONTOUR #	1	-0.1078007E+04
CONTOUR #	2	-0.8300354E+03
CONTOUR #	3	-0.5820640E+03
CONTOUR #	4	-0.6340825E+03
CONTOUR #	5	-0.4861211E+03
CONTOUR #	6	-0.3381498E+03
CONTOUR #	7	-0.1901785E+03
CONTOUR #	8	-0.4220703E+02
CONTOUR #	9	0.1057644E+03

STREAM FUNCTION CONTOUR VALUES.
MIN= 0.0
MAX= 0.7303573E+01

CONTOUR #	1	0.7303572E+00
CONTOUR #	2	0.1460714E+01
CONTOUR #	3	0.2191071E+01
CONTOUR #	4	0.2921428E+01
CONTOUR #	5	0.3651785E+01
CONTOUR #	6	0.4382142E+01
CONTOUR #	7	0.5112499E+01
CONTOUR #	8	0.5842857E+01
CONTOUR #	9	0.6573215E+01

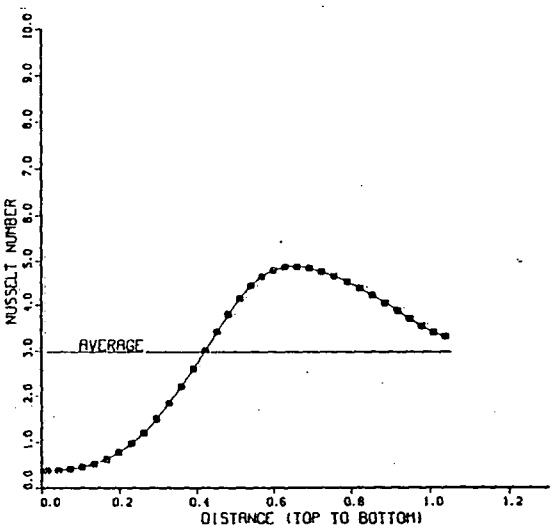

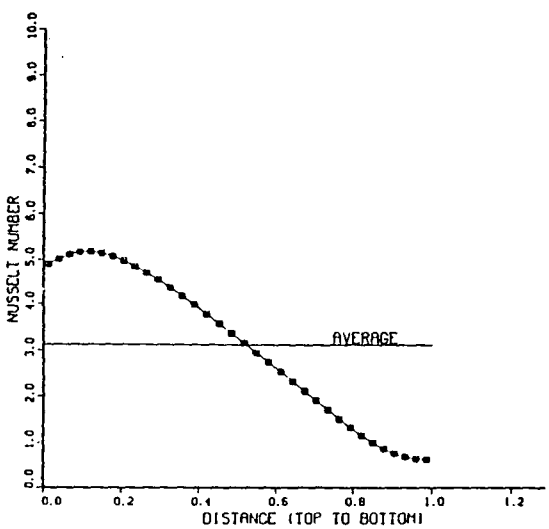

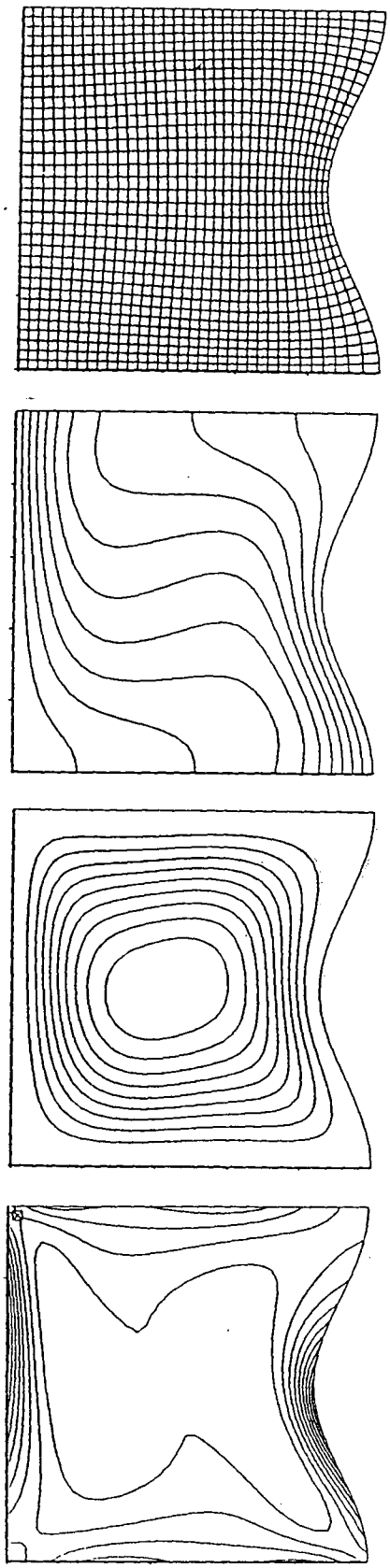

PR= 1.0
RA= 100000.0
DIMENSIONLESS AMPLITUDE= -0.075
AVERAGE NUSSELT NUMBER (RIGHT WALL)= 0.4306437E+01
AVERAGE NUSSELT NUMBER (LEFT WALL)= 0.4534001E+01
LENGTH OF THE WALL(RIGHT)= 0.1052813E+01
LENGTH OF THE WALL(LEFT)= 0.9889620E+00

VORTICITY COUNTOUR VALUES.
MIN= -0.2884367E+04
MAX= 0.6340410E+03

CONTOUR #	1	-0.2622526E+04
CONTOUR #	2	-0.2260686E+04
CONTOUR #	3	-0.1898845E+04
CONTOUR #	4	-0.1537004E+04
CONTOUR #	5	-0.1175163E+04
CONTOUR #	6	-0.8133223E+03
CONTOUR #	7	-0.4514817E+03
CONTOUR #	8	-0.8864063E+02
CONTOUR #	9	0.2722000E+03

STREAM FUNCTION CONTOUR VALUES.
MIN= 0.0
MAX= 0.9870117E+01

CONTOUR #	1	0.9870117E+00
CONTOUR #	2	0.1974023E+01
CONTOUR #	3	0.2961035E+01
CONTOUR #	4	0.3948047E+01
CONTOUR #	5	0.4935059E+01
CONTOUR #	6	0.5922070E+01
CONTOUR #	7	0.6909081E+01
CONTOUR #	8	0.7896093E+01
CONTOUR #	9	0.8883105E+01

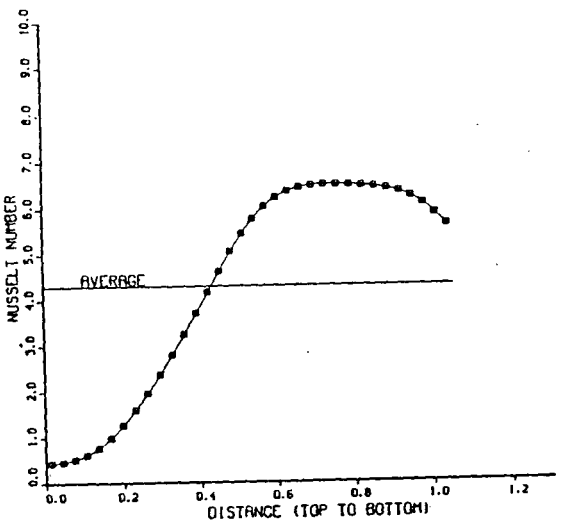

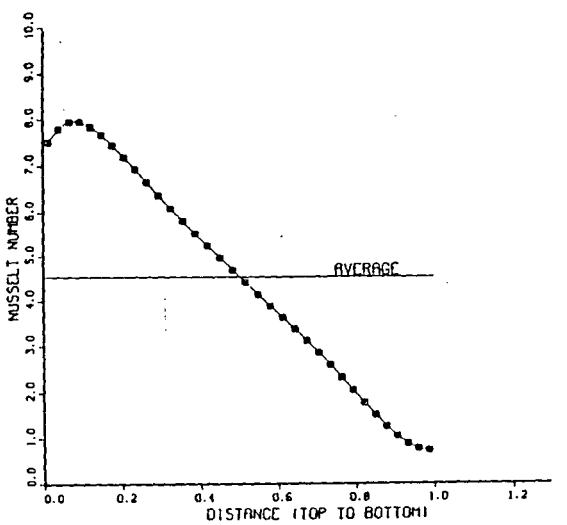

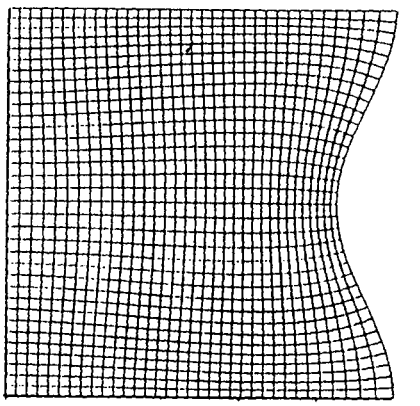

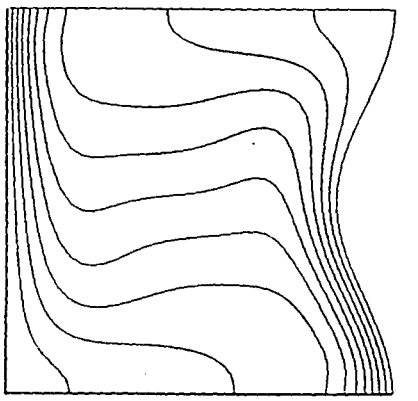

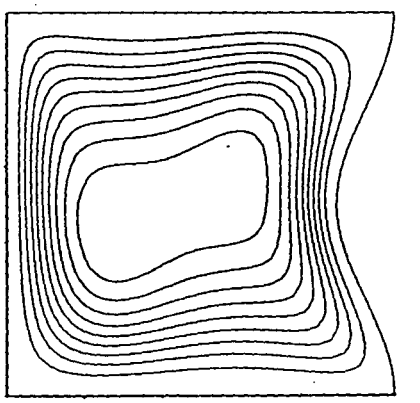

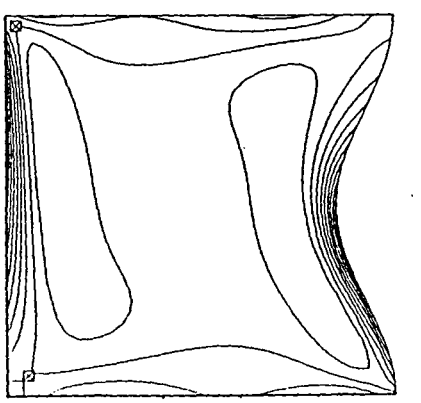

PR= 1.0
RA= 0.0
DIMENSIONLESS AMPLITUDE= 0.0
AVERAGE NUSSELT NUMBER (RIGHT WALL)= 0.1000713E+01
AVERAGE NUSSELT NUMBER (LEFT WALL)= 0.9999542E+00
LENGTH OF THE WALL(RIGHT)= 0.1000000E+01
LENGTH OF THE WALL(LEFT)= 0.1000000E+01

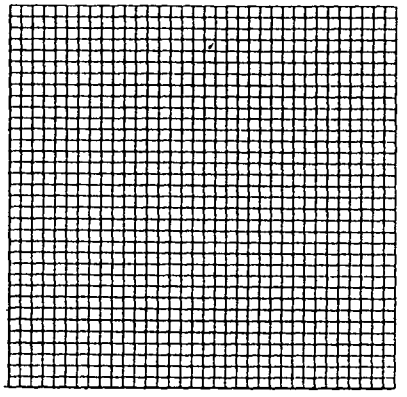

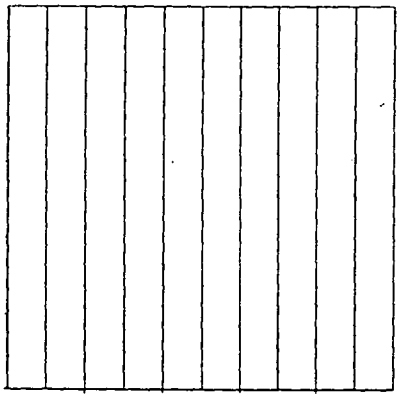

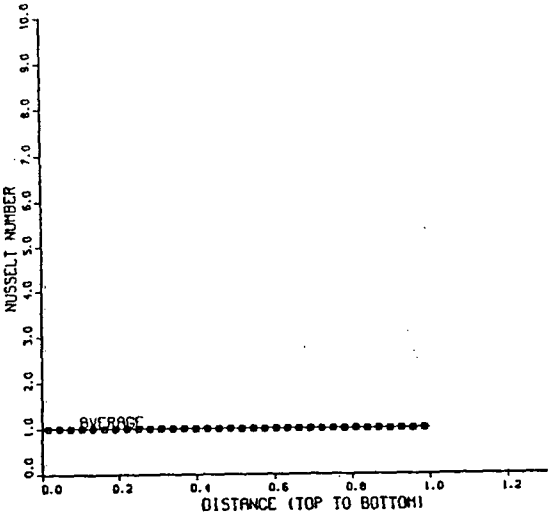

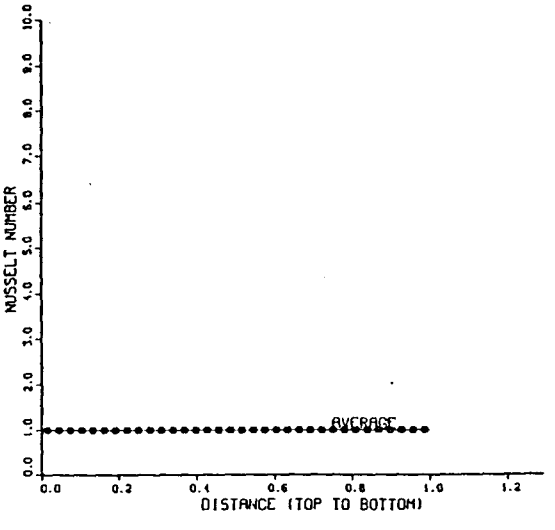

PR= 1.0
RA= 1000
DIMENSIONLESS AMPLITUDE= 0.0
AVERAGE NUSSELT NUMBER (RIGHT WALL)= 0.1117314E+01
AVERAGE NUSSELT NUMBER (LEFT WALL)= 0.1117116E+01
LENGTH OF THE WALL(RIGHT)= 0.1000000E+01
LENGTH OF THE WALL(LEFT)= 0.1000000E+01

VORTICITY COUNTOUR VALUES.
MIN= -0.5111407E+02
MAX= 0.3193279E+02

CONTOUR #	1	-0.4280939E+02
CONTOUR #	2	-0.3450471E+02
CONTOUR #	3	-0.2620003E+02
CONTOUR #	4	-0.1789536E+02
CONTOUR #	5	-0.9590668E+01
CONTOUR #	6	-0.1285980E+01
CONTOUR #	7	0.7018707E+01
CONTOUR #	8	0.1532338E+02
CONTOUR #	9	0.2362808E+02

STREAM FUNCTION CONTOUR VALUES.
MIN= 0.0
MAX= 0.1172150E+01

CONTOUR #	1	0.1172149E+00
CONTOUR #	2	0.2344298E+00
CONTOUR #	3	0.3516449E+00
CONTOUR #	4	0.4688598E+00
CONTOUR #	5	0.5860748E+00
CONTOUR #	6	0.7032897E+00
CONTOUR #	7	0.8205047E+00
CONTOUR #	8	0.9377197E+00
CONTOUR #	9	0.1054935E+01

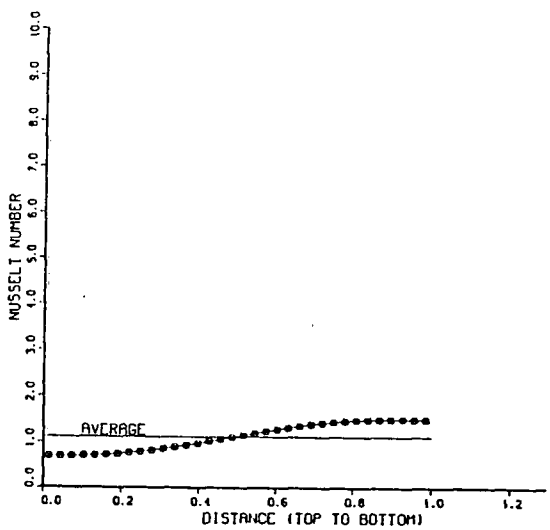

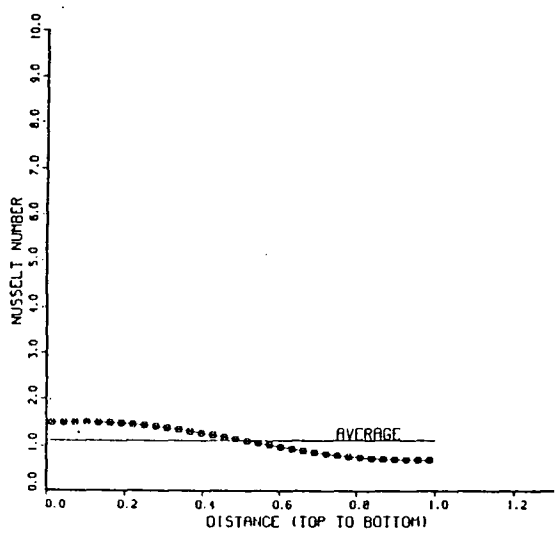

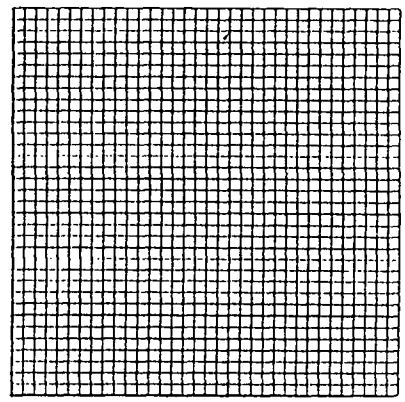

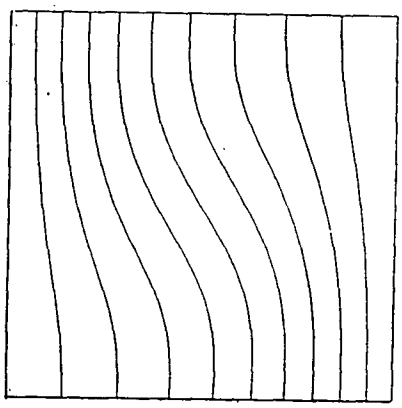

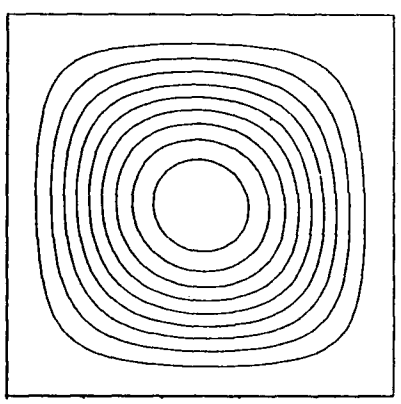

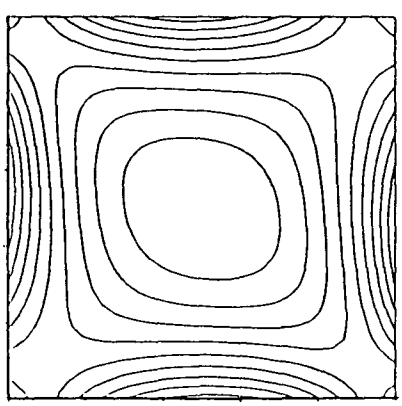

PR= 1.0
RA= 3000.0
DIMENSIONLESS AMPLITUDE= 0.0
AVERAGE NUSSELT NUMBER (RIGHT WALL)= 0.1503907E+01
AVERAGE NUSSELT NUMBER (LEFT WALL)= 0.1503778E+01
LENGTH OF THE WALL(RIGHT)= 0.1000000E+01
LENGTH OF THE WALL(LEFT)= 0.1000000E+01

VORTICITY COUNTOUR VALUES.
MIN= -0.1473275E+03
MAX= 0.6775168E+02

CONTOUR #	1	-0.1258196E+03
CONTOUR #	2	-0.1043117E+03
CONTOUR #	3	-0.8280374E+02
CONTOUR #	4	-0.6129584E+02
CONTOUR #	5	-0.3978792E+02
CONTOUR #	6	-0.1827998E+02
CONTOUR #	7	0.3227921E+01
CONTOUR #	8	0.2473582E+02
CONTOUR #	9	0.4624374E+02

STREAM FUNCTION CONTOUR VALUES.
MIN= 0.0
MAX= 0.2709798E+01

CONTOUR #	1	0.2709798E+00
CONTOUR #	2	0.5418595E+00
CONTOUR #	3	0.8129393E+00
CONTOUR #	4	0.1083919E+01
CONTOUR #	5	0.1354898E+01
CONTOUR #	6	0.1625877E+01
CONTOUR #	7	0.1896858E+01
CONTOUR #	8	0.2167837E+01
CONTOUR #	9	0.2438816E+01

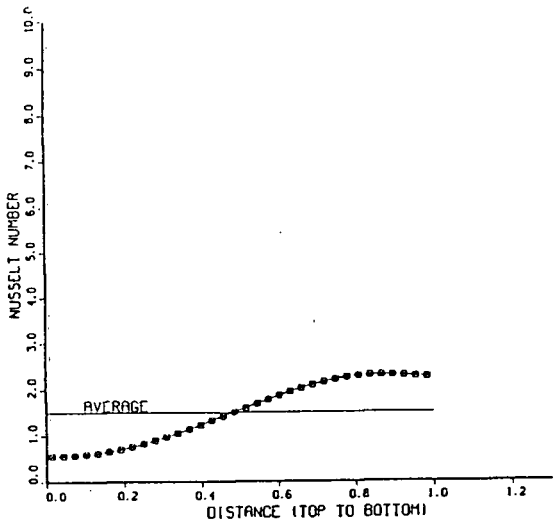

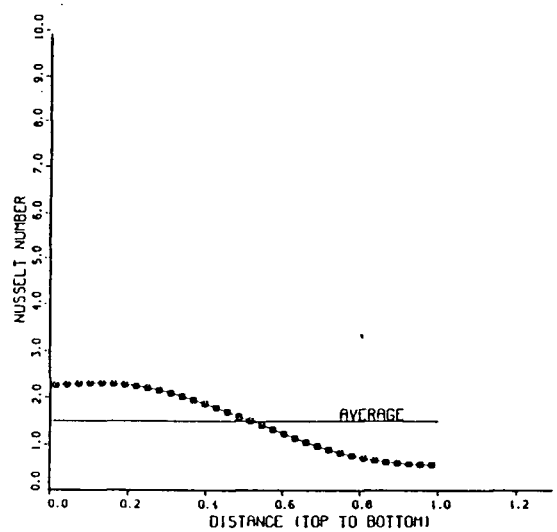

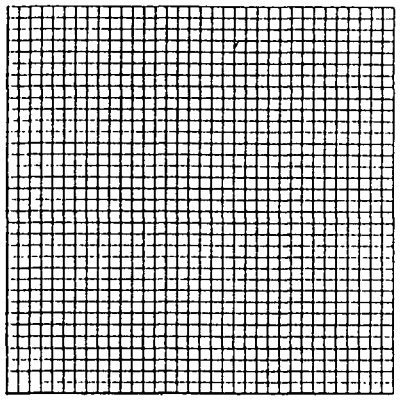

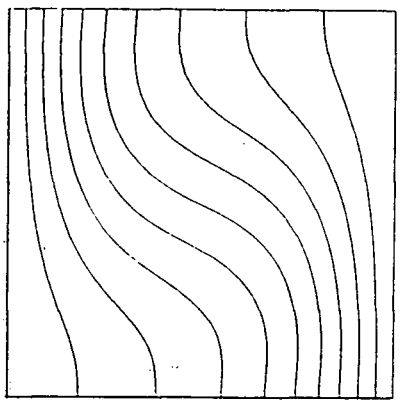

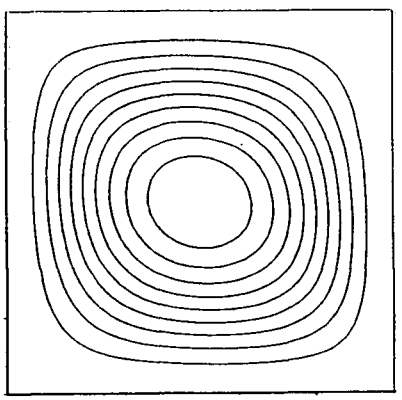

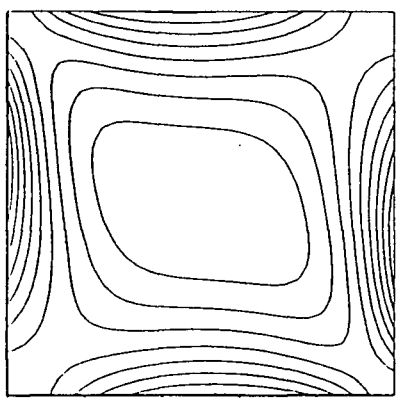

PR= 1.0
RA= 10000.0
DIMENSIONLESS AMPLITUDE= 0.0
AVERAGE NUSSELT NUMBER (RIGHT WALL)= 0.2255569E+01
AVERAGE NUSSELT NUMBER (LEFT WALL)= 0.2255677E+01
LENGTH OF THE WALL(RIGHT)= 0.1000000E+01
LENGTH OF THE WALL(LEFT)= 0.1000000E+01

VORTICITY COUNTOUR VALUES.
MIN= -0.4267256E+03
MAX= 0.1278877E+03

CONTOUR #	1	-0.3712642E+03
CONTOUR #	2	-0.3158030E+03
CONTOUR #	3	-0.2603416E+03
CONTOUR #	4	-0.2048804E+03
CONTOUR #	5	-0.1494192E+03
CONTOUR #	6	-0.9385776E+02
CONTOUR #	7	-0.3849658E+02
CONTOUR #	8	0.1696460E+02
CONTOUR #	9	0.7242578E+02

STREAM FUNCTION CONTOUR VALUES.
MIN= 0.0
MAX= 0.5112517E+01

CONTOUR #	1	0.5112517E+00
CONTOUR #	2	0.1022503E+01
CONTOUR #	3	0.1533754E+01
CONTOUR #	4	0.2045006E+01
CONTOUR #	5	0.2556257E+01
CONTOUR #	6	0.3067508E+01
CONTOUR #	7	0.3578761E+01
CONTOUR #	8	0.4090013E+01
CONTOUR #	9	0.4601265E+01

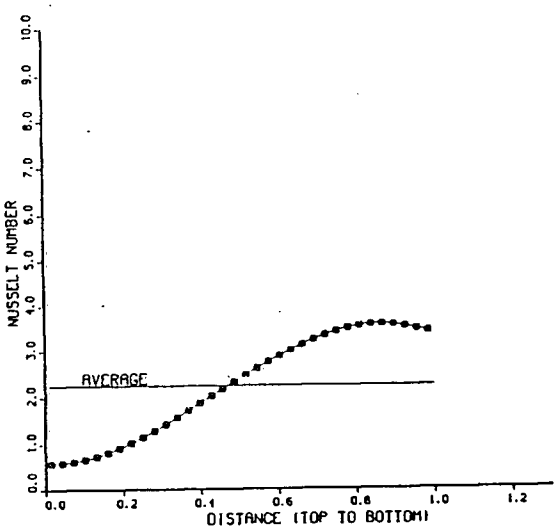

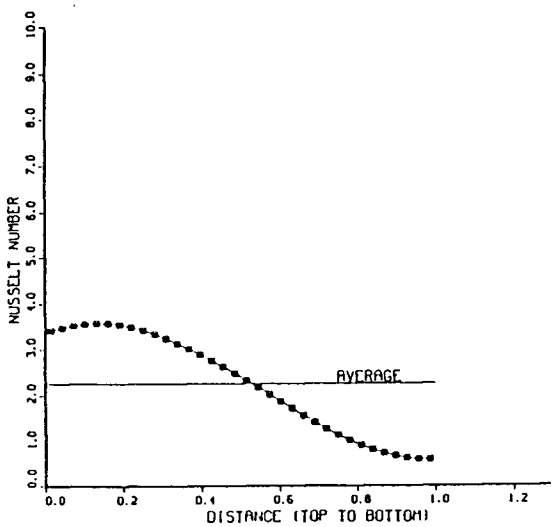

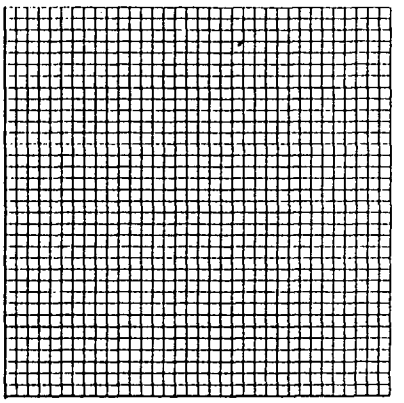

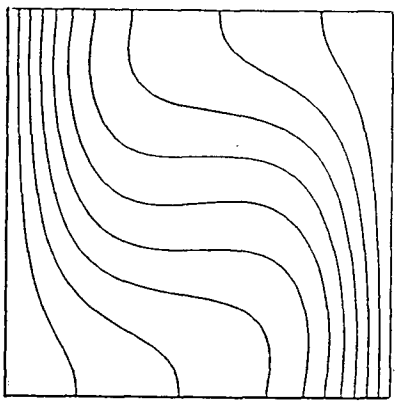

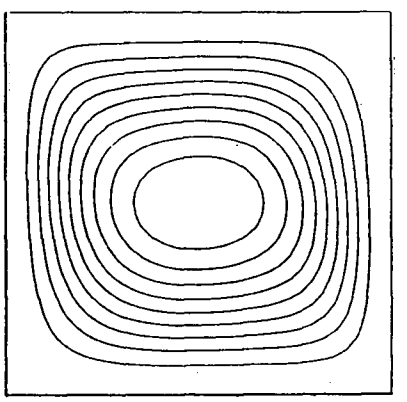

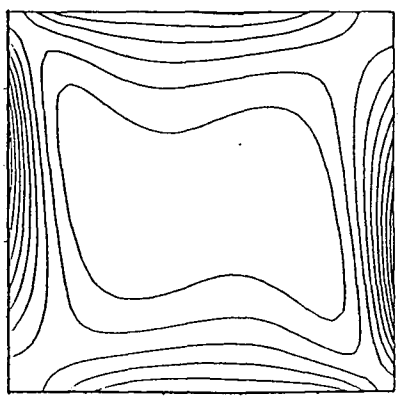

PR= 1.0
RA= 30000.0
DIMENSIONLESS AMPLITUDE= 0.0
AVERAGE NUSSELT NUMBER (RIGHT WALL)= 0.3178328E+01
AVERAGE NUSSELT NUMBER (LEFT WALL)= 0.3179296E+01
LENGTH OF THE WALL(RIGHT)= 0.1000000E+01
LENGTH OF THE WALL(LEFT)= 0.1000000E+01

VORTICITY COUNTOUR VALUES.
MIN= -0.1042259E+04
MAX= 0.2597678E+03

CONTOUR #	1	-0.9120559E+03
CONTOUR #	2	-0.7818533E+03
CONTOUR #	3	-0.6516506E+03
CONTOUR #	4	-0.5214480E+03
CONTOUR #	5	-0.3912458E+03
CONTOUR #	6	-0.2610430E+03
CONTOUR #	7	-0.1308403E+03
CONTOUR #	8	-0.6374512E+00
CONTOUR #	9	0.1285647E+03

STREAM FUNCTION CONTOUR VALUES.
MIN= 0.0
MAX= 0.7335073E+01

CONTOUR #	1	0.7335073E+00
CONTOUR #	2	0.1467014E+01
CONTOUR #	3	0.2200521E+01
CONTOUR #	4	0.2934028E+01
CONTOUR #	5	0.3667535E+01
CONTOUR #	6	0.4401043E+01
CONTOUR #	7	0.5134550E+01
CONTOUR #	8	0.5868058E+01
CONTOUR #	9	0.6601565E+01

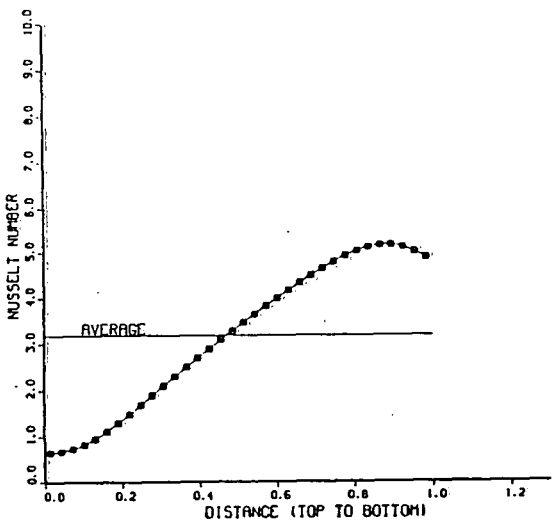

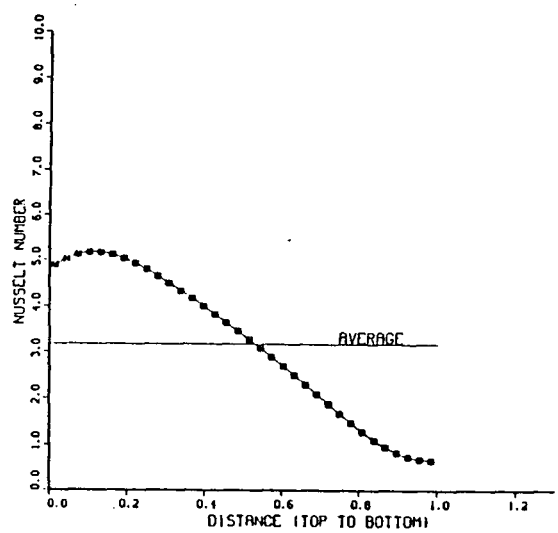

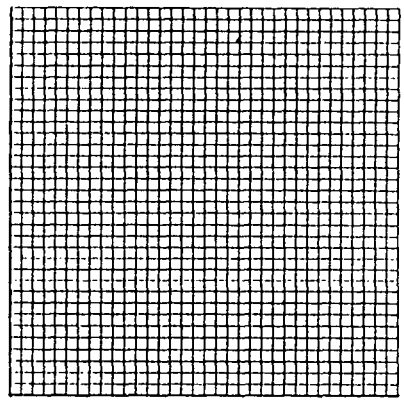

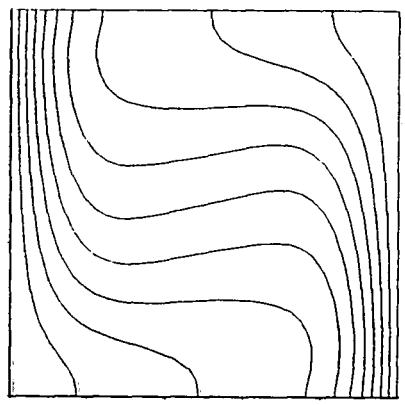

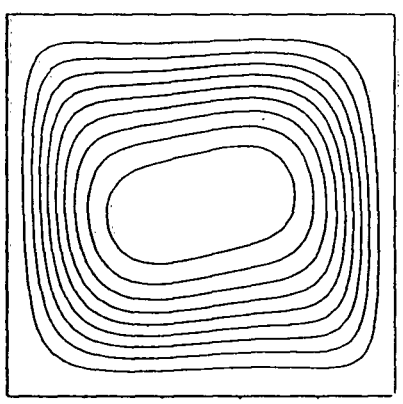

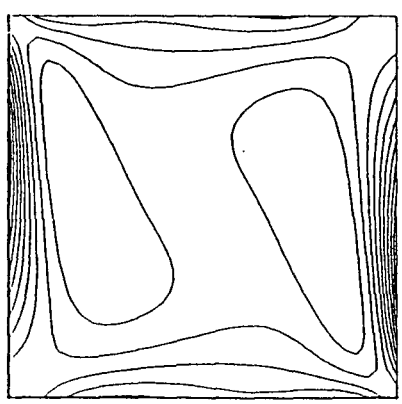

PR= 1.0
RA= 100000.0
DIMENSIONLESS AMPLITUDE= 0.0
AVERAGE NUSSELT NUMBER (RIGHT WALL)= 0.4592916E+01
AVERAGE NUSSELT NUMBER (LEFT WALL)= 0.4592480E+01
LENGTH OF THE WALL(RIGHT)= 0.1000000E+01
LENGTH OF THE WALL(LEFT)= 0.1000000E+01

VORTICITY COUNTOUR VALUES.
MIN= -0.2694243E+04
MAX= 0.6211931E+03

CONTOUR #	1	-0.2362700E+04
CONTOUR #	2	-0.2031156E+04
CONTOUR #	3	-0.1699612E+04
CONTOUR #	4	-0.1368069E+04
CONTOUR #	5	-0.1036525E+04
CONTOUR #	6	-0.7049814E+03
CONTOUR #	7	-0.3734382E+03
CONTOUR #	8	-0.4189453E+02
CONTOUR #	9	0.2896494E+03

STREAM FUNCTION CONTOUR VALUES.
MIN= 0.0
MAX= 0.1014151E+02

CONTOUR #	1	0.1014151E+01
CONTOUR #	2	0.2028301E+01
CONTOUR #	3	0.3042453E+01
CONTOUR #	4	0.4056603E+01
CONTOUR #	5	0.5070755E+01
CONTOUR #	6	0.6084906E+01
CONTOUR #	7	0.7099056E+01
CONTOUR #	8	0.8113208E+01
CONTOUR #	9	0.9127358E+01

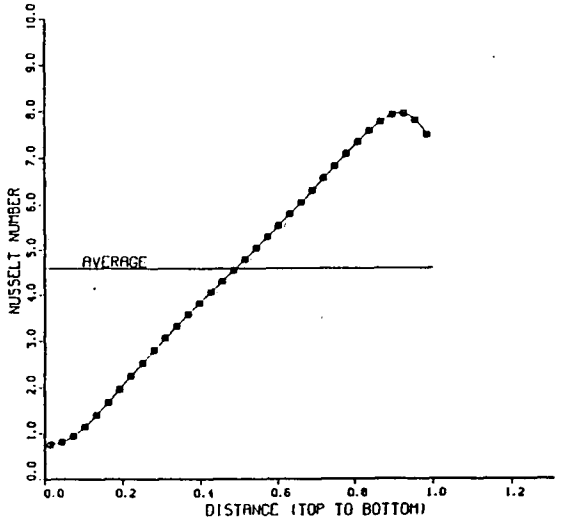

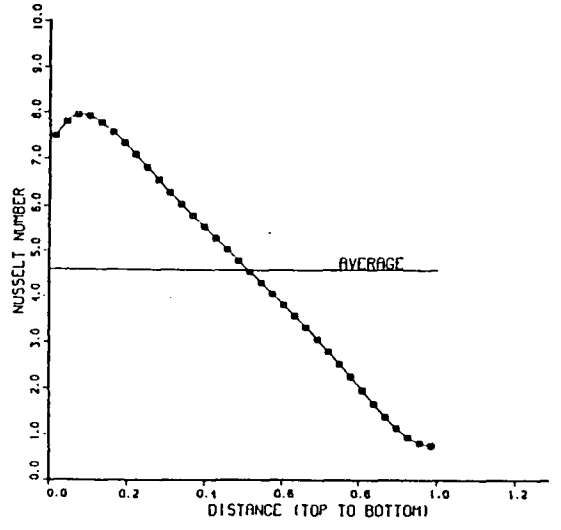

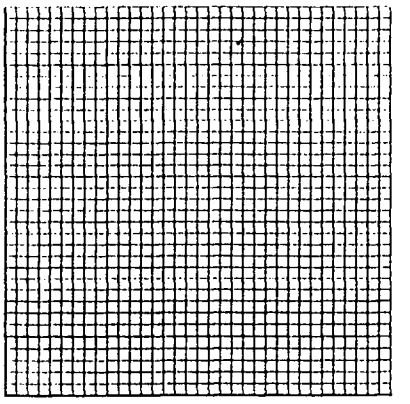

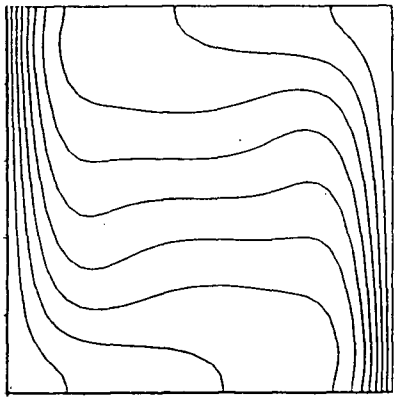

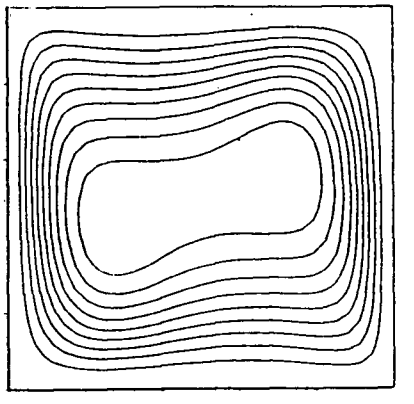

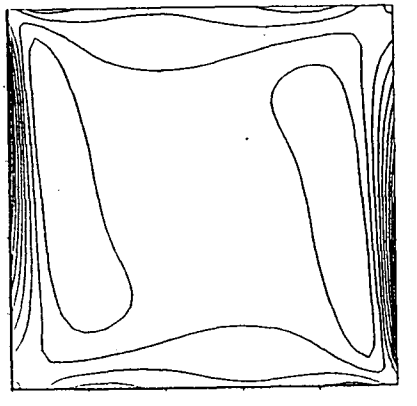

PR= 1.0
RA= 0.0
DIMENSIONLESS AMPLITUDE= 0.075
AVERAGE NUSSELT NUMBER (RIGHT WALL)= 0.8987239E+00
AVERAGE NUSSELT NUMBER (LEFT WALL)= 0.9431577E+00
LENGTH OF THE WALL(RIGHT)= 0.1052813E+01
LENGTH OF THE WALL(LEFT)= 0.1000045E+01

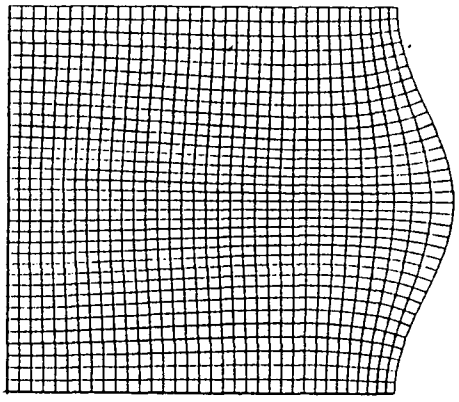

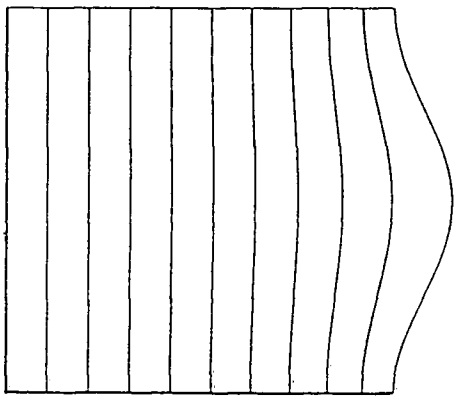

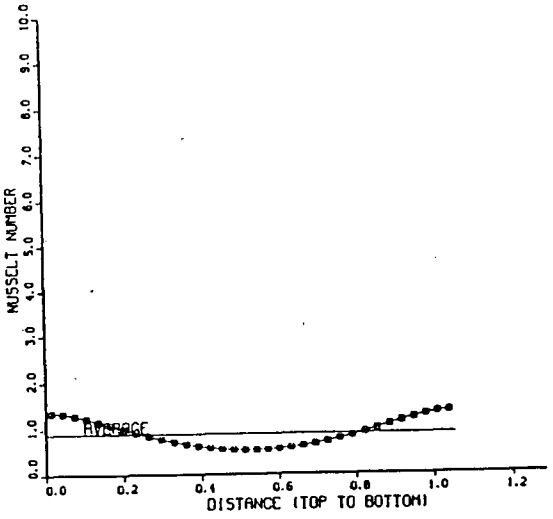

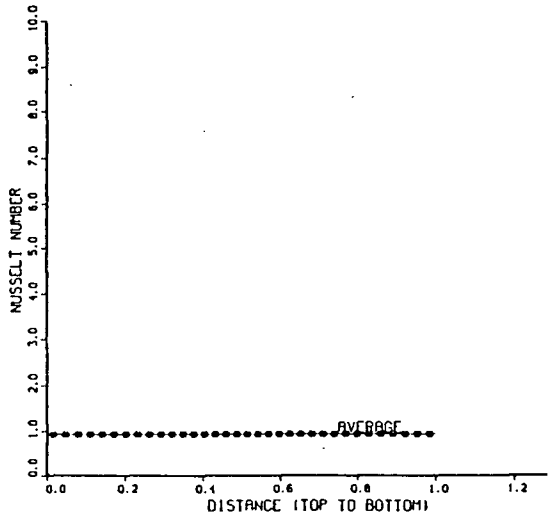

PR= 1.0
RA= 1000.0
DIMENSIONLESS AMPLITUDE= 0.075
AVERAGE NUSSELT NUMBER (RIGHT WALL)= 0.1031169E+01
AVERAGE NUSSELT NUMBER (LEFT WALL)= 0.1085437E+01
LENGTH OF THE WALL(RIGHT)= 0.1052813E+01
LENGTH OF THE WALL(LEFT)= 0.1000045E+01

VORTICITY COUNTOUR VALUES.
MIN= -0.5050365E+02
MAX= 0.3166330E+02

CONTOUR #	1	-0.4228694E+02
CONTOUR #	2	-0.3407027E+02
CONTOUR #	3	-0.2585358E+02
CONTOUR #	4	-0.1763688E+02
CONTOUR #	5	-0.9420181E+01
CONTOUR #	6	-0.1203506E+01
CONTOUR #	7	0.7013189E+01
CONTOUR #	8	0.1522988E+02
CONTOUR #	9	0.2344659E+02

STREAM FUNCTION CONTOUR VALUES.
MIN= 0.0
MAX= 0.1285832E+01

CONTOUR #	1	0.1285832E+00
CONTOUR #	2	0.2571664E+00
CONTOUR #	3	0.3857497E+00
CONTOUR #	4	0.5143330E+00
CONTOUR #	5	0.6429162E+00
CONTOUR #	6	0.7714994E+00
CONTOUR #	7	0.9000826E+00
CONTOUR #	8	0.1028666E+01
CONTOUR #	9	0.1157248E+01

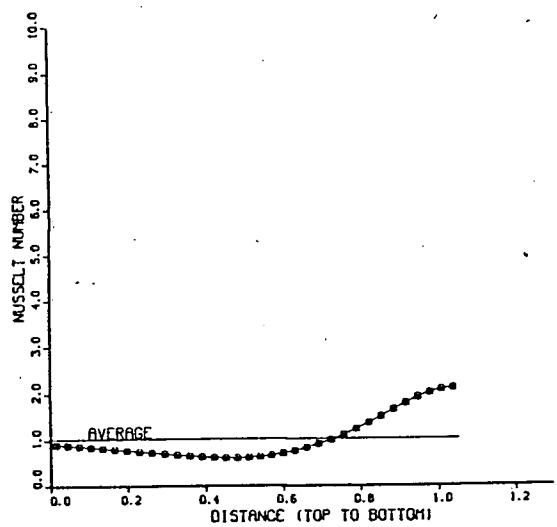

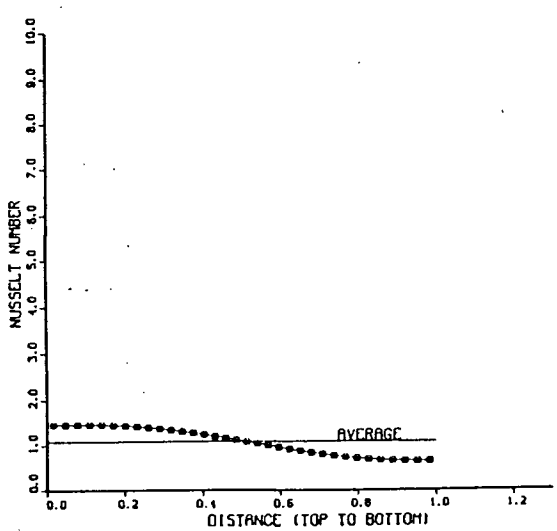

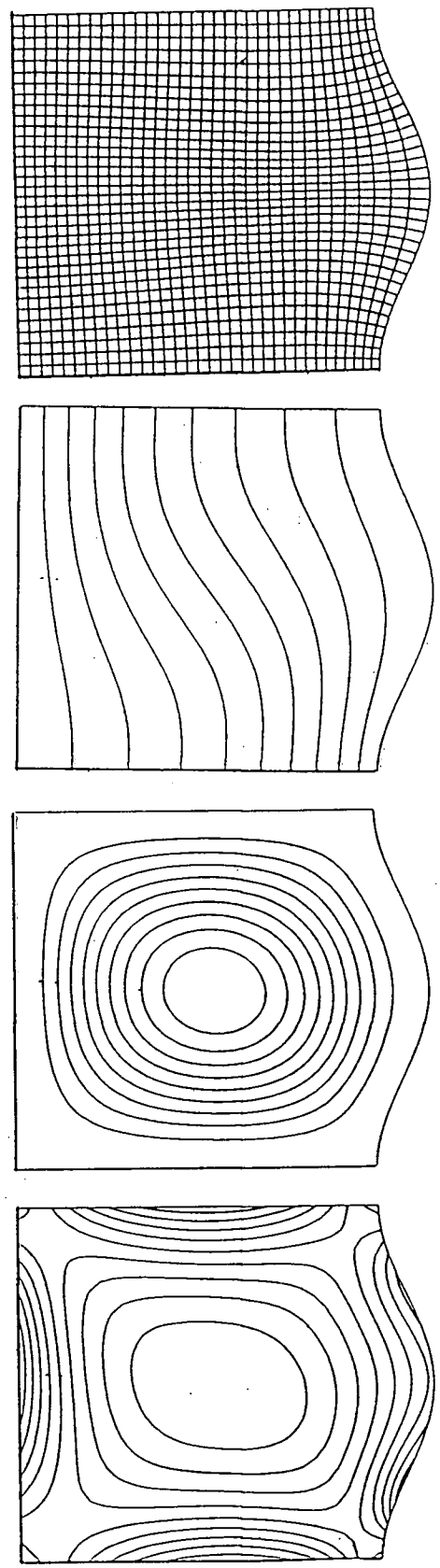

PR= 1.0
RA= 3000.0
DIMENSIONLESS AMPLITUDE= 0.075
AVERAGE NUSSELT NUMBER (RIGHT WALL)= 0.1431821E+01
AVERAGE NUSSELT NUMBER (LEFT WALL)= 0.1507381E+01
LENGTH OF THE WALL(RIGHT)= 0.1052813E+01
LENGTH OF THE WALL(LEFT)= 0.1000048E+01

VORTICITY COUNTOUR VALUES.
MIN= -0.1467118E+03
MAX= 0.6422588E+02

CONTOUR #	1	-0.1256180E+03
CONTOUR #	2	-0.1045242E+03
CONTOUR #	3	-0.8343050E+02
CONTOUR #	4	-0.6233672E+02
CONTOUR #	5	-0.4124285E+02
CONTOUR #	6	-0.2014820E+02
CONTOUR #	7	0.9445801E+00
CONTOUR #	8	0.2203836E+02
CONTOUR #	9	0.4313211E+02

STREAM FUNCTION CONTOUR VALUES.
MIN= 0.0
MAX= 0.2875842E+01

CONTOUR #	1	0.2875842E+00
CONTOUR #	2	0.5751684E+00
CONTOUR #	3	0.8627526E+00
CONTOUR #	4	0.1150336E+01
CONTOUR #	5	0.1437921E+01
CONTOUR #	6	0.1725505E+01
CONTOUR #	7	0.2013088E+01
CONTOUR #	8	0.2300673E+01
CONTOUR #	9	0.2588257E+01

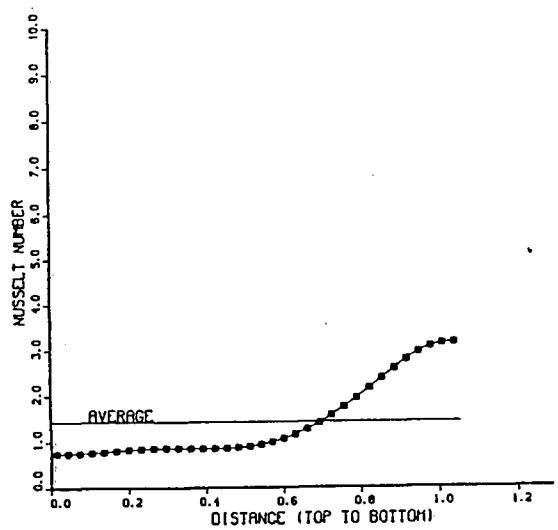

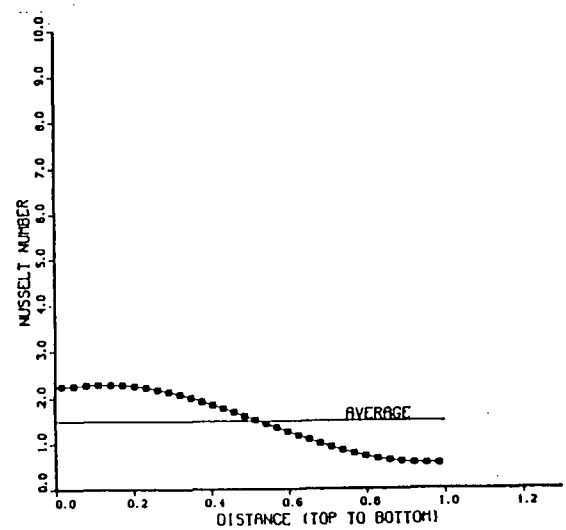

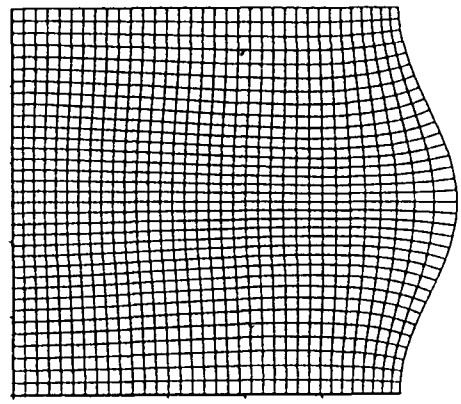

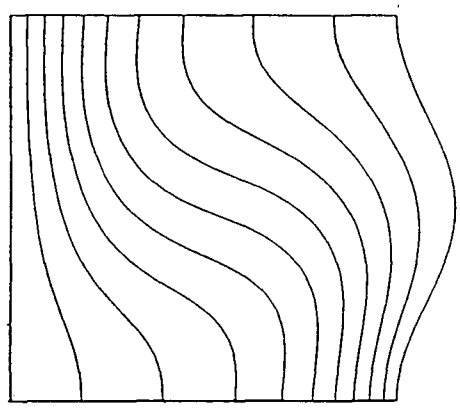

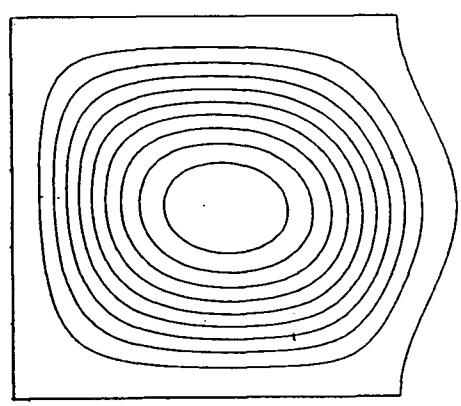

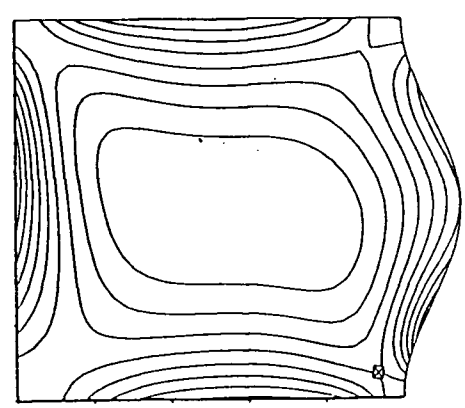

PR= 1.0
RA= 10000.0
DIMENSIONLESS AMPLITUDE= 0.075
AVERAGE NUSSELT NUMBER (RIGHT WALL)= 0.2180868E+01
AVERAGE NUSSELT NUMBER (LEFT WALL)= 0.2286139E+01
LENGTH OF THE WALL(RIGHT)= 0.1052813E+01
LENGTH OF THE WALL(LEFT)= 0.1000045E+01

VORTICITY COUNTOUR VALUES.
MIN= -0.4301121E+03
MAX= 0.1335035E+03

CONTOUR #	1	-0.3737505E+03
CONTOUR #	2	-0.3173889E+03
CONTOUR #	3	-0.2610273E+03
CONTOUR #	4	-0.2046659E+03
CONTOUR #	5	-0.1483044E+03
CONTOUR #	6	-0.9194287E+02
CONTOUR #	7	-0.3558130E+02
CONTOUR #	8	0.2078003E+02
CONTOUR #	9	0.7714165E+02

STREAM FUNCTION CONTOUR VALUES.
MIN= 0.0
MAX= 0.5241264E+01

CONTOUR #	1	0.5241264E+00
CONTOUR #	2	0.1048252E+01
CONTOUR #	3	0.1572379E+01
CONTOUR #	4	0.2096505E+01
CONTOUR #	5	0.2620631E+01
CONTOUR #	6	0.3144758E+01
CONTOUR #	7	0.3668884E+01
CONTOUR #	8	0.4193011E+01
CONTOUR #	9	0.4717136E+01

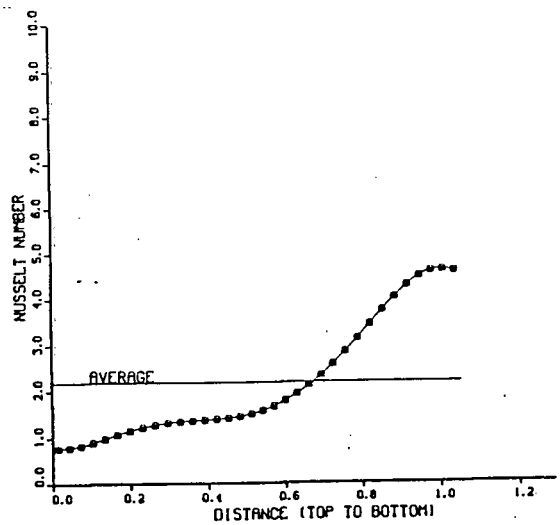

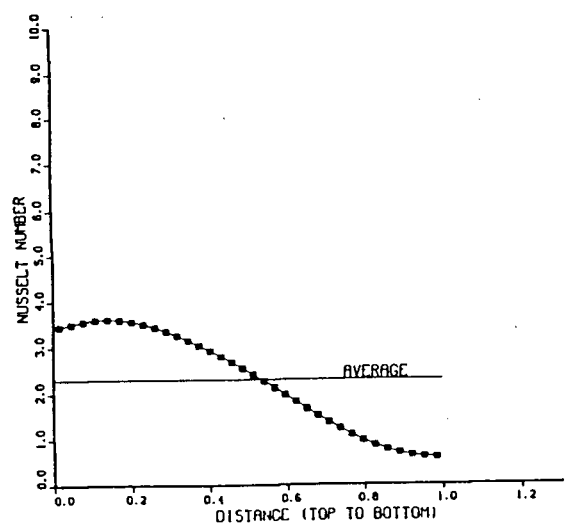

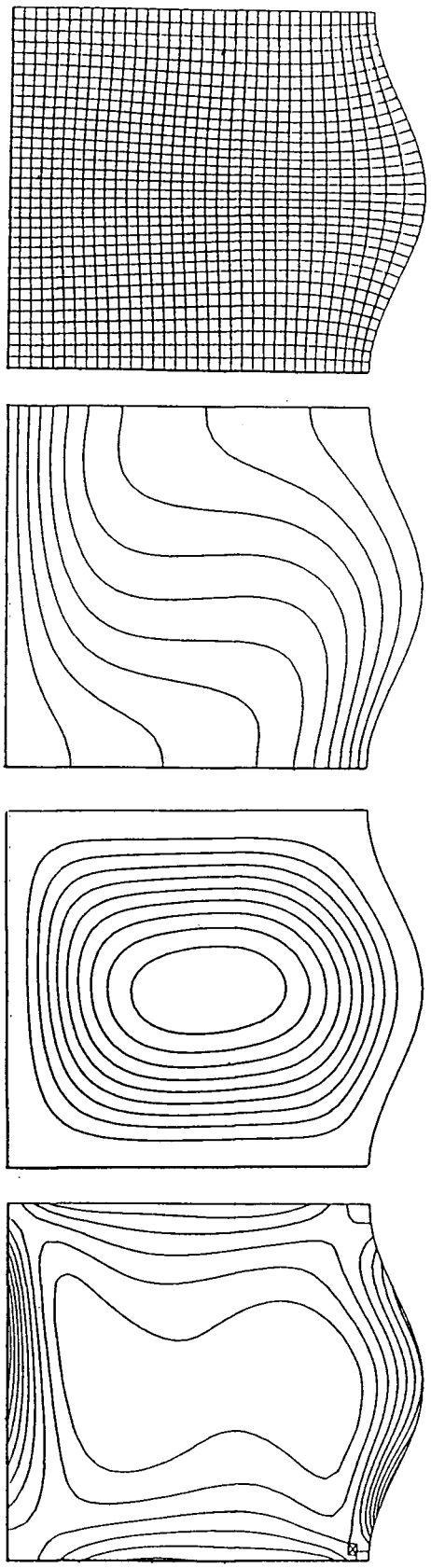

PR= 1.0
RA= 30000.0
DIMENSIONLESS AMPLITUDE= 0.075
AVERAGE NUSSELT NUMBER (RIGHT WALL)= 0.3103331E+01
AVERAGE NUSSELT NUMBER (LEFT WALL)= 0.3266892E+01
LENGTH OF THE WALL(RIGHT)= 0.1052813E+01
LENGTH OF THE WALL(LEFT)= 0.1000045E+01

VORTICITY COUNTOUR VALUES.
MIN= -0.1062268E+04
MAX= 0.2828481E+03

CONTOUR #	1	-0.8277666E+03
CONTOUR #	2	-0.7832451E+03
CONTOUR #	3	-0.6587334E+03
CONTOUR #	4	-0.5242219E+03
CONTOUR #	5	-0.3897102E+03
CONTOUR #	6	-0.2551990E+03
CONTOUR #	7	-0.1206873E+03
CONTOUR #	8	0.1382446E+02
CONTOUR #	9	0.1483362E+03

STREAM FUNCTION CONTOUR VALUES.
MIN= 0.0
MAX= 0.7506384E+01

CONTOUR #	1	0.7506384E+00
CONTOUR #	2	0.1501276E+01
CONTOUR #	3	0.2251915E+01
CONTOUR #	4	0.3002552E+01
CONTOUR #	5	0.3753190E+01
CONTOUR #	6	0.4503830E+01
CONTOUR #	7	0.5254467E+01
CONTOUR #	8	0.6005107E+01
CONTOUR #	9	0.6755745E+01

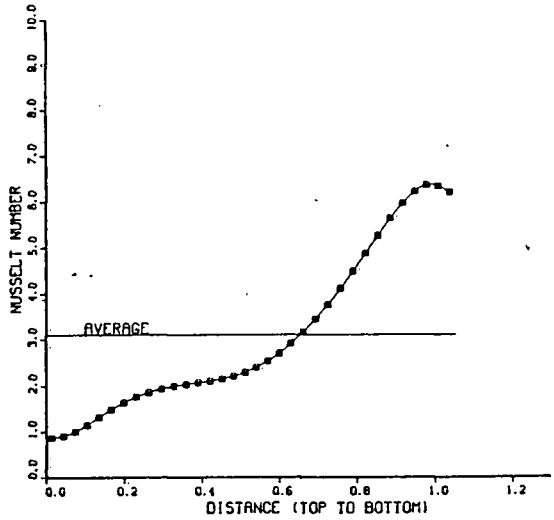

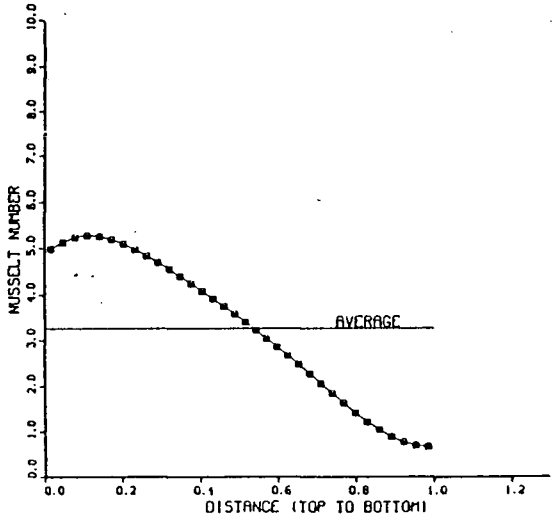

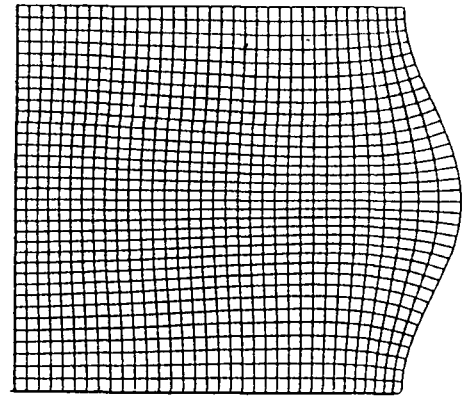

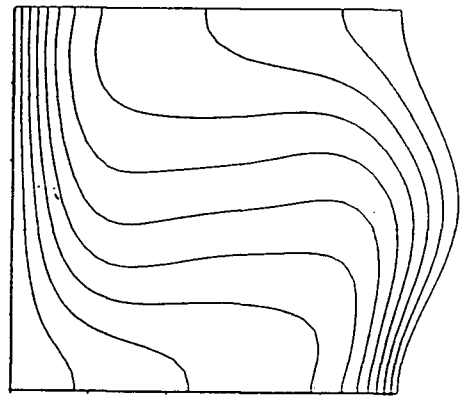

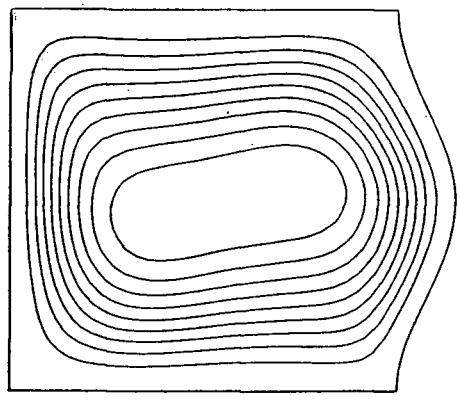

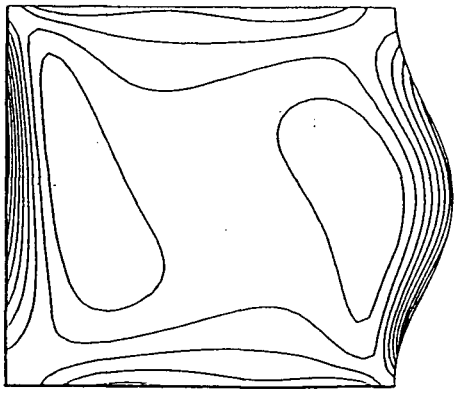

PR= 1.0
RA= 100000.0
DIMENSIONLESS AMPLITUDE= 0.075
AVERAGE NUSSELT NUMBER (RIGHT WALL)= 0.4484457E+01
AVERAGE NUSSELT NUMBER (LEFT WALL)= 0.4721610E+01
LENGTH OF THE WALL(RIGHT)= 0.1052813E+01
LENGTH OF THE WALL(LEFT)= 0.1000045E+01

VORTICITY COUNTOUR VALUES.
MIN= -0.2738948E+04
MAX= 0.6383308E+03

CONTOUR #	1	-0.2401220E+04
CONTOUR #	2	-0.2063493E+04
CONTOUR #	3	-0.1725764E+04
CONTOUR #	4	-0.1388037E+04
CONTOUR #	5	-0.1050309E+04
CONTOUR #	6	-0.7125808E+03
CONTOUR #	7	-0.3748533E+03
CONTOUR #	8	-0.3712500E+02
CONTOUR #	9	0.3006028E+03

STREAM FUNCTION CONTOUR VALUES.
MIN= 0.0
MAX= 0.1075415E+02

CONTOUR #	1	0.1075415E+01
CONTOUR #	2	0.2150828E+01
CONTOUR #	3	0.3226243E+01
CONTOUR #	4	0.4301659E+01
CONTOUR #	5	0.5377073E+01
CONTOUR #	6	0.6452487E+01
CONTOUR #	7	0.7527902E+01
CONTOUR #	8	0.8603317E+01
CONTOUR #	9	0.9678732E+01

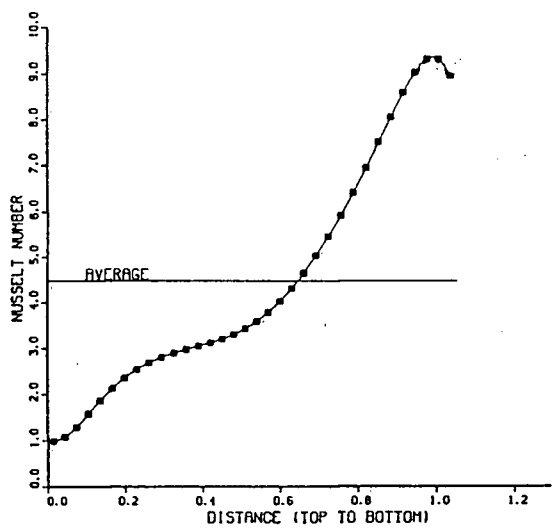

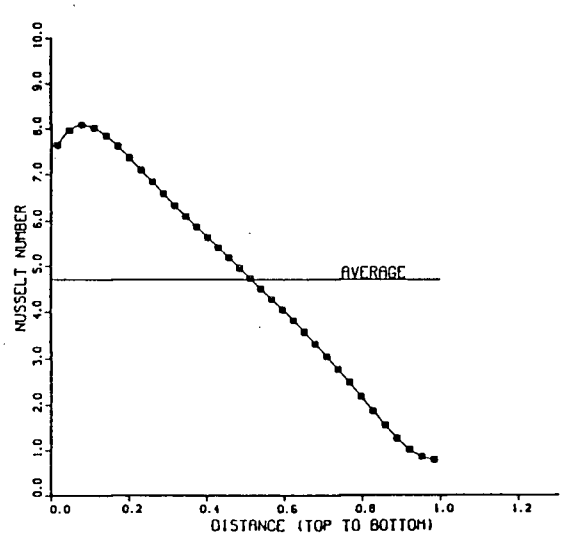

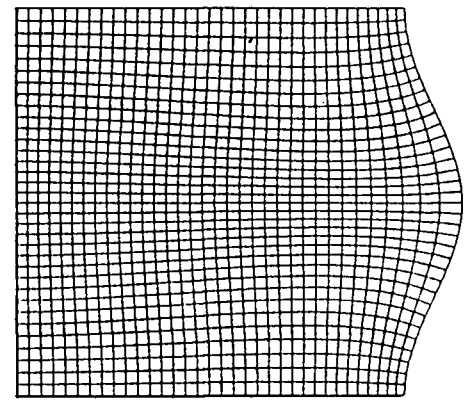

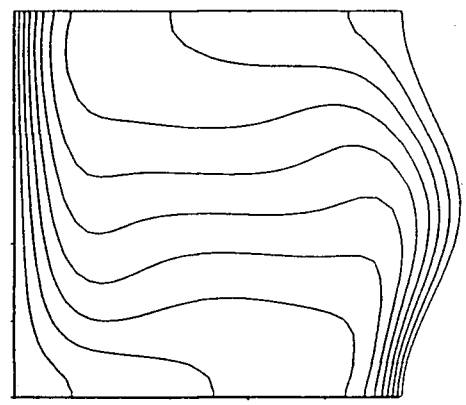

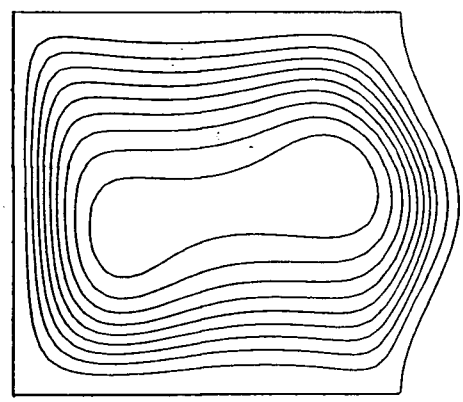

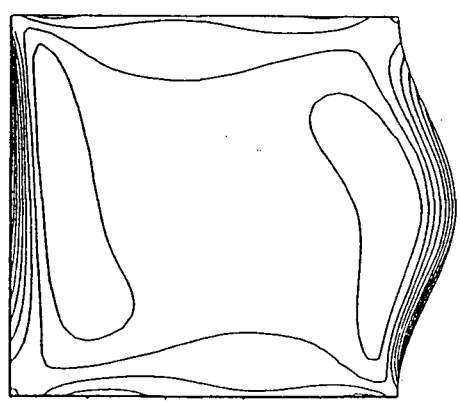

PR= 1.0
RA= 0.0
DIMENSIONLESS AMPLITUDE= 0.150
AVERAGE NUSSELT NUMBER (RIGHT WALL)= 0.7694461E+00
AVERAGE NUSSELT NUMBER (LEFT WALL)= 0.9144906E+00
LENGTH OF THE WALL(RIGHT)= 0.1192486E+01
LENGTH OF THE WALL(LEFT)= 0.1000084E+01

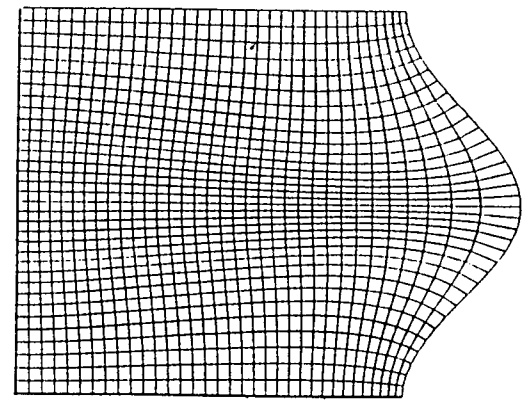

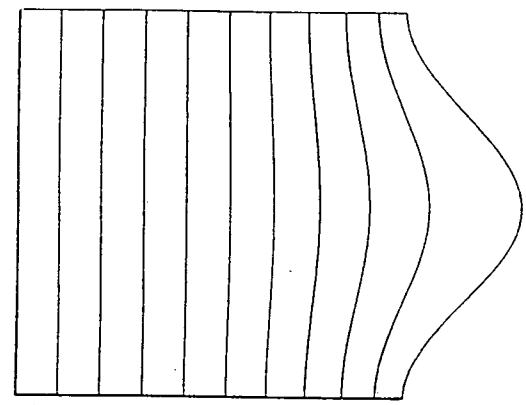

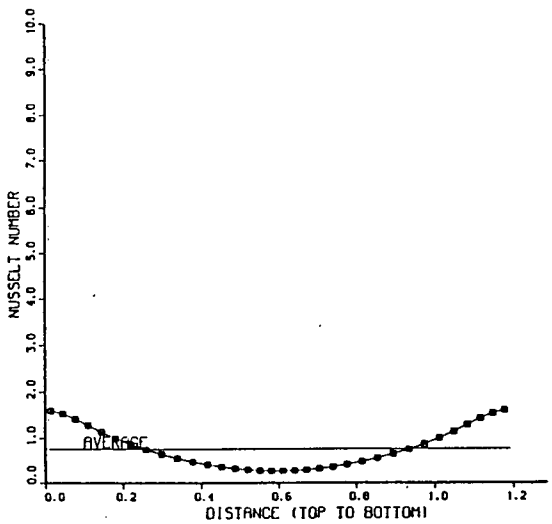

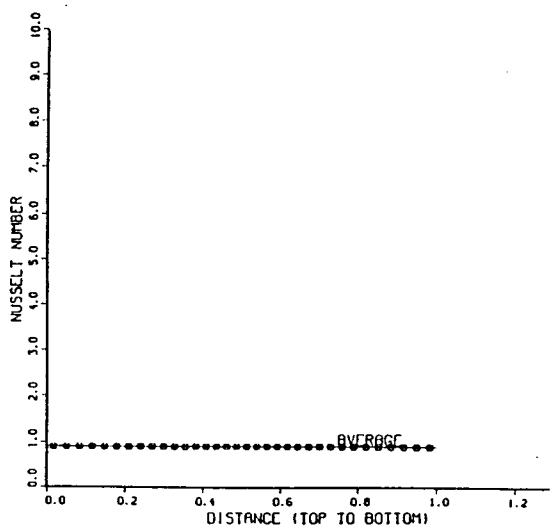

PR= 1.0
RA= 1000.0
DIMENSIONLESS AMPLITUDE= 0.150
AVERAGE NUSSELT NUMBER (RIGHT WALL)= 0.8971367E+00
AVERAGE NUSSELT NUMBER (LEFT WALL)= 0.1069689E+01
LENGTH OF THE WALL(RIGHT)= 0.1192486E+01
LENGTH OF THE WALL(LEFT)= 0.1000084E+01

VORTICITY COUNTOUR VALUES.
MIN= -0.5156377E+02
MAX= 0.3105145E+02

CONTOUR #	1	-0.4330223E+02
CONTOUR #	2	-0.3504073E+02
CONTOUR #	3	-0.2677921E+02
CONTOUR #	4	-0.1851770E+02
CONTOUR #	5	-0.1025618E+02
CONTOUR #	6	-0.1994659E+01
CONTOUR #	7	0.6266861E+01
CONTOUR #	8	0.1452840E+02
CONTOUR #	9	0.2278992E+02

STREAM FUNCTION CONTOUR VALUES.
MIN= 0.0
MAX= 0.1344956E+01

CONTOUR #	1	0.1344956E+00
CONTOUR #	2	0.2689912E+00
CONTOUR #	3	0.4034869E+00
CONTOUR #	4	0.5378825E+00
CONTOUR #	5	0.6724782E+00
CONTOUR #	6	0.8069738E+00
CONTOUR #	7	0.9414694E+00
CONTOUR #	8	0.1075965E+01
CONTOUR #	9	0.1210461E+01

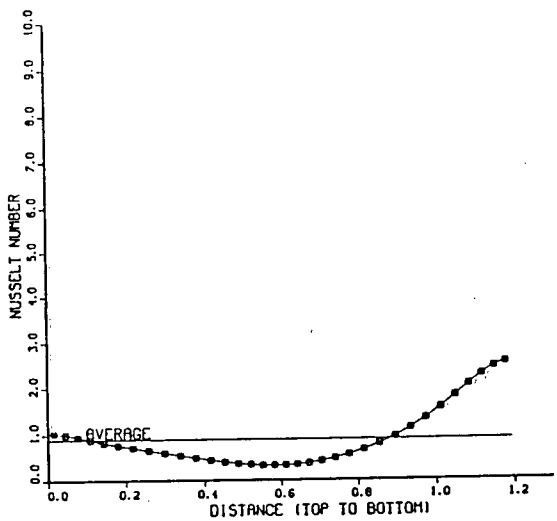

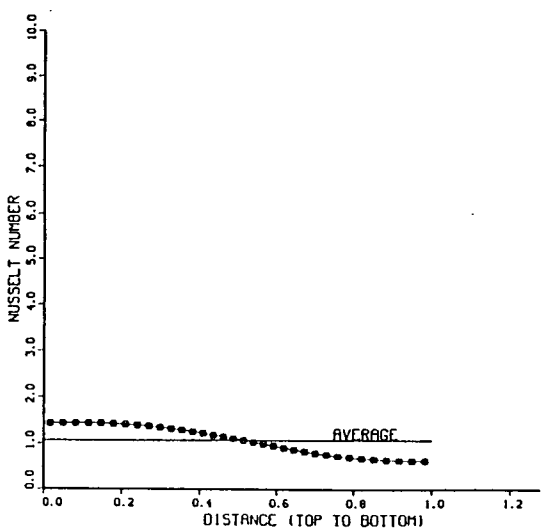

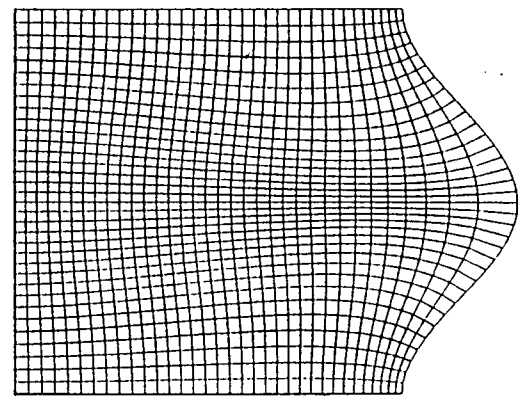

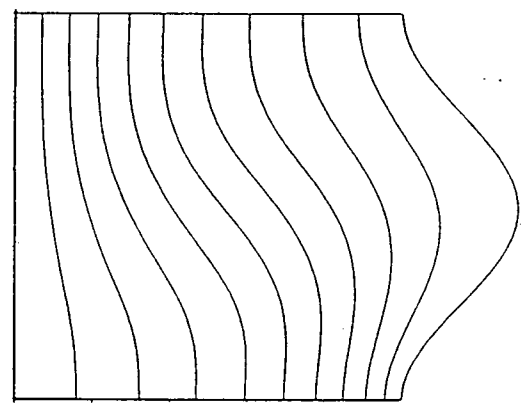

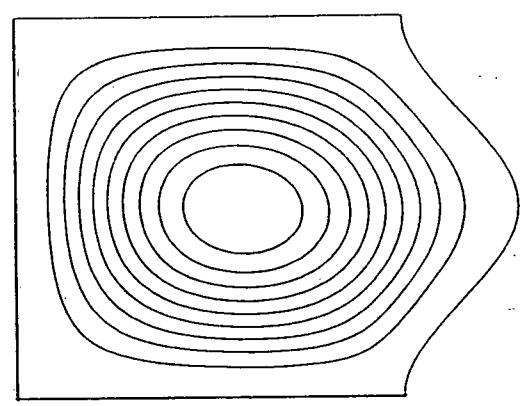

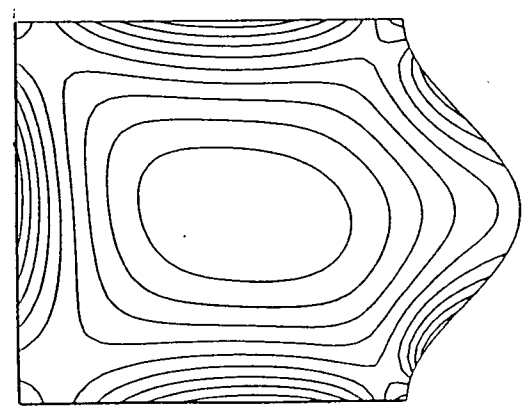

PR= 1.0
RA= 3000.0
DIMENSIONLESS AMPLITUDE= 0.150
AVERAGE NUSSELT NUMBER (RIGHT WALL)= 0.1267410E+01
AVERAGE NUSSELT NUMBER (LEFT WALL)= 0.1511370E+01
LENGTH OF THE WALL(RIGHT)= 0.1192486E+01
LENGTH OF THE WALL(LEFT)= 0.1000084E+01

VORTICITY COUNTOUR VALUES.
MIN= -0.1474019E+03
MAX= 0.6207288E+02

CONTOUR #	1	-0.1264545E+03
CONTOUR #	2	-0.1055070E+03
CONTOUR #	3	-0.8455951E+02
CONTOUR #	4	-0.6361201E+02
CONTOUR #	5	-0.4266454E+02
CONTOUR #	6	-0.2171707E+02
CONTOUR #	7	-0.7685923E+00
CONTOUR #	8	0.2017780E+02
CONTOUR #	9	0.4112538E+02

STREAM FUNCTION CONTOUR VALUES.
MIN= 0.0
MAX= 0.2855637E+01

CONTOUR #	1	0.2855637E+00
CONTOUR #	2	0.5911274E+00
CONTOUR #	3	0.8866911E+00
CONTOUR #	4	0.1182255E+01
CONTOUR #	5	0.1477818E+01
CONTOUR #	6	0.1773380E+01
CONTOUR #	7	0.2068945E+01
CONTOUR #	8	0.2364510E+01
CONTOUR #	9	0.2660072E+01

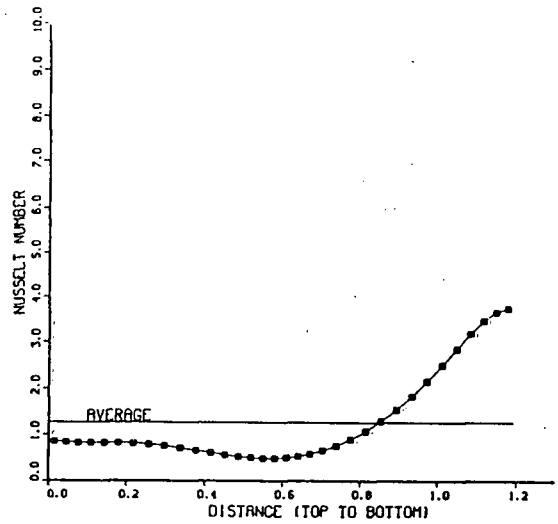

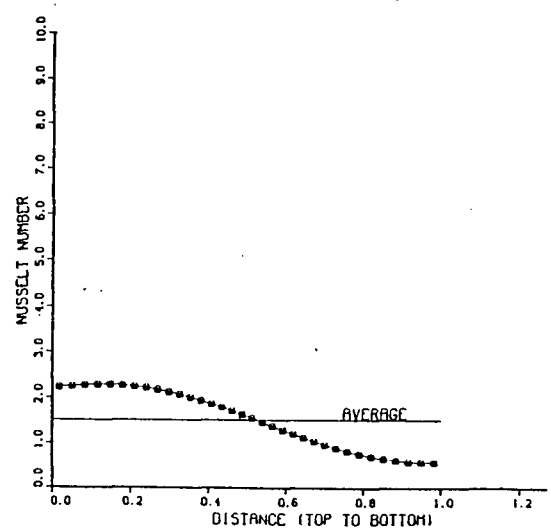

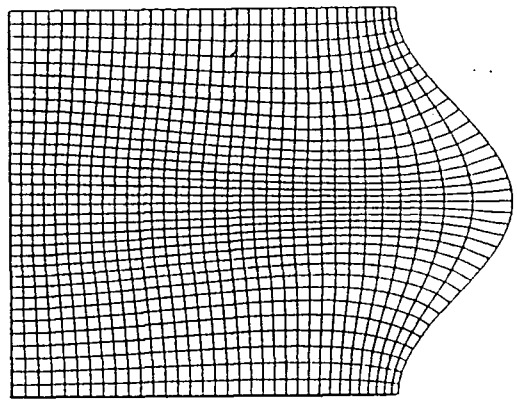

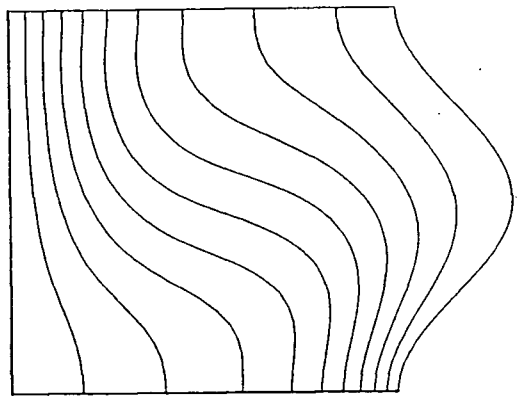

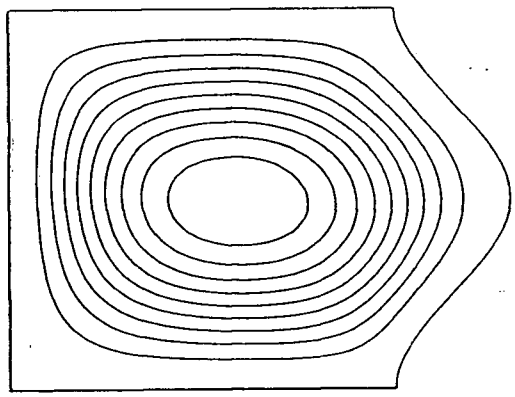

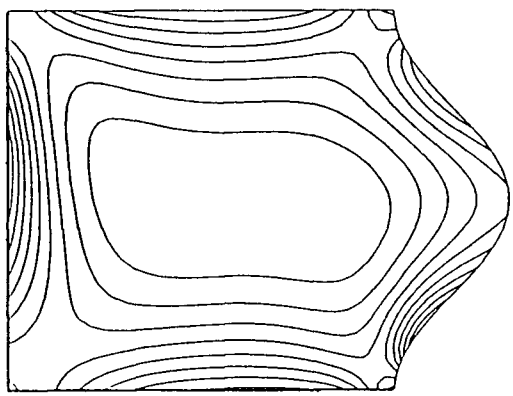

PR= 1.0
RA= 10000.0
DIMENSIONLESS AMPLITUDE= 0.150
AVERAGE NUSSELT NUMBER (RIGHT WALL)= 0.1957571E+01
AVERAGE NUSSELT NUMBER (LEFT WALL)= 0.2334428E+01
LENGTH OF THE WALL(RIGHT)= 0.1192486E+01
LENGTH OF THE WALL(LEFT)= 0.1000084E+01

VORTICITY COUNTOUR VALUES.
MIN= -0.4362793E+03
MAX= 0.1348951E+03

CONTOUR #	1	-0.3791618E+03
CONTOUR #	2	-0.3220444E+03
CONTOUR #	3	-0.2649270E+03
CONTOUR #	4	-0.2078096E+03
CONTOUR #	5	-0.1506921E+03
CONTOUR #	6	-0.9357471E+02
CONTOUR #	7	-0.3645728E+02
CONTOUR #	8	0.2066016E+02
CONTOUR #	9	0.7777734E+02

STREAM FUNCTION CONTOUR VALUES.
MIN= 0.0
MAX= 0.5296778E+01

CONTOUR #	1	0.5296777E+00
CONTOUR #	2	0.1059355E+01
CONTOUR #	3	0.1589033E+01
CONTOUR #	4	0.2118710E+01
CONTOUR #	5	0.2648388E+01
CONTOUR #	6	0.3178065E+01
CONTOUR #	7	0.3707744E+01
CONTOUR #	8	0.4237422E+01
CONTOUR #	9	0.4767098E+01

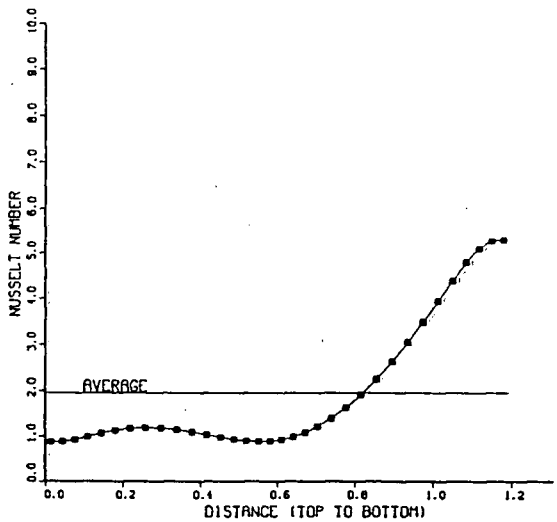

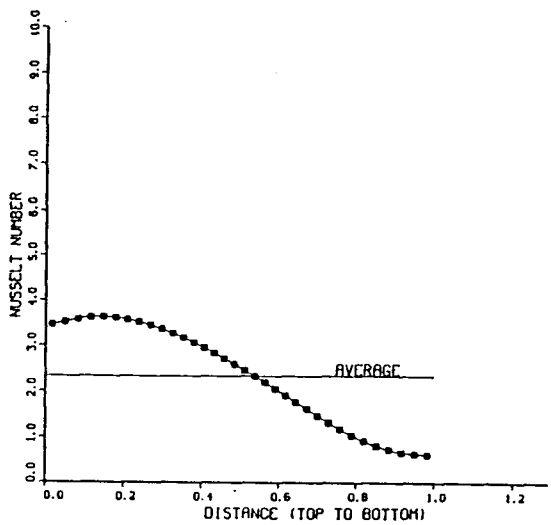

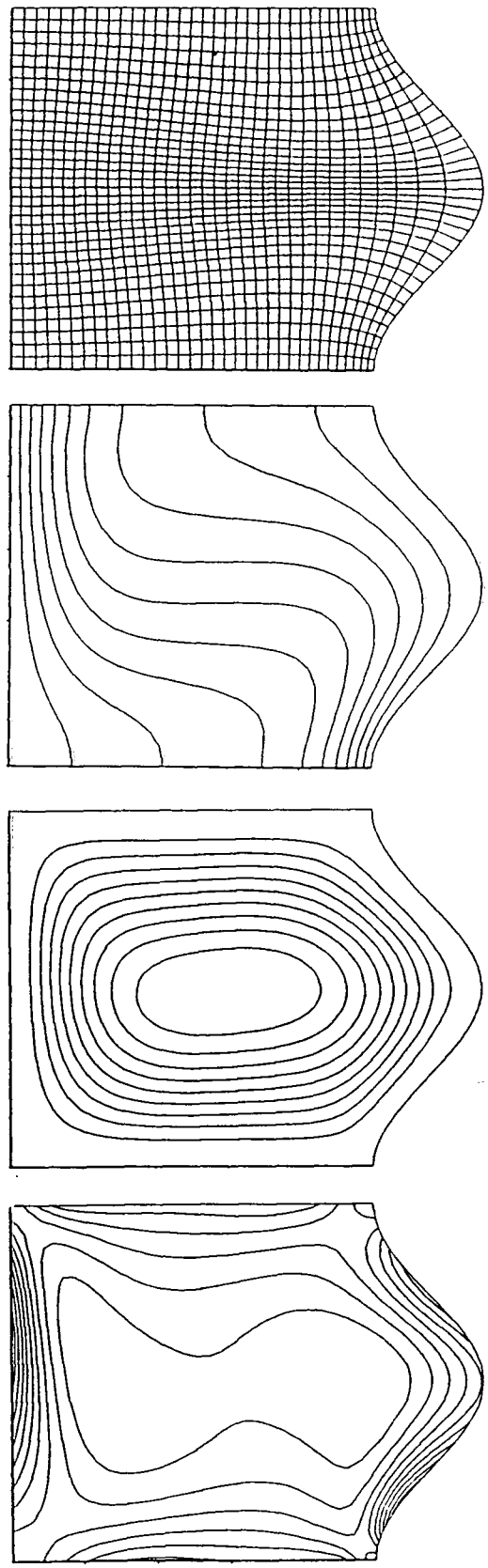

PR= 1.0
RA= 30000.0
DIMENSIONLESS AMPLITUDE= 0.150
AVERAGE NUSSELT NUMBER (RIGHT WALL)= 0.2815608E+01
AVERAGE NUSSELT NUMBER (LEFT WALL)= 0.3356983E+01
LENGTH OF THE WALL(RIGHT)= 0.1182486E+01
LENGTH OF THE WALL(LEFT)= 0.1000084E+01

VORTICITY COUNTOUR VALUES.
MIN= -0.1086954E+04
MAX= 0.2918354E+03

CONTOUR #	1	-0.9490747E+03
CONTOUR #	2	-0.8111958E+03
CONTOUR #	3	-0.6733169E+03
CONTOUR #	4	-0.5354380E+03
CONTOUR #	5	-0.3975591E+03
CONTOUR #	6	-0.2596802E+03
CONTOUR #	7	-0.1218013E+03
CONTOUR #	8	0.1607764E+02
CONTOUR #	9	0.1539565E+03

STREAM FUNCTION CONTOUR VALUES.
MIN= 0.0
MAX= 0.7712517E+01

CONTOUR #	1	0.7712517E+00
CONTOUR #	2	0.1542503E+01
CONTOUR #	3	0.2313754E+01
CONTOUR #	4	0.3085007E+01
CONTOUR #	5	0.3856257E+01
CONTOUR #	6	0.4627510E+01
CONTOUR #	7	0.5398761E+01
CONTOUR #	8	0.6170013E+01
CONTOUR #	9	0.6941264E+01

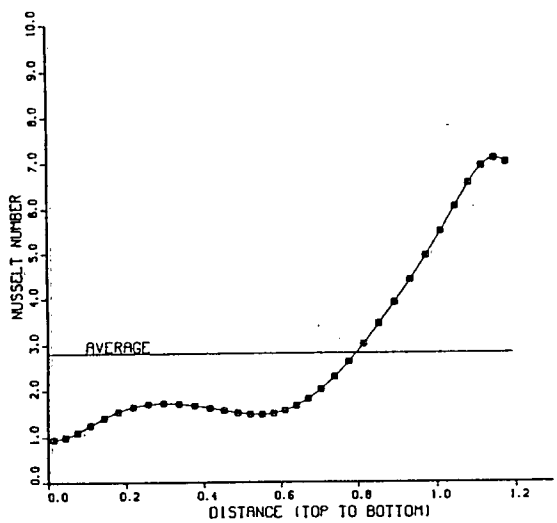

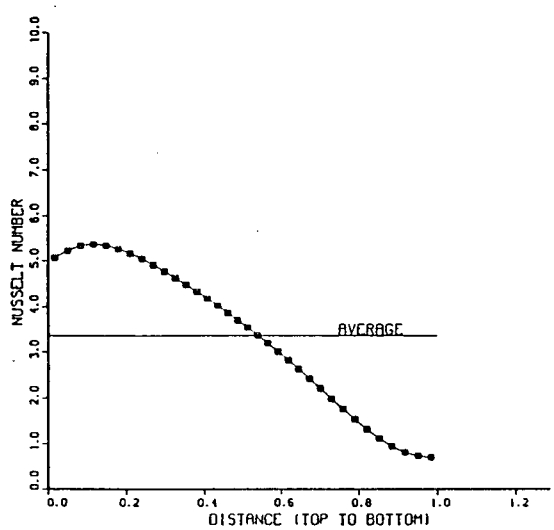

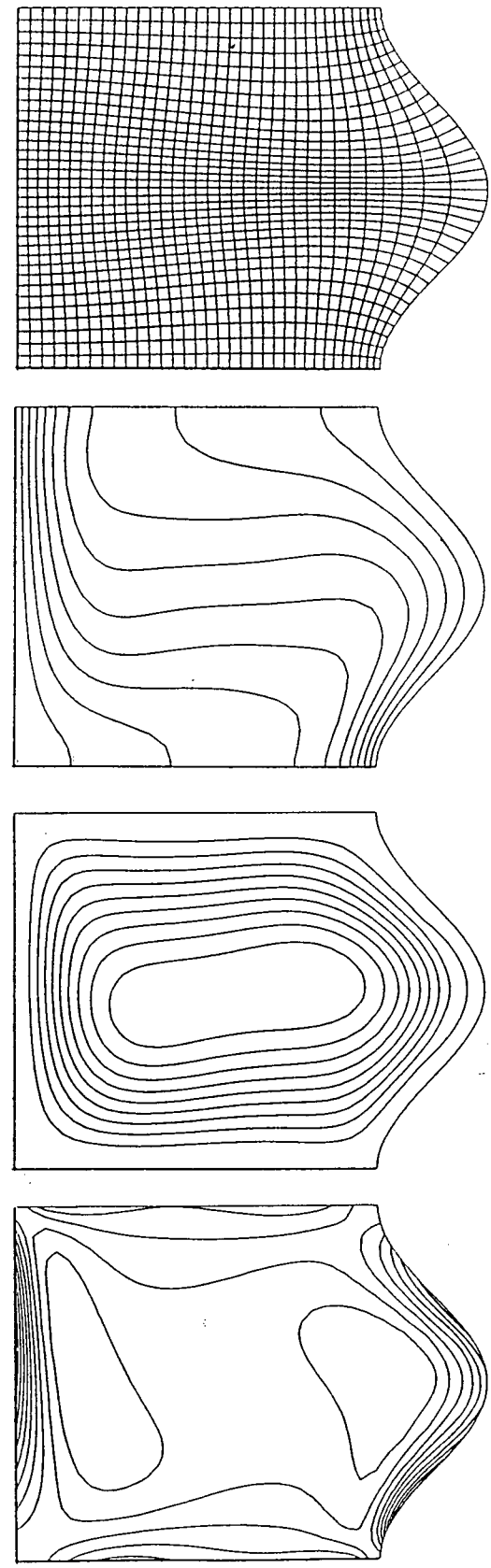

PR= 1.0
RA= 100000.0
DIMENSIONLESS AMPLITUDE= 0.150
AVERAGE NUSSELT NUMBER (RIGHT WALL)= 0.4082529E+01
AVERAGE NUSSELT NUMBER (LEFT WALL)= 0.4881560E+01
LENGTH OF THE WALL(RIGHT)= 0.1192486E+01
LENGTH OF THE WALL(LEFT)= 0.1000084E+01

VORTICITY COUNTOUR VALUES.
MIN= -0.2808643E+04
MAX= 0.6615945E+03

CONTOUR #	1	-0.2461620E+04
CONTOUR #	2	-0.2114596E+04
CONTOUR #	3	-0.1767572E+04
CONTOUR #	4	-0.1420549E+04
CONTOUR #	5	-0.1073525E+04
CONTOUR #	6	-0.7265007E+03
CONTOUR #	7	-0.3794771E+03
CONTOUR #	8	-0.3245313E+02
CONTOUR #	9	0.3145703E+03

STREAM FUNCTION CONTOUR VALUES.
MIN= 0.0
MAX= 0.1133965E+02

CONTOUR #	1	0.1133965E+01
CONTOUR #	2	0.2267930E+01
CONTOUR #	3	0.3401895E+01
CONTOUR #	4	0.4535861E+01
CONTOUR #	5	0.5669826E+01
CONTOUR #	6	0.6803791E+01
CONTOUR #	7	0.7937756E+01
CONTOUR #	8	0.9071722E+01
CONTOUR #	9	0.1020569E+02